UNIVERSITY OF Southampton

University of Southampton Research Repository

Copyright © and Moral Rights for this thesis and, where applicable, any accompanying data are retained by the author and/or other copyright owners. A copy can be downloaded for personal non-commercial research or study, without prior permission or charge. This thesis and the accompanying data cannot be reproduced or quoted extensively from without first obtaining permission in writing from the copyright holder/s. The content of the thesis and accompanying research data (where applicable) must not be changed in any way or sold commercially in any format or medium without the formal permission of the copyright holder/s.

When referring to this thesis and any accompanying data, full bibliographic details must be given, e.g.:

Thesis: Author (Year of Submission) "Full thesis title", University of Southampton, name of the University Faculty or School or Department, PhD Thesis, pagination.

Data: Author (Year) Title. URI [dataset]

University of Southampton

Faculty of Natural and Environmental Sciences

School of Ocean and Earth Science

Advances in the state-of-the-art in the quantitative ecology of the marine megabenthos

Volume 1 of 1

by

Noëlie Marie Aline Benoist

ORCID iD 0000-0003-1978-3538

Thesis for the degree of Doctor of Philosophy

September 2020

UNIVERSITY OF SOUTHAMPTON

ABSTRACT

FACULTY OF NATURAL AND ENVIRONMENTAL SCIENCES
School of Ocean and Earth Science
Thesis for the degree of Doctor of Philosophy

ADVANCES IN THE STATE-OF-THE-ART IN THE QUANTITATIVE ECOLOGY OF THE MARINE MEGABENTHOS

by Noëlie Marie Aline Benoist

This study attempts to advance the quantitative ecology of the megabenthos by (i) adopting and developing the use of mass seabed photography, and by (ii) extending body-size-based ecosystem assessment to this group. The metabolic theory of ecology (MTE) builds from simple bio-energetic assumptions of individual metabolism to make predictions about ecological processes from individual structure and functioning, to community and ecosystem dynamics. Under the 'energetic equivalence rule', or Damuth's rule, the population density of living organisms is related to a -3/4 power of body mass, indicating equal resource acquisition across body-size classes. In the marine environment, meio- to macrobenthic assemblages have be usefully modelled as a notional single trophic level, suggesting energetic equivalence throughout the two fractions. That concept is tested here by extension to the megabenthos.

The body-size structure of benthic assemblages was examined in four contrasting settings: two shelf-sea sites in the Celtic Sea (Greater Haig Fras marine conservation zone; Shelf-Sea Biogeochemistry area), and two deep-sea sites (Porcupine Abyssal Plain sustained observatory, PAP-SO, northeast Atlantic; Clarion-Clipperton Zone, CCZ, northeast Pacific). Imagery data were collected using autonomous underwater vehicles, allowing consistent assessment of the megabenthos in the form of individual-based body-size spectral analyses, over landscape-scale areas encompassing multiple habitat types. For the well-known Celtic Shelf and PAP-SO assemblages, species-specific length-weight relationships were used to derive individual biomass data. However, that was not possible for the poorly studied CCZ fauna, prompting the development of a generalised volumetric method for individual body-mass estimation. The MTE framework was used to investigate the effects of seafloor temperature and resource supply on the stocks and flows of mass and energy at these sites.

The results of this study demonstrate the practical advantage of mass seabed photography in the quantitative ecological assessment of the megabenthos. The volumetric methodology developed overcomes the taxonomic, temporal, and spatial, dependencies known to impact length-weight relationships. The megabenthos body-size distributions produced were broadly consistent across sites, and generally conformed to the MTE expectations, i.e. controlled by both seafloor temperature and resource supply. These results suggest a much greater ecological significance of the megabenthos than has generally been assumed, i.e. at the PAP-SO site they account for 93% of the total metabolically active standing stock carbon biomass, and 27% of total benthic carbon respiration. Individual-based body-size spectral analyses, coupled with the MTE framework, provide a robust baseline for assessing ecological patterns, and for monitoring change.

List of contents

List of tables

List of figures

Chapter 6 Deep-sea sites

Chapter 7 Body-Size Distribution of Contrasting Benthic Assemblages

List of equations

Declaration of Authorship

I, **Noëlie Marie Aline Benoist**, declare that this thesis entitled "**Advances in the state-of-the-art in the quantitative ecology of the marine megabenthos**", and the work presented in it, are my own and has been generated by me as the result of my own original research. I confirm that:

1. This work was done wholly or mainly while in candidature for a research degree at this University;
2. Where any part of this thesis has previously been submitted for a degree or any other qualification at this University or any other institution, this has been clearly stated;
3. Where I have consulted the published work of others, this is always clearly attributed;
4. Where I have quoted from the work of others, the source is always given. With the exception of such quotations, this thesis is entirely my own work;
5. I have acknowledged all main sources of help;
6. Where the thesis is based on work done by myself jointly with others, I have made clear exactly what was done by others and what I have contributed myself;
7. Parts of this work have been published as:

Benoist NMA, Bett BJ, Morris KJ, Ruhl H. 2019. A generalised method to estimate the biomass of photographically surveyed benthic megafauna. *Progress in Oceanography - Special Issue VIS: Northeast Atlantic PAP-SO*, **178**, 102188. DOI: 10.1016/j.pocean.2019.102188

Benoist NMA, Morris KJ, Bett BJ, Durden JM, Huvenne VAI, Le Bas TP, Wynn RB, Ware SJ, Ruhl HA. 2019. Monitoring mosaic biotopes in a marine conservation zone by autonomous underwater vehicle. *Conservation Biology*, **33**(5), 1174-1186. DOI: 10.1111/cobi.13312

Morris KJ, Bett BJ, Durden JM, **Benoist NMA**, Huvenne VA, Jones DO, Robert K, Ichino MC, Wolff GA, Ruhl HA. 2016. Landscape-scale spatial heterogeneity in phytodetrital cover and megafauna biomass in the abyss links to modest topographic variation. *Scientific Reports* **6**, 34080. DOI: 10.1038/srep34080

Simon-Lledó E, Bett BJ, Huvenne VAI, Schoening T, **Benoist NMA**, Jeffreys RM, Durden JM, Jones DOB. 2019. Megafaunal variation in the abyssal landscape of the Clarion Clipperton Zone. *Progress in Oceanography* **170**, 119-133. DOI: 10.1016/j.pocean.2018.11.003

Simon-Lledó E, Bett BJ, Huvenne VAI, Schoening T, **Benoist NMA**, Jones DOB. 2019. Ecology of a polymetallic nodule occurrence gradient: Implications for deep-sea mining. *Limnology and Oceanography*, **64**(5), 1883-1894. DOI: 10.1002/lno.11157

Thompson CEL, Silburn B, Williams ME, Hull T, Sivyer D, Amoudry LO, Widdicombe S, Ingels J, Carnovale G, McNeill CL, Hale R, Marchais CL, Hicks N, Smith HEK, Klar JK, Hiddink JG, Kowalik J, Kitidis V, Reynolds S, Woodward EMS, Tait K, Homoky WB, Kroger S, Bolam S, Godbold JA, Aldridge J, Mayor DJ, **Benoist NMA**, Bett BJ, Morris KJ, Parker ER, Ruhl HA, Statham PJ, Solan M. 2017. An approach for the identification of exemplar sites for scaling up targeted field observations of benthic biogeochemistry in heterogeneous environments. *Biogeochemistry* **135**(1-2), 1-34. DOI: 10.1007/s10533-017-0366-1

Zelada Leon A, Huvenne VAI, **Benoist NMA**, Ferguson M, Bett BJ, Wynn RB. 2020. Assessing the Repeatability of Automated Seafloor Classification Algorithms, with Application in Marine Protected Area Monitoring. *Remote Sensing* **12**(10), 1572. DOI: 10.3390/rs12101572

Signed: .....

Date: .....

Acknowledgements

I would like to thank my supervisor, and mentor, Brian Bett, whose continuous support and guidance throughout this project have been invaluable; your patience and encouragement did make all the difference. Thanks to my supervisory panel, Henry Ruhl, Daniel Jones, Adrian Martin, and Antony Jensen, and to my panel chair, Richard Lampitt, for their assistance during the time of research and writing of the thesis.

So many other people have helped me stay on track and complete this project. I would like to acknowledge all my past and present Deep-Seas colleagues, Kirsty Morris, Aurélie Goineau, Andrew Gates, Tammy Horton, Andrew Gooday, Brett Hosking, Rob Young, Erik Simon-Lledó, Jennifer Durden, Amanda Serpell-Stevens; and fellow researchers, Simone Pfeifer, Anita Hollingsworth, Marla Spencer, and Philip Smith, for the helpful comments and discussions, whether about what's going on in the ocean, or about the weather. Also, thanks to the Marine Geoscience group, in particular, Veerle Huvenne, for the opportunity to go on research cruises, and Tim Le Bas, James Strong, Cat Wardell, and Nils Piechaud, for sharing these experiences. Thank you as well to Claire Laguionie Marchais (NUI Galway), Luciana Génio (ISA), Raissa Hogan (NUI Galway), Corinne Pebody, Sue Hartman, and all the colleagues and students present during the research cruises at the Porcupine Abyssal Plain, and for enlightening my time at sea. I am also thankful to the crew of RRS *James Cook* and RRS *Discovery*, and to the Marine Autonomous and Robotic Systems and the National Marine Facilities groups, for their technical support during my numerous research expeditions, and most importantly, for teaching me how to play cribbage.

Last but not least, I would like to thank my family, my parents, my brothers—Laurent and Stéphane, and my little sister—Elora, and my friends, in particular Anne, Angela, and Franco, for their unconditional love and support over the years. And thanks to you Michael S.W., for your care and endless patience. You are all so fantastic; all this would have been much harder without you.

Nomenclature

APEI	area of particular environmental importance
AUV	autonomous underwater vehicle
B	total ecosystem resource use (mg C m^{-2})
B_i	population respiration at size class i (mg C m^{-2})
CCZ	Clarion-Clipperton Zone
DEB	dynamic energy budget
DOOS	deep-ocean observing strategy
$e^{-E/kT}$	Boltzmann factor
E	activation energy of metabolism (eV)
ECD	equivalent cylindrical diameter (mm)
ECL	equivalent cylindrical length (mm)
EER	energetic equivalence rule
EBV	essential biodiversity variable
EOV	essential ocean variable
EUNIS	European Union Nature Information System
fwwt	fresh wet weight
LM	general linear model
GEBCO	general bathymetric chart of the oceans
GEO BON	global biodiversity observing system
GOOS	global ocean observing strategy
GHF	Greater Haig Fras
GVM	generalised volumetric method
i_0	normalization constant of metabolism (mg C d^{-1})
I_i	individual metabolic rate at size class i (mg C d^{-1})
k	Boltzmann's constant (8.617×10^{-5} eV/K)
LWR	length-weight relationship
MCZ	marine conservation zone
M_E	estimated body mass (g wwt)
M_M	measured body mass (g wwt)
MTE	metabolic theory of ecology
N	total population density (ind. m^{-2})
N_i	population density at size class i (ind. m^{-2})
NERC	Natural Environment Research Council
NOC	National Oceanography Centre
PAP-SO	Porcupine Abyssal Plain sustained observatory
POC	particulate organic carbon
pwwt	preserved wet weight
RRS	Royal Research Vessel
$[R_i]$	power supplied to class i
rt	residence time (d)
SL	standard (linear) length
SSB	Shelf-Sea Biogeochemistry
T	temperature (K)
TOC	total organic carbon content (%)
V_E	estimated body volume (mL)
V_M	measured body volume (mL)
W	total population biomass (g wwt m^{-2}; mg C m^{-2})
W_i	population biomass at size class i (g wwt m^{-2}; mg C m^{-2})
wwt	wet weight

Chapter 1

Introduction

1.1 General introduction

From an ecological perspective, life can be expressed in terms of the interactions among a combination of biological entities, organisms forming a community, and their environment. These ecological energetic interactions are dynamic in space and time, and are sustained by the quality and flows of energy and nutrients that travel through all life compartments. Understanding how biotic and abiotic parameters function together under different spatial and temporal constraints is the goal of all ecologists, so that we can comprehend how natural systems work and thus benefit from them (Calow 1977; Tomlinson et al. 2014).

The marine benthos corresponds to the communities of organisms that live in (infauna), on (epifauna), or near (demersal fauna) the seabed. Benthic organisms are represented by a range of invertebrate taxa varying in size from micrometres to tens of centimetres (Narayanaswamy et al. 2016; Bett 2019), living freely or attached to surfaces, and exhibiting different feeding habits, from filter feeding and detritus feeding to scavenging and predation. Demersal fishes are also a component of the benthos; they have evolve a wide variety of morphological and behavioural adaptations to living on the seafloor, and they mainly feed on other fishes, benthic invertebrates, and zooplankton (Bergstad 2009).

Benthic communities reflect the health of our oceans, and play a key role in the regulation of ecosystem services provided to mankind (Gage and Tyler 1991; Bertness et al. 2001, 2014; Gray and Elliott 2009; Griffiths et al. 2017). For example, they participate in nutrient cycling and carbon sequestration (Schmitz et al. 2013), and represent an important food source for humans (ICES 2008, 2016). Benthic organisms, particularly invertebrates, are so reliant on the quality of their physical environment (e.g. sediment

composition, water quality, and hydrology), and are thus potentially sensitive to sudden environmental changes, they are considered good bio-indicators of the health of aquatic ecosystems (Reynoldson and Metcalfe-Smith 1992; Hiscock et al. 2005; Salas et al. 2006). Although benthic ecology is not a new discipline, our knowledge has been limited to only a small fraction of the global seafloor because of methodological restrictions on sampling the benthos as we go further away from the coastline, and deeper into the ocean (Raffaelli et al. 2003).

There are various ways to monitor the health and productivity of ecosystems, including standing-stock assessment, and taxonomic evaluation for assessing faunal composition and diversity. Biomass is a key ecological variable that informs the fields of conservation, environmental quality assessment, resource management, and the study of the stocks and flows of mass and energy through ecosystems (e.g. Tomlinson et al. 2014) (see chapter 4 section 4.2.1). In the latter case, individual body mass, via the metabolic theory of ecology (MTE), is a critical variable in the assessment of ecosystem-level processes (Brown et al. 2004; Schramski et al. 2015). In the marine environment, recent field studies (Kelly-Gerreyn et al. 2014; Labra et al. 2015; Laguionie Marchais et al. 2020), and theoretical considerations (Bett 2013, 2014), have suggested that there is an increase in the total measured seafloor biomass as larger and larger body sizes are included in those estimates. The largest organisms present, the megafauna, may contribute very substantially to total standing stock biomass, and may play a greater role in the fluxes of mass and energy, than is generally believed (Bett 2019; Laguionie Marchais et al. 2020).

Our quantitative understanding of the stocks and flows of mass and energy through benthic systems has largely been made upon evaluation of the smaller faunal size fractions constituting benthic communities—from micro- to macrobenthos. Assessment of the largest size fraction—the megabenthos, body size ≥ 1 cm (e.g. Bett 2019)—has traditionally been undertaken by trawl sampling (e.g. Gage and Bett 2005), providing the advantage of acquiring physical specimens for taxonomic identification and direct standing stock biomass evaluation. However, that approach is destructive, typically limited to sedimentary habitats, and likely to be semi-quantitative at best (e.g. McIntyre

1956). In a study of the deep-sea megabenthos, Bett et al. (2001) estimated trawling efficiency to be dependent on body size, varying from < 1% for small ophiuroids (e.g. *Ophiocten hastatum*) to 98% for the largest taxa (e.g. holothurian *Psychropotes longicauda*). In response to these limitations, there has been a general increase in the use of seafloor photography to quantify megafaunal assemblages (Durden et al. 2016c), which has recently accelerated with the development of autonomous underwater vehicles (AUVs) (Wynn et al. 2014; Jones et al. 2019) and their use in quantitative benthic ecology (Milligan et al. 2016; Morris et al. 2016; Simon-Lledó et al. 2019a). Seafloor photography from an AUV enables the rapid quantitative survey of large areas that can comprise multiple habitats, in a consistent and non-destructive manner (e.g. Thomson et al. 2017; Benoist et al. 2019a).

The size an organism reaches at maturity is the expression of the effect of individual life history, combined with environmental forces influencing growth. It comes with costs in terms of resource use and energy flow, therefore having a direct effect on productivity. Given the central role that body size plays in determining many biological processes (e.g. metabolism, abundance, biomass, production) (Peters 1983; Brown et al. 2004), it seems only natural to treat organisms in terms of their body size as an alternative to, or in conjunction with, their taxonomic identity. Sheldon and Parsons (1967) and Sheldon et al. (1972) pioneered size-based analysis of marine ecosystem structure and functioning with their work on the size distribution of particles in the pelagic realm, followed by the benthic studies of Schwinghamer (1981) and Warwick (1984).

The present Ph.D. thesis attempts to advance the state-of-the-art in the quantitative ecology of the marine megabenthos by (i) adopting and further developing the use of mass photography by AUV, and by (ii) extending size-based analysis of ecosystem structure and functioning to the largest size fraction of the benthos. It explores the body-size distribution of epibenthic mega-invertebrates and demersal fish communities (megabenthos) at four locations in contrasting environmental settings—two shelf-sea study sites in the Celtic Sea, and two deep-sea sites in the NE Atlantic and NE Pacific. Drawing on large-scale AUV-based photographic surveys, size spectra are constructed for the megabenthos at all sites.

As an introduction to this thesis, the basic notions of the MTE are examined, and empirical examples drawn from previous benthic studies are set in relation to the theory's numerical framework. The following chapters describe the local environmental settings of the four study sites (chapter 2), and the methods used to collect data on the megabenthos (at all locations) and the macrobenthos (at one location), from field sampling to sample processing and data analysis (chapter 3). Chapter 4 provides a background to existing indirect approaches to individual biomass estimation from photographs, comparing the traditional approach based on taxon-specific length-weight relationships (LWRs) to a new, taxon-independent, generalised volumetric method (GVM) that was developed during the course of this Ph.D. (Benoist et al. 2019b). Chapters 5 and 6 give a description of the benthic communities at the shelf- and deep-sea locations, respectively. Chapter 5 is divided into two parts: published work on the use of AUV seabed imagery for broad-scale ecological assessment of shelf-sea megabenthic assemblages, across multiple and mixed habitats (5.A); body-size spectral analysis of shelf-sea assemblages (5.B). Chapter 7 then aims to contrast the body-size distributions from the four sites, and to examine potential links to key environmental factors. This chapter also implements the use of body-size spectra combined with the MTE numerical framework to examine carbon stocks and flows for the integrated benthic ecosystem. The key results of this thesis are summarised in chapter 8, together with some considerations of the broader implications of the improved quantitative analysis of the megabenthos, made possible by photographic assessments and the use of body-size spectra.

1.2 Metabolic theory of ecology

Metabolism reflects the flux and transformation of energy and materials in living organisms, involving exchanges with the environment (from resource uptake to release of altered forms), processing of those resources, and the allocation of energy and materials to survival, growth, and reproduction (Brown et al. 2004; Savage et al. 2004a; Allen and Gillooly 2007). It is determined by the rate at which these processes occur across all biological units from molecules to individuals, and it is often measured as the rate of respiration in heterotrophs, using direct calorimetry or estimation of oxygen

consumption (Elliot and Davison 1975; Peters 1983; Lampert 1984). Metabolic rate can be categorised as (i) basal, or resting, when metabolic requirements are minimum, allowing survival under ideal conditions; (ii) field like, when energy expenditure involves growth and reproduction; or (iii) maximal, when a high level of physical activity is sustained (e.g. predator avoidance).

Metabolic rate is considered to follow (a) an allometric relationship with body mass, and to have (b) an exponential dependence on temperature; thus described by a primary equation for individual metabolic rate (I_i, equation 1.1 in the calculation box on page 8), which forms the basis of the metabolic theory of ecology (Brown et al. 2004). Empirical data across a wide range of terrestrial and aquatic species have shown that individual metabolic rate typically scales as a 3/4 power of body mass across 27 orders of magnitude in mass, from the smallest prokaryotes to the largest metazoans (Peters 1983; West et al. 1997; Savage et al. 2004b; West and Brown 2005; Brey 2010). Brown et al. (2004) suggest that the origin of this mass scaling reflects the fractal-like design of resource distribution in metazoans (i.e. materials are transported through linear networks that branch to supply all parts of the organisms), which is thought to minimize the energy required for distribution (West et al. 1997, 1999; Savage and West 2006).

Criticism and controversies have centred on the scaling of individual metabolic rate with body mass, as reviewed by West and Brown (2005), and discussed by other authors (van der Meer 2006; Maino et al. 2014; Clarke 2017). In particular, the surface law predicts an alternative scaling exponent of 2/3, reflecting the role of body surface area in heat dissipation. In any approach, difficulties remain in accurate measurement of representative, metabolically active, body mass data across taxa, and of metabolic rate. Even though 3/4 might not be a universal metabolic exponent, using it as a parameter in allometric equations that are components of more complex models can lead to adequate approximations.

The MTE numerical framework builds from simple bio-energetic assumptions of individual metabolism to make predictions about ecological processes from individual structure and functioning (e.g. allometry, biomass partitioning, life history), to community (e.g. abundance with body-size distribution, energetic equivalence) and ecosystem dynamics (e.g.

biogeochemical cycling) (Brown et al. 2004; Savage et al. 2004a; Lewis et al. 2008; Yvon-Durocher and Allen 2012; Schramski et al. 2015). Damuth (1981, 1987) reviewed extensively the literature about interspecific scaling of population and body mass among terrestrial mammals and invertebrates. The author noted that the abundance of individuals was inversely related to their size ($M^{-3/4}$); that is, reciprocally to individual metabolic rate ($M^{3/4}$), in such a way that resource acquisition rate was approximately equal across geometric body-size classes (M^0). This is typically referred to as the 'energetic equivalence rule' (EER), or 'Damuth's rule', when the mass-scaling of numerical abundance is a -3/4 power (White et al. 2007). All other things being equal, it implies that within an assemblage feeding on the same resource, no geometric body-size class has an energetic advantage over any other.

At steady state, and under energetic equivalence, population abundance per size class (N_i, equation 1.2) is predicted to decrease (-3/4 power) with increasing body size (i.e. fixed resource supply supports fewer larger individuals) (figure 1.1a), and with increasing temperature (i.e. higher individual metabolic rate). Consequently, biomass per size class (W_i, equation 1.3) is expected to scale as a quarter power of body mass. Similarly, resource use per size class (B_i, equation 1.4) is predicted to be invariant of body size given the body-mass scaling of size-class abundance and individual metabolic rate (i.e. $N_i \times I_i \propto {M_i}^{-3/4} \times {M_i}^{3/4} \propto {M_i}^0$), and to be fixed by resource supply rate per size class (i.e. EER) (Damuth 1981; Allen et al. 2002; Brown et al. 2003, 2004; Lewis et al. 2008; Isaac et al. 2012; Yvon-Durocher and Allen 2012; Sewall et al. 2013; Schramski et al. 2015). Total ecosystem abundance (N), biomass (W), and resource use (B, as respiration), are then the summations of these variables across all size classes represented.

However, in a multi-trophic level system, such as a 'simple' pelagic system where fish feed on zooplankton which feed on phytoplankton, ecologists have long noted that abundance scales as M^{-1}, biomass as M^0, and correspondingly resource use as $M^{-1/4}$ (Sheldon et al. 1972; Brown et al. 2003b, 2004; Lewis et al. 2008; figure 1.1b). This observation of near constant biomass across many doubling body-size classes in pelagic systems is referred to as the 'Sheldon spectrum' (Sheldon et al. 1967). Brown et al.

(2004) interpreted this difference from the simple form of the MTE numerical framework by assuming a predator-prey body-mass ratio of 10^4 , and 10% transfer of energy between trophic levels (see also Jennings et al. 2002; Blanchard et al. 2009; Tsai et al. 2016).

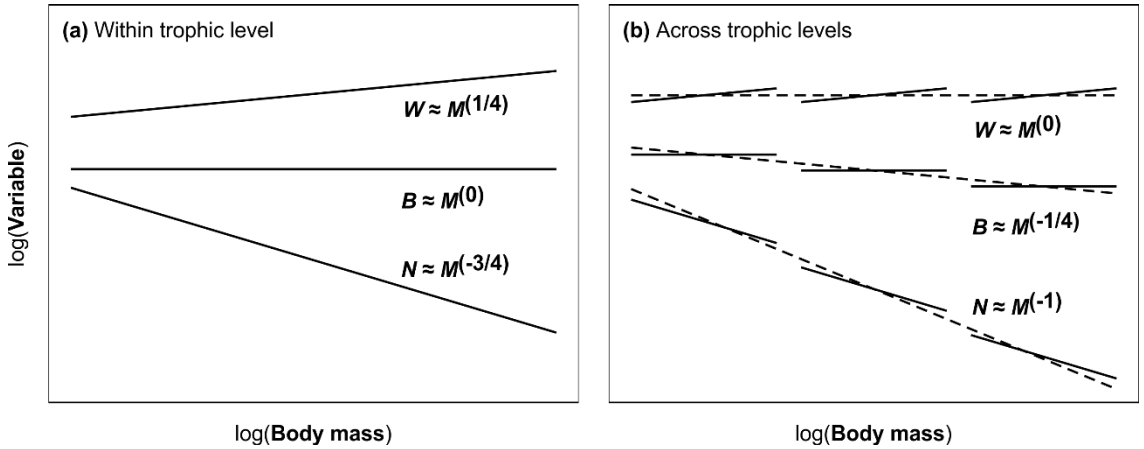

Figure 1.1. Graphical representation of the MTE model of assemblage structure. (a) Within trophic level (continuous lines), a 'simple' system representing an assemblage feeding on a common resource. **(b)** An assemblage represented by three size-based trophic levels (dashed lines), assuming a predator-prey body-mass ratio of 10^4 and a 10% transfer of energy between levels (e.g. pelagic system). Variables: N, faunal abundance (numerical density); W, standing stock biomass; B, resource use as respiration (equations 1.2-1.4, respectively). (Re-drawn from Brown et al. 2004)

Early studies of benthic body-size spectra (e.g. Schwinghamer 1983; Warwick 1984) suggested that they had systematic variations between the conventional faunal body-size categories (micro-, meio-, and macrobenthos) with peaks in biomass or species richness in size classes thought to represent the optimal body-size characteristics of the different benthic lifestyles (sediment-attached, interstitial, and sedentary or of limited mobility, respectively) (figure 1.2). However, more recently Bett (2013, 2014) suggested that these apparent variations might be sampling artefacts such that monotonic abundance and biomass spectra may be a reasonable approximation of the benthic system. For example, the MTE framework can be used to reinterpret existing data such as Mare's (1942) for the biomass and abundance of micro- to macrobenthic organisms for which Bett (2014) found that abundance (biomass) decreased (increased) with body mass having a scaling exponent of -0.81 (0.25), close to the model predictions.

CALCULATION BOX

Body-size class: body-size division based on $\sqrt{2}$ geometric scaling; the geometric mean is used to represent the class.

Size-class individual metabolic rate (I_i; power, e.g. watts per individual), where i_0 is a normalization constant, M_i is geometric mean body mass in class i, $e^{-E/kT}$ is the Boltzmann factor where E is the activation energy of metabolism (0.65 eV) (Brown et al. 2004, 2012), k is the Boltzmann's constant (8.617×10^{-5} eV/K), and T is temperature in kelvin (K).

$$I_i = i_0 \, {M_i}^{3/4} \, e^{-E/kT} \qquad \text{(equation 1.1)}$$

Size-class population abundance (N_i; numerical density, e.g. individuals per unit area), where $[R_i]$ is the power intensity supplied to class i.

$$N_i = [R_i] \, {M_i}^{-3/4} \, e^{E/kT} \qquad \text{(equation 1.2)}$$

Size-class population biomass (W_i; mass density, e.g. grams per unit area).

$$W_i = [R_i] \, {M_i}^{1/4} \, e^{E/kT} \qquad \text{(equation 1.3)}$$

Size-class population respiration (B_i; power intensity, e.g. watts per unit area).

$$B_i = [R_i] \, {M_i}^{0} \, e^{-E/kT} \qquad \text{(equation 1.4)}$$

Under energetic equivalence, $B_i = [R_i]$.

Temperature-correction of size-class data: to simplify the comparison of data from sites having different bottom water temperatures, a correction can be applied based on the temperature dependence of metabolic rate (equation 3 in Gillooly et al. 2001).

Temperature-corrected abundance data ($\boldsymbol{N_{i\,(1.5\,^\circ C)}}$), where $x\,^\circ C$ represents the dataset seafloor temperature, 1.5 °C represents the target seafloor temperature e.g. of a reference site.

$$\boldsymbol{N_{i\,(1.5^\circ C)}} = \boldsymbol{N_{i\,(x^\circ C)}} \, \frac{e^{E/kT_{(x\,^\circ C)}}}{e^{E/kT_{(1.5^\circ C)}}} \qquad \text{(equation 1.5)}$$

1.3 Benthic size spectra

Body-size spectra based on individual body mass rather than mean taxon body mass have long been employed to describe benthic marine assemblages in connection with habitat type, water depth, resource supply, and disturbance gradients (Gerlach et al. 1985; Lampitt et al. 1986; Schwinghamer 1985, 1988; Duplisea and Drgas 1999; Basset et al. 2004; Law et al. 2012, Labra et

al. 2015; Górska and Włodarska-Kowalczuk 2017). Yet, few have been directly compared with the numerical framework provided by the MTE. This is, in part at least, because the datasets were not 'edited' to account for potential sampling artefacts, that can otherwise mask or detract from a continuous trend in abundance and biomass scaling with body size (Bett 2013, 2014; Laguionie Marchais et al. 2020). In addition, field-sampling limitations in terms of quantitative effectiveness and spatial coverage, particularly in the study of the largest body sizes, have limited some of these earlier studies.

Schwinghamer (1985) assessed the size spectra of benthic communities from three locations (around Nova Scotia and south of Bermuda, NW Atlantic) that differed in water depth and sediment characteristics, reporting an overall increase in biomass with body size, despite peaks and troughs thought to be characteristic of the micro-, meio-, and macrofauna size fractions (figure 1.2). The author noted that for each fraction, the sampling methods employed limited biomass estimation to within a certain body-size range, and introduced higher variability at the largest body sizes because of restricted physical sample size.

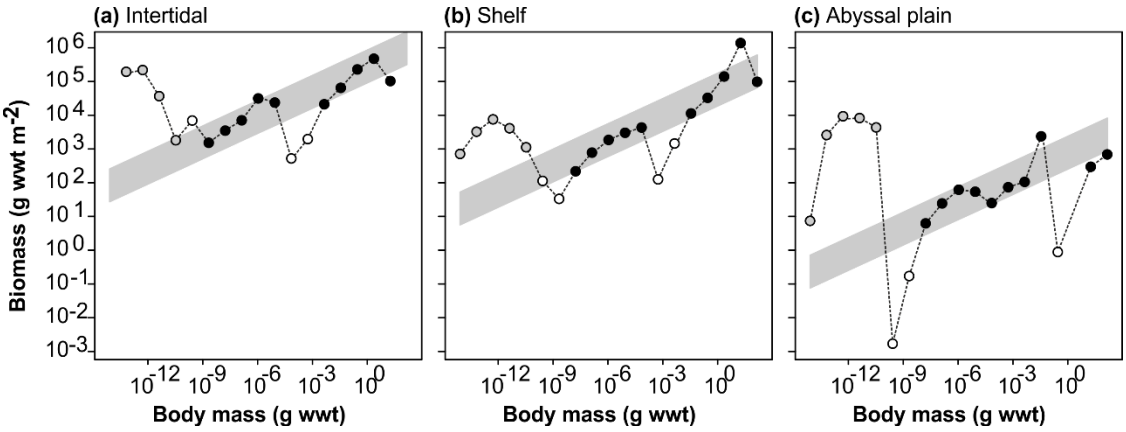

Figure 1.2. Biomass size spectra of intertidal, shelf, and abyssal micro- to macrobenthic assemblages in the NW Atlantic. Re-drawn from Schwinghamer (1985; authors' figure 1) where sampling sites are **(a)** intertidal; **(b)** offshore Scotian Shelf (c. 10-160 m); **(c)** Nares Abyssal Plain (4500-5850 m). Data were pooled by site and summarised to median values. Open symbols are presumed unrepresentative values; grey symbols are microbes; solid symbols are meio- and macrobenthos. Shaded area is MTE model biomass (equation 1.3; 0.25 scaling exponent) for representative non-microbe data.

Similarly, Górska and Włodarska-Kowalczuk (2017) analysed meio- and macrobenthic communities in two open fjords off west Svalbard (Arctic) with

respect to food availability and glacial disturbance. During sample processing, the authors included nematodes in their macrofauna fraction, often omitted in other works, attenuating the apparent 'biomass trough' between the two faunal fractions (figure 1.3). If data from the smallest size classes encountered in sieved samples is considered to be non-quantitative (e.g. Bett 2013, 2014; Laguionie Marchais et al. 2020), then the biomass spectra have scaling exponents close to the MTE model (0.25) in the undisturbed sites (figure 1.3a, b) as opposed to the disturbed site (figure 1.3c). Górska and Włodarska-Kowalczuk (2017) also noted a reduction in the elevation of the biomass spectrum under low food conditions, and a reduction in the maximum body size detected.

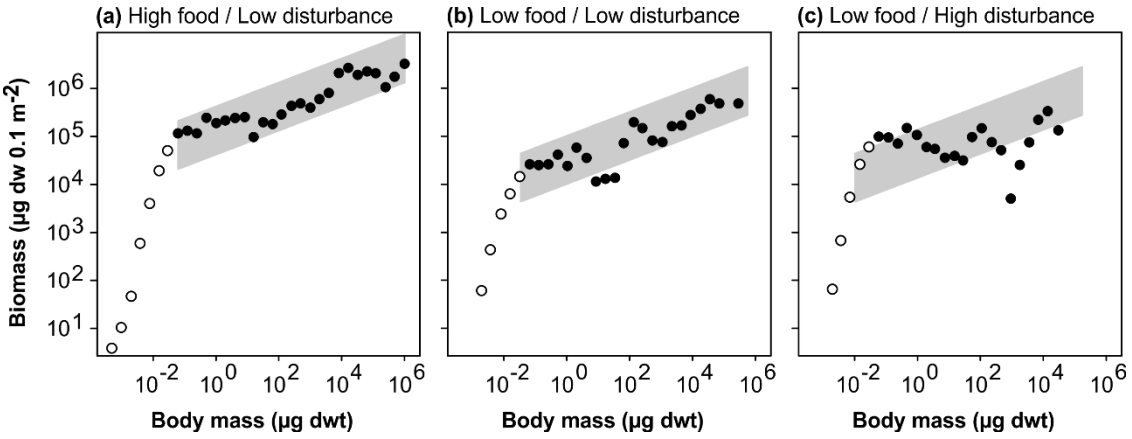

Figure 1.3. Biomass size spectra of open-fjord meio- to macrobenthic assemblages in the Arctic. Re-drawn from Górska and Włodarska-Kowalczuk (2017; authors' figure 3a) where sampling sites were characterised as **(a)** high food availability/low disturbance; **(b)** low food availability/low disturbance; **(c)** low food availability/high disturbance. Open symbols are presumed unrepresentative values. Shaded area is MTE model biomass (equation 1.3; 0.25 scaling exponent).

Labra et al. (2015) studied temporal variation of macro- and megabenthic communities in a shallow sedimentary bay off Chile (SE Pacific; < 25 m water depth), and compared species-based to individual-based approaches for the assessment of abundance and energy use through allometric scaling. They found that energetic equivalence seemed to be apparent across the larger, but not the smaller, size classes. If the potentially unrepresentative data from the smallest size classes is discounted (e.g. Bett 2013, 2014; Laguionie Marchais et al. 2020), abundance has a scaling

exponent close to the MTE model (-0.75) (figure 1.4), i.e. consistent with the EER.

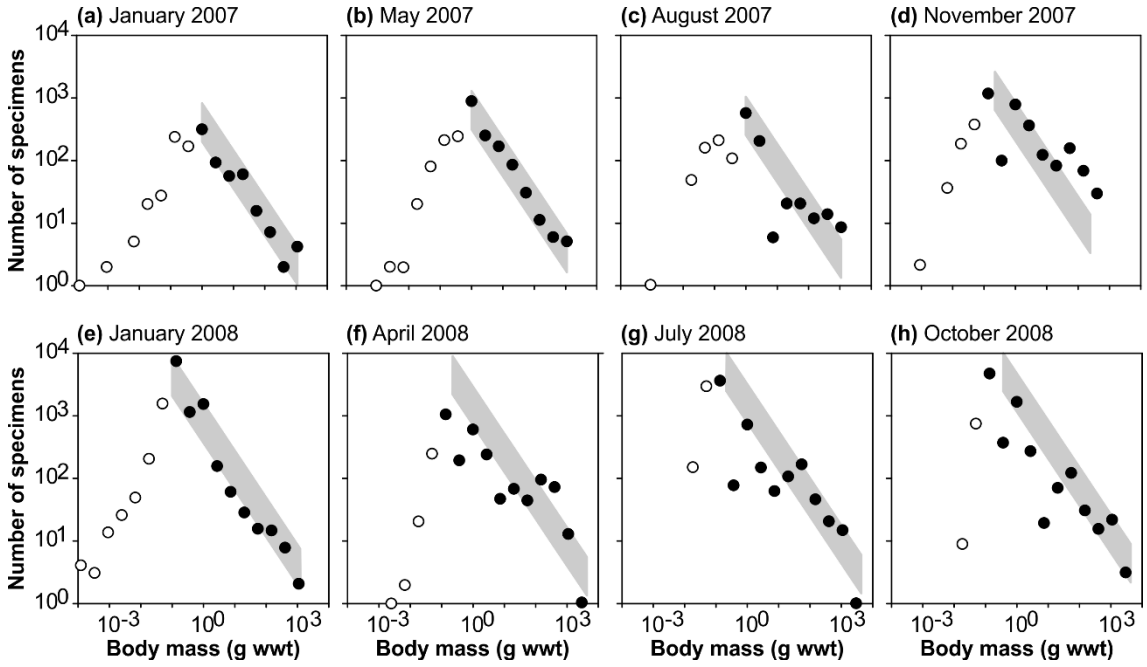

Figure 1.4. Abundance size spectra of shallow marine macro- to megabenthic assemblages in the SE Pacific. Re-drawn from Labra et al. (2015; authors' figure 4) where (a-h) were sampling months. Open symbols are presumed unrepresentative values, Shaded area is MTE model density (equation 1.2; -0.75 scaling exponent).

1.4 Ecological energetics of the benthos

The ocean can be divided into two zones: the shelf sea and the deep sea, as delimited by the 200 m water depth contour, typically marking the transition from continental shelf to the continental slope, and the change from euphotic to mesophotic realms (Lalli and Parsons 1997). With the exception of chemosynthetic ecosystems such as hydrothermal vents and seeps, the deep sea is typically a low temperature, resource-limited system, having no in situ primary production (McClain et al. 2012). Consequently, the deep-sea benthos relies on the flux of particulate organic carbon (POC) exported from the euphotic zone (Etter and Grassle 1992; Johnson et al. 2007); a flux that decreases rapidly with increasing water depth (Rowe 1971; Martin et al. 1987; Marsay et al. 2015).

Recently, Kelly-Gerreyn et al. (2014) modelled the body-size distribution of deep-sea benthic systems to investigate potential links with POC flux. They combined a number of allometric relationships to examine the size-class biomass distribution of meio- and macrobenthos from three locations (Faroe-Shetland Channel, Fladen Ground, Oman Margin) contrasted in terms of water depth (150 to 1660 m), in situ temperature (-1 to 13 °C), and POC flux to the seabed (10 to 40 g C m^{-2} yr^{-1}). Their results showed that the size-class abundance of these invertebrates, in the mass range 1 µg to 28 g wet weight, scaled approximately as $M^{-3/4}$, and their biomass as $M^{1/4}$, i.e. consistent with the simple MTE model. Subsequently, Laguionie Marchais et al. (2020) found that standing stocks of macrobenthos (polychaetes) at Station M in the deep NE Pacific, were also well predicted by the simple MTE model. The authors further demonstrated the value of considering the joint effects of temperature and resource supply on the body-size distribution of benthic assemblages. McClain et al. (2012) obtained similar results in their study compiling data on deep- and shallow-sea organisms globally. For the deep-sea environment, they concluded that chemical energy (i.e. POC flux) played a key role in establishing benthic assemblage structure, and that the effect of temperature was detectable in abundance and biomass data.

To date, testing the use of the simple MTE model with data on the deep-sea benthos has been limited to the meio- and macrobenthos because of a historical limitation on quantitative sampling. However, via recently developed

mass photographic survey by AUVs, it has become possible to generate high-quality, quantitative data on the deep-sea megabenthos (Morris et al. 2014, 2016; Durden et al. 2015a, 2016a; Simon-Llédo et al. 2019a), and those of shelf-sea environments (Thomson et al. 2017; Benoist et al. 2019a). In addition, Durden et al. (2019) recently tested resource uptake body-mass scaling in deep-sea megabenthos assemblages comprised of deposit feeders from two abyssal locations (Porcupine Abyssal Plain sustained observatory, NE Atlantic; Station M, NE Pacific). Their results indicated that ingestion rates in the body mass range 0.2 g to 4.2 kg were consistent (0.81 mass-scaling exponent) with the general metabolic scaling assumed in the MTE model (i.e. 0.75), as had been previously determined for shallow-water marine benthos by Cammen (1979) (0.74 mass-scaling exponent). These works indicate that in both shallow-water and deep-sea environments, the general concept of energetic equivalence (Damuth's rule; White et al. 2007) is at least plausible, and therefore that the simple MTE model may be of value in the quantitative study of the megabenthos.

1.5 Ph.D. thesis aims

The main objective of this thesis is to examine the body-size structure of marine benthic communities contrasted environmentally in terms of local temperature and resource supply, as assessed using seafloor imagery data. Following the MTE predictions that biological and ecological processes scale predictably with body size, the resulting data can be used to further assess the influence of local environmental parameters (e.g. resource supply) in shaping the body-size distribution of the marine benthos. This thesis does not test metabolic theory per se; it examines whether a singular size spectrum can provide a useful summary of the benthic system, and whether the application of the MTE numerical framework can provide a better understanding of the benthic system. Specifically, the aims of this thesis are the following:

1. Construction of quantitative abundance, biomass, and estimated respiration flux, body-size spectra for benthic assemblages.

Body-size spectral analysis of benthic assemblages, as assessed from seabed photography, involved methodological considerations in the generation

of reliable individual body-size data of megabenthos taxa (≥ 1 cm body size), starting from the photogrammetric extraction of individual body-size data to the standardisation of sampling effort across datasets (chapters 3 and 4). The use of mass photography by AUV to resolve ecologically significant information, at broad-scale, across multiple and mixed habitats is demonstrated with the study of benthic assemblages in the Celtic Sea (chapter 5.A).

At one study site, the body-size spectral framework was also extended to smaller benthos, where data of directly sampled macrobenthos (250 µm sieve mesh) was available. Across both faunal fractions studied (macro- and megabenthos), the quantitative aspect of the body-size spectra generated was examined, and the reliable portion of the spectra was used in the subsequent analyses (chapters 5.B and 6).

2. Evaluation of the reliable size spectra of the megabenthos: assessment of consistency in slope between environmentally contrasted assemblages, and of uniformity in intercept with corresponding data of smaller benthos (at one study site only), and subsequent comparison with the MTE predictions.

The shape of the body-size spectra, within and across the megabenthos and the macrobenthos faunal fractions studied, was compared with the MTE predictions for abundance, biomass, and respiration flux, scaling with body size. The following hypotheses were tested:

Hypothesis 1. At each study site, the abundance, biomass, and estimated respiration flux, body-size spectra of megabenthic assemblages follow the same MTE-consistent trends as meio- and macrobenthos, i.e. slopes of -3/4, 1/4, and 0, respectively, as previously observed (Bett 2014; Kelly-Gerreyn et al. 2014; Laguionie Marchais et al. 2020; chapters 5.B and 6).

Hypothesis 2. For the megabenthos, the elevation (intercept) of these slopes is consistent with corresponding data of smaller size fractions of the benthos (e.g. macrobenthos), i.e. the 'single trophic level' model holds across conventional faunal size fractions (chapter 6).

3. Investigation of the effect of environmental temperature and resource supply on the distribution of benthic assemblages: application of temperature-correction to standardize standing stock data, and comparison of the elevation between the slopes.

The effect of local environmental conditions, namely seafloor temperature and resource supply, on the body-size structure of benthic assemblages was investigated with respect to the MTE framework. The following hypothesis was tested:

Hypothesis 3. The elevation of these slopes is consistent with (controlled by) both environmental temperature and resource supply (e.g. POC flux), i.e. standing stocks are expected to decrease with increasing temperature and/or decreasing resource supply (chapter 7).

4. Use the MTE framework for modelling carbon stocks and flows at the seafloor, as illustrated using the deep-sea dataset from the NE Atlantic.

Benthic carbon stocks and flows were modelled assuming a uniform, MTE-based distribution of standing stocks throughout the whole body-size spectrum, i.e. from microbes to megabenthos (chapter 7). The resultant data were assessed to examine the potential contribution of benthic megafauna to biogeochemical cycling at the seafloor.

In this Ph.D. thesis, the hypotheses tested are that the body-size structure of benthic assemblages is primarily driven by the effects of local environmental parameters, namely seafloor temperature and resource supply, and that it follows the simple predictions of the MTE numerical framework, i.e. that standing stocks at the seafloor can be modelled with simple bio-energetic assumptions of individual metabolism.

Chapter 2

Study sites and environmental settings

2.1 Introduction

Ecological data for this Ph.D. thesis were obtained from four locations: two shelf-sea sites on the Celtic Shelf in (i) the Greater Haig Fras marine conservation zone (GHF-MCZ) and (ii) the UK-NERC Shelf-Sea Biogeochemistry (SSB) study areas, and two deep-sea sites at (iii) the Porcupine Abyssal Plain sustained observatory (PAP-SO), NE Atlantic, and in (iv) the Clarion-Clipperton Zone (CCZ), NE Pacific (figure 2.1). At all sites, photographic material of the epifaunal megabenthos was collected prior to the start of this Ph.D. project, and analysed by myself or with other researchers before and throughout the project. At the PAP-SO, trawl samples of the megabenthos were collected during fieldwork to provide baseline data for the establishment of a generalised volumetric method to estimate individual biomass of photographed organisms (chapter 4). Also, from the PAP-SO, directly sampled macrobenthos collected prior to this Ph.D. programme, were analysed for comparison with megabenthos data.

These study sites were selected to test an essential hypothesis of this Ph.D. thesis that local environmental settings, namely seafloor temperature and food supply, exert an influence on the body-size distribution of benthic communities. The present chapter gives a description of the seafloor environment at the four study sites, and a summary is provided in table 2.1.

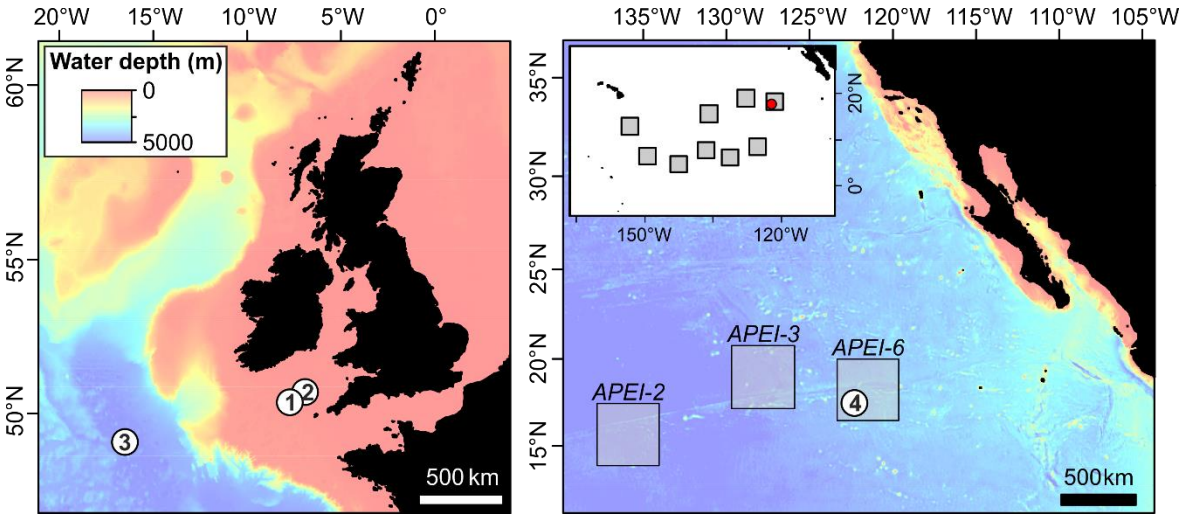

Figure 2.1. Study-site locations. Location of the benthic surveys in the NE Atlantic (left pane) with (1) Greater Haig Fras (GHF), (2) UK-NERC Shelf-Sea Biogeochemistry study area (SSB), (3) Porcupine Abyssal Plain sustained observatory (PAP-SO), and in the NE Pacific (right pane) with (4) Clarion-Clipperton Zone (CCZ) in the a APEI-6 (area of particular environmental importance).

Table 2.1. Environmental variables at the four study sites. Greater Haig Fras (GHF), UK-NERC Shelf Sea Biogeochemistry study area (SSB), Porcupine Abyssal Plain sustained observatory (PAP-SO), and Clarion-Clipperton Zone (CCZ) (figure 2.1). Mean annual seabed water temperature estimated from Locarcini et al. (2018). Mean annual particulate organic carbon (POC) flux to the seabed estimated from Lutz et al. (2007). Mean annual oxygen concentration at the seafloor estimated from Garcia et al. (2018).

	GHF	SSB	PAP-SO	CCZ
Site central sampling position	50.4° N	50.7° N	49.0° N	17.2° N
	7.7° W	9.9° W	16.5° W	122.6° W
Water depth (m)	107	104	4850	4150
Seabed water temperature (°C)	10	10	2.5	1.5
POC flux to seabed (g C m^{-2} yr^{-1})	12.5	12.5	2.5	0.25
Seabed water oxygen concentration (mL L^{-1})	6	6	6	3.5

2.2 Shelf-sea study sites in the Celtic Sea

The two shelf-sea sites are located in the Celtic Sea, a shallow embayment of the NE Atlantic Ocean extending between the margins of the European continental shelf and the coastal waters of the English Channel and Irish Sea (figure 2.1). The Celtic Shelf, together with the nearby North Sea and Irish Sea, has been studied considerably along with the development of fisheries and maritime industries during the 20th century. Greater Haig Fras is a marine conservation zone where a time-series study was initiated in 2012 to assess the potential use of autonomous underwater vehicles as a tool for monitoring UK MCZs (Ruhl 2013; Wynn et al. 2014), and repeated in 2015 and 2018 (Huvenne 2016, 2019) to evaluate temporal variation and repeatability of the field and analytical methods (Zelada Leon et al. 2020[1]). SSB is an area studied as part of the UK-NERC Shelf-Sea Biogeochemistry project that aims to improve European shelf-seas biogeochemical modelling of carbon and nutrients cycles over a range of spatial scales. Geographically close (i.e. c. 110 km apart), GHF and SSB share similar environmental conditions that are presented overleaf. Description of benthic megafauna and demersal fish communities at GHF and at SSB can be found in Benoist et al. (2019a)[2] and

[1] This work was submitted for publication as "Zelada Leon A, Huvenne VA, **Benoist NMA**. (2020). Assessment of the Repeatability of Automated Marine Habitat Mapping Approaches to Support the Monitoring of Marine Protected Areas. Remote Sensing 12(10), 1572. DOI: 10.3390/rs12101572". I did the initial annotation of the photographic data prior to the start of this Ph.D. thesis, and also in coordination with another researcher during this Ph.D. programme, but the analyses reported and the publication process formed part of the thesis.

[2] This work was published as "**Benoist NMA**, Morris KJ, Bett BJ, Durden JM, Huvenne VAI, Le Bas TP, Wynn RB, Ware SJ, Ruhl HA. 2019. Monitoring multiple biotopes in a marine conservation zone by autonomous underwater vehicle. Conservation Biology **33**(5), 1174-1186. DOI: 10.1111/cobi.13312". The publication and supplementary material are available in chapter 5 part A and in appendix A. I did the initial annotation of the photographic data prior to the start of this Ph.D. thesis, and , but the analyses reported and the publication process formed part of the thesis.

Thomson et al. (2017)[1], respectively. The Celtic Sea is generally exposed to a range of human pressures that include a number of maritime industries, such as fisheries for Norway lobster, cuttlefish, and king scallop (ICES 2008). Both GHF and SSB are moderately exposed to bottom trawling pressure (Thomson et al. 2017), GHF to a lesser extent.

On the Celtic Shelf, the main source of inflow water comes from the Atlantic Ocean, and water circulation is strongly influenced by the poleward-flowing slope current (ICES 2008). The Irish Shelf Front, to the south and west of Ireland, is the main oceanographic front in the region, and it marks the boundary between the shelf waters and the offshore North Atlantic waters, causing turbulence and promoting the resuspension of deep-water nutrients. Water currents in the Celtic Sea are dominated by semi-diurnal tidal activity, dissipating high flow energy towards the English Channel and Irish Sea (Sharples and Holligan 2006; Thomson et al. 2017). Topography and tidal amplitude on the shelf vary considerably, and in combination with attenuated wind and wave-induced mixing, are influential to strong thermal stratification during summer, between May and November, whereas during winter, in association with stronger winds and increased bed-stress level, the water column is well mixed (Brown et al 2003; Sharples and Holligan 2006; Thomson et al. 2017). Mean winter seabed temperatures typically range 9-10 °C, increasing to 11-16 °C in the summer months (Thomson et al. 2017).

The Celtic Shelf seafloor tends to decrease southwards in relief, exhibiting a low topographic gradient at both study sites (95-110 m water depth), and comprising multiple substratum types: rock, mobile sediments (mud, sand, coarser material), and mosaics of rock and sediments. In shelf seas, tidal stress largely affects the distribution of sediment types, with

[1] This work was published as "Thompson CEL, Silburn B, Williams ME, Hull T, Sivyer D, Amoudry LO, Widdicombe S, Ingels J, Carnovale G, McNeill CL, Hale R, Marchais CL, Hicks N, Smith HEK, Klar JK, Hiddink JG, Kowalik J, Kitidis V, Reynolds S, Woodward EMS, Tait K, Homoky WB, Kroger S, Bolam S, Godbold JA, Aldridge J, Mayor DJ, **Benoist NMA**, Bett BJ, Morris KJ, Parker ER, Ruhl HA, Statham PJ, Solan M. 2017. An approach for the identification of exemplar sites for scaling up targeted field observations of benthic biogeochemistry in heterogeneous environments. Biogeochemistry **135**(1-2), 1-34. DOI: 10.1007/s10533-017-0366-1". The publication is available in appendix B. I analysed the photographic data of the megabenthos in coordination with another researcher during this Ph.D. programme, and the analyses reported and the publication process formed part of the thesis.

coarser sediments associated with strong tidal currents, whereas finer grains are found in weaker tidal areas, generally depicting a north to south decreasing mean grain size gradient (Sharples and Holligan 2006). The dynamism of tidal activity and the occurrence of benthic storms in the Celtic Sea allow for reworking of these sediments, permitting the formation and movement of bed forms, in particular sand waves of varying magnitude. For example, see figure A.1-2 in appendix A where the wavelength varies between c. 50 cm in coarse sediments and c. 10 cm in sandy sediments at GHF. The SSB site was designated to be a representative UK-shelf area in terms of sediment coverage, comprising vast muddy and sandy grounds, with numerous occurrences of pebbles, cobbles, and boulders embedded in the sediments (Thomson et al. 2017). In addition to these typical sediment types, GHF encompasses what is recorded as the only substantial offshore area of granitic rocky reef in the Celtic Sea, supporting a wide range of sessile and mobile, iconic species (Barrio Froján et al. 2015; Benoist et al. 2019a). The European continental shelf sediments form a regionally important reservoir of carbon, with sediment total organic carbon content (TOC) observed to increase with decreasing grain size from 1.3% to 6.1% in sandy and muddy sediments, respectively (Diesing et al. 2017; Godbold et al. 2017).

Primary productivity is high in the Celtic Sea (Lutz et al. 2007; ICES 2008), which in addition to habitat heterogeneity, promotes megafauna standing stocks and diversity. Diatom-dominated phytoplankton blooms initiate in April and last between a few weeks to two months, and primary production strongly drops in summer when surface waters become nutrient poor (Thomson et al. 2017; Seguro et al. 2019). The breakdown of thermal stratification from November induces the formation of autumn blooms, intensifying the regional temporal dynamism of nutrient fluxes. Davis et al. (2019) recorded integrated values in particulate organic carbon (POC) ranging from 420 ± 64 mmol m^{-2} (± 95% confidence intervals, CI) in spring to 227 ± 23 mmol m^{-2} (± 95% CI) in autumn in the mixed bottom layer (as defined below the thermocline) (Davis et al. 2019). Annual seafloor POC flux averages 12.5 g C m^{-2} yr^{-1} (Lutz et al. 2007).

The amount of dissolved oxygen in seawater is associated to temperature-controlled solubility and respiration of organic carbon. Near-bed

waters in the Celtic Sea are well oxygenated (6 mL L^{-1} mean annual concentration at 100 m water depth) (Garcia et al. 2018). Still, low oxygen zones naturally occur during summer, arising from stratification and seafloor oxygen demand.

2.3 Deep-sea study sites

2.3.1 Porcupine Abyssal Plain, NE Atlantic

The Porcupine Abyssal Plain sustained observatory (PAP-SO) is a 30-year time-series site of international significance located in the subpolar NE Atlantic, between the European continental shelf and the Mid-Atlantic Ridge (figure 2.1) (Hartman et al. 2012). It is a remote location, isolated from the complexities of the adjacent continental slope and Mid-Atlantic Ridge. Scientific research at PAP-SO has focussed on the links between surface processes (physical and biogeochemical) and the supply of POC to the seafloor in shaping benthic communities with regards to biodiversity and ecosystem functioning. The remote seafloor at PAP-SO is little affected by anthropogenic activities, nonetheless litter has often been observed (collected during trawl surveys or seen on imagery; personal observation; Lampitt 2017b, c; Stinchcombe 2017; Hartman 2019; Ruhl 2013, 2019), and studies have shown an accumulation of microplastic particles in the sediments (van Cauwenberghe et al. 2013; see also Maximenko et al. 2019).

The PAP-SO site lies south the main stream of the North Atlantic Current, where the water flow is principally moving from west to east at a relatively weak velocity, and is affected by strong tidal activity (Lampitt et al. 2001). The seafloor at the level abyssal plain (4850 m mean water depth) exhibits modest topographic variation with the presence of small hills (< 100 m elevation) where sensors show there is a higher concentration of suspended organic matter in the water column, resulting in higher standing stocks and

species diversity (Durden et al. 2015a; Morris et al. 2016[1]). Water mixing is subject to inter-annual variability, causing variations in the organic material supplied to the seafloor (Lampitt et al. 2001). Mean annual seafloor temperature is 2.5 °C (Locarcini et al. 2018).

The abyssal seafloor is primarily composed of fine sediments (mud), and show patchy occurrences of overlaying hard substrata in the form of clinker (i.e. burnt coal) generally, and iceberg drop-stones, on the hills (Durden et al. 2015a). Benthic storms occasionally occur in the NE Atlantic but none has been recorded at the PAP-SO site (Lampitt et al. 2001).

Primary production and fluxes of organic matter produced in the overlaying surface water are subject to strong seasonal fluctuation, with the spring bloom occurring mid to late May because of rapid water column stratification (Rice et al. 1994; Bett et al. 2001; Hartman et al. 2010; Lampitt et al. 2001, 2010a, b). Hartman et al. (2010, 2012) have observed progressive warming of surface waters along with increasing stratification, leading to a decline in primary production. The abyssal seafloor is mesotrophic and subjected to high seasonal and inter-annual variation in the quantity and quality of POC flux from surface waters, with apparent POC flux maxima during summer (Lampitt et al. 2001, 2010a, b). Lampitt et al. (2010b) estimated daily POC flux at 3000 m water depth ranging between c. 2 mg C m^{-2} d^{-1} in winter and c. 12 mg C m^{-2} d^{-1} in summer. Annual seafloor POC flux averages 2.5 g C m^{-2} yr^{-1} (Lutz et al. 2007).

The PAP-SO site lies at the beginning of the global ocean conveyor belt, where at the higher latitudes warm surface waters cool down and sink to form well-oxygenated deep waters (6 mL L^{-1} mean annual concentration between 4500-5000 m water depth) (Garcia et al. 2018). Cooling of surface waters implies the upper column is under-saturated in CO_2, which promotes

[1] This work was published as "Morris KJ, Bett BJ, Durden JM, **Benoist NMA**, Huvenne VA, Jones DO, Robert K, Ichino MC, Wolff GA, Ruhl HA. 2016. Landscape-scale spatial heterogeneity in phytodetrital cover and megafauna biomass in the abyss links to modest topographic variation. Scientific Reports **6,** 34080. DOI: 10.1038/srep34080". The publication is available in appendix C. I did the initial annotation of the photographic data in coordination with other researchers prior to the start of this Ph.D. thesis, but the analyses reported represent the result of my own work during the Ph.D. programme.

continuous carbon storage and sink to the seafloor, making the PAP-SO site an important reservoir of carbon (Hartman et al. 2012).

2.3.2 Clarion-Clipperton Zone, NE Pacific

The Clarion-Clipperton Zone (CCZ) is a vast area located in the sub-equatorial NE Pacific, between Hawaii and Mexico, where major geological fractures sculpt the abyssal seafloor within a large east-west-oriented strip delimited to the north and to the south by the Clarion and the Clipperton Fracture Zones. The CCZ seafloor has been the object of scientific and commercial exploration since the 1960s. Targeted for deep-sea mining of polymetallic nodules, a baseline survey was conducted in 2015 to assess benthic habitats and their associated biodiversity (Jones 2015; Ardron et al. 2019; Simon-Lledó et al. 2019a[1], b). The study area was located in the APEI-6 (area of particular environmental importance) (Wedding et al. 2013; Lodge et al. 2014), in the north-easternmost part of the CCZ (figure 2.1), where the abyssal seafloor exhibits a range of north-south ridges and troughs (4000-4300 m water depth), and a chain of seamounts to the south. Anthropogenic disturbance is not suspected in the APEI-6; though test mining has been conducted in other areas of the CCZ (Jones et al. 2017).

Surface waters in the CCZ area are dominated by the westward-flowing Northern Equatorial Current at the north, and by the eastward-flowing Equatorial Counter Current at the south, and are subject to seasonal variability and wind-induced eddies. Bottom waters (> 4000 m water depth) in the Pacific Ocean are formed by the Lower Circumpolar Water formed in the northern North Atlantic, and are affected in the CCZ region by hydrodynamic energy of the near-bottom water layer, which is regulated by global water circulation and tidal processes (Radziejewska 2014). Currents are typically slow, preventing shear bed stress, and limiting sediment resuspension. Nonetheless, studies have shown that the CCZ seafloor is periodically

[1] This work was published as "Simon-Lledó E, Bett BJ, Huvenne VAI, Schoening T, **Benoist NMA**, Jeffreys RM, Durden JM, Jones DOB. 2019. Megafaunal variation in the abyssal landscape of the Clarion-Clipperton Zone. Progress in Oceanography **170**, 119-33. DOI: 10.1016/j.pocean.2018.11.003". The publication is available in appendix D. I did the initial annotation of the photographic data in coordination with a fellow researcher during the course of this Ph.D. programme, but the analyses reported represent the result of my own work during the Ph.D.

disturbed by benthic storms (Radziejewska 2014), which increases spatial and temporal variability of the seafloor environment. Mean annual deep-seafloor temperature is 1.5 °C and shows little variation (Radziejewska 2014; Locarcini et al. 2018).

The seafloor, slightly deepening westward, is primarily composed of fine sediments (mud dominated by very fine silt and clay particles) of biogenic origin (siliceous ooze), and it is exposed to low sedimentation rate of surface-produced organic matter (Radziejewska 2014). Nevertheless, the frequent occurrence of polymetallic (ferromanganese) nodules, between 0.5-20 cm in diameter, overlaying, embedded, or completely buried in the seabed, provides suitable habitat for obligate hard-substrata species (Radziejewska 2014; Simon-Lledó et al. 2019a, b). In the APEI-6, total organic carbon was estimated c. 0.44% of the surface sediments (0-1 cm) (Simon-Lledó et al. 2019a).

Over the entire CCZ surface area, it has been shown that primary productivity tends to decrease from east to west and from south to north. Surface primary production is seasonal and generally lower than at PAP. With only 1-7% of organic matter reaching the seafloor, the CCZ abyss is considered oligotrophic (annual POC flux c. 0.25 g C m^{-2} yr^{-1}) (Lutz et al. 2007). However, ephemeral events, such as sinking of large animal remains, have been documented and reported as important sources of local food supply enrichment (see e.g. Amon et al. 2017c).

Because of microbial respiration and weak water mixing, a pronounced oxygen minimum zone covers the depth range of 300-500 m in the CCZ, measured between 120-2500 m in the eastern part; nonetheless, it does not extend to the seafloor (Radziejewska 2014). Sitting at the end of the global ocean conveyor belt, deep waters at this site are depleted in oxygen due to metabolic processes (3.5-3.7 mL L^{-1} mean annual concentration at 4000-4500 m water depth) (Garcia et al. 2018).

Chapter 3

Materials and methods

3.1 Introduction

The majority of data analysed in this Ph.D. thesis relate to the epifaunal megabenthos assemblages from the four study sites described in chapter 2, as obtained from seafloor image analysis. In this project, the megabenthos was represented by all the organisms observed on these in situ images, and comprised specimens of centimetre to meter-length scale in body size, in the form of individual entities (e.g. Arthropoda, Echinodermata, Mollusca, Fish), and of colonial, encrusting, or morphologically plastic, forms (e.g. Ascidiacea, Bryozoa, Cnidaria, Porifera) (e.g. Bett 2019). Additionally, infaunal macrobenthos assemblages from the PAP site were examined. The macrobenthos consisted characteristically of these invertebrates collected from sediments and retained on a 250-µm-mesh sieve (e.g. Amphipoda, Copepoda [Harpacticoida], Isopoda, Polychaeta) (Narayanaswamy et al. 2016). In the present contribution, all nematodes retained on the sieve were also included in the macrobenthos samples.

Data collection of the two faunal fractions assessed, from field survey to sample processing and analysis, are described in sections 3.2 and 3.3. The primary variables assessed are abundance (numerical density), individual biomass, and estimated population respiration flux, allowing the production of body-size spectra for each variable. For megafauna specimens, individual biomass was estimated from photographic analysis using two approaches: a traditional method based on species-specific allometric considerations, and a new generalised volumetric method (GVM) developed during this Ph.D. programme, based on geometric considerations. The GVM was also employed to estimate individual biomass of macrobenthos taxa. Both methods are succinctly described in section 3.4, and are fully explained in chapter 4. The construction of individual-based body-size spectra is detailed in section 3.5. Analytical methods applied to compare quantitatively the body-size

distributions of environmentally contrasted benthic assemblages against the metabolic theory of ecology (MTE) are developed in section 3.6. Section 3.7 briefly presents the approach employed to test the practical use of MTE at the assemblage level, in a simple assessment of seafloor carbon stocks and flows modelling. Data standardization and limitations are presented in section 3.8.

3.2 Data collection for epifaunal megabenthos assemblages

3.2.1 AUV photographic field survey

Landscape-scale photographic surveys of the seabed were conducted with the AUV *Autosub6000* at all sites except at the SSB study area where the AUV *Autosub3* was employed (figure 3.1). For each survey, the AUV was set to dive at a target altitude of 2.5-3.2 m above the seabed, and at a target vehicle speed of 1.2-1.4 m s^{-1}. The two AUVs were fitted with identical photographic systems; the camera used (Point Grey Research Grasshopper 2, 5.0 MP, colour) was oriented vertically beneath the AUV, rendering a typical imaged seabed area of 0.9-2.4 m^2. Pictures were recorded every 0.85-1.00 s using a National Oceanography Centre xenon strobe unit (11 J), providing continuous coverage of the seabed at all sites. General field methodology at each study site is presented hereafter, and summary metadata are provided in table 3.1 together with corresponding references to cruise reports for additional technical details.

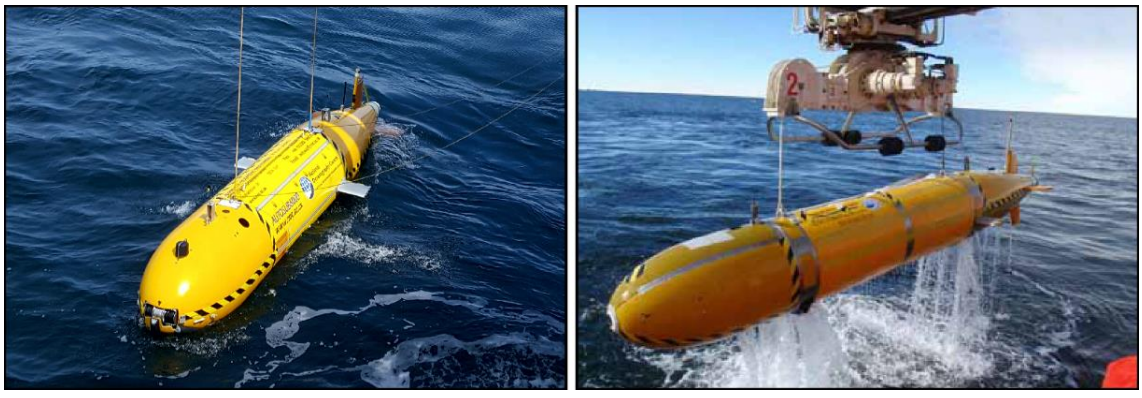

Figure 3.1. AUVs employed during the photographic surveys at the four study sites. *Autosub6000* (left) and *Autosub3* (right).

Table 3.1. Summary metadata of the AUV photographic surveys of the epifaunal megabenthos at the four study sites. Greater Haig Fras (GHF-1, 2012; GHF-2, 2015), UK-NERC Shelf-Sea Biogeochemistry study area (SSB), Porcupine Abyssal Plain (PAP), Clarion-Clipperton Zone (CCZ) (see figure 2.1 in chapter 2, and figures 3.2-3.5 in the section below). The number of image units refers to the number of seafloor images analysed in each dataset with corresponding area surveyed. Images were analysed in the form of tiles or as individual image (see details in section 3.2.2).

	GHF-1	**GHF-2**	**SSB**	**PAP**	**CCZ**
Cruise number	D377	JC124	DY034	D378	JC120
AUV mission number	M58	M87	M466/467/468	M53/54/55/56	M79/81/83
Cruise report	Ruhl (2013)	Huvenne (2016)	Ruhl (2016)	Ruhl (2013)	Jones (2015)
Date of sampling	25-26 Jul. 2012	12 Aug. 2015	20, 24, 26 Aug. 2015	17, 19, 20, 21 Jul. 2012	01, 07, 10 May 2015
Site central position	50° 22.0' N	50° 22.0' N	50° 43.0' N	48° 56.0' N	17° 38.0' N
	007° 42.1' W	007° 42.1' W	006° 54.0' W	016° 34.0' W	123° 51.5' W
AUV target altitude (m)	3.2	3.2	2.5	3.2	3.2
AUV target speed (m s^{-1})	1.2	1.2	1.4	1.2	1.2
Image capture rate (s^{-1})	0.86	0.86	1.0	0.86	0.85
Typical image unit area (m^2)	7.29	7.26	0.93	13.18	1.71
Number of image units	2637 tiles	708 tiles	4160 single images	6472 tiles	10,052 single images
	(5-image units)	(5-image units)		(10-image units)	
Total area surveyed (m^2)	19,223	5,142	3,876	85,294	18,582
Seafloor pixel resolution (mm)	0.59	0.50	0.42	0.49	0.59

Greater Haig Fras. GHF-MCZ (107 m mean water depth) was selected to conduct a time-series investigation of the benthos using AUV technology, on the merit that this study site comprises multiple habitat types ranging from soft sediments to hard substrata. Photographic material was obtained from the RRS *Discovery* cruise D378 baseline survey in 2012 (GHF-1) (Ruhl 2013), and from the RRS *James Cook* cruise JC124 repeat survey in 2015 (GHF-2) (Huvenne 2016). Both photographic surveys were carried out as four north-south transect lines, and a crossing line that targeted a rock outcrop of slightly elevated terrain (figure 3.2). The two missions took place during summer and followed similar field procedures; however, the time of AUV operation marks the main difference between the two surveys (night time in 2012, day time in 2015).

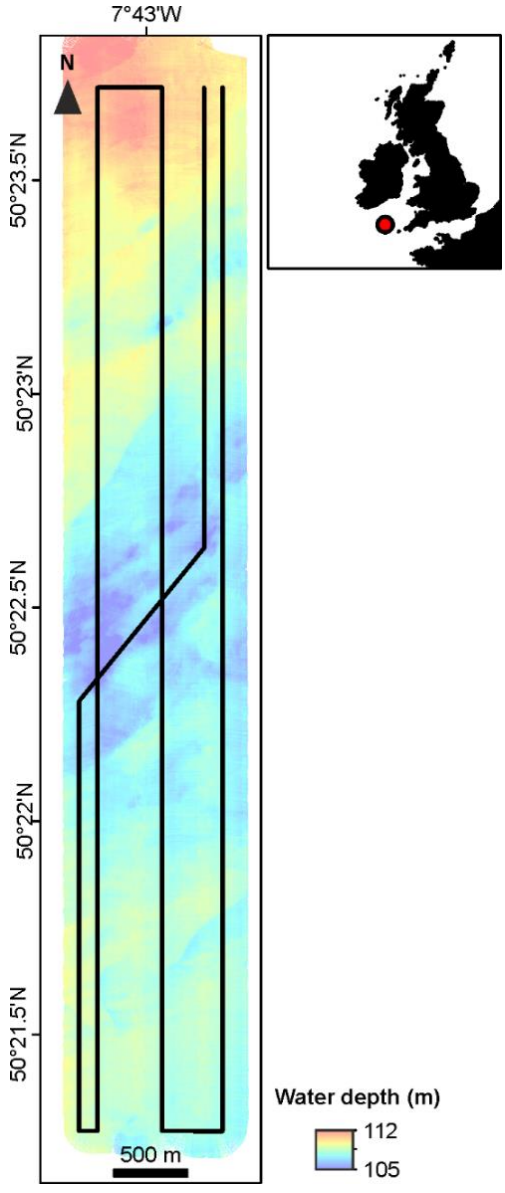

Figure 3.2. AUV photographic survey at the Greater Haig Fras marine conservation zone. GHF-MCZ (red circle) is shown in relation to the UK, Ireland, and France on the top right map. Photographic transects (black lines) surveyed in 2012 and 2015 are overlaid on bathymetric map obtained from multibeam swath survey during RRS *Discovery* cruise D378 (Ruhl 2013).

SSB study area. The UK-NERC SSB programme consisted of several cruises spanning from 2014 to 2015 (Thomson et al. 2017). For this contribution, photographic material was acquired at the SSB sites (104 m mean water depth) during the RRS *Discovery* cruise DY034 in summer 2015 (Ruhl 2016). The photographic survey consisted of three AUV deployments targeting three main seafloor habitat types: site G, sandy sediments; site H, muddy sediments with a component of hard substratum type; site I, muddy sediments (figure 3.3). Each survey occurred over night, and was designed to contain a minimum of six transect lines at 150 m (site I) and 250 m (sites G and H) line spacing.

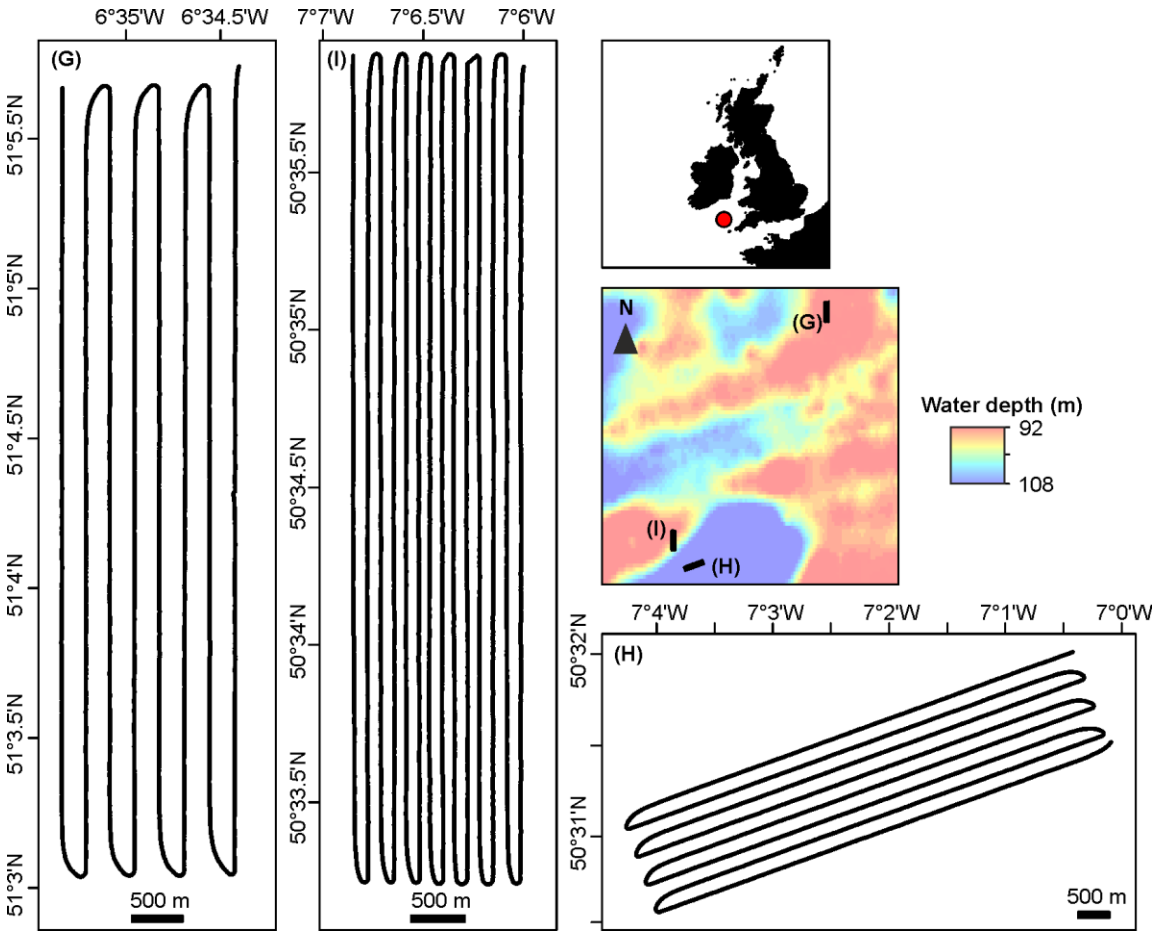

Figure 3.3. AUV photographic survey at the UK-NERC Shelf-Sea Biogeochemistry study area. SSB (red circle) is shown in relation to the UK, Ireland, and France on the top right map. The locations of sites G, H, and I, are shown on a bathymetric map obtained from GEBCO data.

Porcupine Abyssal Plain sustained observatory. The photographic survey at PAP-SO (4850 m mean water depth) occurred during the RRS *Discovery* cruise D378 in summer 2012 (Ruhl 2013), and it comprised four AUV deployments on a small hill (c. 250 m altitude) and its surrounding flat abyssal seabed (figure 3.4). The deployments were designed to include fine-scale surveys (100 m line spacing within a 1-km^2 box) at the base of the hill and in the plain areas, and broad-scale surveys (1000 m line spacing in a c. 100-km^2 region) in the plain area.

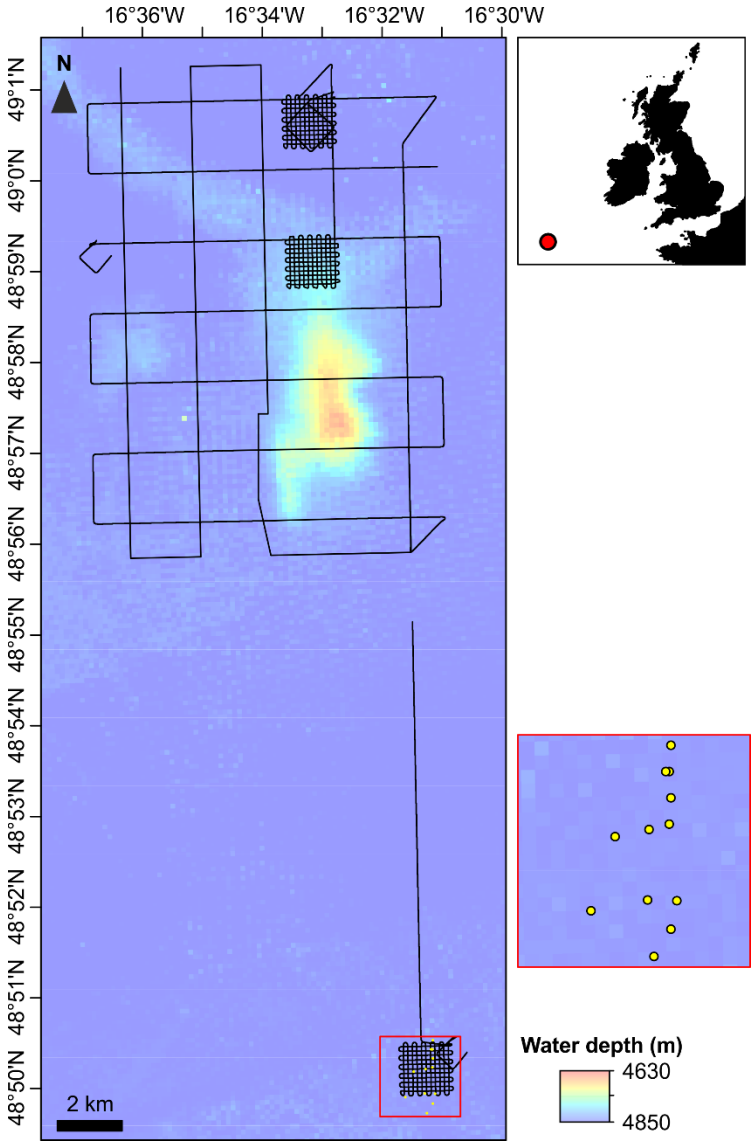

Figure 3.4. AUV photographic survey and Megacorer survey at the Porcupine Abyssal Plain sustained observatory. PAP-SO (red circle) is shown in relation to the UK, Ireland, and France on the top right map. Broad-scale and fine-scale AUV photographic transects (black lines) and macrobenthos samples (yellow dots in red box in the SE corner) are overlaid on a bathymetric map obtained from GEBCO data. No seafloor photograph was possible on the high ground of the hill resulting in breaks in the survey lines.

Clarion-Clipperton Zone. Baseline ecological mapping at the CCZ study site (4150 m mean water depth) was undertaken during the RRS *James Cook* cruise JC120 in spring 2015 (Jones 2015). To capture the seafloor geological variation at the CCZ, a set of three stratified random surveys were designed to include the top of a ridge (4000-4100 m water depth band), the base of a trough (4200-4300 m), and the plain area (4100-4200 m). The AUV collected seafloor images across forty 1.8-km-long transects in the plain and in the ridge locations, and twenty 900-m-long transects in the trough area (figure 3.5).

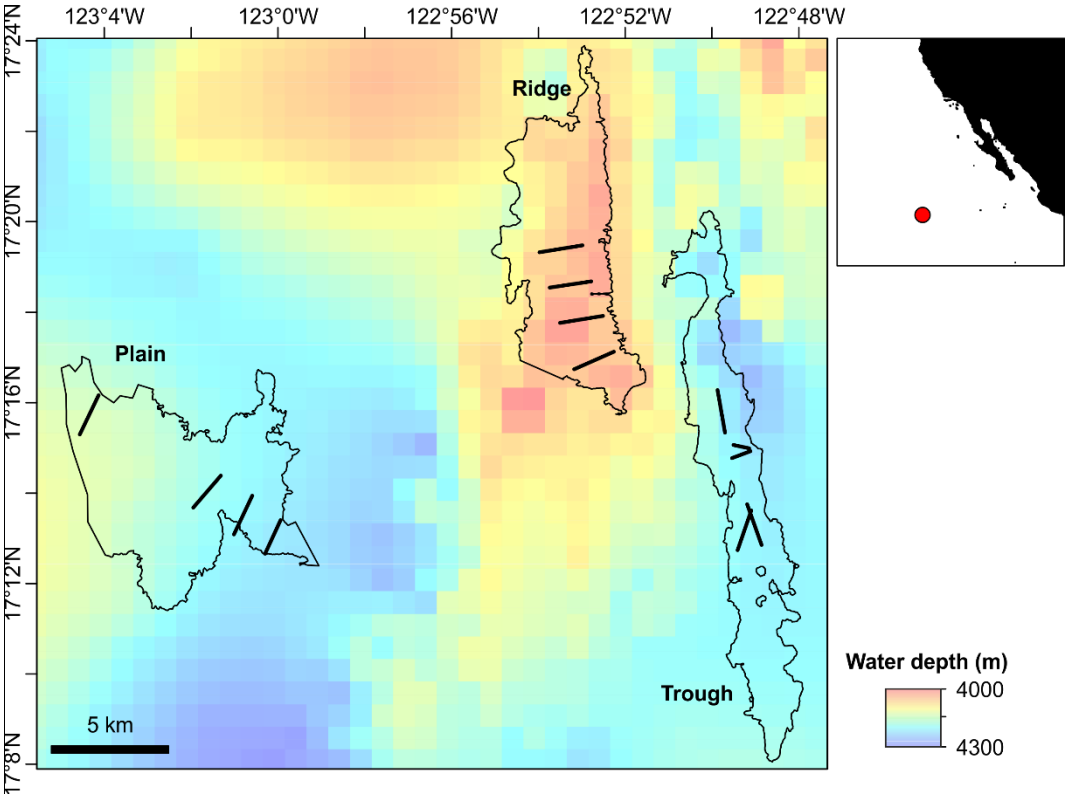

Figure 3.5. AUV photographic survey at the Clarion-Clipperton Zone. Study area in the CCZ (red circle) is shown in relation to Mexico on the top right map. Photographic transects (black lines) in each stratum (plain, ridge, trough) are overlaid on a bathymetric map obtained from GEBCO data. Only those transects analysed in the present study are displayed.

3.2.2 Image processing

Individual images were processed to improve visual quality (non-uniform illumination and colour correction), and georeferenced from vehicle navigation (Morris et al. 2014). For GHF and PAP, consecutive images were mosaicked into five- and ten-image units, respectively, subsequently referred to as 'tiles' (Morris et al. 2014). Tiling was undertaken to remove overlapped areas of seabed from consecutive photographs, and to reduce the data management overhead by decreasing the number of images analysed, and the size of the resultant data matrices. For CCZ, images were not mosaicked into tiles, hence every second image was discounted to avoid overlap between consecutive images, and to prevent double counting. Given the AUV's operational altitude and speed at SSB, there was no overlap between images, thus individual images were analysed. This yielded image units (individual photographs or tiles) of varying seabed area (0.90-13.00 m^2; table 3.1). Only photographs taken between 1.9 and 4.1 m altitude were included in the analysis in order to ensure consistency in specimen detection and identification. Images, or tiles, located at the corners of the transect lines (i.e. where the AUV turned to start a new line) were discounted from the analysis.

3.2.3 Image analysis

Sample photographic unit. Photographic data from the four study sites were analysed to extract ecologically relevant data of the epifaunal megabenthos (taxonomic identification, individual body-size measurement) within their local environment. Single-photograph-, or tile-data generation, referred to as annotation, was undertaken using Image-Pro Plus (V7.0, Media Cybernetics Inc.) (GHF, Benoist et al. 2019a; appendix A; SSB, Thomson et al. 2017; appendix B; PAP, Morris et al. 2014; appendix C), or the web-platform BiigleDias (V2.0, Langenkämper et al. 2017) (CCZ, Simon-Lledó et al. 2019a; appendix D). Photographic sampling units were annotated in random order to avoid potential spatial and/or temporal bias in the resultant data (Durden et al. 2016b).

Seabed assessment. Seabed photographs were categorised into habitat categories on the basis of substratum type (shelf-sea sites) and terrain geomorphology (deep-sea sites). At GHF and SSB, seabed was visually

classified into hard substratum (bedrock, boulder, cobble), coarse sediment (sand with shells, pebbles, granules), sand, and mud (very fine sediments with evident burrows and animal markings) (Thomson et al. 2017; Benoist et al. 2019a). Depending upon coverage of hard substratum type (i.e. 0-10% absent, 10-50% minority area, 50% majority area) on an individual image (SSB), or a tile (GHF), photographic units were then grouped into sedimentary (i.e. mud, sand, and/or coarse), intermediate (i.e. hard minority), or hard (i.e. hard majority) habitats. At PAP, small hills (< 100 m elevation) were separated from the surrounding level abyssal plain (c. 4850 m water depth) (Morris et al. 2016). At CCZ, submarine topography was divided into flat abyssal plain (4100-4200 m water depth), ridge (< 4100 m water depth), and trough (> 4200 m water depth) (Simon-Lledó et al. 2019a).

Faunal assessment. All megabenthos data reported in the thesis derive from either physical samples from the seafloor, or from AUV photographs taken within c. 2.5-3.2 m of the seafloor, consequently all data are regarded to represent the benthic system (endobenthos, epibenthos, suprabenthos, and hyperbenthos). Epibenthic invertebrate megafauna specimens and demersal fish (≥ 1 cm body size) were counted, measured (as presented in section 3.4, and fully described in chapter 4), and identified to the lowest taxonomic or morphotype unit possible (species/species groups/higher taxa) (e.g. see Althaus et al. 2015; appendices E and F). In the case of colonial and encrusting organisms, individual colonies or patches were measured. Solitary tubicolous polychaetes, bivalves, and gastropods were observed on images but excluded from the analyses to avoid inclusion of empty tubes/shells. At PAP-SO, xenophyophores ('giant' protozoan Foraminifera) (e.g. Kamenskaya et al. 2015, 2016; Gooday et al. 2017a, b) and demersal fish fauna were observed, but were not quantified in this project (see Milligan et al.'s (2016) study of the spatial distribution of abyssal fish assemblages at PAP-SO). At the CCZ study site, xenophyophores dominated the megabenthos assemblages in terms of numerical abundance (Simon-Lledó et al. 2019a) and were included in this project. Nonetheless, as a result of the difficulty in estimating the biomass of these taxa, and in simply recognizing living specimens (Levin and Gooday 1992; Hughes and Gooday 2004; Gooday et al. 2018), the subsequent biomass assessment of xenophyophores remains at an exploratory stage (see

section 3.4 and chapter 6). Where specimens could not be assigned to a taxonomic unit or morphotype, they were recorded as indeterminate (< 2% total specimens) and excluded from subsequent analyses.

3.3 Data collection for infaunal macrobenthos assemblages

3.3.1 Multi-corer field survey

Macrobenthos samples were collected from the 'PAP Central coring area' (500 m radius of nominal centre point, 48° 50.22' N 016° 31.27' W; 4850 m mean water depth) (figure 3.4), using a Bowers and Connelly Megacorer (figure 3.6), during the FS *Meteor* cruise ME108 in 2014 (Lampitt 2017b), and during the RRS *Discovery* cruise DY032 in 2015 (Lampitt 2017c). In total, twelve samples were collected, with three to seven core tubes (10-cm internal diameter) per sample (figure 3.4; table 3.2). Core samples were processed for preservation on board of the vessels following standard procedures (Lampitt 2017b, c). Briefly, cores were extruded and sliced into five layers (0-1, 1-3, 3-5, 5-10, 10-15-cm sediment horizons) and placed in UN certified bottles. Before slicing, the supernatant water at the top of the core was siphoned onto a 250-µm-mesh sieve, and transferred into the first sediment horizon bottle. Sediment samples were fixed in 4% buffered formaldehyde seawater solution for later analysis. Only the first top three sediment layers (i.e. 0-1, 1-3, 3-5 cm) were analysed in this Ph.D. thesis, corresponding to 0.503 m^2 seabed area sampled in total.

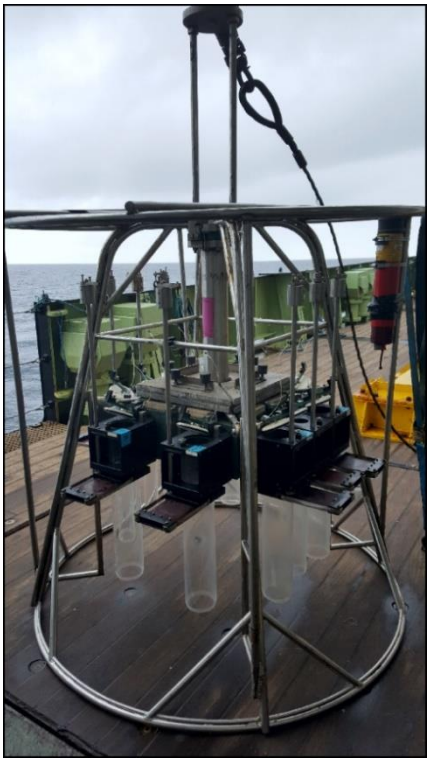

Figure 3.6. Bowers and Connelly Megacorer employed during the multi-corer survey at the 'PAP Central coring area'.

Table 3.2. Summary metadata of the Megacorer surveys of the infaunal macrobenthos at PAP-SO. Cruise and station number (no.), sampling date and location, and number of core tubes for each sample collected. Only 6/7 core tubes were gathered from the ME108-773 3-5-cm horizon layers. See figure 3.4 for the corresponding map.

Cruise no.	Station no.	Date of sampling	Latitude	Longitude	No. core tubes
ME108	745	12 Jul. 2014	48° 50.08' N	016° 31.15' W	6
ME108	746	12 Jul. 2014	48° 50.06' N	016° 31.15' W	6
ME108	752	13 Jul. 2014	48° 50.07' N	016° 31.16' W	7
ME108	758	14 Jul. 2014	48° 50.01' N	016° 31.15' W	7
ME108	773	16 Jul. 2014	48° 50.05' N	016° 31.16' W	7
ME108	805	19 Jul. 2014	48° 50.07' N	016° 31.18' W	6
DY032	16	25 June 2015	48° 50.17' N	016° 31.61' W	3
DY032	17	25 June 2015	48° 50.48' N	016° 31.28' W	3
DY032	22	26 June 2015	48° 50.21' N	016° 31.29' W	4
DY032	23	26 June 2015	48° 50.45' N	016° 31.47' W	3
DY032	61	29 June 2015	48° 50.21' N	016° 31.12' W	6
DY032	71	29 June 2015	48° 50.00' N	016° 31.25' W	6

3.3.2 Faunal sediment sample processing

All sediment core samples (i.e. across the two cruises and all deployments) were pooled together by horizon layer prior to sieve-based sorting on a 250-µm-mesh sieve in laboratory, and preservation in ethanol. All macrobenthos taxa retained on the sieve were counted and identified to class level under a stereomicroscope. All nematodes retained on the sieve were included in this analysis as part of the macrobenthos samples.

3.3.3 Macrobenthos sample analysis

Macrobenthos samples were analysed to generate individual body-mass data. Each specimen was observed using a Leica Mz7.5 stereomicroscope (Meyer Instruments) (magnification range from 6.3 to 50, providing adequate field width to comprise the entire specimen), photographed using a Nikon Coolpix 4500 digital camera, and sketched and measured (as detailed in section 3.4) using a camera lucida (figure 3.7).

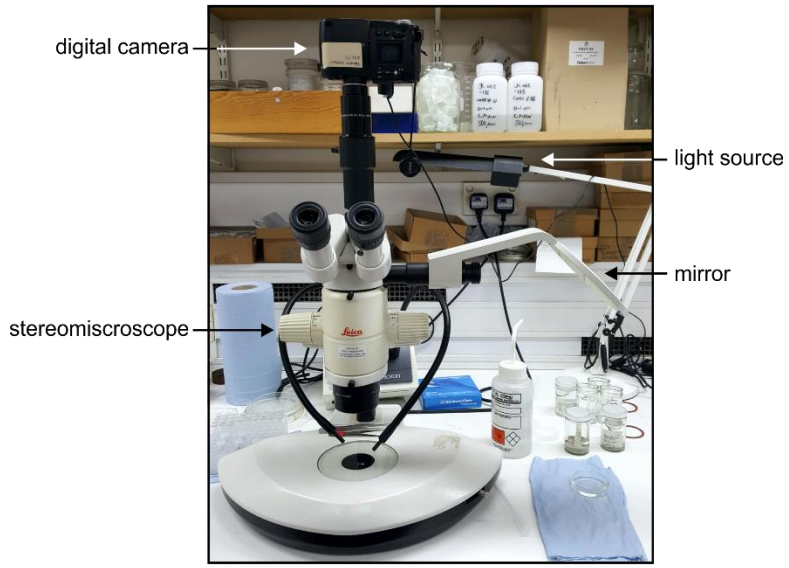

Figure 3.7. Stereomicroscope with camera lucida used to analyse macrobenthos samples. Individual macrobenthic specimens (including nematodes retained on a 250-µm-mesh sieve) were observed using a stereomicroscope, photographed using a digital camera, and sketched and measured using a camera lucida.

3.4 Individual biomass estimation

For the megafauna photographic samples, two approaches were employed for generating the primary variable, i.e. individual body mass, assessed in this Ph.D. thesis. Both procedures, fully described in chapter 4, required the measurement of one or two body dimensions per specimen. At GHF and at PAP, a traditional method based on species-specific allometric considerations was employed. A single standard linear dimension (SL in mm) was measured for each individual, and where possible, specimen body-size measurements were converted to estimated gram wet weight biomass (M_E in g wwt) via existing length-weight relationships (LWRs) (as detailed in section 4.2.3; equation 4.1) (GHF: Arnaud and Do-Chi 1977; Coull et al. 1989; Merella et al 1997; Richardson et al. 2000; Robinson et al. 2010; Silva et al. 2013; appendix A; PAP: Durden et al. 2016a). At SSB and at CCZ, a new generalised volumetric method (GVM) (Benoist et al. 2019b) developed during this Ph.D. programme, based on geometric considerations, was employed. Two dimensions were measured for each individual. The dimensions determined, equivalent cylindrical diameter (ECD in mm) and equivalent cylindrical length (ECL in mm), were representative of a cylinder of equivalent volume, translated to estimated biovolume (V_E in mL) using the equation of a cylinder (equation 4.3), and converted to gram wet weight biomass (M_E in g wwt) assuming a tissue volumetric density of 1.056 (as detailed in section 4.3.2).

For the macrobenthos at PAP, and for the xenophyophores at CCZ, the GVM was also employed. At CCZ, a subset of the fauna (metazoan and protozoan) was re-measured to produce ECD and ECL, and those measurements were then extrapolated to the rest of the specimens (as detailed in chapter 6 section 6.2.3.1; equation 6.1). Macrobenthic polychaete taxa collected in sediment cores are often damaged (incomplete) during the subsequent sample processing (i.e. sieving). For these specimens, ECL was estimated using the regression equation between ECL and ECD as obtained from the measurement of intact specimens (see details in section 6.2.3.2; equation 6.2a). As mentioned previously, it is practically impossible to estimate the biomass of xenophyophore specimens from photographic assessment alone (Hughes and Gooday 2004). Nonetheless, Levin and Gooday

(1992) and Gooday et al. (2018) estimated the biomass (i.e. protoplasm) of xenophyophores as little as 0.01-5% of their body size. In this contribution, the body size of individual xenophyophores was estimated using the GVM, with subsequent corrections for deriving body size into protoplasmic biomass (as detailed in section 6.2.3.3).

3.5 Construction of body-size spectra

An individual-based approach (White et al. 2007), rather than species-based using mean individual size, was employed in this Ph.D. thesis to assess the body-size structure of benthic assemblages. This permitted an assessment of the different assemblages at the organism level without averaging data by taxon, which could potentially mask the influence of rare, large, individuals in the observed size-structure trend, at the community level.

Individual-based body-size spectra are created by plotting the measurement of an ecological variable (e.g. density, biomass, respiration flux) on the y-axis against discrete body-size classes on the x-axis. In this analysis, spectra were constructed using $\sqrt{2}$ geometric size classes, where each class is c. 1.41 the biomass of the class below/above. This yielded 29 classes ranging from 0.5 µg to 9.7 mg for macrofauna data, and 44 classes ranging from 1.2 mg to 3.6 kg for megafauna data (figure 3.8; appendix G). One exceptionally large isopod was recovered on top of a core at station DY032-023, and retained in this analysis for illustration purpose. Its body mass was estimated at 0.12 g, thus entering the megafauna body-size spectrum range.

Each specimen was then assigned a body-size class, and the total abundance (N_i in number of individuals, ind.), estimated biomass (W_i in g wwt), and estimated respiration flux (B_i in mg C d^{-1}; see below), per size class, were standardized to seabed area (m^2). Each variable was then used to produce abundance- (N in number of individuals m^{-2}), biomass- (W in g wwt m^{-2}), and estimated-respiration-flux (B in mg C m^{-2} d^{-1}) body-size spectra.

In chapters 5 and 6, size-class respiration flux (B_i) was calculated from individual metabolic rate (I_i) using Hemmingsen's (1960) equation for standard metabolic rate of poikilotherms at 20 °C (equation 3.1), with a site-specific temperature-correction (i.e. GHF and SSB, 10 °C; PAP, 2.5 °C; CCZ, 1.5 °C) (Gillooly et al. 2001), and multiplied by size-class abundance (N_i):

$$I_i = 0.14\, M_i^{3/4} \qquad \text{(equation 3.1)}$$

where I_i is in watt, and M_i is body mass in kilogram. As mentioned in chapter 1 section 1.2, there are debates around the scaling value of individual metabolic rate with body mass (e.g. see West and Brown 2005 and van der Meer 2006). Nonetheless, a considerable amount of empirical evidence show that individual metabolic typically scale with 3/4 power of body mass, as Brey (2010) demonstrated using almost 23,000 datasets of aquatic metazoans. For carbon stocks and flows assessment in chapter 7, size-class respiration flux was calculated using equation 3.1, testing a range of normalisation constants that were found in the literature (Brey 2010; McClain et al. 2012; Laguionie Marchais et al. 2020), in order to assess the model sensitivity (as detailed in section 7.2.2).

Where applicable, wet weight biomass was converted to carbon (C) units using the conversion factors for dry/wet mass (0.2152), and for carbon/dry mass (0.3587) provided by Brey et al. (2010). Similarly, where I_i was estimated in watts (equation 3.1), it was then converted to mg C d^{-1} units using the conversion factors for watt/joule d^{-1} (86400), and for joule/mg C (40.6) provided by Brey et al. (2010). The dependant variables (N, W, B) and the independent variable (M) are typically illustrated on a logarithmic scale, allowing better visualisation of their inter-relationships across the range of body sizes encountered, spanning from four (GHF-1) to nine (PAP-SO) orders of magnitude (figure 3.8).

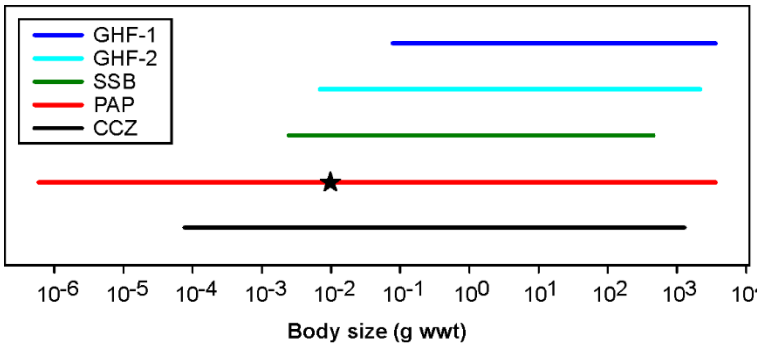

Figure 3.8. Graphical representation of the body-size ranges assessed at each study site. Greater Haig Fras (GHF-1, 2012; GHF-2, 2015), UK-NERC Shelf-Sea Biogeochemistry study area (SSB), Porcupine Abyssal Plain (PAP), Clarion-Clipperton Zone (CCZ). The star denotes the end of the macrofauna spectrum and the start of the megafauna spectrum at PAP.

There are two ways of reading a body-size spectrum. Horizontally, it depicts the range of body sizes comprising the faunal assemblage studied, where the smallest and the largest body sizes are likely to be determined by the sampling method, and the sampling extent, respectively (see next section). Vertically, the spectrum shows the intensity response of the variable assessed (e.g. abundance, biomass, respiration flux), and how the variable varies with body size. On the abundance spectrum, the location of the peak is thought to be sampling-method dependant, and to denote the starting point of the representative quantitative data (Bett 2013, 2014), with its elevation an expression of environmental and biological constraints. To the left of the peak, specimens are under-sampled because they are too small to be consistently sampled or observed. Above it, physical sample size, particularly the total number of specimens encountered, ultimately determines how far the spectrum extends to the right.

3.6 Analytical methods

To assess body-size distributions in respect to the metabolic theory framework, it was necessary to account for the inevitable sampling artefact resulting in under-sampling of the small-sized specimens (Bett 2013, 2014). Thus, only the reliable quantitative data were considered, i.e. the right-hand tail of the abundance-size distribution. In addition, to limit the impact of 'noisy' data in the largest size classes represented, a minimum number of ten individuals per size class was maintained by merging abundance data between consecutive size classes where necessary, and by dividing the resultant data by the number of classes merged.

At each site, abundance, biomass, and estimated respiration flux were compared against the MTE predictions using a linear regression model in Minitab (V18.1, Minitab Inc.). Edwards et al. (2017, 2020) tested the effect of data type (body mass or length) and resolution, and the effect of binning that data for conducting body-size spectral analyses. The authors recommend the use of a maximum likelihood estimate (MLE) method, based on binning that considers body-mass-data counts, where each count represents species-specific values within its respective size bin. The MLE was also tested, and the results (i.e. *b* exponent) were analogous to those obtained using the linear

regression model. They are not present in this thesis, but will be the object of a future publication in a relevant journal.

Seafloor temperature varied substantially between the four study sites, complicating direct comparison of body-size distribution of standing stocks. To standardise the influence of temperature, abundance data were corrected to a 1.5 °C equivalent (i.e. using CCZ as the reference site; chapter 1 equation 1.5) (Gillooly et al. 2001). Temperature-correction permitted direct comparison of the influence of other local environmental variables (e.g. POC flux to the seabed) in structuring the four benthic communities studied. Variation between sites was considered using a general linear model (LM) in Minitab. LM is a simplification of multiple linear regression, and it is a useful statistical framework for comparing how several variables (e.g. site, faunal abundance) affect different continuous variables (e.g. body size). Homogeneity of the body-size distribution slopes was assessed using an interaction term between 'site' (factor) and 'body size' (covariate).

3.7 Estimation of seafloor carbon stocks and flows

The PAP study was used as an example to evaluate the practical use of the MTE predictions in estimating seafloor carbon stocks and flows, in a similar fashion to Laguionie Marchais et al's. (2020) study of the benthos at Station M in the NE Pacific. In this project, the approach was built upon the abundance-size spectrum obtained for the PAP-SO megabenthic assemblage (see results in chapter 6 section 6.3.1 and corresponding discussion). The method is fully described in chapter 7 section 7.2.2.

3.8 Sampling effort and limitations

In quantitative ecological analysis, sample size is the primary limitation for collecting enough (quantifiable) data on the assemblage of interest (megabenthos and macrobenthos in the present), and for subsequently processing and analysing the data within the time limit available. This is achieved by surveying large seabed areas (megabenthos; in terms of the number of photographs collected), and collecting several sediment cores (macrobenthos), for producing sufficient sample replication. In particular, sampling effort associated with sample size varies across the body-size

spectrum within each faunal fraction, so that many smaller individuals are detected in comparison to the larger ones whose record becomes random at inappropriate sample scale, because home-range size, or animal space use, increases with increasing body size (Damuth 1981; Peters 1983; Jetz et al. 2004; Tamburello et al. 2015).

In photographic assessment of the megabenthos using AUVs, biological data ultimately depend upon the quality and the quantity (i.e. seabed coverage) of the photographs collected. The optimal resolution size (10-30 mm in the present study) for consistent specimen detection, taxonomic identification, and body-size measurement, is established by the quality of the photographs collected, which is determined by the vehicle's altitude and diving position (i.e. heading, pitch, and roll, influenced by local water currents), the camera settings, the water column conditions (e.g. particle backscatter associated with turbidity), and the subsequent photographic processing applied to improve the visual outcomes (see section 3.2.2). Thus, when sampling and analysing multiple photographic datasets analysed by one or several users, it is essential to standardize field and laboratory methodologies (i.e. photographic processing and analysis) (Durden et al. 2016b, c).

Standardizing ecological data, within and across datasets, is commonly achieved using a similar level of taxonomic identification, and by normalizing image data to seabed area. Taxonomic identification was conducted at GHF and at PAP where faunal assemblages are well-known to science (Durden et al. 2016a; Benoist et al. 2019a and references therein), with the primary intent of using species-specific LWRs in the estimation of individual biomass. At SSB and at CCZ, taxonomic identity was not required to apply the GVM; it was completed nonetheless for faunal diversity and community composition assessment (Thomson et al. 2017; Simon-Lledó et al. 2019a).

Similarly, macrobenthos data obtained from sediment cores depend upon the number of cores collected, and on the processing techniques applied prior and post preservation in laboratory. Sieve-mesh size is the primary determinant of optimal-resolution size (Gage et al. 2002; Pavithran et al. 2009; Bett 2013, 2014; Narayanaswamy et al. 2016), with some organisms that are expected to be retained, yet, pass through because they are damaged, thin and/or elongated, or soft bodied.

Individual-based body-size spectra can be used as a tool for controlling the quality of sampling effort allocated to the range of sizes observed among the taxa present. This is well demonstrated between the two GHF datasets, between the GHF and the SSB datasets, and within the CCZ dataset (figure 3.9). At GHF, field methodology and sample processing were similar in 2012 and in 2015, and the 'optimum' size detected between the surveys was consistent (c. 4-7 g wwt) (figure 3.9a). However, a first small peak abundance below the 'optimum' size is evident at GHF-2, resulting from the records of a single taxon, the cup coral *Caryophyllia smithii*, an iconic species in the area, expected to be found on bedrock. Annotating individuals smaller than the 'optimum' size would not disturb the overall biomass interpretation, however, numerical density and community composition analyses would be biased towards the smallest size classes because they would be over-represented. Thus, it may represent wasted effort in the general process of image annotation.

SSB is the only study area where the AUV was set to dive at a lower target altitude (i.e. 2.5 m instead of 3.2 at the other sites) (table 3.1), enabling the record of smaller individuals. Despite sharing a similar faunal assemblage to GHF, the 'optimum' size at SSB was determined at 0.2 g wwt (figure 3.9a), reflecting the influence of AUV altitude on faunal detection. Thus, the body-size range at CCZ (figure 3.9c) extends towards smaller individuals in comparison to all the other sites (figure 3.9a, b) despite field methodology and sample processing being held constant (with the exception of altitude at SSB). Also, at the CCZ site, a preliminary assessment of the size spectrum revealed the presence of a single crustacean taxon (c. 800 individuals) associated to the small secondary peak abundance following the 'optimum' size (figure 3.9c). This taxon was subsequently identified as a pelagic red crab (similar, if not identical, to *Pleuroncodes planipes*) (Robinson et al. 2004; Pineda et al. 2016), and considered to represent a mass food fall. Consequently, these data were discounted from the subsequent size-spectra analyses.

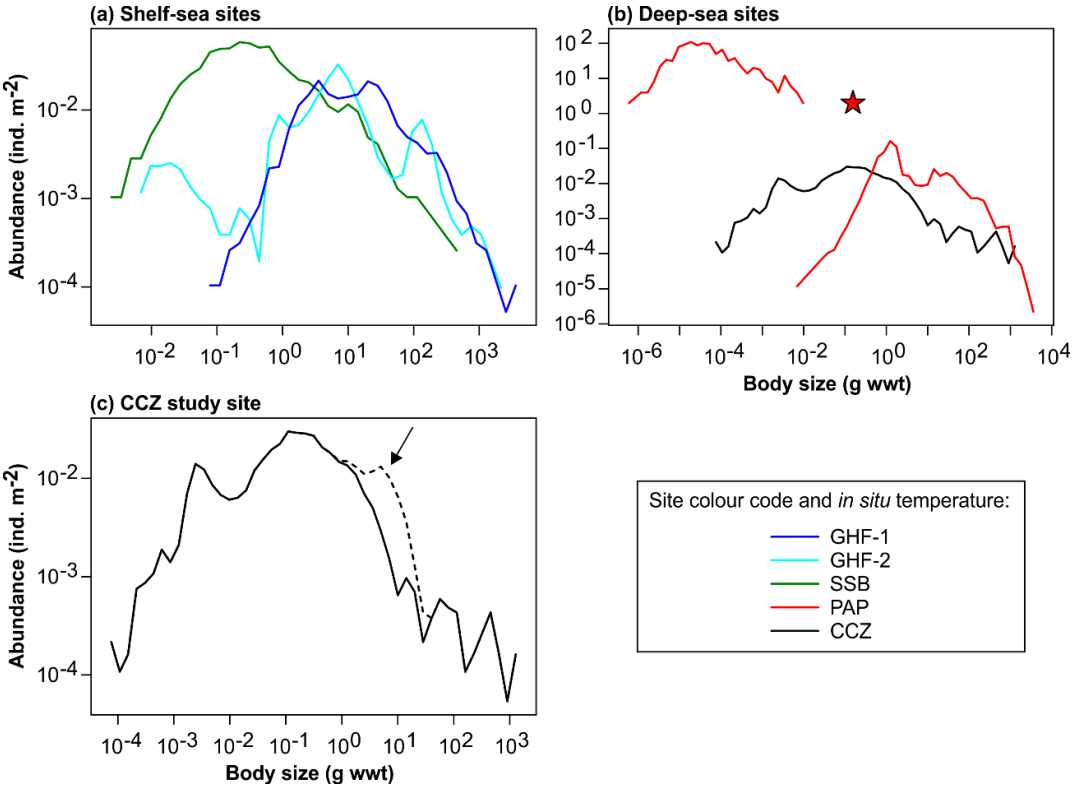

Figure 3.9. Body-size distribution of abundance at the four study sites. (a) Shelf-sea sites: Greater Haig Fras (GHF-1, 2012; GHF-2, 2015), UK-NERC Shelf-Sea Biogeochemistry study area (SSB). **(b)** Deep-sea sites: Porcupine Abyssal Plain (PAP), Clarion-Clipperton Zone (CCZ). The star denotes the presence of a single, exceptionally, large isopod in the macrobenthos data at PAP. **(c)** Distribution of pelagic red crab carcasses at the CCZ study site (dashed line), with corresponding peak abundance indicated by the arrow.

Chapter 4

A generalised volumetric method to estimate the biomass of photographically surveyed benthic megafauna

Benoist NMA[a,b], Bett BJ[a], Morris KJ[a], Ruhl HA[a,c]

[a] National Oceanography Centre, Southampton SO14 3ZH, UK
[b] University of Southampton, Southampton SO14 3ZH, UK
[c] Monterey Bay Aquarium Research Institute, California 95039, USA

Published in Progress in Oceanography*, September 2019, **178**: 102188. DOI: 10.1016/j.pocean.2019.102188.* *Literature cited can be found in the reference section of the Ph.D. thesis, supplementary material to the research publication, and the acknowledgements, are provided in appendix E. As presented in this chapter, the different sections, figures, and tables, were renumbered sequentially to comply with the formatting of the other chapters. The research highlights and the graphical abstract are also presented in this chapter.*

Highlights

- Individual body mass is key to estimating stocks and flows of carbon and energy.
- Biomass estimation from seafloor photographs may be particularly problematic.
- A generalised volumetric method (GVM) to estimate individual biomass is proposed.
- The GVM is at least as effective as the length-weight relationship (LWR) approach.
- The GVM offers several significant advantages over the LWR approach.

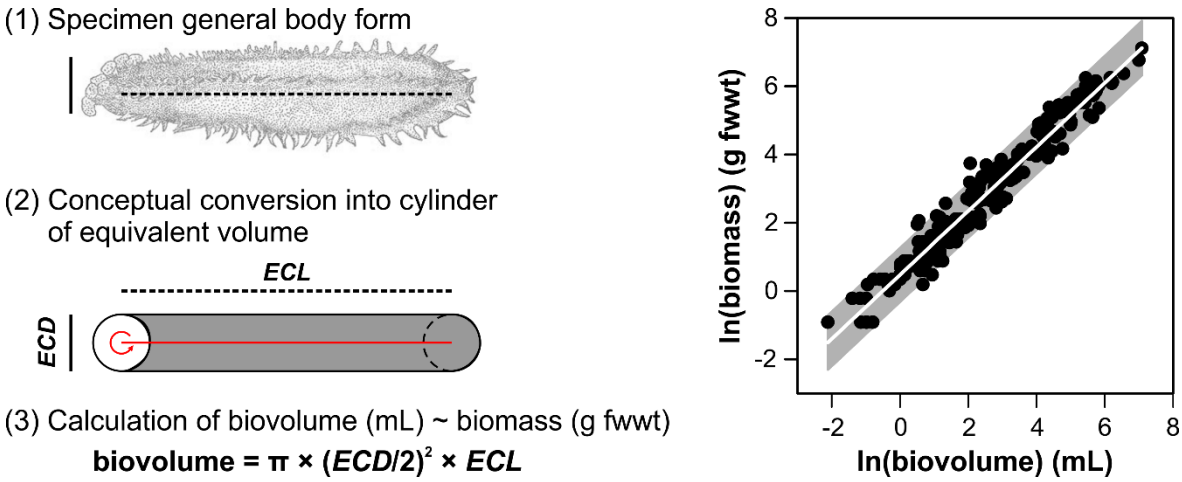

A generalised volumetric method (GVM) to estimate individual biomass of photographed seafloor specimens can overcome the systematic, temporal and spatial variation, associated with the traditional length-weight relationship method. The GVM models specimen body volume **(1)** as a cylinder of equivalent volume **(2)**. The two body measurements corresponding to an equivalent cylindrical diameter (*ECD*) and to an equivalent cylindrical length (*ECL*) are converted into biovolume (mL) **(3)**, which corresponds closely to fresh wet weight biomass (g fwwt).

4.1 Abstract

Biomass is a key variable for understanding the stocks and flows of carbon and energy in the environment. The quantification of megabenthos biomass (body size ≥ 1 cm) has been limited by their relatively low abundance and the difficulties associated with quantitative sampling. Developments in robotic technology, particularly autonomous underwater vehicles, offer an enhanced opportunity for the quantitative photographic assessment of the megabenthos. Photographic estimation of biomass has typically been undertaken using taxon-specific length-weight relationships (LWRs) derived from physical specimens. This is problematic where little or no physical sampling has occurred and/or where key taxa are not easily sampled. We present a generalised volumetric method (GVM) for the estimation of biovolume as a predictor of biomass. We validated the method using fresh trawl-caught specimens from the Porcupine Abyssal Plain Sustained Observatory (northeast Atlantic) and we demonstrated that the GVM has a higher predictive capability and a lower standard error of estimation than the LWR method. GVM and LWR approaches were tested in parallel on a photographic survey in the Celtic Sea. Among the 75% of taxa for which LWR estimation was possible, highly comparable biomass values and distribution patterns were determined by both methods. The biovolume of the remaining 25% of taxa increased the total estimated standing stock by a factor of 1.6. Additionally, we tested inter-operator variability in the application of the GVM, and we detected no statistically significant bias. We recommend the use of the GVM where LWRs are not available, and more generally given its improved predictive capability and its independence from the taxonomic, temporal, and spatial, dependencies known to impact LWRs.

Keywords: ecology; benthos; body size; biovolume; photography; image analysis; northeast Atlantic; Porcupine Abyssal Plain; Celtic Sea

4.2 Introduction

A census of biomass on Earth is important to understanding both the structure and the functioning of the biosphere (Bar-On et al. 2018). Population and assemblage biomass, together with individual body size (mass), are generally seen to be critical variables in the assessment of the stocks and flows of mass and energy in marine ecosystems (e.g. Tomlinson et al. 2014). These stocks and flows influence the primary ecosystem goods and services that the marine environment provides, and in turn, monitoring their status is likely to be essential to achieving the corresponding sustainable development goals (United Nations General Assembly 2015). In the following, we consider the need for benthic biomass data, the current synthesis of global megabenthos data (large fauna living on or near the seafloor), and the suitability of the currently predominant biomass estimation method.

4.2.1 Biomass as an essential variable

The Framework for Ocean Observing (e.g. Lindstrom et al. 2012) indicates a region of overlap between the essential biodiversity variables (EBVs) of the global biodiversity observing system (GEO BON) (Kissling et al. 2018) and the essential ocean variables (EOVs) of the global ocean observing system (GOOS) (Muller-Karger et al. 2018), within which the variable body mass lies. Body mass directly, or indirectly, features in several EBVs: (a) population abundance (as a proxy for numerical abundance); (b) population structure by age/size class; (c) body mass; (d) physiological traits (as a key predictor of metabolism and related traits) (e.g. Peters 1983); and (e) secondary productivity (as a key predictor) (e.g. Banse and Mosher 1980). Assessment of these EBVs is considered relevant to Aichi Biodiversity Targets 4-12 and 14-15 for the maintenance and the restoration of biological ecosystems by 2020 (GEO BON 2011; Pereira et al. 2013).

Recent examinations of EOVs (e.g. Constable et al. 2016; Miloslavich et al. 2018; Levin et al. 2019) have made frequent references to abundance and to biomass variables, and occasional references to body-mass spectra, in connection with zooplankton, fish, and benthic invertebrates. The GOOS currently recognises stock assessments of marine biota groups, including benthic invertebrate stocks, as ‘emerging’ EOVs (www.goosocean.org,

accessed September 2019). The deep ocean observing strategy (DOOS) (Levin et al. 2019) recommends the consideration of EOVs and of 'emerging' EOVs, with the addition of individual body size and of sponge-habitat cover (www.deepoceanobserving.org, accessed September 2019). There is general agreement in the identification of biomass as a key variable in the EBVs by GEO BON, and in the biology and ecosystem EOVs by GOOS and DOOS.

Given the central roles that individual body size and total biomass play in the stocks and flows of mass and energy through marine ecosystems, it seems clear that they should be established as EOVs. Selection as an essential variable is not determined by the variable's perceived 'value' or 'need' alone. The expert panels and other researchers that consider candidate EOVs necessarily give regard to many factors (e.g. Miloslavich et al. 2018); key among these are likely to be: (a) impact, i.e. scientific and societal relevance; (b) feasibility, i.e. monitoring scalability and practicality; and (c) cost effectiveness, i.e. scientific and operational capacity. Given that body mass already features in multiple EBVs of the GEO BON, its impact for ecological research seems clear. It is therefore timely and of particular significance, for both the scientific community and conservation practitioners, to establish a method for the estimation of individual body size and total biomass that (i) has general, broad-scale, application, (ii) can readily be adopted for use in multiple environments by a wide range of users, and (iii) can be achieved using readily available existing technologies.

4.2.2 Existing benthic megafauna biomass data

In the marine environment, recent field studies (Kelly-Gerreyn et al. 2014; Labra et al. 2014; Laguionie Marchais et al. 2020) and theoretical considerations (Bett 2013, 2014) have suggested that total estimated seafloor biomass increases with the mean, or maximum, body size of the organisms included in the study. In effect, the largest organisms present, e.g. benthic megafauna (megabenthos; ≥ 1 cm body size), contribute substantially to the 'true' total standing stock biomass in the system (Bett 2019). Seafloor megafaunal assemblages are often assessed by trawl sampling (e.g. Gage and Bett 2005); however, this approach is typically limited to sedimentary habitats and is likely to be semi-quantitative at best (e.g. McIntyre 1956; Uzmann et

al. 1977; Bett et al. 2001). Moreover, trawling, be it for scientific sampling or commercial fishing purposes, is a rather destructive process (e.g. Huvenne et al. 2016) and thus should be avoided if possible; a factor that may be of concern in time-series studies (e.g. Billett et al. 2010). In response to these limitations, there has been a general increase in the use of seafloor photography to quantify megabenthos assemblages (Durden et al. 2016c), which has recently accelerated with the development of autonomous underwater vehicles (AUVs) (Wynn et al. 2014; Jones et al. 2019) and their use in quantitative seafloor ecology (Morris et al. 2016; Simon-Lledó et al. 2019a). AUV-based seafloor photography enables the rapid quantitative survey of large areas that can comprise multiple habitats in a consistent and non-destructive manner (e.g. Morris et al. 2014; Marzinelli et al. 2015; Milligan et al. 2016; Benoist et al. 2019a).

Wei et al. (2010) provide a major compilation and assessment of global benthic biomass (from bacteria to megabenthos) that is widely cited (129 Web of Science Core Collection citations, May 2019), and that has been used as the basis of other major works, e.g. to predict future trends of seafloor biomass in response to climate change (Jones et al. 2014; 58 Web of Science Core Collection citations, May 2019). However, the megabenthos biomass data synthesised by Wei et al. (2010) encompasses records based on bottom-trawl catches and photographic surveys, potentially introducing mismatches in the spatial scale observed and in the body sizes and the taxonomic groups assessed. We examine the possible significance of this methodological variation in our evaluation of available methods below.

4.2.3 Photographic estimation of individual biomass

Generating quantitative ecological data from large sets of seafloor photographs poses a number of challenges including specimen detection and identification, biomass estimation, and data standardization. Durden et al. (2016a) provide a brief review of existing methodology that essentially comprise two options: (i) calculating the product of numerical density and of a representative value for the individual biomass of a particular taxon, or (ii) the use of a taxon-specific length-weight relationship (LWR) approach. Both methods require access to existing morphometric data on the taxa of interest,

which are frequently unavailable in poorly studied geographic regions, in particular deep-water environments, or for the attached fauna of hard substratum habitats.

Nevertheless, the LWR approach is commonly employed in both the analyses of photographic surveys (e.g. Durden et al. 2015) and of trawl catches (e.g. Robinson et al. 2010). These conversions are typically expressed as an allometric equation of the form:

$$M_E = a \times SL^b \qquad \text{(equation 4.1)}$$

where M_E is estimated body mass, SL is a defined standard linear body dimension, and a and b are taxon-specific constants obtained by log-log regression of measured body mass on SL, and consequently require adequate prior data for the taxon in question (e.g. Durden et al. 2016a). These two constants are an expression of life history and local environmental settings (i.e. ecological factors affecting individual metabolism) (e.g. Peters 1983). In biological terms, the b parameter (or allometry coefficient) is indicative of the rate of weight gain relative to growth in length (see equation 4.2 below). The LWR method is attractive for both its simplicity and its ability to generate biomass estimates for individual specimens, such as are required in the study of individual-based body-size spectra (Edwards et al. 2017; Laguionie Marchais et al. 2020), or any research involving the structuring role of body size in ecosystems (e.g. Sewall et al. 2013; Lewis et al. 2018; Durden et al. 2019).

Durden et al. (2016a) accessed a database of some 47,000 specimens of megabenthos collected by otter trawl from the Porcupine Abyssal Plain sustained observatory (PAP-SO; 4850 m water depth, northeast Atlantic) to produce LWRs for 34 morphotypes (species/species groups/higher taxa) (e.g. Althaus et al. 2015). A typical otter-trawl catch from the PAP-SO returns specimens from between 60 and 80 morphotypes, and the current morphotype catalogue for photographic studies in the area has some 70 morphotypes (Durden et al. this issue*; Hosking et al. this issue*). However, despite the high research effort at PAP-SO (Billett and Rice 2001; Lampitt et al. 2010; Hartman et al. 2012; "Guest editors" this issue*), LWRs are only available for

* Progress in Oceanography Special Issue VIS: Northeast Atlantic PAP-SO, 2019, **178**

approximately half of the taxa present. Similarly, Robinson et al. (2010) undertook a major beam-trawl survey of 283 stations in the North Sea, encountering 497 benthic fish and invertebrate taxa, from which they were able to produce LWRs for 216 taxa, i.e. approximately half of the taxa present. Of those 216 LWRs, only 95 were based on 50 or more specimens. Nine of these invertebrate species were sufficiently numerous and widespread in their geographic distribution to analyse temporal (year of sampling) and spatial (north or south of the 50 m isobath) variation in the LWRs. The authors detected statistically significant temporal and/or spatial variations in the LWRs of seven of those species (see also Stoffels et al. 2003).

Potential temporal (and spatial) variation in the a and the b parameters of LWRs are linked to the concept of condition factor (or condition index), as frequently implemented in studies of fish populations (e.g. Froese 2006). The condition factor is essentially a ratio of measured specimen body mass to the mass predicted from the specimen's length. Froese (2006) provides a formula for calculating relative weight (W_{rm}) as:

$$W_{rm} = 100 \times W / a_m L^{b_m} \qquad \text{(equation 4.2)}$$

where W is specimen weight, L is specimen length, and a_m and b_m are the geometric means of the available LWR parameters. In terms of statistical significance, the number of specimens used to calculate a LWR can be expected to impact its reliability. We examine the possible significance of systematic variation in condition factor in our evaluation of available methods below.

4.2.4 The need for a generalised method

LWRs are potentially subject to systematic, temporal and spatial variation, and may be highly taxon-specific. Consequently, the use of LWRs out of temporal, spatial, or taxonomic, context may result in substantial systematic error. More fundamentally, taxon-specific LWRs simply do not exist for the vast majority of megafaunal species, imposing an immediate severe limitation on the general application of this approach. Environmental assessments, particularly in relation to deep-sea mineral resource exploitation, are now regularly being conducted in very poorly known areas where physical sampling of the megafauna is rare or absent (e.g. Gates et al. 2017; Durden

et al. 2018; Stratmann et al. 2018), demonstrating a growing need for a more tractable method of taxon-independent biomass estimation.

Consequently, we have developed a taxon-independent method for the estimation of biovolume from geometric considerations of photographed specimens as a proxy for biomass. Similar biovolume-based approaches are well established for small organisms (microbes: Saccà 2017; phytoplankton: Jiménez et al. 1987; Hillebrand et al. 1999; Sun and Liu 2003; zooplankton: Alcaraz et al. 2003; Mustard and Anderson 2005; copepods, nematodes: Baguley et al. 2004; Di Mauro et al. 2011; Jung et al. 2012; Moore et al. 2013; Mazurkiewicz et al. 2016; gastropods: McClain 2004), and fossil invertebrates (Novack-Gottshall 2008). Briefly, these approaches select a geometric form to represent approximately the biovolume of a given taxon, then make the measurements necessary to estimate the volume of the selected geometric form. Further conversion of biovolume to units of (fresh) wet weight mass, carbon mass (C), or energy (e.g. joule) can be achieved via established factors (e.g. Brey et al. 2010).

In this contribution, we describe and test a generalised volumetric method (GVM) for the estimation of megafaunal specimen biovolume, as an estimator of biomass, from photographic observations. We first validated the method against measured specimen mass and volume using a collection of fresh trawl-caught specimens from the PAP-SO site. The full methodology was then trialled by two operators in a case study of benthic ecology based on a large photographic dataset derived from AUV surveys on the Celtic Shelf (100 m water depth, northeast Atlantic), where both sedimentary and hard substratum habitat types occur. Comparative assessments of the conventional taxon-specific LWR approach and the proposed taxon-independent GVM are provided, together with an assessment of inter-operator variation in biovolume and biomass estimation.

4.3 Materials and Methods

4.3.1 Evaluation of current methods

4.3.1.1 Field methods

To evaluate the influence of field method, megabenthos biomass data (invertebrates and fish) from the Wei et al. (2010) dataset, limited to deep-sea records (water depth > 200 m), were separated into trawl catches and photographic surveys. A general linear model (LM) of log(biomass) on water depth by method of biomass estimation was developed using the Minitab software package (v18.1; Minitab, Inc.).

4.3.1.2 Length-weight relationship (LWR) method

To examine the characteristics of the LWR method for predicting individual biomass, we examined morphometric data for the large holothurian *Psychropotes longicauda* (*n* = 984) from 15 trawl catches spanning seven research cruises (different years) to the PAP-SO. This species is a biomass dominant at PAP (e.g. Billett et al. 2010) and easily identified in both trawl-catches and seafloor photographs. Corresponding LWRs were examined by linear regression (preserved wet weight ~ standard body length), and temporal variation (between individual catches and years) by LM (preserved wet weight ~ standard body length × trawl or × year), as performed in Minitab. The relative weight of *P. longicauda* specimens was calculated using equation 4.2, with the a_m and b_m parameters taken to be the cruise (year) values. Non-parametric tests (Spearman's rank correlation and Mood's median test; Minitab) were used to further examine variations in relative weight.

4.3.2 A generalised volumetric method (GVM)

The GVM models specimen body volume as a cylinder, and therefore it requires two defining measurements that correspond to the radius (measured as the diameter) and the length of an equivalent cylindrical object. This approach represents a much-simplified approximation of the full range of body forms exhibited by benthic megafauna. Consequently, the method requires the user to compress conceptually the specimen into a cylinder of approximately equivalent volume. **(1)** The user must first choose the most appropriate axis

of rotation for the cylinder; this will become the dimension along which length is measured. The choice of an 'appropriate' axis is essentially determined by the general body plan and the orientation of the photographed specimen (figure 4.1). **(2)** The next choice is an appropriate equivalent cylindrical diameter (*ECD*) perpendicular to the axis of rotation, i.e. given the chosen axis of rotation, what is the most appropriate representative diameter for a conceptually compressed cylinder in that orientation? **(3)** Finally, given that choice of *ECD*, what is the most appropriate equivalent cylindrical length (*ECL*) that will best estimate the volume of the cylinder (figures 4.1 and 4.2)? The estimated specimen biovolume (V_E) is then calculated as:

$$V_E = \pi \times (ECD/2)^2 \times ECL \qquad \text{(equation 4.3)}$$

The process is simplest to conceive in the case of vermiform organisms (figure 4.2a, b); however, it is readily translated to a wide range of morphologies (figure 4.2c-l). The method is necessarily subjective in that the measurements are not made between distinct morphological features, but they are instead aimed at the most effective volumetric representation. The method is, therefore, **(*recommendation 1*)** best implemented by users with zoological knowledge of the taxa involved and, preferably, **(*recommendation 2*)** with experience in directly handling comparable physical specimens. It is simplistic but affords considerable flexibility in practical application, enabling the user to deal with varying specimen orientation and/or partially obscured specimens. From experience, **(*recommendation 3*)** our primary advice to potential users is to retain a simple focus on the objective of estimating the tissue biovolume of the specimen in question, including its appendages if they make an appreciable contribution to the organism's volume. The user should avoid the temptation of making a 'standard measurement' if that has been their previous practice, and treat each specimen encountered as a new case. The method draws on the user's prior knowledge and experience of three-dimensional morphology; consequently, that knowledge is a prerequisite for successful operation.

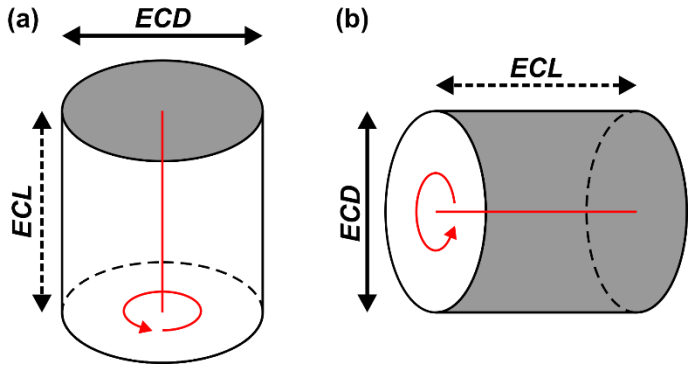

Figure 4.1. Body dimensions of a conceptualised cylindrical specimen as observed from **(a)** a vertical or **(b)** a horizontal orientation. The observed body surface (shaded), the axis of orientation (red line), the equivalent cylindrical diameter (*ECD*; solid dimension line), and the equivalent cylindrical length (*ECL*; dashed dimension line) are illustrated.

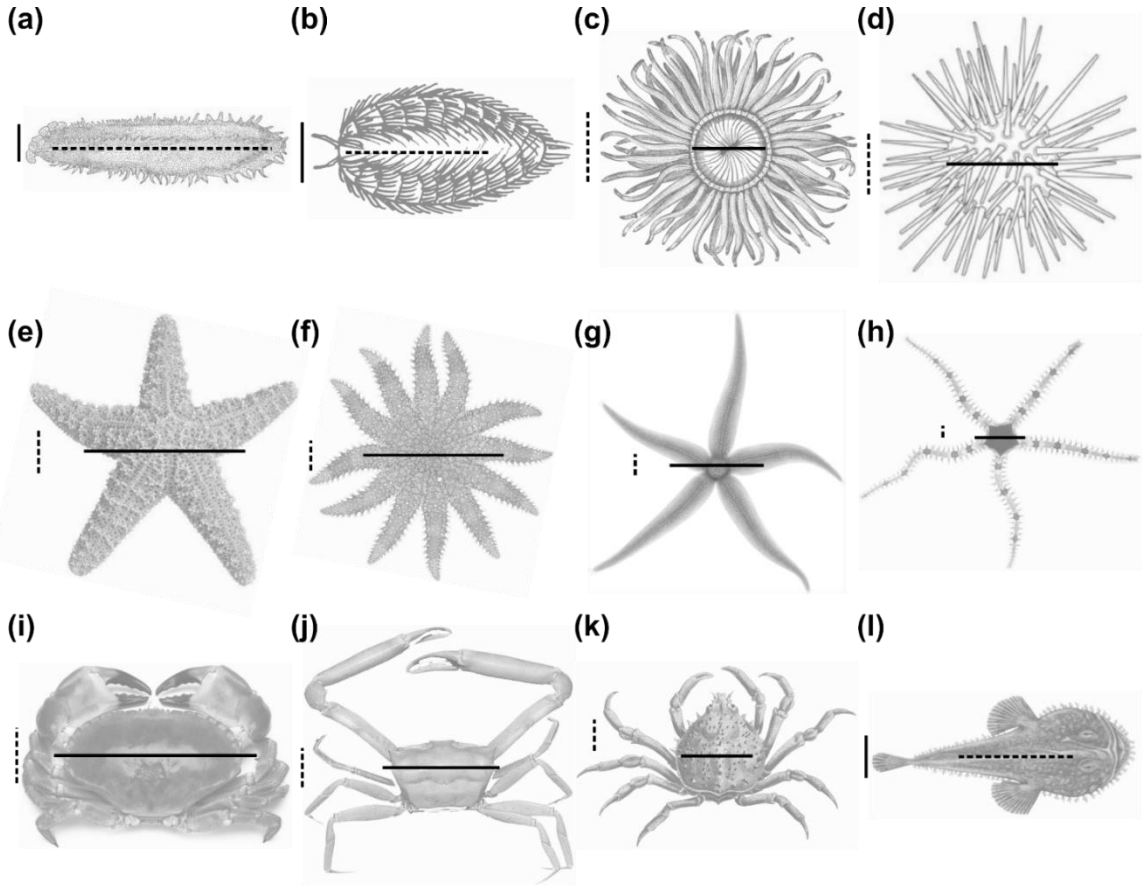

Figure 4.2. Examples of the application of generalised volumetric method measurements to a range of benthic megafauna body forms. The corresponding equivalent cylindrical diameter (*ECD*; solid line) and equivalent cylindrical length (*ECL*; dashed line) measurements are illustrated. **(a)** Holothuroidea. **(b)** Polychaeta. **(c)** Anthozoa. **(d)** Echinoidea. **(e-g)** Asteroidea. **(h)** Ophiuroidea. **(i-k)** Brachyura. **(l)** Actinopterygii.

The GVM is readily adapted to colonial, encrusting, or morphologically plastic, forms (e.g. Ascidiacea, Bryozoa, Cnidaria, Porifera). In colonial forms, the user can opt to estimate the colony as a unit, or to make estimates for the unitary components (zooids, polyps). For example, with close-encrusting colonies and Porifera, the user can estimate an ECD to best represent the areal extent of the subject and then estimate an ECL to best represent the typical thickness of the corresponding layer of biological tissue. With erect colonial Cnidaria (e.g. Octocorallia), the user can (a) estimate the biovolume of each single polyp with a representative contribution of connecting tissue; (b) estimate the biovolume of a single polyp with a representative contribution of connecting tissue, and apply a multiplier for the number *n* of polyps in the colony (i.e. ECL is replaced by $ECL \times n$ in equation 4.3); or (c) estimate an ECD representative of stem tissue thickness and then estimate an ECL that represents the total length of the tissue-bearing stem. A very similar approach can be applied to branching Porifera. With other sponge growth forms, the user can readily adopt similar methods, for example: (i) laminar, ECD to represent the plate area, ECL to represent the plate tissue thickness; (ii) cup/goblet/barrel forms, ECD to represent one-half of the outer surface of the cup, ECL to represent double the cup tissue thickness. Again, our primary advice to potential users is to retain a simple focus on the objective of estimating the tissue biovolume of the specimen in question (***recommendation 3***).

4.3.3 Method validation with physical specimens

Fresh specimens of benthic invertebrate megafauna and demersal fish were collected from the Porcupine Abyssal Plain Sustained Observatory site (PAP-SO; 48° 50' N 016° 30' W) at 4850 m water depth (Hartman et al. 2012), using a semi-balloon otter trawl during the RRS *Discovery* cruises DY050 in 2016 (Stinchcombe 2017) and DY077 in 2017 (Lampitt 2017c). In total, 206 intact specimens were selected for direct physical measurement on board and subsequent indirect photographic body-size measurement. The test specimens were chosen to represent a wide range of body shapes, sizes (five orders of magnitude), taxonomic identities (six phyla, 34 taxa) (appendix E), and ecological characteristics (deposit feeder, filter feeder, predator, scavenger, mobile, sessile).

4.3.3.1 Direct measurement of specimens

Blotted individual fresh wet weight (fwwt) biomass (M_M) was recorded to the nearest 0.1 g using a motion-compensated electronic balance (POLS S-182 Marine Onboard Scale, Lorrimar Weighing Ltd.). Fresh biovolume (V_M) was measured by displacement using a measuring cylinder suited to the specimen size (100, 250, 1000, or 2000 mL) and recorded to the nearest 0.5, 1.0, 5.0, or 10.0 mL, respectively. Specimen biomass and biovolume ranged c. 0.5-1225 g and 0.5-1210 mL, respectively.

4.3.3.2 Indirect measurement of specimens

Each fresh specimen was then photographed (Fujifilm FinePix F550EXR) from above (i.e. high oblique, near perpendicular view), in a position to match the typical view obtained from seafloor AUV-survey photographs (e.g. dorsal view of squat lobster with tail folded beneath body, dorsal view of shrimp, oral view of anemone) (figure E.1). Photograph-derived body-size measurements were then made at 0.5 mm resolution, typical of seafloor survey photographs (e.g. Morris et al. 2014), via image analysis software (Image-Pro Plus, v7.0, Media Cybernetics Inc.). Three body dimensions were recorded from each specimen: (i) GVM equivalent cylindrical diameter (ECD), (ii) GVM equivalent cylindrical length (ECL), and (iii) LWR standard linear body dimension (SL), as employed in previously established PAP-SO taxon-specific LWRs (i.e. Durden et al. 2016a). The ECD and ECL measurements were converted to estimated biovolume (V_E) using equation 4.2, i.e. the proposed GVM approach. The SL measurement was converted to fresh wet weight biomass (M_E) using equation 4.1, i.e. the LWR method detailed by Durden et al. (2016a).

4.3.3.3 Analytical approach

Relationships between measured and estimated specimen mass and volume were examined by regression. We primarily based our assessment on the predictive results of model I ordinary least squares (OLS) regression, as implemented in Minitab (Sokal and Rohlf 1995), on the premise that our focus was the prediction of mass from estimated volume (V_E), or from standard length (SL), and that the test specimens were deliberately selected (i.e. intact) rather than randomly sampled from the trawl catches. We carried out OLS regressions on the native variables and on their transformation to natural

logarithms to acknowledge potential inhomogeneity of variance. In reporting regression results, we have included the 'Predicted R^{2}' statistic (Minitab 2013); this is based on a leave-one-out cross-validation approach and assesses how well the model predicts new observations (see e.g. Allen 1971). In addition, we also carried out model II regressions (Legendre and Legendre 1998) that are suited to the assessment of functional relationships where both variables are measured with error, and where the focus is on the symmetric relationship between the two variables, rather than the asymmetric case of predicting one from the other. We implemented two forms of model II regression: (i) ranged major axis (RMA) using the 'lmodel2' package (v1.7-3) (Legendre 2018), and (ii) standardised major axis (SMA) using the 'smatr' package (v3) (Warton et al. 2012), in the R environment (v3.3.2) (R Core Team 2016). These various regression techniques are extensively discussed by Warton et al. (2006) and Legendre (2018).

4.3.4 Method trial in a photographic case study

Seafloor images were obtained from three shelf-sea locations in the Celtic Sea, northeast Atlantic, c. 100 m water depth (Thompson et al. 2017), using the AUV *Autosub3* (McPhail et al. 2009) during the RRS *Discovery* cruise DY034 in 2015 (Ruhl 2015). The AUV was programmed to survey at a target altitude of 2.5 m above the seafloor, yielding a nominal resolution of c. 0.5 mm per pixel. The optical axis of the camera was approximately perpendicular to the seafloor, with the AUV's pitch and roll angles recorded for subsequent image processing. General field method and subsequent image processing and assessment were as described by Morris et al. (2014, 2016), with data generated from 4160 images, representing c. 4000 m^{2} of seafloor.

4.3.4.1 Image analysis

All benthic invertebrate megafauna and demersal fish (≥ 1 cm body size) observed were counted and identified to the lowest taxonomic or morphotype unit (table E.1). As defined above, three body dimensions were recorded per specimen: ECD, ECL, and SL. Where specimens could not be assigned to a taxonomic unit or morphotype, they were recorded as indeterminate (< 1% of specimens) and excluded from subsequent analyses. Specimen body-size measurements were converted to estimated volume (V_E) using equation 4.3,

i.e. the GVM approach, and to estimated mass (M_E) using equation 4.1, i.e. the LWR approach, where possible (via conversion factors obtained from the literature; Coull et al. 1989; Richardson et al. 2000; Robinson et al. 2010; Silva et al. 2013; Durden et al. 2016a). The biovolume of all identifiable specimens recorded was estimated using the GVM; however, LWRs were only available for c. 75% of the taxa encountered. To enable direct comparison of the two methodologies, we refer to biovolume estimates for only those specimens for which M_E could be calculated as $V_{E-partial}$. Each seafloor image was also visually classified to habitat type: (i) hard substrata (boulder, cobble; total 54 m^2), (ii) sand (1169 m^2), (iii) mud (2034 m^2), and (iv) mosaic where there was substantial hard substratum present in sand or mud (10-50% areal coverage; 618 m^2) (e.g. Benoist et al. 2019a). To acknowledge the likely inhomogeneity of variance and the unbalanced sampling design, standing stock data (biovolume or biomass standardised to seafloor area observed) were $\log_{10}$-transformed and assessed using Welch's ANOVA (Welch 1951) with subsequent pairwise comparisons made using the Games-Howell method (Games and Howell 1976), as implemented in Minitab.

4.3.4.2 Inter-operator variation assessment

Two operators (O1, O2) were trained jointly to apply GVM body-size measurements on a selection of photographed individual megabenthos specimens representative of the range of taxa encountered in the study area. Training consisted of repeat measurements of the selected specimens and joint quality/control assessment of the resultant data to minimise intra- and inter-operator inconsistencies. This process yielded two final training samples of 130 paired specimen records ($V_{E-training}$). Each operator then independently processed a set of c. 2400 images. A subset of 20% of those images was analysed by both operators (i.e. c. 480 images common to O1 and O2), yielding two field samples of estimated standing stock (M_E, $V_{E-partial}$, V_E). To measure variability in standing stock estimates between operators, the training and the field datasets were randomly resampled with replacement to establish an appropriate measure of inter-operator error in standing stock estimation using a modified form of bootstrapping (Davison and Hinkley 1997). This process was repeated 10,000 times using a custom script implemented in the R environment (R Core Team 2016). For each dataset,

total standing stock ($V_{E-training}$, M_E, $V_{E-partial}$, V_E) was calculated for each bootstrap sample, and the 95% confidence interval (CI) of relative difference between operators was estimated using the simple percentile method (Davison and Hinkley 1997). To give context to the inter-operator variability estimates, the overall relative variability in field standing stock was also estimated using the same method for the same sampling unit size (i.e. 10,000 resamples with replacement of c. 480 images from the complete image set).

4.4 Results and Discussion

4.4.1 Evaluation of current methods

4.4.1.1 Trawl sample versus photographic survey

Figure 4.3 presents the megabenthos biomass data (invertebrates and fish) from the Wei et al. (2010) dataset as divided into trawl catch and photographic survey methods. These data suggest substantial underestimation of biomass when based on trawl catches. More formally, the LM of log(biomass) on water depth by method reveals a statistically significant effect of method ($F_{1,220}$ = 76.4, p < 0.001) and no statistically significant interaction between water depth and method ($F_{1,219}$ = 0.75, p = 0.388). Consequently, the model predicts a common slope for the response of log(biomass) to water depth for both methods of -3.75 × 10^{-4}, with a 95% CI of -4.32 ×10^{-4} to -3.17 × 10^{-4} that does not encompass the slope originally published (i.e. -3.07 × 10^{-4}) (Wei et al. 2010). In particular, note the substantial offset in the estimated intercepts: trawl 1.73 (95% CI 1.59, 1.88) and photo 3.01 (95% CI 2.87, 3.15). This equates to a factor of 20 underestimation of biomass at a given water depth by trawl catch relative to photographic survey.

We suggest that this substantial, systematic, methodological bias should be carefully considered, particularly when estimates of standing stock biomass are being produced (e.g. Wei et al. 2010), and where those estimates are being used in future climate change scenario forecasts (e.g. Jones et al. 2014). The current state of knowledge may be substantially biased towards underestimated stocks of seafloor biomass. Figure 4.3 illustrates two additional biomass estimates from the PAP-SO site as provided by recent photographic assessments (Durden et al. 2015a; Morris et al. 2016). The

mean value of these estimates, 258 mg C m^{-2} (photographic data), is over two orders of magnitude greater than the corresponding estimate from the original regression of 2 mg C m^{-2} (pooled trawl and photographic data) (Wei et al. 2010). The 'true' trawl estimate of PAP-SO megabenthos biomass (invertebrate only) is 17 mg C m^{-2}, based on 44 otter trawls covering the period 1989-2005 (Billett et al. 2001, 2010). We conclude that the state-of-the-art in megabenthos biomass estimation (e.g. Wei et al. 2010) is generally a factor of 20 below the likely true value, and may be underestimated by a factor of 200+ locally. This is not a new observation, nor is the potential use of underwater photography to tackle the issue a new solution (e.g. McIntyre 1956; Uzmann et al. 1977; Bett et al. 2001). We therefore suggest that there is both a clear need and scope for substantial improvement via the widespread adoption of photographic-survey-based megabenthos biomass estimation.

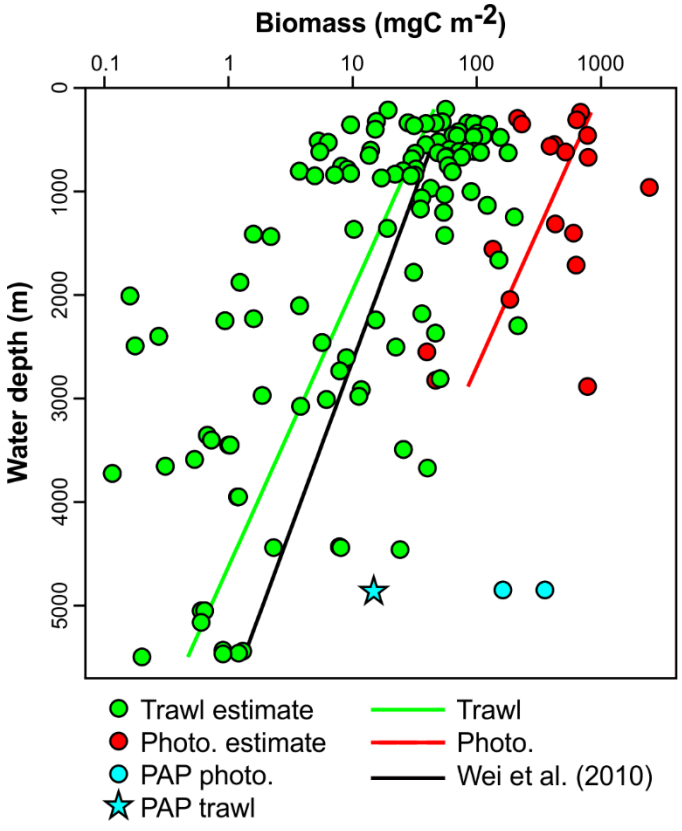

Figure 4.3. Megabenthos biomass as a function of water depth and estimation method: trawl catches and photographic surveys. Data shown are as compiled by Wei et al. (2010) with the addition of (i) two values for the Porcupine Abyssal Plain Sustained Observatory site derived from recent photographic assessments (Durden et al. 2015a; Morris et al. 2016), and (ii) the 'true' trawl estimate of PAP-SO megabenthos biomass (invertebrate only; Billett et al. 2001, 2010), with units of mass converted from fresh wet weight to carbon mass using the coefficients provided by Brey et al. (2010). Lines represent regressions of log(biomass) on water depth: (i) black, original regression provided by Wei et al. (2010), with general linear model results for (ii) green, trawl catches, and (iii) red, photographic surveys.

4.4.1.2 Evaluation of LWR method

Illustrated in its linear form, the LWR for *P. longicauda* demonstrates the rather diffuse nature of that relationship (figure 4.4). For example, a specimen of 20 cm standard length ($19.5 < SL \leq 20.5$ cm) has an observed weight range of 84-358 g preserved wet weight (pwwt), and a predicted weight range of 203-226 g pwwt using the LWR method. Although the LWR approach may superficially appear to be an exact numerical method, i.e. individual biomass is obtained mathematically from a standard measurement, it is effectively an approximate technique, with the predicted value ranging 40% to 170% of the true value in this example.

The LWR illustrated in figure 4.4 represents a composite of 15 trawl catches from seven cruises spanning almost 15 years. When the identities of individual catches, or cruises, are included in a LM, statistically significant variation is evident in both cases (trawls $F_{1,14} = 3.54$, $p < 0.001$; cruises $F_{1,6} = 4.97$, $p < 0.001$), and in both cases there are statistically significant interactions with standard body length (length × trawl $F_{1,14} = 2.86$, $p < 0.001$; length × cruise $F_{1,6} = 2.77$, $p = 0.011$). Consequently, there are statistically significant differences in both the a and the b parameters among trawls and cruises (e.g. figure 4.5). Such variation calls in to question the selection of the most appropriate value for these parameters in the case of *P. longicauda* or indeed any other species.

Figure 4.6 illustrates the variation in the relative weight of *P. longicauda* by year of sampling. Spearman's rank correlation of relative weight and standard body length indicated the effective independence of these measures ($r_{s984} = -0.037$, $p = 0.247$). A Mood's median test detected statistically significant temporal variation in relative weight ($\chi^2_6 = 136.8$, $p < 0.001$). In effect, specimens collected in 2005 and 2015-2017 were c. 15% heavier at a given length than the general LWR prediction, and those collected in 2004, 2011, and 2013 were c. 15% lighter than the prediction. Such systematic temporal variation could, for example, be linked to the known intra- and inter-annual variation in the supply of organic matter to the seafloor in this location (e.g. Bett et al. 2001). This, again, calls in to question the selection of the most appropriate LWR parameter values for *P. longicauda* or any other species.

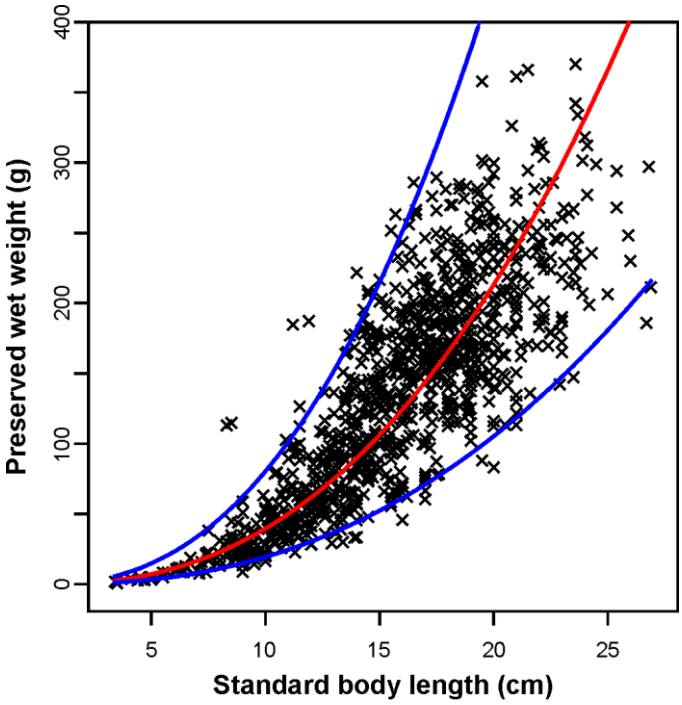

Figure 4.4. Length-weight relationship of the holothurian *Psychropotes longicauda* sampled from the Porcupine Abyssal Plain Sustained Observatory between 2004 and 2017.Scatter plot of individual values with corresponding log-log regression (red line) and associated 95% prediction interval (blue lines); $F_{1,982}$ = 4232.4, p < 0.001, R^2 = 81.1%, $W = 0.442 \times SL^{2.42}$.

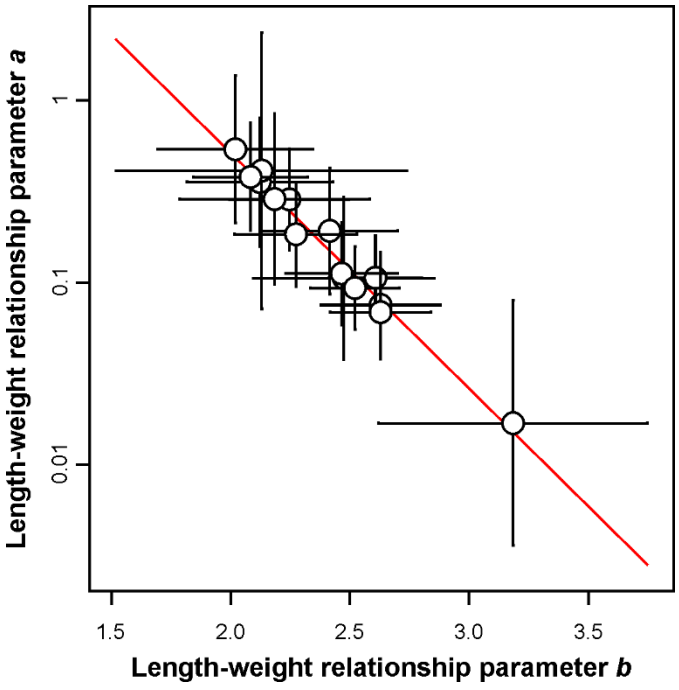

Figure 4.5. Variation in length-weight relationship (LWR) of the holothurian *Psychropotes longicauda* sampled from the Porcupine Abyssal Plain Sustained Observatory between 2004 and 2017.For each trawl catch, the *a* and the *b* parameters of the LWR are illustrated, together with corresponding 95% confidence intervals. The red line represents the log-linear regression of *a* on *b*.

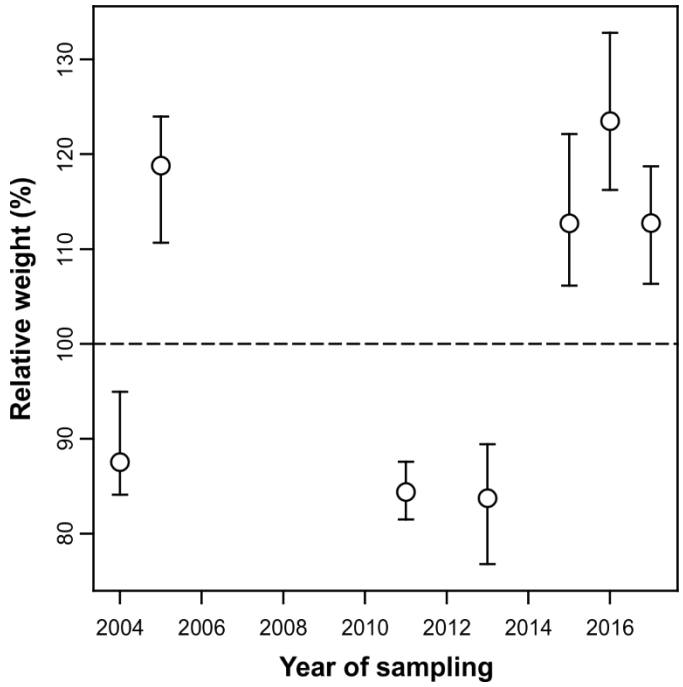

Figure 4.6. Temporal variation in the relative weight (specimen weight/LWR-predicted weight; equation 4.2) of the holothurian *Psychropotes longicauda* from the Porcupine Abyssal Plain Sustained Observatory between 2004 and 2017. The median value is presented with corresponding 95% confidence interval. Dashed line serves as reference line.

4.4.2 Validation with physical specimens

We tested the relationships between direct physical measurement (M_M, V_M) and indirect photographic body-size measurement (M_E, V_E) obtained from a variety of trawl-caught specimens from the PAP-SO study site (appendix E). All of the relationships examined between measured and estimated mass and volume yielded strong and statistically significant Pearson's product-moment correlations (r), ranging between 0.897 for $M_M \sim M_E$ to 0.997 for $M_M \sim V_M$ (table 4.1). Consequently, there was only minor variation between the regression slope coefficients estimated by the model I (table 4.2) and the model II (table 4.3) methods. Indeed, in most cases the 95% CI of the regression slope encompasses the value 1.0; the primary exception being the relationship $M_M \sim M_E$ that yielded substantially lower slope values (c. 0.6; tables 4.2 and 4.3).

Similarly, ordinary least squares regressions were all statistically significant and exhibited good predictive capacity with predicted R^2 ranging between 76.1% for $M_M \sim M_E$ to 99.4% for $M_M \sim V_M$ (table 4.2). All OLS regression coefficients were statistically significant, except in the case of the intercept for $M_M \sim V_M$ in both linear and logarithmic forms, suggesting a very close correspondence between body mass and body volume (table 4.2). In other words, for every additional mL in body volume, body mass is expected

to increase by c. 1 g fwwt, suggesting an average tissue volumetric mass density of 1.053 (linear) and 1.058 (logarithmic; figure 4.7a; table 4.2), with very similar values derived from the linear forms of RMA (1.056) and SMA (1.056) model II regressions (table 4.3).

Table 4.1. Relationships between biomass and biovolume of megabenthos specimens from the Porcupine Abyssal Plain Sustained Observatory, as directly measured and photographically estimated using the generalised volumetric method and the length-weight-relationship approach. Pearson's product-moment correlation coefficients (r) of measured ($_M$) and estimated ($_E$) specimen mass (M_M, M_E; g fwwt) and volume (V_M, V_E; mL), for linear (lin.) and logarithmic (log.) relationships (in all cases n = 206, and p < 0.001).

Variable	M_M (lin., log.)	V_M (lin., log.)	M_E (lin., log.)
V_M (lin., log.)	0.997, 0.981		
M_E (lin., log.)	0.897, 0.977	0.901, 0.960	
V_E (lin., log.)	0.952, 0.934	0.954, 0.923	0.907, 0.941

Table 4.2. Predictive capacity of photographic methods to estimating body size. Model I linear regressions between measured and photographically estimated body size of megabenthos specimens from the Porcupine Abyssal Plain Sustained Observatory, using the generalised volumetric method and the length-weight-relationship approach. Results of model I ordinary least squares regression analyses of measured ($_M$) and estimated ($_E$) specimen mass (M_M, M_E; g fwwt) and volume (V_M, V_E; mL). (Pred., predicted; CI, confidence interval; ***, p < 0.001).

Equation	$F_{[1,204]}$	R^2 (%)	Pred. R^2 (%)	Intercept 95% CI	$t_{[204]}$	Slope 95% CI	$t_{[204]}$
$M_M = 1.250 + 1.053\ V_M$	35768***	99.4	99.4	(-0.543, 3.043)	1.37	(1.042, 1.064)	189***
$\ln(M_M) = 0.056 + 0.996\ \ln(V_M)$	5254***	96.3	96.2	(-0.036, 0.147)	1.20	(0.968, 1.023)	72.5***
$M_M = 13.91 + 0.982\ V_E$	1992***	90.7	89.7	(6.831, 20.99)	3.87***	(0.939, 1.026)	44.6***
$\ln(M_M) = 0.472 + 0.938\ \ln(V_E)$	4303***	95.5	95.4	(0.381, 0.562)	10.3***	(0.910, 0.966)	65.6***
$M_M = 20.49 + 0.547\ M_E$	844***	80.5	76.1	(10.32, 30.67)	3.97***	(0.510, 0.584)	29.1***
$\ln(M_M) = 0.408 + 0.837\ \ln(M_E)$	1386***	87.2	86.9	(0.248, 0.568)	5.03***	(0.793, 0.882)	37.2***
$V_M = 12.11 + 0.931\ V_E$	2057***	91.0	89.4	(5.500, 18.72)	3.61***	(0.891, 0.972)	45.4***
$\ln(V_M) = 0.504 + 0.908\ \ln(V_E)$	2403***	92.2	92.0	(0.387, 0.622)	8.48***	(0.872, 0.945)	49.0***

Table 4.3. Functional relationship between photographically estimated and measured body size. Model II linear regression between measured and photographically estimated body size of megabenthos specimens from the Porcupine Abyssal Plain Sustained Observatory, using the generalised volumetric method and the length-weight-relationship approach. Results of model II regression (RMA, ranged major axis; SMA, standardised major axis) analyses of measured ($_M$) and estimated ($_E$) test specimen mass (M_M, M_E; g fwwt) and volume (V_M, V_E; mL). (CI, confidence interval).

Equation	RMA intercept (95% CI)	RMA slope (95% CI)	SMA intercept (95% CI)	SMA slope (95% CI)
$M_M \sim V_M$	1.019 (0.199, 1.830)	1.056 (1.045, 1.067)	1.028 (-0.766, 2.822)	1.056 (1.045, 1.067)
$\ln(M_M) \sim \ln(V_M)$	0.002 (-0.077, 0.079)	1.014 (0.987, 1.042)	0.001 (-0.039, 0.040)	1.015 (0.988, 1.042)
$M_M \sim V_E$	10.62 (7.517, 13.58)	1.032 (0.987, 1.078)	10.65 (3.497, 17.80)	1.031 (0.989, 1.076)
$\ln(M_M) \sim \ln(V_E)$	0.410 (0.335, 0.483)	0.962 (0.934, 0.992)	0.180 (0.141, 0.220)	0.960 (0.932, 0.989)
$M_M \sim M_E$	13.34 (8.703, 17.66)	0.614 (0.573, 0.657)	13.78 (3.378, 24.18)	0.610 (0.574, 0.648)
$\ln(M_M) \sim \ln(M_E)$	0.226 (0.082, 0.362)	0.899 (0.853, 0.948)	0.101 (0.031, 0.171)	0.897 (0.853, 0.942)
$V_M \sim V_E$	9.210 (6.330, 11.97)	0.975 (0.933, 1.018)	9.109 (2.437, 15.78)	0.977 (0.937, 1.018)
$\ln(V_M) \sim \ln(V_E)$	0.397 (0.297, 0.492)	0.950 (0.913, 0.990)	0.177 (0.126, 0.228)	0.946 (0.910, 0.983)

Among the fresh specimens, the proposed GVM appeared to have good predictive capability for both volume (predicted R^2 89.4-92.0%; figure 4.7c) and mass (89.7-95.4%; figure 4.7b), which exceeded that of mass prediction by the conventional LWR method (76.1-86.9%; table 4.2). In practical terms, the standard deviation of the estimate was 47.1 g fwwt for the GVM and 68.1 g fwwt for the LWR method, where the corresponding value from directly measured volume was 11.6 g fwwt.

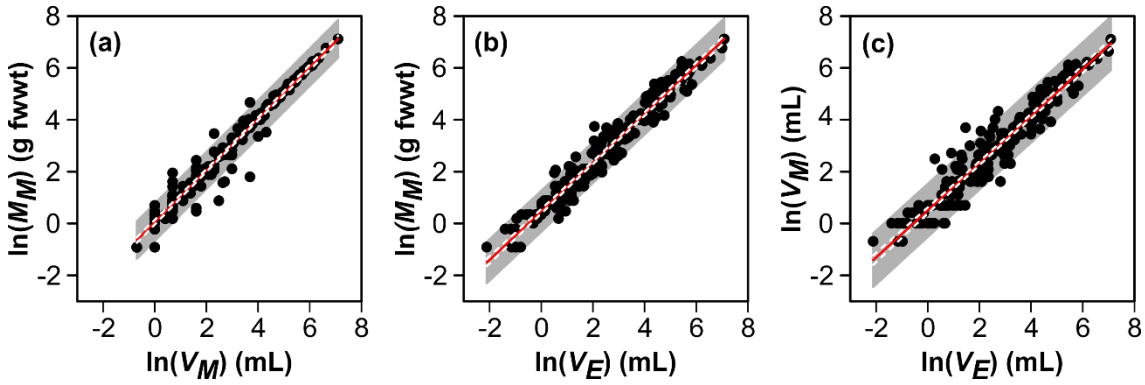

Figure 4.7. Comparison of measurements and estimates of volume and biomass of fresh megabenthos specimens from the Porcupine Abyssal Plain Sustained Observatory. Log-log linear regressions. **(a)** Measured mass (M_M) on measured volume (V_M). **(b)** Measured mass (M_M) on geometrically estimated biovolume (V_E; equation 4.3). **(c)** Measured biovolume (V_M) on geometrically estimated biovolume (V_E). Solid red lines are regressions, dashed white lines are corresponding 95% confidence intervals, and shaded areas the corresponding 95% prediction intervals.

Although the estimation of mass from standard length is a commonly applied technique, it is not entirely surprising that the proposed GVM has an improved predictive capacity. The estimation of mass from a single measured dimension (*SL*) relies on a consistent relationship between the measured dimension and the two unmeasured dimensions, whereas the volumetric approach measures two dimensions, with the second-dimension measurement (*ECD*) subjectively modified to be representative of the third unmeasured dimension. Further, as previously discussed, the mass of an individual of a given standard length may be, for example, substantially influenced by its life stage, physical condition, feeding success, health, season, and geographic location (e.g. Meyer 1989; Primavera et al. 1998; Kimmerer et al. 2005; Méthot et al. 2012; Mahé et al. 2016; Zilli et al. 2017).

The volumetric assessment of individual biomass is frequently used in the study of microscopic and small-bodied organisms (Baguley et al. 2004; Mustard and Anderson 2005; Novack-Gootshall 2008; Mazurkiewicz et al. 2016). Studies of macro- and megafaunal marine organism biovolume have previously been used as an indicator of relative biomass, or the physical space occupied by individuals (McClain 2004; Jones et al. 2007; McClain and Boyer 2009). In the present study, we have been able to compare directly mass estimates by our proposed taxon-independent GVM and the taxon-specific LWR method, where those relationships were derived from a very extensive measurement database of c. 47,000 specimens (Durden et al. 2016a). The GVM appears to outperform the traditional LWR method, having a higher predicted R^2 value and lower standard error of estimate value. The generalised volumetric estimate (V_E) does requires the user to measure two body dimensions (*ECD*, *ECL*). Nonetheless, the additional time (cost) of making the second measurement is small compared to the full process of locating a specimen within an image, identifying that specimen, and making a single measurement (*SL*). The proposed method is taxon, time, and location independent, offering considerable benefits that are further explored in the following case study.

4.4.3 Celtic Sea case study trial

In total, 2896 specimens from eight phyla and 92 taxa were measured from photographs using both the GVM and the LWR approach (appendix E). The estimated range for individual biovolume (V_E) was 0.001 mL to 16.98 L, and for biomass (M_E) 0.001 g to 17.35 kg. Total standing stock estimated by the GVM was very similar to that estimated with the LWR method ($V_{E\text{-}partial}$ 7.74 × 10^{-3} mL m^{-2}, M_E 7.34 × 10^{-3} g m^{-2}). No statistically significant differences were detected between $V_{E\text{-}partial}$ and M_E estimates for the total surveyed area, or within the individual habitat types encompassed by the survey (figure 4.8). Similarly, both methods illustrated the same pattern and detected the same statistically significant differences between habitat types ($V_{E\text{-}partial}$ $F_{3,267}$ = 46.69, $p < 0.001$; M_E $F_{3,266}$ = 53.13, $p < 0.001$). The same pattern and statistically significant differences were also apparent in the total biovolume data, i.e. including those taxa for which LWR estimation was not possible (V_E $F_{3,274}$ = 131.67, $p < 0.001$). However, there were appreciable increases in estimated standing stock from the M_E and $V_{E\text{-}partial}$ values to the V_E values (figure 4.8). By application to the full range of taxa present, the GVM increased the total standing stock estimate over the LWR method by a factor of 1.6 for the total seafloor area surveyed, by about double in the case of mosaic and mud habitats, and around four-fold on hard substrata.

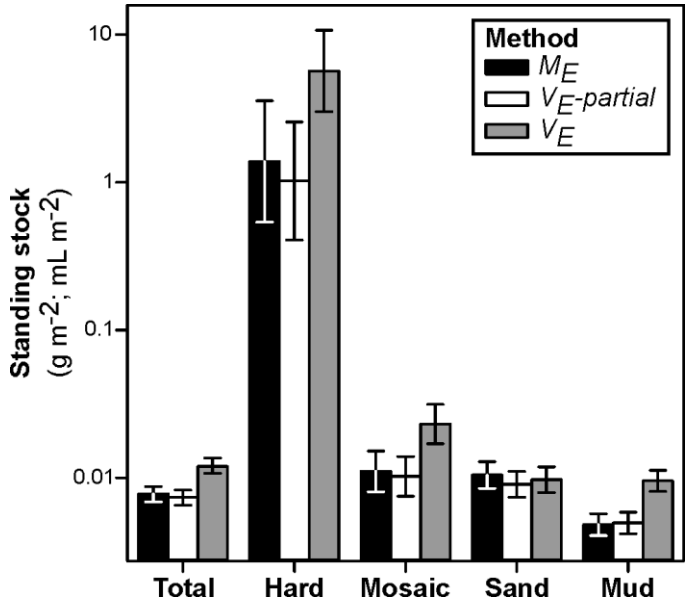

Figure 4.8. Celtic Sea megabenthos standing stock biomass by habitat type and estimation method. The mean value is presented with 95% confidence interval, as estimated using the length-weight-relationship (LWR) approach (M_E, g m^{-2}; equation 4.1) and the generalised volumetric method (mL m^{-2}; equation 4.3), excluding ($V_{E\text{-}partial}$) and including (V_E) those taxa for which LWR estimation was not possible.

The potential advantage of the GVM, compared to the LWR method, was well demonstrated in the Celtic Sea case study trial. This region encompasses substantial areas of mixed substratum types (mosaics of hard rock and mobile sediments) that are not easily surveyed using physical sampling methods, such that photography may be the only uniformly applicable approach to stock assessment across habitat types. Estimated biovolume ($V_{E\text{-}partial}$) was highly consistent with the biomass estimates (M_E) obtained by the LWR method, suggesting at least an equal performance for the proposed method. Further, the volumetric method enabled the assessment of the c. 25% of taxa for which no LWR data were available (mainly bryozoans, sponges, and colonial cnidarians). Located in the European Atlantic shelf seas, the fauna of this study area is very well known with a substantial literature from which to derive LWR conversion factors (Coull et al. 1989; Robinson et al. 2010; Silva et al. 2013; Benoist et al. 2019a). However, in marine regions lacking that information, the proposed taxon-independent GVM offers the prospect of useful standing stock assessments despite a lack of taxon-specific information. In addition, the volumetric approach enables the assessment of those organisms that do not exhibit a distinctive body form or that are rarely sampled as complete entities (e.g. sponges, colonial and encrusting taxa).

The Celtic Sea dataset was produced by two different operators trained to apply GVM body-size measurements using a common training image dataset. Following that training, there was no statistically significant difference in the total volume estimated ($V_{E\text{-}training}$) between operators O1 and O2 (figure 4.9a). This preliminary test was further expanded in the full field trial. As suggested by Durden et al. (2016b, c), a subset of images was analysed by both operators to quantify potential inter-operator bias in the estimation of mass and volume using both the LWR and the GVM approaches. There were no statistically significant differences in estimated biomass (M_E) or estimated biovolume ($V_{E\text{-}partial}$, V_E) between operators (figure 4.9b-d). Note also that the field sample relative variability was appreciably greater than the inter-operator relative variability for both LWR and GVM approaches (figure 4.9b-d).

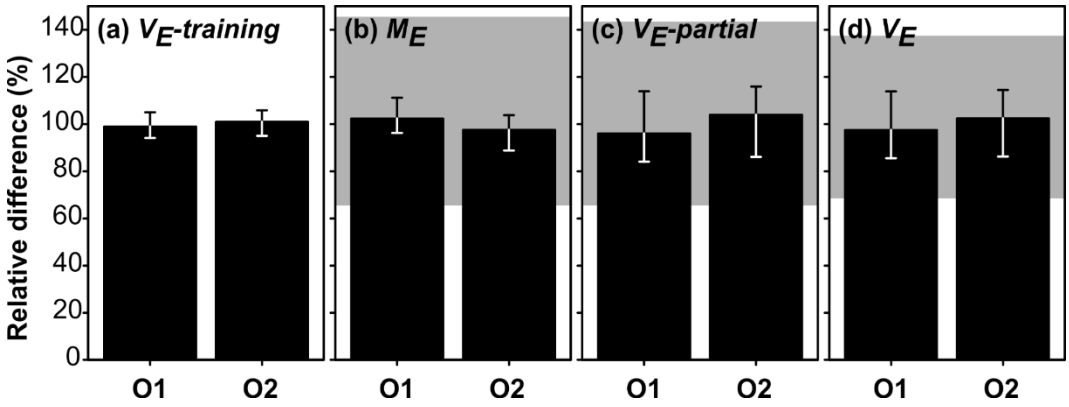

Figure 4.9. Inter-operator variability in the estimation of Celtic Sea megabenthos standing stock biomass. Variability, as 95% confidence interval of individual operator mean value, is illustrated as relative difference (%) from the joint mean value (i.e. 100%) of the two operators (O1, O2). **(a)** Total biovolume estimated by the generalised volumetric method (GVM) for an initial training dataset (V_E-*training*). **(b)** Total survey biomass estimated using the length-weight-relationship (LWR) approach (M_E, i.e. equation 4.1). **(c-d)** Total survey biovolume estimated using the GVM, excluding (c; $V_{E\text{-}partial}$, i.e. equation 4.3) and including (d; V_E, mL) those taxa for which LWR estimation was not possible. The shaded bands (b-d) represent the variability, as 95% confidence intervals, of the full survey estimates of the corresponding standing stock parameter (i.e. M_E, $V_{E\text{-}partial}$, V_E).

4.4.4 Generalised volumetric method

Individual body size and total biomass of the megabenthos are essential variables given their central roles in the regulation of marine ecosystems. Yet, the lack of an appropriate and cost-effective method, applicable at broad scale, has limited their consideration in the framework for ocean observing. The increasing use of robotic technologies, remotely operated vehicles and particularly autonomous underwater vehicles, to study the seafloor, has delivered new opportunities for the quantitative assessment of the megabenthos across a range of spatial scales and environments. The collection and analysis of large amounts of photographic data (digital stills, digital video, chemical films) does bring new challenges, including the estimation of biomass in the absence of physical specimens or prior knowledge of LWRs. In these cases, we suggest that the use of the generalised volumetric method (GVM) offers an effective means to estimate biovolume. Indeed, given that the volumetric method appears to outperform the length-weight-relationship method even where extensive prior information is available (e.g. PAP-SO and UK Celtic Sea sites), we would suggest that it is considered for use more generally. We would also again note that there is clear evidence that LWRs can exhibit substantial taxon, time, and location, specificities that have the

potential to introduce appreciable biases to biomass estimates where those variations in LWRs are not known or controlled. It may also be worth noting that to describe how individuals acquire and use energy, some ecological models adopt biovolume as their main body-size currency, such as dynamic energy budget (DEB) models (Kooijman 2000) that typically include 'structural length' (i.e. biovolume$^{1/3}$) as a primary variable (e.g. Sousa et al. 2010), under the assumption that most physiological processes are volume dependant.

The GVM does require the user to convert virtually the specimen into a compressed cylinder of equivalent volume in order to best estimate *ECD* and *ECL*. We would therefore recommend the user should have significant zoological experience, be familiar with the morphology of the taxa involved, and ideally, have prior experience with handling comparable physical specimens (see recommendations in section 4.3.2). The GVM necessarily incorporates a subjective element in this conceptual specimen-to-cylinder conversion. Consequently, multiple users contributing to a common dataset should inter-calibrate their approach, as we have illustrated in the Celtic Sea case study trial. It may be impossible to eliminate all such differences in measurement within and between analyses (e.g. Mazurkiewicz et al. 2016); however, some simple precautions, such as randomisation, can readily be implemented (see recommendations in Durden et al. 2016b, c). For example, in the Celtic Sea case study trial, we ensured that each operator was randomly allocated images from the full image set available to avoid bias between AUV deployments and between habitat types. Similarly, we randomised the order in which each operator assessed images in order to avoid temporal variation in the operator's performance being unintentionally translated into spatial variation, had the images been analysed in the original field sequence.

There are clearly opportunities for further development of the generalised volumetric method. One is in the automation of the basic process, as has been achieved for particulate organic matter (Iversen et al. 2010) and nematode biovolume assessment (Moore et al. 2013; Mazurkiewicz et al. 2016). This could be more challenging in the case of megabenthos in seafloor photographs; firstly, because the complex background (i.e. the seafloor) makes in situ specimen delineation more involved, and secondly, because of

the wide variety of body shapes exhibited across taxa. Nevertheless, automation could be achieved through recent rapid advances in machine vision and in machine learning (Schoening et al. 2012, 2016; Langenkämper and Nattkemper 2017). Machine recognition of basic morphological types could enable automated application of our proposed method. A second challenge will be to improve the conversion of estimated biovolume (fresh wet weight mass) to units of carbon mass and energy that may be particularly valuable in the application of numerical modelling frameworks such as the metabolic theory of ecology (Brown et al. 2004) and DEB (Kooijman 2000) models in the assessment of ecosystem stocks and flows. Conversions from wet weight are widely available (e.g. Brey et al. 2010) and serve as a useful approximation, i.e. by assumption of volumetric mass density (e.g. 1.056; see 3.2. Validation with physical specimens).

4.5 Conclusions

Biomass is a key ecological variable that informs the fields of conservation, environmental quality assessment, resource management, and the study of the stocks and flows of mass and energy through ecosystems. It is featured as an essential biodiversity variable (EBV) and as an 'emerging' essential ocean variable (EOV), prompting the need for a method for the measurement of individual biomass, which is broadly applicable and which can be readily adopted by a wide range of users. In seafloor imagery, the traditional LWR approach employed to derive individual biomass relies on pre-existing taxon-specific data and may be subject to systematic, temporal and spatial variation. The LWR method is also restricted to readily sampled taxa that have a fixed body form. These significant limitations may be overcome with the taxon-independent generalised volumetric method described here. The predictive ability of the GVM, in accuracy and in precision, appears to at least equal that of the LWR approach, and it has much more general and much more immediate applicability.

Chapter 5

Shelf-sea sites

This chapter is divided in two parts. Part A is a published work that I undertook during this Ph.D. programme, which deals with the ecological assessment of benthic megafauna assemblages in a marine conservation zone on the Celtic Shelf, using mass photography by autonomous underwater vehicle (Benoist et al. 2019a). Part B is the body-size spectral analysis of the two shelf-sea megabenthic assemblages assessed in this thesis.

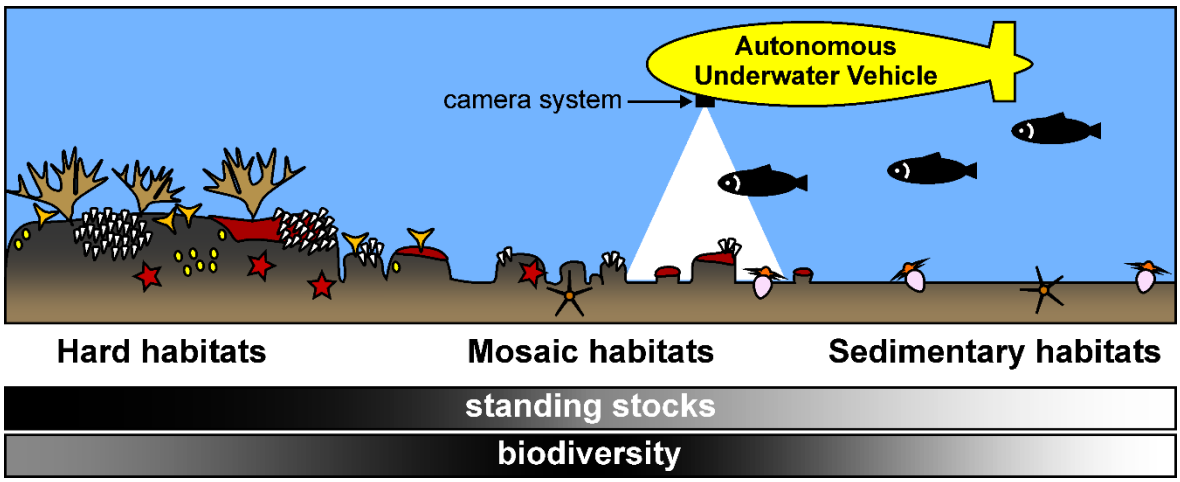

AUVs offer a solution to monitoring challenges posed by the mixed habitats and growing spatial extent of marine protected areas globally. Photographic survey by autonomous underwater vehicle offers an effective and efficient means of surveying large areas of seafloor and multiple habitat types to a common, consistent, and repeatable standard. (Graphical abstract; Benoist et al. 2019a)

Part 5.A

Monitoring mosaic biotopes in a marine conservation zone by autonomous underwater vehicle

Benoist NMA[a,b], Morris KJ[a], Bett BJ[a], Durden JM[a,b,c], Huvenne VAI[a], Le Bas TP[a], Wynn RB[a], Ware SJ[d], Ruhl H[a]

[a] National Oceanography Centre, Southampton SO14 3ZH, UK
[b] University of Southampton, Southampton SO14 3ZH, UK
[c] University of Hawaii, Honolulu HI 96822, USA
[d] Centre for Environment Fisheries and Aquaculture Science, Lowestoft NR33 0HT, UK

Published in Conservation Biology*, March 2019, **33**(5), 1174-1186. DOI: 10.1111/cobi.13312. Literature cited can be found in the reference section of the Ph.D. thesis, supplementary material to the research publication and the acknowledgements are provided in appendix A. As presented in this chapter, the different sections, figures, and tables, were renumbered sequentially to comply with formatting of the other chapters. The graphical abstract is presented on the preceding cover page of this chapter.*

5.A.1 Abstract

The number of marine protected areas (MPAs) has increased dramatically in the last decade and poses a major logistic challenge for conservation practitioners in terms of spatial extent and the multiplicity of habitats and biotopes that now require assessment. Photographic assessment by autonomous underwater vehicle (AUV) enables the consistent description of multiple habitats, in our case including mosaics of rock and sediment. As a case study, we used this method to survey the Greater Haig Fras marine conservation zone (Celtic Sea, northeast Atlantic). We distinguished 7 biotopes, detected statistically significant variations in standing stocks, species density, species diversity, and faunal composition, and identified significant indicator species for each habitat. Our results demonstrate that AUV-based photography can produce robust data for ecological research and practical marine conservation. Standardizing to a minimum number of individuals per sampling unit, rather than to a fixed seafloor area, may be a valuable means of defining an ecologically appropriate sampling unit. Although composite sampling represents a change in standard practice, other users should consider the potential benefits of this approach in conservation studies. It is broadly applicable in the marine environment and has already been successfully implemented in deep-sea conservation and environmental impact studies. Without a cost-effective method, applicable across habitats, it will be difficult to further a coherent classification of biotopes or to routinely assess their conservation status in the rapidly expanding global extent of MPAs.

Keywords: marine protected area; seafloor; benthos; biotope classification; mosaic habitats; ecological metrics

5.A.2 Introduction

Acquiring ecological data is key to basic biological research, monitoring change in biodiversity, and the development of effective conservation actions. Achieving those aims in a timely and cost-effective manner remains a significant challenge in terrestrial and aquatic systems. In both cases, drones – unmanned aerial vehicles (UAVs) and autonomous underwater vehicles (AUVs) – promise significant advances in capability (Anderson and Santana-Gaston 2013; Wynn et al. 2014).

Marine protected areas (MPAs) have long been suggested as a tool for maintaining and restoring biodiversity (Woodcock et al. 2017), and the designation of numerous MPAs is now driving the need for better and more cost-effective description and quantification of the biological assemblages present and their habitats. Autonomous underwater vehicles are an established technology in seafloor research (Durden et al. 2016c) and appear to be an effective tool in science- and conservation-driven studies both in shelf-sea (Marzinelli et al. 2015) and deep-sea (Morris et al. 2016) environments. They offer rapid, nondestructive data collection, access to a wide range of habitats, and reduced survey costs (Wynn et al. 2014). AUV data can improve the quantification of conservation metrics (Durden et al. 2016a) and may be of particular value in habitats where remote sampling methods are ineffective, such as reef or rock habitats (Tolimieri et al. 2008).

MPAs typically encompass multiple habitats, and the use of varying samplers (e.g. grabs, trawls, towed cameras) has limited the degree to which the resultant data can be synthesized across substratum types. The European Nature Information System (EUNIS) provides a classification of habitats and biotopes that has been influential in standardizing habitat description (Costello 2009), although its limitations have become evident as conservation-based marine mapping has expanded. In particular, important mixed, or mosaic, marine habitats "cannot be represented using the current EUNIS classification system as it only recognizes separate rock or sediment habitats" (Galparsoro et al. 2012: page number 2634). Mosaic habitats likely play a key role in the connectivity that underpins the functioning of MPA networks (Olds et al. 2016), and how they might best be classified remains an area of active debate (Dauvin 2015). It is the rule-based hierarchical nature of EUNIS (e.g. rock or

sediment) that poses the problem, which may similarly impact other hierarchical systems (Harris 2012).

Where habitat-type-dependent field methods are employed, a single biotope classification scheme can be difficult or impossible to operate (van Rein et al. 2009). Different field methods also introduce major mismatches in both the spatial scale observed and in the corresponding body sizes and taxonomic groups assessed. These difficulties could be reduced and the full potential of AUV-based monitoring realized if visual assessment by photography could be implemented usefully across multiple biotopes. The benefits include use of common scales and methods across habitats and consequently a common classification scheme; explicit recording of the species and habitats that underpin MPA designation and legislation; and direct evidence of violating activities from indicators such as trawl marks and human debris. However, as Galparsoro et al. (2012) indicate, two questions remain: how robust are visually based classifications and what constitutes an appropriate sampling unit in photographic assessments?

To tackle these questions, we undertook an AUV survey in the Greater Haig Fras marine conservation zone (MCZ) (Wynn et al. 2014) (figure 5.A.1a, b). Nested within the MCZ is the Haig Fras special area of conservation (SAC) that includes a bedrock outcrop reef. The MCZ has substantial areas of mixed rock-sediment habitat that are difficult to assess by physical sampling. We used AUV data to investigate whether mosaic biotopes can be adequately described and discriminated on the basis of visual data; to establish potential links between biotope characteristics and substratum type and complexity, to demonstrate the potential effectiveness of the method; and to examine the influence of sampling unit choice in a practical conservation assessment of complex habitats.

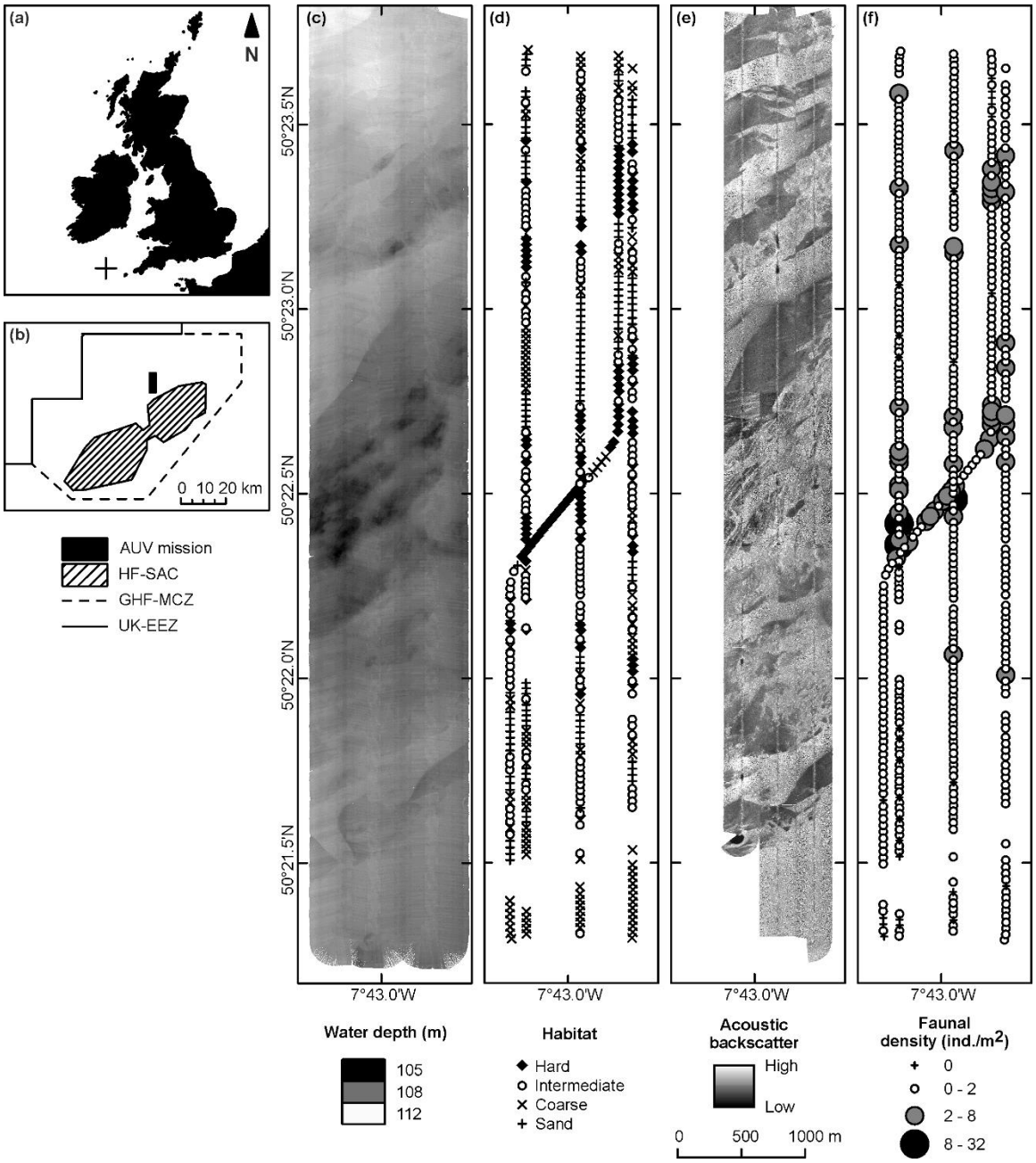

Figure 5.A.1. AUV photographic survey. (a) Location of the Greater Haig Fras marine conservation zone (GHF-MCZ) in the Celtic Sea, **(b)** area of autonomous underwater vehicle survey and adjacent Haig Fras special area of conservation within the GHF-MCZ, **(c)** bathymetry, **(d)** photographic habitat classification (hard, ≥ 50% seafloor cover by bedrock, boulder, cobbles; intermediate, ≥ 10% seafloor cover by bedrock, boulder, cobbles; coarse, > 90% seafloor cover by gravelly sand, granules, pebbles, shells; sand, > 90% seafloor cover by sand), (e) sidescan sonar backscatter intensity, and **(f)** photographic estimate of faunal numerical density (combined invertebrates and demersal fish; > 1 cm body length).

5.A.3 Methods

5.A.3.1 Field survey

All data were derived from a 16-hour deployment of the AUV *Autosub6000* in July 2012 (Ruhl 2013) during which the vehicle undertook three dives: swath bathymetry survey (dive 1) (figure 5.A.1c); photographic survey from a target altitude of 3.2 m above the seafloor with a Point Grey Research Grasshopper 2 camera (Morris et al. 2014) (dive 2); and a sidescan sonar survey (dive 3) (figure 5.A.1e). The swath bathymetry and sidescan sonar survey methods are detailed, but we used only data from the single photographic survey dive (duration 225 minutes) in our analyses here. The photographic survey was carried out as 4 north-south transect lines and 1 crossing line (figure 5.A.1d, f) that targeted a rock outcrop of slightly elevated terrain (figure 5.A.1c) with sinuous striations in the sonar view (figure 5.A.1f).

5.A.3.2 Image data generation

Images were processed to improve non-uniform illumination and color representation, rectified to a common scale (0.59 mm/pixel), georeferenced, and mosaicked into groups of five consecutive images (tiles) (Morris et al. 2014). In total 2637 such tiles were produced, each representing approximately 7.3 m^2 of seabed. Tiling was undertaken to remove overlap from consecutive photographs and as a practical convenience to reduce the data management overhead. Tiles were assessed in random order to avoid bias through knowledge of spatial proximity (Durden et al. 2016b). We present results from three distinct sampling units: tile (primary sampling element, physical scale approximately 7.3 m^2, variable number of specimens); composite area (multiple tiles, approximately 150 m^2, variable number of specimens); composite individuals (multiple tiles, approximately 150 specimens, variable seabed area) (table 5.A.1).

Three primary substratum types were recorded: hard substrata (bedrock, boulder, cobbles), coarse sediments (gravelly sand, granules, pebbles, shells), and sand. A primary substratum type was attributed based on majority (≥ 50%) tile area, and a secondary type was recorded if present (≥ 10%). The combination of primary and secondary types yielded four mixed, or

mosaic, substratum categories (e.g. Post et al. 2011) (appendix A). For presentation and analysis, the substratum classes were simplified into summary habitats (table 5.A.1): hard habitats with hard primary substratum, intermediate habitats with hard secondary substratum, and coarse habitats and sand habitats (jointly referred to as sedimentary habitats) where hard substratum was absent. We did not observe coarse and sand mosaic-habitat during the survey. Litter and other human debris on the seabed were also recorded (appendix A).

Table 1. 5.A.1. Photographic effort by habitat and substratum type, given as total survey and composite sample values (Ind., individuals).

		Total				Composite area			Composite individuals		
Habitat	**Substratum[a]**	**Tiles**	**Area (m^2)**	**Area (%)**	**Ind.**	**n**	**Area (m^2)[b]**	**Ind.[b]**	**n**	**Area (m^2)[b]**	**Ind.[b]**
Hard	H	121	882	4.6	2832	6	147	472	19	16	149
Hard	Hc	211	1564	8.1	3648	10	156	265	59	27	147
Hard	Hs	214	1656	8.6	4135	10	165	414	61	27	148
Intermediate	Ch	584	4255	22.1	1476	29	146	51	12	355	148
Intermediate	Sh	119	874	4.5	389	6	145	65	12	73	130
Coarse	C	669	4836	25.2	446	33	146	14	3	1612	149
Sand	S	719	5156	26.8	966	36	143	27	6	859	138
Mean							150	187		229	147
Total		2637	19223	100.0	12892	130			84		

[a] Primary substratum (H)ard, (C)oarse, and (S)and, secondary substratum corresponding lower case.

[b] Mean of replicates.

Invertebrates and demersal fish (> 1 cm body length) were counted, measured, and identified to the lowest taxonomic or morphotype unit possible (e.g. Althaus et al. 2015). For colonial and encrusting organisms, the greatest diameter of individual colonies, or patches, was measured. Solitary tubicolous polychaetes, bivalves, and gastropods were observed but excluded from the analyses to avoid inclusion of empty tubes or shells. Indeterminate specimens (< 1% of total) were excluded from subsequent analyses. Body-size measurements were converted to estimated gram wet weight biomass via existing length-weight relationships (appendix A).

5.A.3.3 Faunal community analysis

We considered the complete set of tiles to represent the total statistical population (i.e. assessments were carried out within that population) and made no statistical inference beyond that population. Our primary objective was to test for biological differences between habitats; therefore, we first grouped the tiles by substratum type. In our case, and in many marine settings, a single photograph (or tile) was insufficient to establish a useful estimate of species diversity or species composition. Consequently, we compiled data from multiple tiles to form our sampling units (replicates). Given the non-independent nature of consecutive tiles and the inevitable occurrence of spatial autocorrelation (Legendre 1993), we compiled the data from individual tiles at random within substratum type to form composite-area sampling units of approximately 150 m^2 per replicate (table 5.A.1). A simplified illustration of this method and formal testing of the randomization process are given in the appendix A. We tested the effect of sampling unit choice in the same manner (composite-individuals sampling units of approximately 150 individuals per replicate) (table 5.A.1 and appendix A).

For density and biomass analyses, individual tile data were log-transformed and assessed using Welch's one-way analysis of variance (ANOVA). Subsequent pairwise comparisons were made using the Games-Howell method, as implemented in Minitab (version 17) (Minitab Limited, Coventry, United Kingdom). To estimate density and biomass at physical scales greater than a single tile, data were repeatedly, randomly, accumulated with replacement to form larger physical samples of 2 to 724 tiles, and a median value was derived from the repeats (in R environment) (R Core Team 2016).

For faunal diversity and composition analyses, replicate-level data (composite area and composite individuals) (table 5.A.1) were assessed. Faunal diversity was assessed by sample-based rarefaction to estimate taxon richness (Sest) (Colwell et al. 2012), the exponential form of the Shannon index (expH′) (Magurran 2004), and the inverse form of Simpson's index (1/D) (Magurran 2004), as calculated via 1000 randomizations without replacement for Sest, and with replacement for expH' and 1/D, in EstimateS (version 9.1.0) (Colwell 2013). Faunal composition was assessed by 2-

dimensional non-metric multidimensional scaling ordination based on the Bray-Curtis dissimilarity of log-transformed faunal density data and subsequent analysis of similarities (ANOSIM), all implemented using PRIMER (version 6.1.11) (Quest Research Limited, Auckland, New Zealand) (Clarke and Warwick 1994). Morphotype specificity and fidelity to particular substratum types was assessed by the indicator value method, as implemented in the R package indicspecies (De Cáceres and Legendre 2009), and by two-way indicator species analysis (TWINSPAN) (Hill 1979), as implemented in the software package PC-ORD (version 4) (Wild Blueberry Media Limited Liability Company, Corvallis, United States of America) with 5 logarithmically arranged density levels. To evaluate the choice of sampling unit we produced auto-similarity curves (Schneck and Melo 2010), as employed by Durden et al. (2016b) in an assessment of seabed photography. The method calculates the average Bray-Curtis dissimilarity between pairs of composite samples formed from increasing numbers of tiles by random resampling of the original data within habitat type (1000 times without replacement; in R environment).

5.A.4 Results

5.A.4.1 Standing stocks

Whether assessed using tile-level or composite-area-replicate data, faunal density exhibited a statistically significant difference between habitats (Welch's ANOVA, $p < 0.001$) (figure 5.A.2a, b); hard habitats had the highest density and coarse the lowest. All pairwise comparisons were significant (Games-Howell, $p < 0.05$). Area-scaled density by habitat followed the same trends; apparent median density rapidly stabilized with seabed area assessed in all habitats (figure 5.A.2c). Faunal biomass also varied significantly between habitats when assessed using tile-level data (Welch's ANOVA, $p < 0.001$) (figure 5.A.2a); hard habitats had the highest biomass and coarse the lowest. Pairwise comparisons indicated significant differences between all habitats (Games-Howell, $p < 0.05$), except between intermediate and sand (Games-Howell, $p = 0.14$). When assessed using composite-area-replicate data, biomass also varied significantly between habitats (Welch's ANOVA, $p < 0.001$) (figure 5.A.2b); however, the magnitude of differences was

substantially reduced. Pairwise comparisons indicated significant differences between all habitats (Games-Howell, $p < 0.05$), except between intermediate and sand (Games-Howell, $p = 0.98$) and between coarse and sand (Games-Howell, $p = 0.15$). Area-scaled biomass by habitat followed the same trends; however, apparent median biomass was slow to stabilize with seabed area assessed. Estimated biomass in hard habitat stabilized at approximately 650 m^2 and in other habitats at approximately 2000 m^2 (figure 5.A.2d).

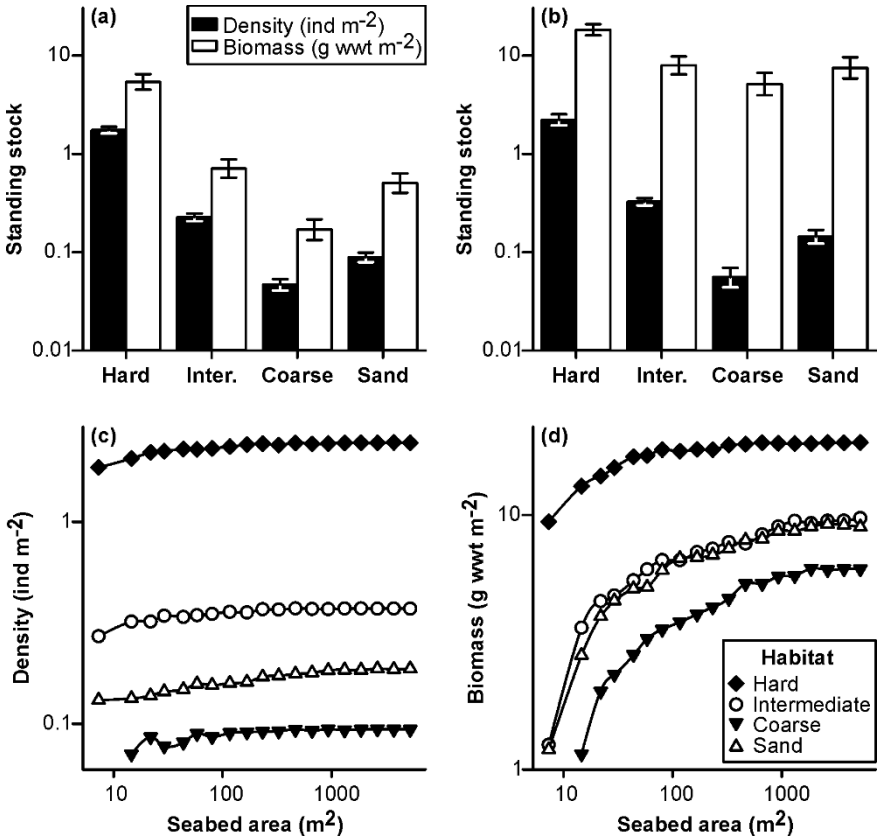

Figure 5.A.2. Standing stock by habitat determined at **(a)** tile scale (c. 7.3 m^2) and **(b)** composite area sample scale (c. 150 m^2), illustrated as geometric mean and 95% confidence interval, together with **(c)** median density, and **(d)** median biomass estimated from increasingly large seabed areas.

5.A.4.2 Faunal diversity

Assessed by composite-area replicates, taxon richness (Sest) exhibited statistically significant differences between habitats; hard and intermediate were notably richer than coarse or sand habitats (figure 5.A.3a). However, these differences were less clear-cut when rarefied by number of individuals (figure 5.A.3d). In contrast, heterogeneity diversity (expH') and dominance

diversity (1/D) showed consistent, statistically significant differences between intermediate and other habitats whether rarefied by area or individuals. Intermediate habitat was the most diverse and sand the least (figure 5.A.3b, c, e, f). These patterns were consistent whether analysed based on composite-area or composite-individuals replicates (figure 5.A.3g, h).

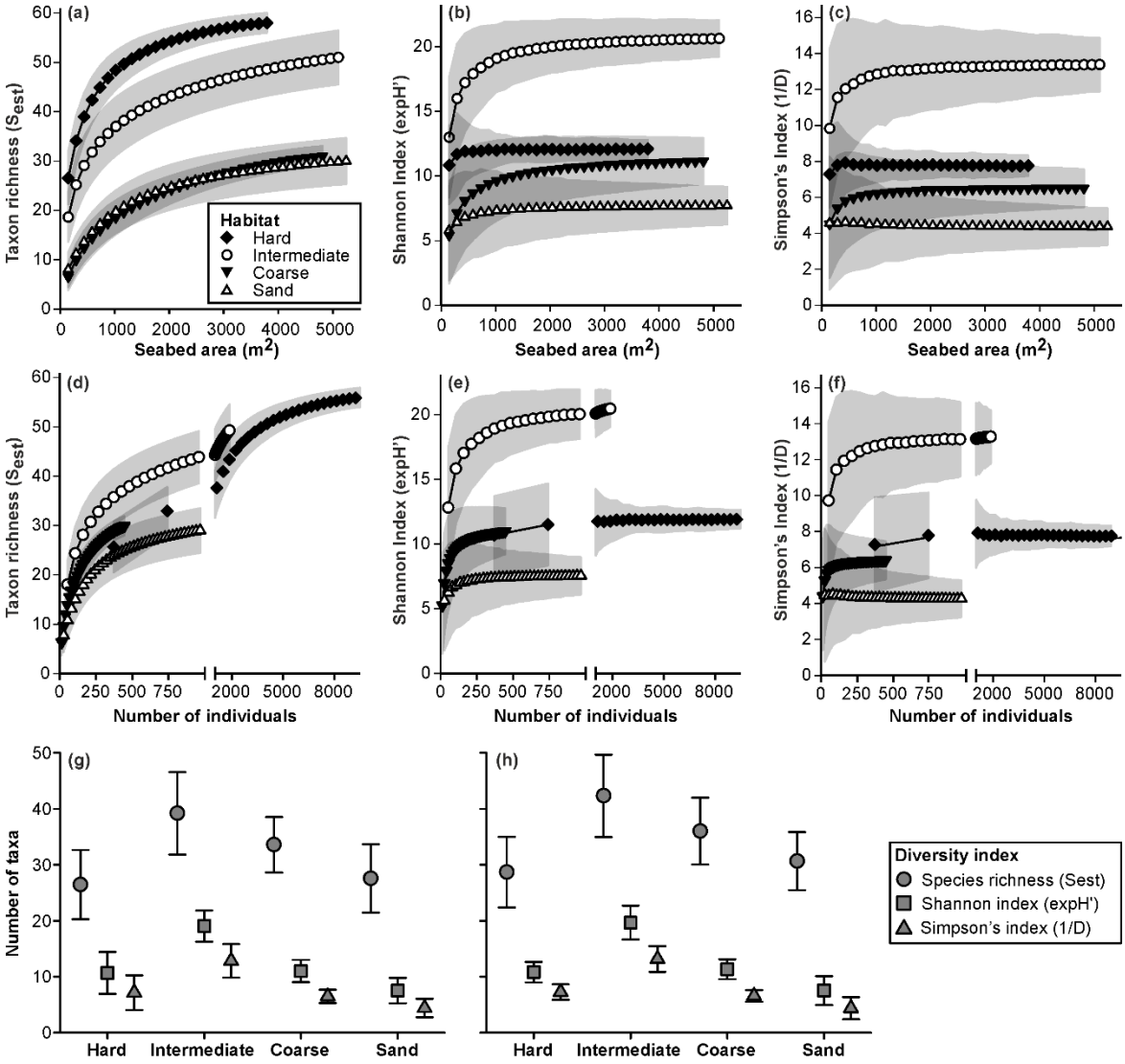

Figure 5.A.3. Sample-based rarefaction of diversity by habitat for **(a-g)** composite area samples, and **(h)** composite individuals samples, as mean and 95% confidence interval (shaded area or error bar). (g) Simplified results for composite area samples, illustrated at an approximately equal number of individuals (364-375) across habitats. (h) Simplified results for composite individual samples, illustrated for the three-sample case, having an approximately equal total number of individuals (446-483) across habitats.

5.A.4.3 Faunal composition

Faunal composition in composite-area replicates varied significantly with substratum type (ANOSIM, R = 0.80, $p < 0.001$). Ordination suggested three distinct sample groupings, corresponding with the hard, intermediate, and sedimentary habitats (figure 5.A.4a), that were ordered by the relative occurrence of hard substratum. Within each of these three primary groups, samples were also well ordered by the relative occurrence of coarse and sand substrata (appendix A). All pairwise comparisons of faunal composition by substratum type were statistically significant (ANOSIM R = 0.36-1.00, $p < 0.05$) (appendix A). Indicator species analysis suggested numerous taxa as statistically significant indicators for hard habitats, single taxa for the intermediate and coarse habitats, and three taxa for the sand habitat (table 5.A.2 and appendix A). Two-way indicator species analysis (TWINSPAN) almost perfectly divided the samples into the visually determined summary-habitat classes, on the basis of faunal composition alone. All hard (n = 26), intermediate (35), and coarse (33) samples were correctly classified; 4 of the 36 sand samples were misclassified as coarse (table 5.A.2).

Faunal composition in composite-individuals replicates also showed very clear groupings, corresponding with the hard, intermediate, and sedimentary habitats, and separation of the coarse and sand habitats (figure 5.A.4b). All pairwise comparisons of faunal composition between habitats were statistically significant with strong differentiation in most comparisons (ANOSIM R = 1.0, $p \leq 0.002$), except between coarse and sand, which were nonetheless statistically significant (ANOSIM R = 0.53, $p = 0.036$). Auto-similarity curves for the 4 summary habitats varied considerably when assessed in terms of seabed area sampled (figure 5.A.4c). That variability was substantially reduced when assessed in terms of the number of individuals sampled (figure 5.A.4d), reflecting the major difference in faunal density between habitats (e.g. figure 5.A.2). To achieve a target assemblage description level of 0.75 self-similarity, composite-area samples would vary from 90 to 1840 m^2 between habitats or from 140 to 220 specimens per composite-individuals sample.

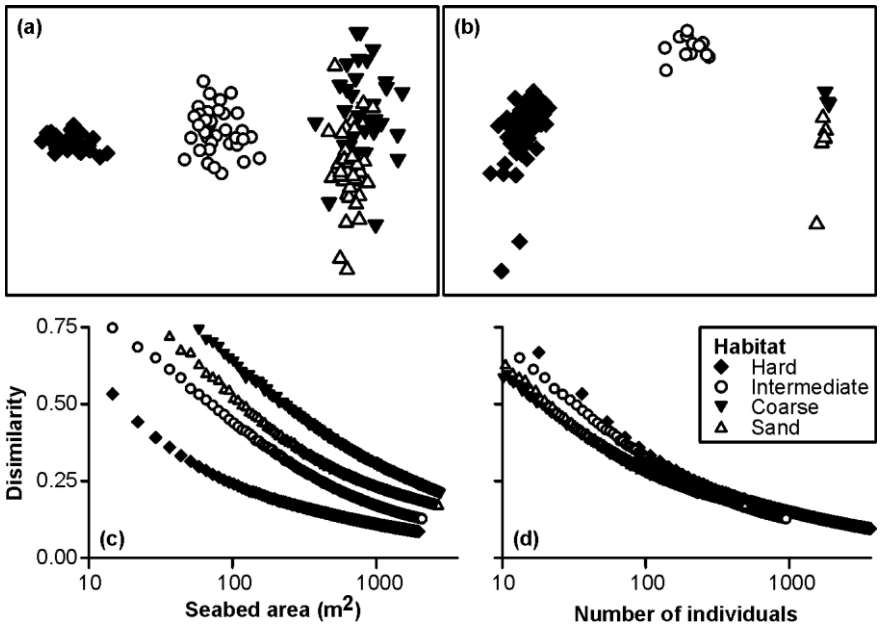

Figure 5.A.4. Variation in faunal composition and auto-similarity with habitat type. (hard, ≥ 50% seafloor cover by bedrock, boulder, cobbles; intermediate, ≥ 10% seafloor cover by bedrock, boulder, cobbles; coarse, > 90% seafloor cover by gravelly sand, granules, pebbles, shells; sand, > 90% seafloor cover by sand). **(a)** 2-dimensional non-metric multidimensional scaling ordination of Bray-Curtis dissimilarity of log-transformed numerical density of combined invertebrates and demersal fish (> 1 cm body length) in composite-area samples and in **(b)** composite-individuals samples, and auto-similarity curves plotted by **(c)** seabed area sampled and **(d)** number of individuals sampled.

Table 5.A.2. Summary of indicator species analyses. Indicator species (bold) and preferentially occurring taxa are listed together with corresponding composite area sample groups, and frequency of occurrence in (H)ard, (I)ntermediate, (C)oarse, and (S)and habitats.

Two-way indicator species analysis					**Indicator species analysis**				
D1[a]	**Taxa**	**D2[a]**	**Taxa**	**Samples[b]**	**Taxa[c]**	**Frequency (%)**			
						H	**I**	**C**	**S**
1	**Bryozoa 01** Porifera 23 Axinellidae spp.	1.1	**Axinellidae spp.** *Porella* sp. *Parazoanthus* sp.	26 × H	***Parazoanthus* sp.**	100.0	34.3	3.0	0.0
					Axinellidae spp.	100.0	77.1	0.0	0.0
					***Porella* sp.**	100.0	74.3	0.0	0.0
					Porifera 20	100.0	28.6	0.0	0.0
					Salmacina dysteri	100.0	65.7	0.0	5.6
					***Munida* sp.**	100.0	74.3	3.0	5.6
					Echinus esculentus	96.2	37.1	0.0	0.0
					***Reteporella* spp.**	100.0	40.0	0.0	5.6
					Stichastrella rosea	100.0	60.0	27.3	19.4
					***Antedon* spp.**	80.8	28.6	3.0	2.8
		1.2	Anthozoa 34 Anthozoa 39 *Lepidorhombus whiffiagonis*	35 × I	**Anthozoa 39**	7.7	42.9	12.1	2.8
2	Perciforme spp. 10 Gadidae spp. Paguridae 02	2.1	***Bolocera* spp.** Anthozoa 16	33 × C 4 × S	**Paguridae 01**	3.8	0.0	21.2	8.3
		2.2	**Paguridae 02** **Cerianthid 01** **Anthozoa 03**	32 × S	**Perciforme spp. 10**	0.0	5.7	6.1	33.3
					***Liocarcinus* spp.**	0.0	5.7	3.0	25.0
					Hippoglossoides platessoides	3.8	2.9	0.0	19.4

[a] First (1) and second (2) hierarchical divisions of samples.

[b] Number of samples from each habitat classified in corresponding division.

[c] Statistically significant ($p < 0.05$) indicator species, note only top 10 of 28 are listed for hard habitats.

5.A.5 Discussion

The area surveyed was characterized by the presence of sand and coarser-grained sedimentary environments, together with outcropping bedrock, boulder, and cobble substrata. We believe that the variety and complexity of the physical environment of the Greater Haig Fras marine conservation zone represents a good test area for the conservation assessment of other large marine protected areas. From an ecological perspective, the presence of hard substrata exerted a strong positive control on faunal density, biomass, and total species richness; mosaic habitats substantially enhanced faunal diversity; and all habitats and mosaics supported distinct faunal assemblages. Photographic assessment provided a uniform field- and data-analysis method across rocky and sedimentary habitats that enabled us to make a direct assessment of multiple biotopes and their occurrence in mosaic form. This ability to resolve ecologically significant information, at broad-scale, across multiple and mixed habitats, suggests that the AUV-based photographic survey was an effective and efficient practical conservation tool in the present case and indicated its potential value in other similarly complex marine habitats.

5.A.5.1 Mosaic habitats

Intermediate habitats, or mosaics of hard substratum within a sedimentary matrix, represented one quarter of the seafloor area observed. Their ecological characteristics were largely predictable as an admixture of their component habitats and consistent with a simple ecotone concept (Odum and Barrett 2005). Faunal density in intermediate habitats was significantly different from, and transitional to, both hard and sedimentary habitats. Regardless of whether rarefied by individuals or seabed area, heterogeneity diversity measures were significantly elevated in intermediate habitats over both hard and sedimentary habitats. This suggests that the addition of the two assemblages (i.e. hard and sedimentary) acted to reduce the dominance component of diversity in the combined assemblage.

When taxon richness was assessed as species density (Whittaker et al. 2001), intermediate habitats were significantly different from, and transitional to, both hard and sedimentary habitats (hard > intermediate > coarse ~

sand). However, when assessed as number of species per individual, the habitats were not statistically distinct and were ordered differently (intermediate > coarse > hard > sand). Species density and total faunal density exhibited the same pattern and might both be controlled by resource availability. In contrast, heterogeneity diversity appeared to exhibit a different pattern related to seafloor-habitat complexity: uniform sediment (sand) < mixed sediment (coarse) < topographically complex cobble, boulder, or bedrock (hard) < mosaicked hard substratum islands in a sedimentary matrix (intermediate). Environmental heterogeneity is thought to be a key driver of species richness (Yang et al. 2015), as was evident in our study, although the effect was more pronounced in the case of heterogeneity diversity.

Mosaic habitats are thought to play a key role in the connectivity of marine ecosystems, in terms of both secondary productivity and the maintenance of biological diversity (Olds et al. 2016). They can represent corridors, or stepping-stones, facilitating the movement of organisms and thereby facilitating processes between dispersed primary habitats. In the case of Haig Fras, the SAC protects what is thought to be the only substantial area of offshore rocky reef habitat in the Celtic Sea. The substantial presence of mosaic habitats in our survey area, and more widely in the Celtic Sea (Thompson et al. 2017), indicates both the potential connectivity of dispersed rocky reefs in the region and the need to protect some of that mosaic habitat in the background environment. These observations provide strong support for the calls to both record (classify) and quantify these mosaic habitats (e.g. Galparsoro et al. 2012; Dauvin 2015). There is also an obvious need to define the physical scale at which the occurrence of mosaics is practically assessed and at which conservation policies might be applied. The quality of the intervening matrix environment may determine the effectiveness of connectivity (Baum et al. 2004) and has been a matter of concern in terrestrial conservation schemes (Donald and Evans 2006).

5.A.5.2 Practical conservation

The UK has implemented over 200 MPAs, with over 27 million km^2 of MPA now designated globally (UNEP-WCMC and IUCN 2019). The routine monitoring of such a large network implies substantial financial costs. We

consider that AUV-based assessment offers a cost-effective solution (Wynn et al. 2014). Our survey can be approximated as a 20-km track accomplished at 1.38 m/s (2.7 knots) (i.e. approximately 4-hour duration). Fitting an identical camera and image storage system to a towed platform, or remotely operated vehicle, and operating at 0.26 m/s (0.5 knots), the survey would require at least 21 hours of ship time. In the case of a towed platform, sea state (swell waves) can be expected to render about 25% of images unusable. Therefore, the effective survey speed is 0.20 m/s, and the full survey would require at least 28 hours of ship time. Consequently, in the case of our survey, the AUV-based approach offers a potential 86% saving on ship-time cost or carbon footprint compared with an equivalent towed camera survey, and perhaps a 96% saving if the ship carries out other useful work for three hours while the AUV is submerged.

In terms of cost effectiveness and conservation effectiveness, survey design may be a key factor, raising two fundamental questions: what sampling unit is required to obtain suitably accurate and precise data (Galparsoro et al. 2012) and how should the survey be conducted (Foster et al. 2014)? Our study demonstrates that AUV photography can provide enhanced information on the nature of the substratum and its associated fauna. The distribution of the identified habitat types closely matched the sidescan sonar mapping, suggesting consistency and accuracy in the visual assessment method. That we were able to detect statistically significant differences in the key ecological parameters (standing stock, species richness and diversity, faunal composition, and indicator taxa) suggests the technique can produce suitably robust data. Visual monitoring also provided direct evidence of human impacts in the form of lost or discarded fishing gear and plastic debris at the seabed (appendix A).

Although our survey was undertaken in a fixed grid form, suited to the complete bathymetric and sidescan sonar mapping of the area, our subsequent treatment of the photographic data changed the character of the biological survey. By partitioning the seafloor into substratum types and then randomly forming sampling units within those types, we converted the non-random grid survey to a form of a posteriori stratified random sampling scheme. We were able to visually identify seafloor habitat type at a much

smaller physical scale (1 m^2) than we think is necessary to appropriately sample the associated fauna (≥ 150 m^2). This point may be particularly important in the development of cost-effective monitoring for complex marine habitats.

There are many potential options for AUV survey design (Foster et al. 2014); however, their implementation may require prior knowledge of environmental stratification and (or) the appropriate sampling unit. Consequently, the combined a posteriori stratification and composite sampling that we have adopted here may have broad, cost-effective, general application in many marine systems, perhaps particularly in spatially complex environments (Huvenne et al. 2011; Thornton et al. 2016). Our approach is potentially applicable to any image data set that can be partitioned into ecologically relevant subsets based on some known or identifiable environmental variable or variables. For example, Morris et al. (2016) segregated their data by topographic height to contrast the ecology of a small abyssal hill with that of the surrounding plain (northeast Atlantic); Simon-Lledó et al. (2019c) assessed ecological variation over a manganese nodule occurrence gradient in the Clarion-Clipperton Zone (northeast Pacific), partitioning their data by seafloor nodule coverage with an automated detection technique (Schoening et al. 2017); and Simon-Lledó et al. (2019b) assessed the long-term impact of simulated deep-sea mining in the Peru Basin (southeast Pacific) by segregating their data on proximity to 26-year-old seabed plough marks.

Our results suggest that parameters of conservation value exhibit various responses to the choice of sampling unit, primarily linked to the number of specimens encompassed. Numerical density (figure 5.A.1c) was essentially insensitive to unit size, contrary to biomass density (figure 5.A.1d) that was highly sensitive to unit size. Bett (2019) examined how estimated biomass may vary with sampling unit size given a power-law distribution of individual body sizes. We found that estimated species richness (figure 5.A.3a,d) was linked to sampling unit size, as have many previous authors (e.g. Sanders 1968; Colwell et al. 2012), and that similarly faunal composition (figure 5.A.4) was substantially influenced by unit size. In the case of biomass and species richness, unit size had a direct impact on the value (accuracy) of the

measured parameter. In the case of faunal composition, unit size affects the variability (precision) of resulting assessments (i.e. the ability to define, discriminate, or monitor the status of a given assemblage or biotope). Simon-Lledó et al. (2019a) reached similar conclusions in their assessment of the effect of sampling unit size on the description of deep-sea megabenthos assemblages based on AUV photography.

Anderson and Santana-Garcon (2015) tackled the issue of variability in faunal composition in a manner similar to ours. They pooled subsamples and asked how many original smaller-scale sampling units were needed to provide a reasonable measure of community structure for comparative analysis. Defining what is reasonable is likely to require case-by-case consideration of specific survey objectives. Forcino et al. (2015) considered the appropriate minimum number of specimens per sampling unit across a broad range of terrestrial and aquatic community types. They suggested a minimum number of 58 individuals per unit as adequate for multivariate analyses. However, they noted that number is likely to be higher if assemblage evenness and taxon richness are high, and ecological contrasts (in space or time) are low.

We based our assessment of the appropriate number of individuals per sampling unit on a target within-habitat dissimilarity between replicates of 0.25, yielding a range of approximately 150-250 individuals per composite sample across habitats. We aimed at standardizing sampling effort between habitat-specific samples by equalizing dissimilarity between samples within the habitats of interest, rather than simply standardizing by seabed area examined. At a more complex level, an optimized data-analysis strategy could potentially entail habitat-based rules, in our case: sand ≥ 150 and hard ≥ 250 individuals per composite sample.

Whether based on the auto-similarity curve approach we have adopted or the assessment of multivariate dissimilarity-based standard error developed by Anderson and Santana-Garcon (2015), we suggest that users consider the potential value of defining their sampling units in terms of number of individuals rather than automatically adopting an area-defined unit. We suspect this approach may have broad application in marine conservation studies, particularly those based on photographic assessments, and should be simple to implement for mass photography from both ROVs and AUVs. We

recognize this may represent a substantial departure from standard practice; nevertheless, we suggest users consider the potential benefits to their own conservation-status assessment and monitoring objectives. To produce reliable comparative assessments of marine benthic diversity, the number of individuals examined needs to be controlled (Sanders 1968), and this requirement could be valuably expanded to assessments of biomass density and faunal composition.

Marine environmental monitoring and conservation capability is increasing rapidly with the availability of new technology (e.g. Jones et al. 2019). Methods for the automated classification of seafloor images are being developed in the quantification of phytodetritus cover (Morris et al. 2016), the characterization of manganese nodule fields (Schoening et al. 2017), and the identification and coverage estimation of kelp forests (Marzinelli et al. 2015), corals, and macroalgae (Monk et al. 2018). However, the routine wide-spread use of automated detection and recognition of individual seafloor species occurrences is not yet possible, although progress seems certain in the coming years. We consider that AUVs are a mature technology (several commercial systems are available for photographic and acoustic mapping work) that offer a practical step change in marine conservation capability. The use of mass photography to achieve such aims will, however, require some change in common practices. Given the goals of cost savings per survey and use of a common method across biotopes and habitats, such change may be a key part of achieving a practical means to more effectively monitor the world’s growing network of MPAs.

Part 5.B

Body-size ecological assessment

5.B.1 Introduction

The two shelf-sea sites assessed in this Ph.D. thesis—the Greater Haig Fras marine conservation zone (GHF-MCZ) and the UK-NERC Shelf-Sea Biogeochemistry (SSB) study area—are both located on the Celtic Shelf. As described in chapter 2 (see also chapter 5.A), these two sites comprise multiple habitat types ranging from mobile sediments (muddy, fine, and coarser-grained sands) to hard substrata (cobbles, boulders, bedrock outcrop). Located on the temperate NE Atlantic shelf (c. 100 m water depth, 10 °C annual mean seabed temperature), the two sites are subject to high primary productivity (POC flux 12.5 g C m^{-2} yr^{-1}) and seasonality patterns (e.g. Davis et al. 2019). Megabenthic assemblages (invertebrates and demersal fish; $\geq$ 1 cm body length) (e.g. Bett 2019) were characterized from photographic analysis in terms of their constituent organisms across the different habitats, and standing stocks (abundance and biomass; Thomson et al. 2017; Benoist et al. 2019a; chapter 5.A.; appendices A and B), and flux (as respiration; this thesis), were quantified. To answer the main objectives (1, 2) of this Ph.D. thesis presented in chapter 1, spectral analyses of the body-size distributions of abundance, biomass, and estimated respiration flux, at the assemblage level, were performed and compared to the metabolic theory of ecology (MTE) (Brown et al. 2004) model.

Study of the body-size structure of two shelf-sea megabenthic assemblages will provide insight into community functioning, on the basis that body size relates to physiological processes (Peters 1983). The MTE model

predicts that the abundance and biomass-size spectra have slopes of -3/4 and 1/4, respectively, and that respiration flux is invariant (slope of 0), with body size. The model also predicts that the elevation of these slopes informs on both environmental temperature and resource supply. In the case of the GHF-MCZ and the SSB study sites that exhibit similar local environmental conditions, the slopes are expected to show consistent elevation. Deviation from the model may reflect the influence of uncontrolled environmental variables and/or anthropogenic impacts, as the two sites differ in their exposure to human activities; GHF was officially designated as a marine protected area in 2016 (Joint Nature Conservation Committee 2018), while the SSB study sites experience significant fishing pressure (Thomson et al. 2017).

This chapter describes the megabenthic assemblages at the GHF-MCZ and at the SSB study area, and it explores the body-size structure of these two assemblages. Ecological data consisted of three large-scale datasets of seafloor images, including two datasets collected at GHF in 2012 (GHF-1) and 2015 (GHF-2). Field survey and subsequent image processing and analysis are presented in chapter 3, and specific methodological and analytical considerations are detailed in the methods section below. Two methods were employed for generating individual body-size data: a taxon-specific length-weight relationship (LWR) approach was used with megabenthos data from the GHF site (Benoist et al. 2019a and references therein; chapter 5.A; appendix A), and a taxon-independent GVM (Benoist et al. 2019b; chapter 4) with megabenthos data from the SSB site. Spectral analyses were achieved at site scale and for each of the seafloor habitats visually identified. Considering the large proportion of demersal fish encountered during the Celtic Shelf surveys, analyses were firstly conducted excluding fish in order to examine their influence on the body-size structure of the assemblages observed. The results presented in this chapter will be compared to those of chapter 6 that deals with deep-sea megabenthic assemblages; and chapter 7 will describe how the environmental conditions (i.e. temperature and POC flux to the seabed) affects the body-size structure of shelf- and deep-sea assemblages.

5.B.2 Methods

Detailed descriptions of the field methodology employed to collect seafloor imagery data, of the photographic processing applied to the raw photographic sampling units, and of the subsequent image analysis steps, are provided in chapter 3 section 3.2, and metadata are summarised in table 3.1. Indirect estimation of individual biomass data of photographed megabenthic fauna are described fully in section 3.4, and in chapter 4. The analytical methods followed to assess the body-size distribution of the assemblage studied are defined in sections 3.5 and 3.6. These are recapitulated briefly in the sections below, and the sampling limitations specific to the analysis of these three photographic datasets are discussed at the end of this chapter.

5.B.2.1 AUV-based seabed imagery

Large-scale ecological surveys were conducted in the GHF-MCZ (GHF-1, 2012, 19,223 m^2 seabed area; Ruhl 2013; GHF-2, 2015, 5142 m^2 seabed area; Huvenne 2016; figure 3.2) and in the SSB study area (2015, 3876 m^2 seabed area; Ruhl 2016; figure 3.3) using autonomous underwater vehicles (AUVs) (figure 3.1). Seafloor images were processed to improve visual quality following Morris et al.'s (2014) methodology, and at GHF, they were mosaicked into five-image tiles (c. 7 m^2 seabed area), whereas at SSB, they were analysed individually (c. 1 m^2 seabed area). The AUV operated at 3.2 m altitude above the seafloor at GHF, and at 2.5 m altitude at SSB, yielding images with nominal seafloor pixel resolutions of c. 0.55 mm px^{-1} and c. 0.40 mm px^{-1}, respectively.

5.B.2.2 Image data generation

Seafloor images were analysed for the substratum type and for observations of epibenthic invertebrate megafauna and demersal fish (count, taxonomic identification, body-size measurement) (GHF-1, Benoist et al.

2019a; chapter 5.A; appendix A; GHF-2, Ferguson et al. in prep.[1]; SSB, Thomson et al. 2017; appendix B). The seafloor was categorised into sedimentary (M, mud; S, sand; C, coarse sediments), intermediate (I; rocks + sediments), and hard habitats (H; bedrock outcrop, boulders, cobbles), on the basis of presence/absence and areal coverage of hard substratum type (appendix A). All specimens, unitary and colonial forms, ≥ 1 cm in body length or in diameter, were retained in the analysis, with the exception of solitary tubicolous polychaetes (Sabellidae spp., Serpulidae spp.), bivalves (Pectinidae spp.), and gastropods (Trochidae spp.), to avoid inclusion of empty tubes/shells. Specimens that could not be identified at the phylum level (i.e. referred to as indeterminate; < 1% total) were excluded from subsequent analysis.

5.B.2.3 Individual biomass estimation

The three photographic datasets acquired at GHF (GHF-1, GHF-2) and at SSB were analysed by independent image analysts for seabed habitat classification, and for taxonomic assessment and individual body-size measurement of benthic specimens. Located in the northern European Atlantic shelf seas, the fauna at these two sites is well known; yet to ensure consistency in specimen identification, a morphotype catalogue was developed based on existing literature (e.g. Althaus et al. 2015; appendix F). Substantial morphometric data, obtained from long-lasting fisheries science on the Celtic Shelf, enabled the use of a length-weight relationship (LWR) approach for the estimation of individual biomass (M_E in g wwt; chapter 4 equation 4.1) (Arnaud and Do-Chi 1977; Coull et al. 1989; Merella et al 1997; Richardson et al. 2000; Robinson et al. 2010; Silva et al. 2013; Benoist et al. 2019a; appendix A). LWRs were available for 77% (65%) of the taxa identified in 2012 (2015) at GHF, and for 74% of the taxa at SSB, ruling out some of the four most abundant taxa recorded at the two sites, i.e. colonial, encrusting, or morphologically plastic forms (Axinellidae spp., Cnidaria sp. 1 and sp. 2,

[1] This study is currently in preparation for publication as "Ferguson M, **Benoist NMA**, Bett BJ, Morris K, Laguionie Marchais C, Ruhl H, Le bas T, Wynn RB, Huvenne VAI. (in prep.). [preliminary title] Repeat monitoring in a marine conservation zone using seabed AUV photography." I did the initial annotation of the photographic data in coordination with an undergraduate student during the course of this Ph.D. programme, but the analyses reported represent the result of my own work during the Ph.D.

Parazoanthus sp., *Porella* sp., and Bryozoa sp. 1). An alternative generalised volumetric method (GVM) based on geometric considerations of individual body shape was developed during the course of this Ph.D. programme, and tested with the SSB dataset (Benoist et al. 2019b; chapter 4 equation 4.3). Those results revealed no statistically significant differences between LWR- and GVM-derived biomass assessments, and the GVM enabled the inclusion of specimens for which no morphometric data was available in the literature. Therefore, at SSB, GVM-derived individual biomass data were used in this analysis. The cup corals *Caryophyllia smithii* were enumerated in 2012 at GHF, but their biomass was not estimated, except in 2015.

5.B.2.4 Standing stock analysis

Benoist et al. (2019a) investigated the effect of sample size on the resultant standing stocks of density and biomass between the habitats identified at GHF-1, comparing tile-level data (c. 7 m^2 seabed area) to composite-area-level (c. 150 m^2 seabed area) data (chapter 5.A). To create such units, the authors followed a composite-sample approach (Nussbaum and Gilbert 2001) by compiling individual tiles at random within habitat type. They found that standing stocks were significantly different between habitats, yet in the case of biomass, the magnitude of differences was substantially reduced. In this Ph.D. thesis, standing stocks at GHF and at SSB, excluding and including demersal fish data, between habitats, were evaluated using tile-level data. Individual tile data were log-transformed and assessed using Welch's one-way ANOVA (Welch 1951), with subsequent pairwise comparisons made using the Games-Howell method, as implemented in Minitab (V18.1, Minitab Inc.).

5.B.2.5 Body-size spectral analysis

Individual-based body-size spectra of abundance (N_i in ind. m^{-2}), biomass (W_i in g wwt m^{-2}), and estimated respiration flux (B_i in mg C m^{-2} d^{-1}), were constructed using $\sqrt{2}$ geometric body-size classes (M_i in g wwt) (appendix G). B_i was calculated from individual metabolic rate (I_i) using Hemmingsen's (1960) equation for standard metabolic rate of poikilotherms at 20 °C, with a site-specific temperature-correction (i.e. 10 °C; details in chapter 3 section 3.5; equation 3.1) (Gillooly et al. 2001), and multiplied by size-class

abundance (N_i). In the present analysis, the normalisation constant employed in equation 3.1 converted to 0.0259 mg C d^{-1}. A minimum number of ten individuals per size class was maintained by merging abundance data between consecutive size classes where necessary. All variables are presented on log_{10} axes, where on the x-axis each class is c. 1.41 the size of the class above/below. Size spectra were produced for each site, and each seafloor habitat types, and both excluding and including demersal fish. The contribution of phyla to size-class abundance is presented for both sites, with at GHF a comparison between the 2012 and the 2015 surveys.

The right-hand sides (Bett 2013, 2014) of abundance, biomass, and estimated respiration flux, spectra were compared against the MTE predictions using a linear regression model in Minitab (V18.1, Minitab Inc.). For comparison of body-size spectra between habitats, regression analyses were performed with abundance data, where habitats with a hard substratum component (i.e. hard and intermediate) were grouped together, distinguishing them from sedimentary habitats (GHF, coarse and sand; SSB, sand and mud).

5.B.2.6 Sampling limitations

Differences in field operations, photographic-sample processing, and data acquisition (i.e. specimen detection, body-size measurement, and estimation of individual biomass) are fully presented in chapter 3 and briefly considered here; these will be discussed in more detail in the conclusion chapter.
(1) The AUV photographic surveys were carried out at different altitudes in the GHF and in the SSB study sites (average difference of 70 cm), introducing bias in 'optimal' body-size detection between the datasets. This did not impact interpretation of the results, only that reliable data were available from smaller size classes at SSB. (2) The photographic samples at GHF were analysed in the form of five-image tiles, whereas at SSB they were assessed individually, presenting disparity in the scale of photographic analysis. (3) The difference in sample size between the 2012 and the 2015 datasets at GHF leads to some inconsistency in detecting the largest specimens present, particularly in sedimentary habitats where the largest individuals were observed (i.e. demersal fish). (4) Several image analysts assessed the three datasets, potentially introducing individual analysis bias in terms of specimen

detection, identification, and body-size measurement. (5) Morphotypes inhabiting tubes or shells were excluded from this analysis on the premise that it was impossible to determine whether they were alive or dead. (6) Two methods were employed to estimate individual biomass: (i) the taxon-specific LWR approach precluding the inclusion of certain morphotypes for which no standard body-size measurement was applicable (i.e. colonial, encrusting, or morphologically plastic forms), or for which no morphometric data were available in the literature; and (ii) the taxon-independent GVM approach that allowed the inclusion of all morphotypes observed. (7) Specimens that were observed partially or that were present above the seabed were allocated the mean individual biomass of their corresponding morphotype, leading to all such occurrences being associated with a single body-size class (i.e. reduced body-size class resolution).

5.B.3 Results

5.B.3.1 Greater Haig Fras marine conservation zone

5.B.3.1.1 Megabenthic assemblage description

The total faunal abundance at GHF varied from 0.67 ind. m^{-2} in 2012 (GHF-1) (Benoist et al. 2019a) to 1.03 ind. m^{-2} in 2015 (GHF-2) (Ferguson et al. in prep.) (figure 5.B.1). Porifera, Cnidaria, Bryozoa, and Echinodermata, were the dominant phyla contributing 81-90% of the megabenthic assemblage across the surveys. In particular, Axinellidae spp., *Parazoanthus* sp., *Porella* sp., *Porania pulvillus*, and Bryozoa sp. 1, were the most abundant morphotypes observed, and in slightly different relative abundances between years. The number of demersal fish recorded between years increased from 0.03 ind. m^{-2} to 0.81 ind. m^{-2}. Whether excluding or including fish data in 2012 and in 2015, standing stock density exhibited a statistically significant difference between habitats (Welch's ANOVA, $p < 0.001$), with hard habitats having the highest density, and coarse the lowest. All pairwise comparisons were significant (Games-Howell, $p < 0.001$), except between coarse and sand in 2015 (invertebrates only, Games-Howell, $p = 0.993$; fish included, $p = 0.983$).

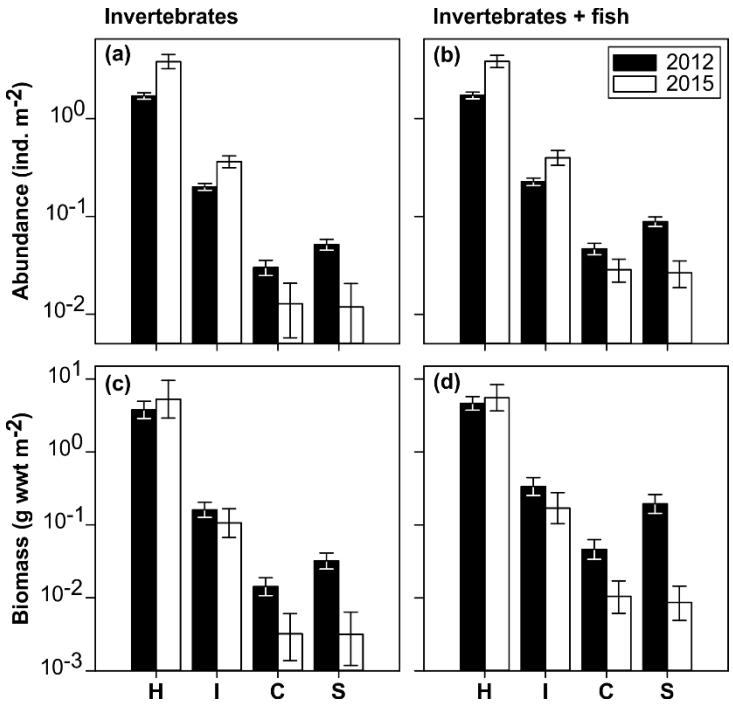

Figure 5.B.1. Megabenthos standing stocks at Greater Haig Fras by summary habitat. (a, b) Total faunal abundance (N in ind. m^{-2}) and **(c, d)** biomass (W in g wwt m^{-2}) of megabenthic invertebrates (left panel) and combined invertebrates and demersal fish (right panel) in 2012 and 2015, illustrated as geometric mean values with corresponding 95% confidence intervals. H, hard habitats. I, intermediate habitats (rocks + sediments). C, coarse sands. S, finer sands.

The total faunal biomass, as estimated using LWRs, varied from 9.4 g wwt m^{-2} in 2012 (Benoist et al. 2019a) to 5.5 g wwt m^{-2} in 2015 (Ferguson et al. in prep.) (figure 5.B.1). Fish, Echinodermata, Cnidaria, and Arthropoda, were the biomass-dominant phyla contributing 98-99% of the assemblage in both surveys (figure 5.B.2). The biomass-dominant taxa were Gadidae (in 2012 only), *Echinus esculentus*, *Bolocera* sp., *Luidia ciliaris*, and *Munida* sp. Whether excluding or including demersal fish data in 2012 and in 2015, standing stocks biomass also varied significantly between habitats (Welch's ANOVA, $p < 0.001$), with hard habitats having the highest biomass, and coarse the lowest. All pairwise comparisons were significant (invertebrates only, Games-Howell, $p < 0.001$), except between intermediate and sand in 2012 (invertebrates + fish, Games-Howell, $p = 0.14$), and between coarse and sand in 2015 (invertebrates only, Games-Howell, $p = 1.00$; including fish, Games-Howell, $p = 0.958$).

A total of 74 distinct morphotypes in nine phyla were recorded in 2012 (Benoist et al. 2019a), and 67 morphotypes (same phyla) in 2015 (Ferguson et al. in prep.), with 47 morphotypes common to both surveys. Of the 27 morphotypes present in 2012 only, 13 were rare (i.e. $n \leq 5$ ind. recorded in total) and two were relatively abundant (Cerianthid sp. 1, $n = 181$ ind.; Gadidae spp., $n = 514$ ind.). Of the 20 morphotypes present in 2015 only, 12

were rare and one was relatively abundant (Porifera sp. 26, *n* = 206 ind.). The relative contribution, in terms of abundance, of the morphotypes common to both surveys is overall similar in 2012 and 2015, with the largest difference attributed to Bryozoa sp. 1 that increased from 0.04 ind. m^{-2} to 0.27 ind. m^{-2}.

The observed pattern in standing stocks distribution between habitats was somewhat similar in both surveys, although higher estimates in 2015 were evident in hard and intermediate habitats, and lower estimates in the sedimentary habitats (sand and coarse) (figure 5.B.1). Demersal fish were more abundant in the sedimentary and intermediate habitats. Confidence intervals around the mean abundance and biomass values are generally wider in 2015, particularly in the sedimentary habitats, likely as a result of the smaller sample sizes analysed.

5.B.3.1.2 Body-size spectra at GHF

Individual biomass ranged from 0.06 g wwt (Asteroidea sp. 2) to 3.2 kg (*Luidia ciliaris*) in 2012, and from 0.007 (*Caryophyllia smithii*) to 1.4 kg (*L. ciliaris*) in 2015. As indicated previously, Echinodermata, Fish, and Cnidaria, were the major contributors to both abundance and biomass standing stocks in 2012 and in 2015 (figure 5.B.2). Echinodermata covered all body-size classes in 2012 (except class c. 1.8 kg geometric mean), and from size class c. 0.1 g wwt in 2015. Demersal fish dominated larger size classes (> 57 g wwt) in 2012, whereas in 2015 they were more abundant in smaller size classes (< 1 g wwt). Cnidaria spread across almost the whole spectrum in 2012, as opposed to 2015 where they were concentrated in the smallest size classes (< 0.01 g wwt). In both surveys, Arthropoda span similar body-size classes yet with differing contribution; a peak abundance is visible at c. 10 g wwt in 2012, whereas it is somewhat levelled between classes in 2015. During both surveys, *Munida* sp. was the main contributor to Arthropoda biomass, with specimens generally smaller in 2015, i.e. top abundance at class c. 40 g wwt in 2012 vs. at class c. 7 g wwt in 2015.

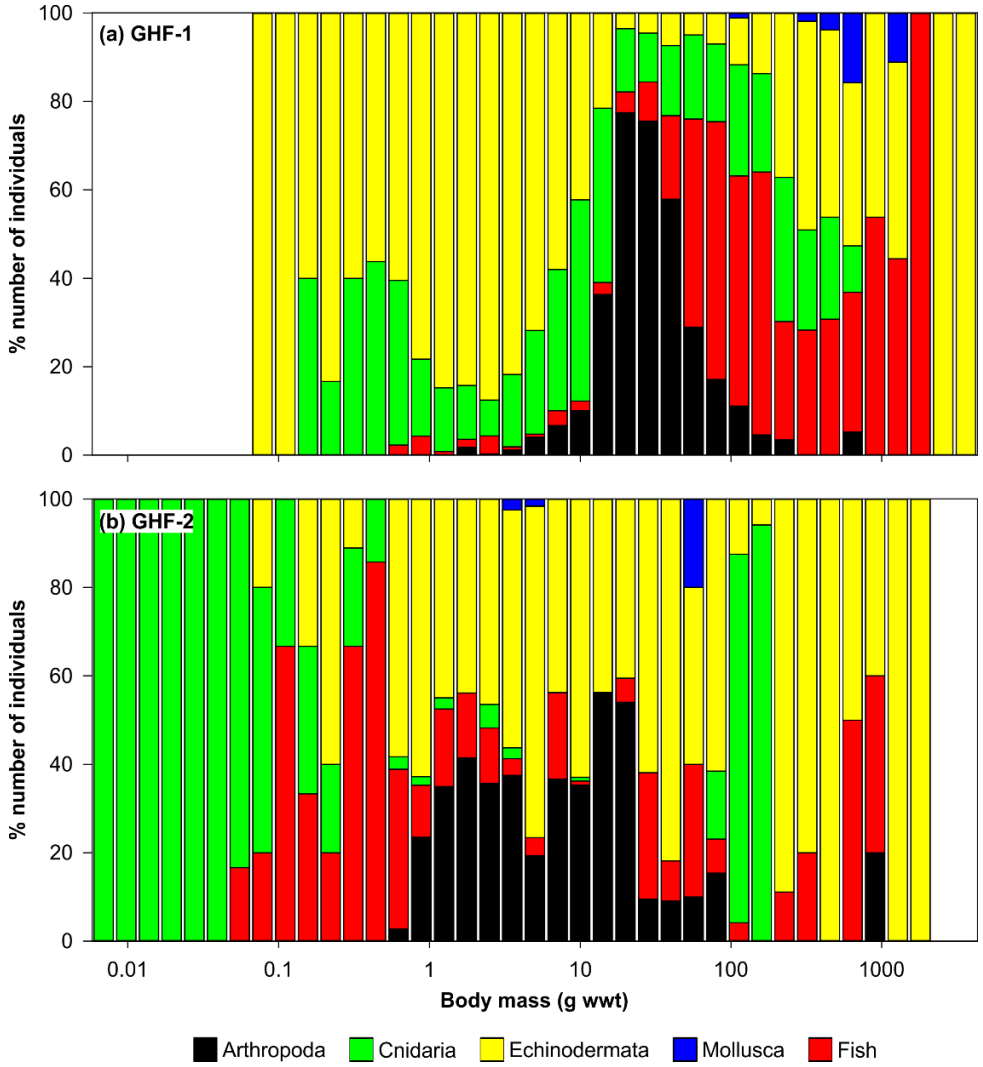

Figure 5.B.2. Contribution of phyla to total size-class abundance estimated at Greater Haig Fras marine conservation zone. (a) GHF-1, 2012. **(b)** GHF-2, 2015.

The individual-based body-size spectra span 32 classes in 2012, and 37 classes in 2015 (figure 5.B.2), and revealed a peak abundance at 3.5 g wwt and at 7.1 g wwt, respectively (figure 5.B.3), marking the starting point of the right-hand side of the spectra (Bett 2013, 2014) (figure 5.B.4). In 2012, a secondary peak of abundance is visible at size class 20.0 g wwt, associated with the hermit-crab Paguridae sp. 2, which was among the dominant taxa during this survey (maximum of 5.2 ind. m^{-2} recorded in a single tile). In 2015, *C. smithii* was also among the dominant taxa in the assemblage. Though, this taxon occupied only the lowest range of body-size classes (0.001 to 0.02 g wwt, i.e. below the 'optimal' resolution size), where a first small peak abundance is visible. A secondary peak is observed between 113.1 and 160.0 g wwt, linked to high abundances of the anemones *Bolocera* sp. and

Anthozoa sp. 37. All *Urticina* specimens were present in one body-size class (160.0 g wwt).

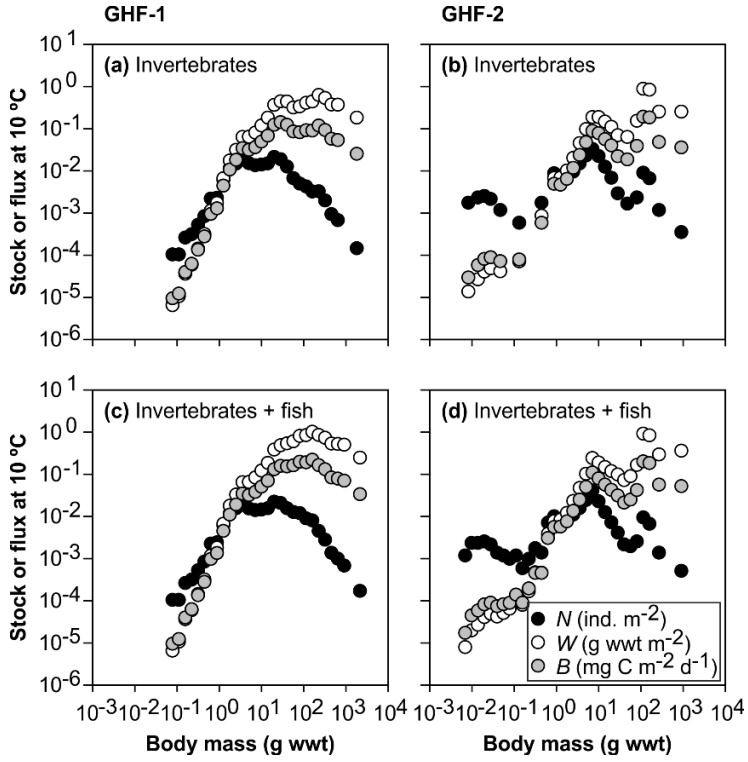

Figure 5.B.3. Megabenthos body-size spectra at Greater Haig Fras marine conservation zone. Body-size distribution of abundance (N_i in ind. m^{-2}), biomass (W_i in g wwt m^{-2}), and estimated respiration flux (B_i in mg C m^{-2} d^{-1}) against body size (M_i in g wwt) at Greater Haig Fras at in situ temperature (i.e. 10 °C) in 2012 (GHF-1; left pane) and in 2015 (GHF-2; right pane). **(a, b)** Invertebrates. **(c, d)** Combined invertebrates and demersal fish.

5.B.3.1.3 Abundance, biomass, and respiration flux against MTE predictions at GHF

Data at GHF were summarized well by the MTE predictions (figure 5.B.4, table 5.B.1). In 2012 and in 2015, invertebrate abundance decreased with body size with slopes of -0.71 and -0.74, respectively, not significantly different from the MTE prediction of -0.75. Combined with demersal fish, abundance decreased with slopes of -0.66 (2012), and -0.71 (2015); also not significantly different from the MTE prediction. Invertebrate biomass increased with body size with slopes of 0.27 (2012), and 0.25 (2015), not significantly different from 0.25 in 2012 only. Combined with demersal fish, biomass increased with slopes of 0.33 (2012), and 0.28 (2015), not significantly different from the MTE prediction (2012 only). Invertebrate respiration flux was invariant with body size with slopes ranging between 0.03 (2012) and 0.01 (2015), not significantly different from 0.00. Including demersal fish,

respiration flux scaled with body size with slopes of 0.09 (2012) and 0.04 (2015), also significantly different from the MTE prediction. Intercept values (i.e. related to resource supply) for abundance, biomass, and respiration flux, ranged between 0.0589 and 0.0959 across both surveys.

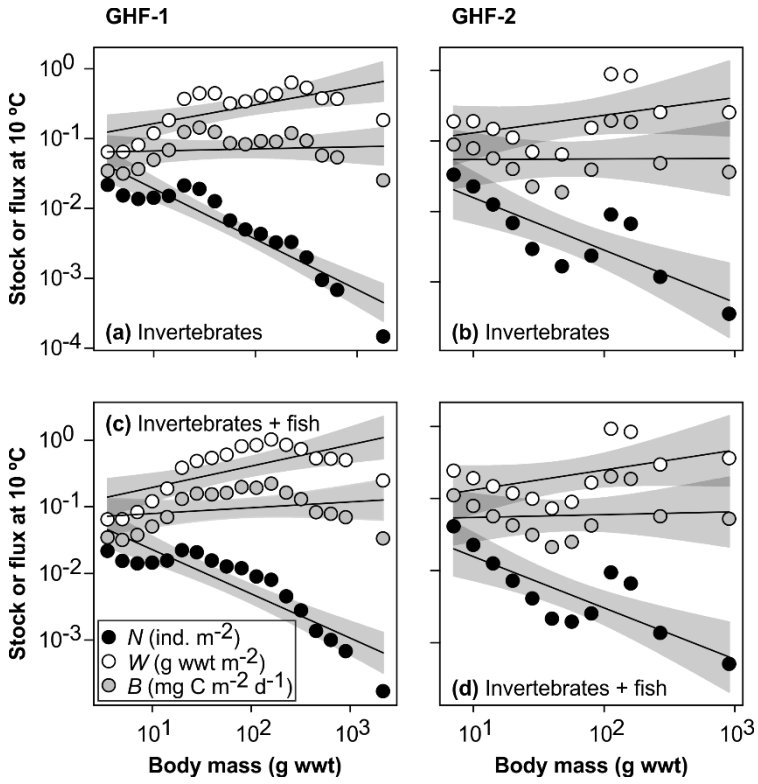

Figure 5.B.4. Megabenthos right-hand side body-size spectra at Greater Haig Fras marine conservation zone. Body-size distribution of abundance (N_i in ind. m^{-2}), biomass (W_i in g wwt m^{-2}), and estimated respiration flux (B_i in mg C m^{-2} d^{-1}) against body size (M_i in g wwt) at Greater Haig Fras at in situ temperature (i.e. 10 °C) in 2012 (GHF-1) and in 2015 (GHF-2). **(a, b)** Invertebrates. **(c, d)** Combined invertebrates and demersal fish. Black lines are regression lines. Shaded areas are 95% confidence intervals. See table 5.B.1 for the corresponding regression equations.

Table 5.B.1. Spectral analyses of stocks and flux at Greater Haig Fras marine conservation zone. Regression analysis for abundance (N_i in ind. m^{-2}), biomass (W_i in g wwt m^{-2}), and estimated respiration flux (B_i in mg C m^{-2} d^{-1}) against body size (M_i in g wwt) for the megabenthic assemblages **(a)** excluding and **(b)** including demersal fish, at in situ temperature (i.e. 10 °C) in 2012 (GHF-1) and in 2015 (GHF-2). See figure 5.B.4 for corresponding plots. **p < 0.01, ***p < 0.001, ns: not significant. *(to be continued)*

(a) Invertebrates

Regression	Equation	Slope 95% CI	N	F	r^2
Abundance (ind. m^{-2})					
GHF-1	$N_i = 0.0959\ M_i^{-0.72}$	-0.88, -0.56	17	91.12***	0.86
GHF-2	$N_i = 0.0872\ M_i^{-0.74}$	-1.13, -0.36	11	19.37**	0.68
Biomass (g wwt m^{-2})					
GHF-1	$W_i = 0.0840\ M_i^{0.27}$	0.10, 0.44	17	11.68**	0.44
GHF-2	$W_i = 0.0736\ M_i^{0.25}$	-0.14, 0.64	11	2.14 ns	0.19
Respiration (mg C m^{-2} d^{-1})					
GHF-1	$B_i = 0.0647\ M_i^{0.03}$	-0.13, 0.19	17	0.20 ns	0.01
GHF-2	$B_i = 0.0589\ M_i^{0.01}$	-0.38, 0.39	11	0.00 ns	0.00

Table 5.B.1. *(Continued)*

(b) Invertebrates + demersal **fish**

Regression	Equation	Slope 95% CI	N	F	r^2
Abundance (ind. m^{-2})					
GHF-1	$N_i = 0.0995\ M_i^{-0.66}$	-0.84, -0.64	18	58.63***	0.79
GHF-2	$N_i = 0.0804\ M_i^{-0.71}$	-1.06, -0.36	12	20.11**	0.67
Biomass (g wwt m^{-2})					
GHF-1	$W_i = 0.0881\ M_i^{0.33}$	0.14, 0.52	18	13.33**	0.45
GHF-2	$W_i = 0.0697\ M_i^{0.28}$	-0.08, 0.63	12	3.00 ns	0.23
Respiration (mg C m^{-2} d^{-1})					
GHF-1	$B_i = 0.0673\ M_i^{0.09}$	-0.09, 0.27	18	1.16 ns	0.06
GHF-2	$B_i = 0.0543\ M_i^{0.04}$	-0.31, 0.39	12	0.06 ns	0.01

5.B.3.1.4 Habitat-specific body-size distribution of abundance at GHF

The body-size distribution of abundance at GHF during both surveys was somewhat different between habitat types, being steeper in sedimentary habitats, whether including or excluding demersal fish (figure 5.B.5, table 5.B.2). In hard and in intermediate habitats, the invertebrate right-hand side of the spectra span 19 size classes in 2012, and 16 classes in 2015. The addition of demersal fish data (GHF-1, 20 classes; GHF-2, 16 classes) did not cause any obvious difference change in distribution, with most morphotypes binned as singletons, except Gadidae specimens that were more numerous per body-size class, and mainly present in the middle section of the right-hand side of the spectra. At GHF-2, more consecutive classes needed to be merged in order to ensure a minimum of ten individuals per class, i.e. represented by the evident trough on the data plot, and by the last data point (figure 5.B.5a, c; appendix G). In sedimentary habitats, the invertebrate right-hand side of the spectra span 12 size classes in 2012, and 10 classes in 2015, where in both cases almost all classes post peak abundance needed to be merged in order to ensure a minimum of ten individuals per class. The addition of demersal fish data (GHF-1, 14 classes; GHF-2, 13 classes) clearly changed the slope of the abundance distribution with body size at GHF-1, which appears less steep and with increased precision (i.e. narrower 95% CI around the regression line). The intercepts of the spectra were similar between 2012 and 2015 in hard habitats, whereas spectral data were clearly more elevated in 2012 in sedimentary habitats.

Data in hard habitats were summarized better by the MTE prediction than in sedimentary habitats, where the distribution of abundance is clearly steeper, whether including or excluding demersal fish (table 5.B.2). In 2012 and in 2015, invertebrate abundance decreased with body size with slopes of -0.65 in hard habitats, not significantly different from the MTE prediction of -0.75. Combined with fish, abundance decreased with slopes of -0.59 (2012) and -0.72 (2015); also not significantly different from the MTE prediction. In sedimentary habitats, invertebrate abundance decreased with body size with slopes of -1.49 (2012) and -0.92 (2015), not significantly different from the MTE prediction of -0.75, with rather expanded confidence limits around the regression line in 2012. Combined with fish, abundance decreased with slopes of -1.06 (2012) and -1.13 (2015); significantly different from the MTE prediction, and steeper than expected. Intercept values (resource supply) generally ranged between 0.0133 and 0.1161 across habitat types, reaching rather high values of 0.6887 and 1.4997 in sedimentary habitats in 2012, excluding and including fish, respectively.

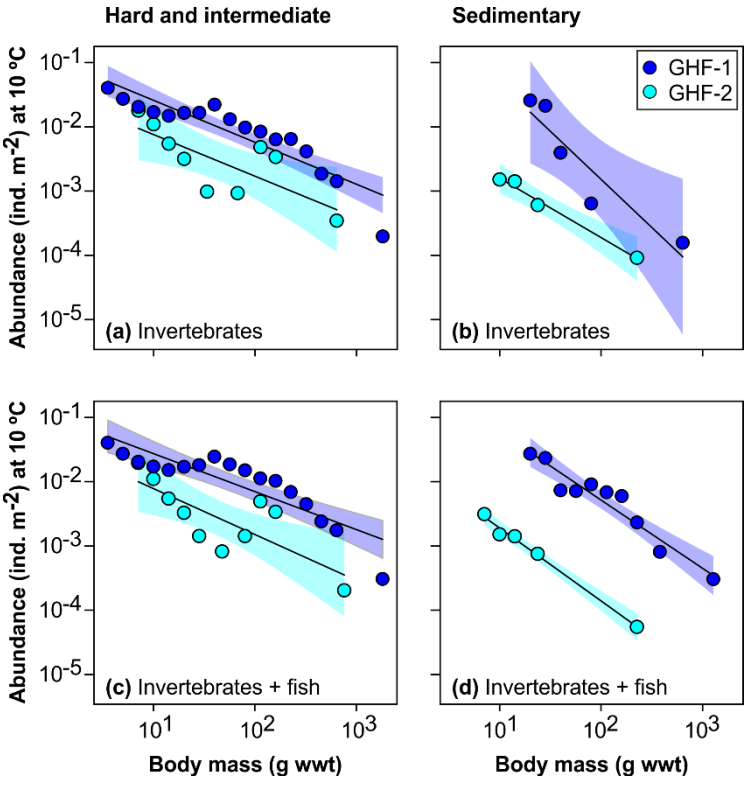

Figure 5.B.5. Megabenthos right-hand side body-size spectra of abundance by habitat type at Greater Haig Fras marine conservation zone. Body-size distribution of abundance (N_i in ind. m^{-2}) against body size (M_i in g wwt) at Greater Haig Fras, at in situ temperature (i.e. 10 °C) in 2012 (GHF-1) and in 2015 (GHF-2), in the hard and intermediate habitats (i.e. with a substantial proportion of hard substratum types) by comparison to the sedimentary habitats (i.e. coarse and fine sediments). **(a, b)** Invertebrates. **(c, d)** Combined invertebrates and demersal fish. Solid lines are regression lines. Shaded areas are 95% confidence intervals. See table 5.B.2 for the corresponding regression equations.

Table 5.B.2. Spectral analyses of megabenthos abundance by habitat type at Greater Haig Fras marine conservation zone. Regression analysis for abundance (N_i in ind. m^{-2}) against body size (M_i in g wwt) for the megabenthic assemblages **(a)** excluding and **(b)** including demersal fish, at in situ temperature (i.e. 10 °C) in 2012 (GHF-1) and in 2015 (GHF-2). See figure 5.B.5 for corresponding plots. *p < 0.05, **p < 0.01, ***p < 0.001, ns: not significant.

(a) Invertebrates

Regression	Equation	Slope 95% CI	N	F	r^2
Hard and intermediate habitats					
GHF-1	$N_i = 0.1161\ M_i^{-0.65}$	-0.82, -0.49	17	69.28***	0.82
GHF-2	$N_i = 0.0337\ M_i^{-0.65}$	-1.15, -0.15	9	9.42*	0.57
Coarse and sand habitats					
GHF-1	$N_i = 1.4997\ M_i^{-1.49}$	-2.57, -0.42	5	11.68**	0.44
GHF-2	$N_i = 0.0133\ M_i^{-0.92}$	-1.26, -0.59	4	141.61**	0.99

(b) Invertebrates + demersal **fish**

Regression	Equation	Slope 95% CI	N	F	r^2
Hard and intermediate habitats					
GHF-1	$N_i = 0.1067\ M_i^{-0.59}$	-0.77, -0.42	17	52.39***	0.78
GHF-2	$N_i = 0.0405\ M_i^{-0.72}$	-1.19, -0.25	10	12.29**	0.61
Coarse and sand habitats					
GHF-1	$N_i = 0.6887\ M_i^{-1.06}$	-1.31, -0.81	10	94.30***	0.92
GHF-2	$N_i = 0.0257\ M_i^{-1.13}$	-1.32, -0.95	5	382.82***	0.99

5.B.3.2 Shelf-Sea Biogeochemistry study area

5.B.3.2.1 Megabenthic assemblage description

The total faunal abundance at the SSB study site was 0.74 ind. m^{-2}, with Cnidaria, Echinodermata, Arthropoda, and Fish contributing 91% of the megabenthic assemblage present (figure 5.B.6) (Thomson et al. 2017). The most abundant morphotypes observed were Asteroid sp. 7, Cnidaria sp. 1 and 2 (pennatulids), Anthozoa sp. 34, Ophiuroid sp. 1, and Paguridae sp. 3. Demersal fish were recorded principally in sandy and muddy habitats, and to a lower extent in intermediate habitats. Whether excluding or including fish data, standing stocks density exhibited a statistically significant difference between habitats (Welch's ANOVA, p < 0.001), with hard habitats having the highest density, and sand and mud the lowest. All pairwise comparisons were significant (Games-Howell, p < 0.001), except between sand and mud (invertebrates, Games-Howell, p = 0.986; combined with fish Games-Howell, p = 0.848).

The total faunal biomass, as estimated using the GVM, was 9.12 g wwt m^{-2}, with Fish, Echinodermata, and Arthropoda the main contributors (figure 5.B.6). Despite their low numerical influence to faunal density, demersal fish were the main contributor to assemblage biomass, representing c. 80% of the megabenthos studied in intermediate and in sand habitats, and up to c. 95% in muddy habitats. Four anglerfish, *Lophius piscatorius*, were recorded, accounting for c. 50% of the total megafauna biomass estimated at SSB, with one individual estimated at 16 kg. Excluding fish, the biomass-dominant taxa were Paguridae sp. 2, *Astropecten irregularis*, *Asterias rubens* (n = 1 specimen only), *Luidia sarsii*, and *Goneplax rhomboides*. Whether excluding or including demersal fish data, standing stock biomass also varied significantly between habitats (Welch's ANOVA, $p < 0.001$), with hard habitats having the highest biomass and sand the lowest. All pairwise comparisons were significant (Games-Howell, $p < 0.001$), except between intermediate and sand (invertebrates + fish, Games-Howell, $p = 0.14$), and between sand and mud (invertebrates, Games-Howell, $p = 1.00$; invertebrates + fish, Games-Howell, $p = 0.998$).

A total of 92 distinct morphotypes in eight phyla were recorded, with 39 rare (i.e. $n \leq 5$ ind. recorded in total), and three relatively abundant (Asteroid sp. 7, n = 430; Cnidaria sp. 2, n = 374; Anthozoa sp. 34, n = 278). Among these morphotypes, 56 were also observed at GHF-MCZ. The morphotypes observed in the SSB area only were predominantly found in muddy habitats, e.g. pennatulids Cnidaria sp. 1 and 2, Paguridae sp. 3, Caridea, *G. rhomboides*.

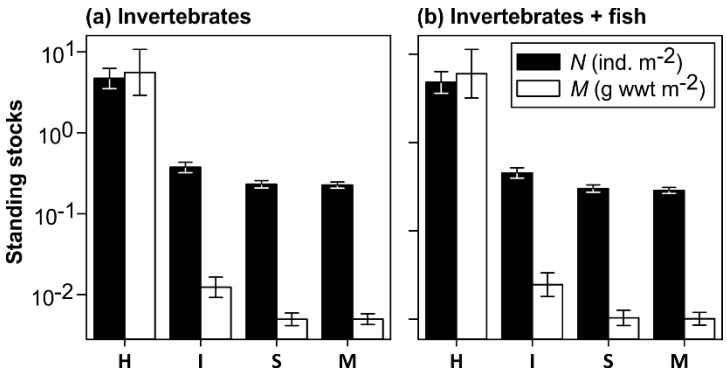

Figure 5.B.6. Megabenthos standing stocks at UK-NERC Shelf-Sea Biogeochemistry (SSB) study area by summary habitat. Total faunal abundance (N in ind. m^{-2}) and biomass (W in g wwt m^{-2}) of **(a)** megabenthic invertebrates and **(b)** combined invertebrates and demersal fish, illustrated as geometric mean values with corresponding 95% confidence intervals.

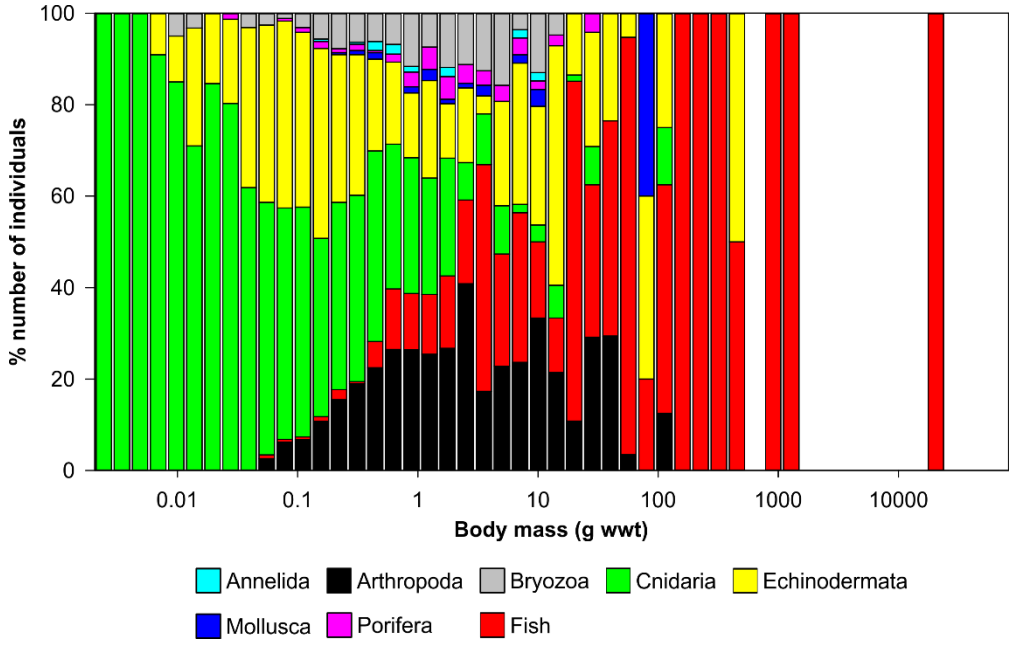

Figure 5.B.7. Contribution of phyla to total size-class abundance estimated at the UK-NERC Shelf-Sea Biogeochemistry (SSB) study area.

5.B.3.2.2 Body-size spectra at SSB

Individual biomass ranged from 0.002 g wwt (Anthozoa sp. 16) to 16.2 kg (*L. piscatorius*). Cnidaria were the most abundant in smaller body-size classes < 1 g wwt, and demersal Fish dominated the larger size classes > 10 g wwt (figure 5.B.7). Arthropods were spread in the middle of the spectrum between c. 0.1 g wwt and c. 100 g wwt. Echinodermata were found principally in smaller classes, and few occurrences of larger specimens > 20 g wwt were recorded. Annelida, Bryozoa, and Porifera occupied the left hand-side of the spectrum < 30 g wwt.

The individual-based body-size spectrum span 39 classes (figure 5.B.7) and showed a unimodal distribution of abundance with body mass, with a peak abundance at 0.22 g wwt (invertebrates only), and at 0.63 g wwt (invertebrates + fish) (figure 5.B.8), marking the starting point of the right-hand side of the spectra (Bett 2013, 2014) (figure 5.B.10). Three 'outlier data' points at size classes 3.5, 20.0, and 56.5 g wwt comprised almost entirely specimens of Clupeiforme sp. 2, Perciforme sp. 3, and Gadidae, respectively, which were observed either partially (i.e. at the edge of an image) or above the seabed, and which were uniformly allocated the mean body mass of the corresponding taxon. The need to make a representative estimate of the body

size for every specimen encountered, instead of using a mean value, is further discussed in section 5.B.4.2, and suggestions for improvements are provided in chapter 8.

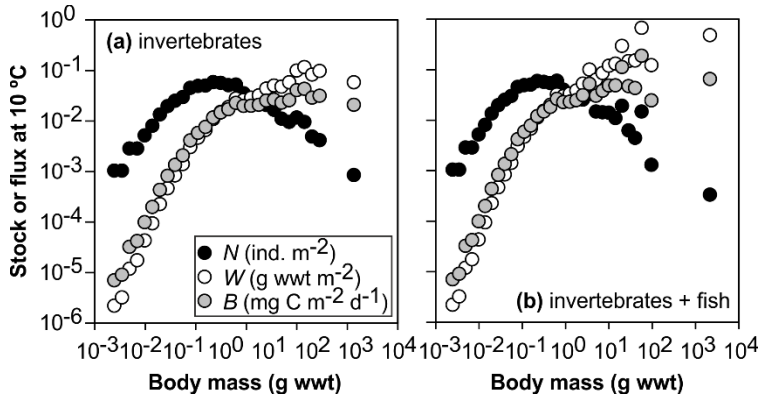

Figure 5.B.8. Megabenthos body-size spectra at the UK-NERC Shelf-Sea Biogeochemistry study site. Body-size distribution of abundance (N_i in ind. m^{-2}), biomass (W_i in g wwt m^{-2}), and estimated respiration flux (B_i in mg C m^{-2} d^{-1}) against body size (M_i in g wwt) at SSB at in situ temperature (i.e. 10 °C). **(a)** Invertebrates. **(b)** Combined invertebrates and demersal fish.

5.B.3.2.3 Abundance, biomass, and respiration flux against MTE predictions at SSB

Data at SSB were summarized well by the MTE predictions (figure 5.B.9, table 5.B.3). Invertebrate abundance decreased with body size with slope of -0.62, and -0.59 when combined with demersal fish, close but significantly different from the MTE prediction of -0.75. Biomass increased with body size with slopes of 0.34 (invertebrates only), and 0.39 (invertebrates + fish), not significantly different from 0.25. Respiration flux exhibited a slight increase with body size with slopes of 0.13 (invertebrates only), and 0.16 (invertebrates + fish), close but significantly different from 0.00. Intercept values for abundance, biomass, and respiration flux, ranged between 0.0218 and 0.0478.

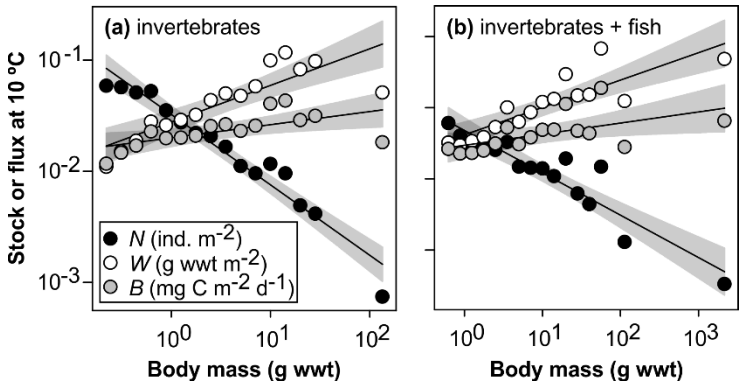

Figure 5.B.9. Megabenthos right-hand side body-size spectra at the UK-NERC Shelf-Sea Biogeochemistry study site. Body-size distribution of abundance (N_i in ind. m^{-2}), biomass (W_i in g wwt m^{-2}), and estimated respiration flux (B_i in mg C m^{-2} d^{-1}) against body size (M_i in g wwt) at SSB at in situ temperature (i.e. 10 °C). Black lines are regression lines. Shaded areas are 95% confidence intervals. See table 5.B.3 for the corresponding regression equations.

Table 5.B.3. Spectral analyses of stocks and flux at the UK-NERC Shelf-Sea Biogeochemistry study site. Regression analysis for abundance (N_i in ind. m^{-2}), biomass (W_i in g wwt m^{-2}), and estimated respiration flux (B_i in mg C m^{-2} d^{-1}) against body size (M in g wwt) for the megabenthic assemblages **(a)** excluding and **(b)** including demersal fish, at in situ temperature (i.e. 10 °C). See figure 5.B.9 for corresponding plots. *p < 0.05, **p < 0.01, ***p < 0.001, ns: not significant.

(a) Invertebrates

Regression	Equation	Slope 95% CI	N	F	r^2
Abundance (ind. m^{-2})					
SSB	$N_i = 0.0323\ M_i^{-0.62}$	-0.70, -0.54	16	286.33***	0.95
Biomass (g wwt m^{-2})					
SSB	$W_i = 0.0276\ M_i^{0.34}$	0.23, 0.44	16	45.81***	0.77
Respiration (mg C m^{-2} d^{-1})					
SSB	$B_i = 0.0218\ M_i^{0.13}$	0.05, 0.21	16	12.19**	0.47

(b) Invertebrates + demersal **fish**

Regression	Equation	Slope 95% CI	N	F	r^2
Abundance (ind. m^{-2})					
SSB	$N_i = 0.0478\ M_i^{-0.59}$	-0.73, -0.46	16	92.37***	0.87
Biomass (g wwt m^{-2})					
SSB	$W_i = 0.0415\ M_i^{0.39}$	0.25, 0.52	16	38.98**	0.74
Respiration (mg C m^{-2} d^{-1})					
SSB	$B_i = 0.0323\ M_i^{0.16}$	0.02, 0.29	16	6.38*	0.31

5.B.3.2.4 Habitat-specific body-size distribution of abundance at SSB

The body-size distribution of abundance at SSB between habitats followed similar patterns as was observed at GHF, whether excluding or including demersal fish (figure 5.B.10; table 5.B.4). The intercepts were slightly higher in hard and in intermediate habitats in comparison to sedimentary habitats, and slopes were consistent across habitats. In hard and in intermediate habitats, the invertebrate right-hand side of the spectrum spanned 18 size classes, and 21 including fish data. The addition of demersal fish data did not cause any obvious difference to the distribution in hard and in sedimentary habitats, however abundance data were more scattered in sedimentary habitats, with 'outlier data' comprising most specimens of the taxa Clupeiforme sp. 2, Perciforme sp. 3, and Gadidae, binned into size classes 3.5 g wwt, 20 g wwt, and 57 g wwt, respectively.

Data were summarized well by the MTE prediction in all habitat types, whether including or excluding demersal fish (table 5.B.4). In hard and in intermediate habitats, invertebrate abundance decreased with body size with a slope of -0.64, and of -0.68 when combined with fish, not significantly different from the MTE prediction of -0.75. In sedimentary habitats, invertebrate abundance decreased with a slope of -0.61 (invertebrates only), and of -0.51 (invertebrates + fish), significantly different from the MTE prediction. Confidence intervals around the regression line of invertebrate body-size distribution were narrower in sedimentary habitats by comparison to hard and intermediate habitats. An opposite pattern was evident when combined with fish data, i.e. 95% CIs were wider around the regression line in sedimentary habitats. Intercept values ranged between 0.0217 and 0.1121 across habitat types, and were generally higher in hard and in intermediate habitats.

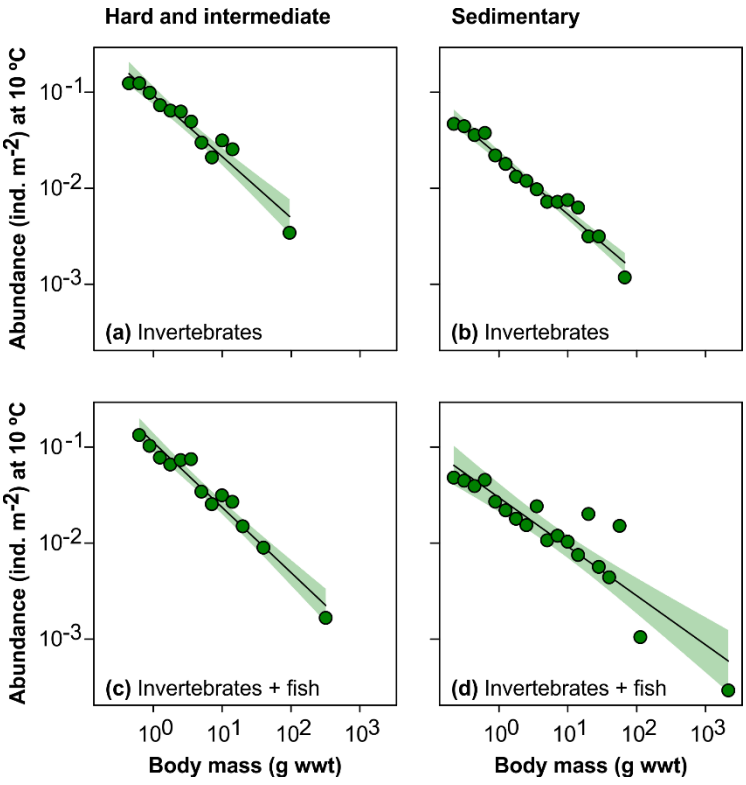

Figure 5.B.10. Megabenthos right-hand side body-size spectra of abundance by habitat type at the UK-NERC Shelf-Sea Biogeochemistry study site. Body-size distribution of abundance (N_i in ind. m^{-2}) against body size (M_i in g wwt) at SSB, at in situ temperature (i.e. 10 °C), in the hard and intermediate habitats (i.e. with a substantial proportion of hard substratum types) by comparison to the sedimentary habitats (i.e. sand and mud sediments). **(a, b)** Invertebrates. **(c, d)** Combined invertebrates and demersal fish. Solid lines are regression lines. Shaded areas are 95% confidence intervals. See table 5.B.4 for the corresponding regression equations.

Table 5.B.4. Spectral analyses of megabenthos abundance by habitat type at the UK-NERC Shelf-Sea Biogeochemistry study site. Regression analysis for abundance (N_i in ind. m^{-2}) against body size (M_i in g wwt) for the megabenthic assemblages **(a)** excluding and **(b)** including demersal fish, at in situ temperature (i.e. 10 °C), in the hard and intermediate habitats (i.e. with a substantial proportion of hard substratum types) with by comparison to the sedimentary habitats (i.e. sand and mud sediments). See figure 5.B.10 for corresponding plots. *p < 0.05, **p < 0.01, ***p < 0.001, ns: not significant.

(a) Invertebrates

Regression	Equation	Slope 95% CI	N	F	r^2
Hard and intermediate habitats					
SSB	$N_i = 0.0926\, M_i^{-0.64}$	-0.75, -0.52	12	157.12***	0.94
Sand and mud habitats					
SSB	$N_i = 0.0217\, M_i^{-0.61}$	-0.67, -0.54	16	409.17**	0.97

(b) Invertebrates + demersal **fish**

Regression	Equation	Slope 95% CI	N	F	r^2
Hard and intermediate habitats					
SSB	$N_i = 0.1121\, M_i^{-0.68}$	-0.77, -0.59	13	257.15***	0.96
Sand and mud habitats					
SSB	$N_i = 0.0298\, M_i^{-0.51}$	-0.63, -0.39	19	83.70***	0.83

5.B.4 Discussion

5.B.4.1 General description

The two shelf-sea sites surveyed—the Greater Haig Fras marine conservation zone (GHF-MCZ) and the UK-NERC Shelf-Sea Biogeochemistry (SSB) study area—were characterised by extensive areas of mixed substratum types ranging from muddy to sandy and coarser-grained sediments, together with hard substrata in the form of boulders and cobbles, either isolated or as patches. These various habitats occurred alone and in various mixtures, or mosaics, from 1 m to > 1 km physical length scales. As assessed by seabed photography, the GHF study area had an approximately equitable spatial extent of hard (21%), intermediate (i.e. hard + sediments; 27%), coarse (25%), and sand (27%) habitats (Benoist et al. 2019a; chapter 5.A). The SSB study site was primarily composed of muddy (52%) and sandy (30%) sediments, but also comprised intermediate (16%) and a very low proportion of hard (1%) habitats (Thomson et al. 2017; appendix B). As presented by Benoist et al. (2019a), the presence of hard substrata at GHF exerted a strong positive control on faunal density, biomass, and total species richness, with distinct faunal assemblages identified between habitats (chapter 5.A).

Environmental heterogeneity is thought to be a key driver of species richness (Stein et al. 2014; Yang et al. 2015), as was evident in the present study, although the effect was more pronounced in the case of heterogeneity diversity measures (chapter 5.A). Rees et al. (1999) noted that in UK shelf seas, coarse substrata supported increased diversity, and suggested that 'coarser' sediments offered more attachment points for sessile species, and more refuges for mobile species. Similarly, in a major survey of the continental margin off northern Norway, Buhl-Mortensen et al. (2012) found that the abundance, biomass, and diversity of the macro- and megabenthos increased with the complexity of the seabed habitat. The use of photographic assessments provided a uniform field- and data-analysis methodology across the rocky and the sedimentary habitats, which enabled a direct assessment of multiple biotopes and their occurrence in mosaic form. This ability to resolve ecologically significant information, at broad scale, across multiple and mixed habitats, suggests that AUV-based photographic survey was an effective and

efficient research tool in the present case, and indicated its potential value in other similarly complex marine habitats.

The benthic assemblages observed at the two study sites comprised taxa commonly recorded in the Celtic Sea (Rees et al. 1999). The assemblages were statistically distinct between all habitat types considered, and useful indicator species were identified for each GHF habitat (Benoist et al. 2019a; appendix A). In the context of potential change over time, indicators may shift in abundance and/or biomass, and such changes may warrant further investigation into the implication(s) for such change on ecological metrics, for instance total assemblage biomass, diversity, or the presence of taxa that have driven legislation (e.g. Perkins et al. 2017). Ellis et al. (2013) identified six assemblages from beam trawls in the Celtic Sea; their "outer shelf" assemblage (50-175 m water depth) was consistent with the observations across both study areas. Following a similar approach, Ellis et al. (2000) classified the assemblages of the contiguous Irish Sea, indicating in that case that the weight of cobbles and boulders taken in the catch was a useful predictor of assemblage type, suggesting the potential significance of mosaic habitats aliased by trawl sampling. However, the scale of the trawl samples assessed by Ellis et al. (2000, 2013; c. 500-3500 m in length) precluded the detection of assemblages specific to substratum types or mosaics that were detected directly in the present surveys.

The presence/absence of some morphotypes between years may be the result of sampling differences, i.e. night survey (2012) vs. day survey (2015), and differences in image processing may have impacted the visual outcome and therefore the graphic interpretation/analysis. Furthermore, despite consistency in specimen detection and identification between operators, a certain degree of annotation bias remains, e.g. numerous small specimens of demersal fish were observed in 2015 only and identified as Actinopterii sp. 1; they were not classified as Gadidae on the basis that they clearly differed in size compared to those Gadidae recorded in 2012. Also, the difference in sample size between surveys (2012, 19,223 m^2 seabed area; 2015, 5142 m^2) may have had a bearing on the record of the largest, rarest, specimens (i.e. animal space use scales positively with body size) (Jetz et al. 2004).

5.B.4.2 Body-size structure

Quantitative individual biomass data of megabenthic assemblages (invertebrates and demersal fish) were obtained from photographic analysis using two methods, and were used to assess the body-size distribution of abundance, biomass, and estimated respiration flux. At GHF, length-weight relationships (LWRs) were employed (Benoist et al. 2019a and references therein; appendix A). The fauna at GHF is well known, however this method is species-specific, and its valid application may be dependent upon season (or year) and location (e.g. Benoist et al. 2019b; chapter 4). Furthermore, a rather large component of the fauna (sessile colonial and encrusting forms found in rocky habitats) could not be included in this study due to the inability to estimate their body mass from standard linear measurement. In contrast, the volumetric approach employed at SSB enabled estimates of individual body-mass data across the full range of specimens recorded (Thomson et al. 2017; Benoist et al. 2019b; chapter 4). Individual biomass of those morphotypes for which no LWR was available in the literature, ranged on average between 0.27 g wwt (Cnidaria sp. 2) and 18 g wwt (*Alcyonium digitatum*), i.e. close to the peak-abundance point of the corresponding spectrum.

Overall, body-size spectra depicted a unimodal distribution of abundance (figures 5.B.3 and 5.B.8), with secondary peaks that may reflect true increase/decrease in the abundance of some taxa, or be the result of individual annotator bias (Durden et al. 2016b). For example, at GHF-2, high numbers of the cup coral *C. smithii* were recorded in the smallest size classes (i.e. below the minimum 'optimum' size). This is an iconic species of the area, and it is likely expected to be encountered in rocky habitats, resulting in an increase in sampling effort allocated to this taxon. On the other hand, some specimens that were observed partially and/or off the seabed, were allocated the mean body mass of their corresponding morphotype, generating 'spikes' in the overall body-size distribution as a result of their bulk assignment to a single size class, instead of being spread across the spectrum. This can be limiting in terms of the quantitative representation of the body-size structure of an assemblage.

Body-size spectral analyses require organism-level information that can only be achieved by estimating the body size of each individual, instead of using a mean value of the corresponding taxon (see chapter 8 for suggestions of improvements). This important issue can be dealt with via the volumetric approach, as it has been done with the SSB data (Benoist et al. 2019b; chapter 4) and with the Clarion-Clipperton Zone deep-sea data (Simon-Lledó et al. 2019a; chapter 6). Edwards et al. (2017, 2020) tested the effect of data type (body mass or length) and resolution, and the effect of binning that data for conducting body-size spectral analyses. The authors recommend the use of a maximum likelihood estimate (MLE) method, based on binning that considers body-mass-data counts, where each count represents species-specific values within its respective size bin[1].

These analyses of body-size spectra provide insights on the necessity of standardising the sampling effort allocated to the observation and identification of specimens, particularly in the case of using a LWR method. Nevertheless, as Schwinghamer (1988) noted, community assessment based on individual body-size analysis can be a powerful alternative to taxonomic analysis, particularly in areas where ecological and natural history knowledge of the fauna is limited (see also Henseler et al. 2019).

5.B.4.3 Body-size distributions and MTE predictions

The body-size distribution of the megabenthic assemblages (invertebrates only, and combined with demersal fish) observed at the two shelf-sea sites assessed, generally matched the predictions of the metabolic theory of ecology (Brown et al. 2004) (figures 5.4 and 5.9; tables 5.2 and 5.3). The addition/removal of fish from the assessment had little impact on the spectra, other than right-side extension, suggesting that a simple MTE-type model may be adequate. Body mass was a strong predictor of abundance distribution, indicating an equivalent distribution of resources and materials within the body-size range studied, referred to as the 'energy equivalence rule' (EER) (Damuth 1981). Cammen (1979) studied the influence of the organic

[1] The MLE method (Edwards et al. 2017) was tested at each site using the right-side slopes of abundance spectra, including and excluding demersal fish. The MLE results (i.e. *b* exponent) showed no difference to those presented in the present thesis. They are not shown in this thesis, but will be the object of a future publication in a relevant journal.

content of the sediment and detritus on the ingestion rate of benthic deposit feeders and detritivores, and the author's results revealed a strong size dependency of resource acquisition, independently of species identity, with mass scaling close to the MTE prediction (i.e. 0.75). Basset et al (2012) considered various datasets across terrestrial and aquatic environments to assess the effect of resource limitation on the allometric scaling of resource ingestion. The authors showed that, on average, the scaling exponent was close to the MTE model, and concluded on the dependence of (i) individual metabolic requirements on body size, (ii) individual resource ingestion rates on resource availability, and (iii) resource availability on individual body size. They also showed that under limited resource conditions, scaling exponent was generally low (c. 0.40).

The results obtained in this Ph.D. thesis agree with those from other shallow-water environments. For example, Labra et al. (2015) studied the body-size distribution of macro- and megabenthic assemblages in a small bay off Chile (SE Pacific), and found that the energetic equivalence rule held for the right-hand side of the body-size distribution assessed (see chapter 1 section 1.3; figure 1.4). The authors also found a temporal response in the abundance-body-size distribution of the assemblages assessed, where the peak abundance shifts in response to seasonal effects (primary productivity and hypoxia) on reproductive patterns, yet with a consistent decline in abundance with body mass, following the EER. Bergstad (2009) reviewed that, beyond an 'optimal' body-size, most demersal fish assemblages exhibit exponential decline in abundance with increasing body mass. The author indicated that coexisting species likely partition resources in order to reduce competition and promote growth and survival.

Biomass and respiration flux distribution with body size showed greater departures from the MTE predictions. Photographic acquisition of individual body-mass data is subjected to many sources of error. In some cases, the measured body dimension, the first step to the estimation of body mass, might misrepresent the true body dimension of the specimen. For example, some specimens are often observed curved or retracted (i.e. soft-bodied organisms), from a lateral angle (rather than downward) when attached to rocks (e.g. anemones), or partially buried in the sediment or partially hidden

under rocks (e.g. sea stars, ophiuroids, squat lobsters), resulting in under-/over-estimation of their body mass. In addition, differences in some specimens' altitude over the seabed may reveal slight over-estimation of their biomass in the particular case where rocks are more elevated than the surrounding seabed. The allocation of a misrepresented allometric LWR in the calculation of individual body mass (e.g. at GHF), i.e. in the case of a specimen identified to morphotype level, despite careful selection of the most representative known species (in terms of shape and body-size range), might distort the final value. Using the body volume of a specimen as a proxy for biomass, as tested with the SSB dataset (see also assessment at the CCZ site; chapter 6), provided robust quantitative individual body-mass data over the full range of specimens observed without the need to omit some taxa/specimens (Thomson et al. 2017; Benoist et al. 2019b; chapter 4), as was the case in the GHF datasets.

Finally, the application of a single equation (chapter 1 equation 1.1), with a temperature-corrected normalisation coefficient obtained from Hemmingsen's (1960) data, to calculate all specimens' individual metabolism within a size class, is attractive from a modelling perspective but may be overly simplistic (see chapter 7 where individual metabolism was calculated using a range of temperature-corrected normalisation coefficients found in the literature, in order to estimate seafloor carbon stocks and flows) (see also Laguionie Marchais et al. (2020)). Though Childress (1995), and more recently McClain et al. (2012), showed that marine benthic groups showed lesser or no decline in their metabolic rate with increasing depth (see also Childress et al. 1990; Drazen and Seibel 2007; Brey 2010; Seibel and Drazen 2007). Individual metabolic rates do, however, exhibit a wide range of species-specific factors (Brey 2010; McClain et al. 2012).

The MTE model in hard and in intermediate habitats better predicted habitat-specific distribution of abundance with body size in comparison to sedimentary habitats at GHF, where the regression slope was closer to -1 than to -0.75. Blanchard et al. (2009) compared the body-size distribution of pelagic predators (fish and invertebrate epifauna) and benthic detritivores (infaunal macrobenthic filter and deposit feeders) from the North Sea, revealing steeper slopes in the former assemblages. Their model accounted for

trophic interactions and the recycling of material that occurs in aquatic ecosystems between pelagic predators and benthic detritivores. The authors determined that biological processes (i.e. growth and mortality) occurred at faster rates in predators, and concluded that external forces (e.g. fishing pressure) disturbed the natural balance of benthos functioning, such that the removal of larger specimens, parallel to increases of smaller individuals, resulted in steeper slopes.

At SSB, abundance-body-size distributions were predicted well by the MTE model, yet the slope value was slightly higher in sedimentary habitats when data comprised both invertebrates and demersal fish. Despite an overall reduction in fishing mortality for shellfish and fishes in the Celtic Sea since the late 1990s, fishery activities (i.e. extraction of targeted large species), and abrasion (associated with bottom trawling and dredging), remain two major regional human-induced pressures in the area, ultimately affecting the state of benthic habitats, faunal communities, and food webs (ICES 2016). Targeting large ground fish alters the size structure and functioning of the benthos, by leaving available their portion of resources to the rest of the community, eventually promoting the development of smaller specimens (Blanchard et al. 2009). In their meeting report, Petchey and Delgrano (2010 and references therein) review the use of body-size spectra as indicators of ecological status, showing the generality of steeper abundance with body-size distributions in disturbed communities.

The MTE model was well represented by both the GHF and the SSB megabenthos assemblages, at site-scale, and between the different habitat types assessed (hard and sedimentary). The intercept values were somewhat similar at GHF in 2012 and in 2015 (c. 0.1 mg C m^{-2} d^{-1}), and higher than at SSB (c. 0.03 mg C m^{-2} d^{-1}); indicative of higher resource supply at GHF (tables 5.B.2 and 5.B.3). The substantial occurrence of rocky substratum types at GHF, serving as more effective habitat for suspension feeders, may promote the enhanced capture of suspended particulate organic matter, by increased advection both vertically and horizontally across the area surveyed (Benoist et al. 2019a; chapter 5.A). Diesing et al. (2017) determined that mud content in surface sediments is the most important factor in determining seafloor POC concentration, with higher POC content associated with muddy sediments.

Though, the authors noted that conversely, gravelly sands contributed highly to the POC stocks of the northern European continental shelf. The benthic stocks at SSB are likely to be depleted by comparison to GHF, as a result of the fishing pressure experienced in the central Celtic Sea (Thomson et al. 2017; ICES 2016). Chapter 7 provides more detail and discussion on the direct comparison of standing stocks scaling with a selected body-size range between the two shelf-sea megabenthic assemblages.

5.B.4.4 Concluding remarks

Shelf seas cover just about 9% of the Earth's ocean surface (Harris et al. 2014), yet they support 15-20% of the global marine primary production (Wollast 1998). The European continental shelves, in particular in the North Sea and in the Celtic Sea, have been extensively studied as key systems in the global carbon cycle, permitting to evaluate the monetary importance of shelf-sea sediments (de Haas et al. 2002; Thomson et al. 2017; Luisetti et al. 2019). These "blue carbon" ecosystems (Smith-Godfrey 2016) are thus important for Human society, and they require adequate and sustainable management. Nonetheless, seafloor carbon stocks are vulnerable to habitat disturbance (e.g. associated to fishing activity) and climate change in general, potentially impacting all levels of the marine food web. The use of individual body size can be of great value for assessing ecosystem services, where body-size spectral analyses, in the form of a service-oriented framework, may improve our understanding of the response of benthic organisms in the face of climate change and anthropogenic pressure (Blanchard et al. 2004, 2005, 2009; Petchey and Delgrano 2010; Rees et al. 2012; Godbold et al. 2013; Datta and Blanchard 2016; Henseler et al. 2019).

Chapter 6

Deep-sea sites

6.1 Introduction

The two deep-sea sites assessed in this Ph.D. thesis were located at the Porcupine Abyssal Plain sustained observatory (PAP-SO) in the NE Atlantic, and in the Clarion-Clipperton Zone (CCZ) in the NE Pacific. As described in chapter 2, these two sites exhibit large-scale topographic structures: small hills (< 100 m elevation) are a feature of the abyssal seafloor at PAP (4850 m water depth), and ridges and troughs (300 m elevation gradient) sculpt the seafloor at the CCZ study area (4150 m water depth). These two sites are primarily composed of mud sediments, with patchy occurrences of overlaying hard substrata of different size and areal cover (PAP-SO, clinker and iceberg drop stones; Durden et al. 2015a, 2016a; CCZ, polymetallic nodules; Simon-Lledó et al. 2019a, b). The annual seafloor temperature is generally low (PAP, 2.5 °C; CCZ, 1.5 °C) (Locarcini et al. 2018), and so are POC fluxes to the seabed (PAP-SO, 2.5 g C m^{-2} yr^{-1}; CCZ, 0.25 g C m^{-2} yr^{-1}) (Lutz et al. 2007). Megabenthic assemblages (invertebrates and demersal fish; ≥ 1 cm body length) (e.g. Bett 2019) were characterised from photographic analysis in terms of their constituent organisms across the different habitats (i.e. topographic strata), and standing stocks (abundance and biomass; Morris et al. 2016; Simon-Lledó et al. 2019a; appendices C and D), and flux (as respiration; this thesis), were quantified. To answer the main objectives (1, 2) of this Ph.D. thesis presented in chapter 1, spectral analyses of the body-size distributions of abundance, biomass, and estimated respiration flux, at the assemblage level, were performed and compared to the metabolic theory of ecology (MTE) (Brown et al. 2004).

Study of the body-size structure of two deep-sea megabenthic assemblages will provide insight into community functioning, on the basis that body size relates to physiological processes (Peters 1983). The MTE model predicts that the abundance and biomass-size spectra have slopes of -3/4 and

1/4, respectively, and that respiration flux is invariant (slope of 0), with body size. The model also predicts that the elevation of these slopes informs on both environmental temperature and resource supply. In the present assessment, the PAP site exhibits slightly higher environmental temperature (c. 1 °C difference), and much higher resource supply to the seafloor (c. 900% increase) by comparison to the CCZ site. In comparison to the two shelf-sea sites in the Celtic Sea analysed previously (chapter 5.B), demersal fish account for very little in terms of numerical density at the two deep-sea sites (c. 1% relative abundance) (Milligan et al. 2016; Simon-Lledó et al. 2019a). However, despite their position in the food web, or feeding habit (i.e. predatory and/or scavenging diet, known to change in time depending on resource availability and/or opportunity), fish still obtain their main resource from the common supply of organic matter shared with the rest of the invertebrate megabenthos, or at least benefit from enhanced potential prey biomass. Fish biomass contribution may have an influence on the overall megabenthos body-size spectrum; therefore, spectral analyses at the CCZ study site in the present chapter exclude and include demersal fish data. Fish were excluded from the original PAP image annotation as they formed part of a separate research project (Milligan 2015; Milligan et al. 2016). The trend in invertebrate body-size distribution at these two sites is expected to be consistent but to show disparity in elevation (intercept) in response to variation of local environmental characteristics.

In addition, data for smaller benthos (250 µm mesh size) from the PAP-SO site were available and analysed in complement of the megabenthos data. At CCZ, xenophyophores (‘giant’ protozoan Foraminifera) (e.g. Kamenskaya et al. 2015, 2016; Gooday et al. 2017a, b) represented a considerable fraction of the megabenthos (c. 85% relative abundance) (Simon-Lledó et al. 2019a). However, Hughes and Gooday (2004) indicate that photographic assessment alone cannot validate whether the specimens are alive or dead. Despite being considered part of the megabenthos (e.g. Bett 2019) given their comparable body size (up to 20 cm), the biomass (i.e. protoplasm) of xenophyophores is thought to be as little as 0.01-5% of their test volume (Levin and Gooday 1992; Gooday et al. 2018). Therefore, spectral analyses at the CCZ study site were performed excluding and including xenophyophores. The newly

developed generalised volumetric method (GVM) (Benoist et al. 2019b; chapter 4) was used to estimate CCZ xenophyophore body volume, and simple approximations (Levin and Gooday 1992; Gooday et al. 2018) were tested to calculate their protoplasmic contribution to GVM-derived biovolume.

The deep sea is a resource-limited system (McClain et al. 2012) where its constituent benthic fauna relies almost exclusively on the exported resource supply produced at the ocean surface (Etter and Grassle 1992; Johnson et al. 2007). It is expected that the body-size distribution from small (macrobenthos) to larger (megabenthos) fauna at PAP-SO follows a uniform pattern (slope and intercept), on the basis that the combined assemblages comprise of primary consumers across the entire body-size range assessed. Deviation from the model may reflect the influence of uncontrolled environmental variables, and/or that the deep-sea benthos represents a rather more complex trophic structure than a simple, single (or multi-mixed), trophic level system.

This chapter describes the megabenthic assemblages at the PAP-SO and at the north-eastern CCZ study sites, and it explores the body-size structure of the two assemblages considered. Ecological data consisted of large-scale datasets from seafloor images from both sites, and of directly sampled macrobenthos from the PAP-SO site. Field survey and subsequent sample processing and analysis are fully presented in chapter 3, and specific methodological and analytical considerations are detailed in the methods section below. Two methods were employed for generating individual body-size data: a taxon-specific length-weight relationship (LWR) approach was used with megabenthos data (invertebrates) from the PAP-SO site (Durden et al. 2016a), and a taxon-independent GVM (Benoist et al. 2019b; chapter 4) for macrobenthos from PAP-SO and for megabenthos (invertebrates, demersal fish, xenophyophores) from the CCZ study site. Spectral analyses were achieved at site scale and for each topographic stratum (i.e. abyssal plain, hill, ridge, and trough). The results presented in this chapter will be compared to those of chapter 5.B that dealt with shelf-sea megabenthic assemblages; chapter 7 will describe how environmental conditions (i.e. temperature and POC flux to the seabed) affect the body-size structure of shelf- and deep-sea assemblages.

6.2 Methods

Detailed descriptions of the field methodology employed to collect seafloor imagery data, of the photographic processing applied to the raw photographic sampling units, and of the subsequent image analysis steps, are provided in chapter 3 section 3.2, and metadata are summarised in table 3.1. For directly sampled macrobenthos, description of the field methodology, and of the sediment core samples processing and analysis, are detailed in section 3.3. Indirect estimation of individual biomass data from photographed megabenthos specimens, and of directly sampled macrobenthos specimens, are described fully in section 3.4, and in chapter 4. The analytical methods followed to assess the body-size distribution of the assemblage studied are defined in sections 3.5 and 3.6. These are recapitulated briefly below, and the sampling limitations specific to this analysis are discussed at the end of this chapter.

6.2.1 AUV-based seabed imagery

Large-scale ecological surveys were conducted at the PAP-SO site (2012, 85,294 m^2 seabed area; Ruhl 2013; chapter 3 figure 3.4) and in the area of particular environmental interest 6 (APEI-6) in the north-eastern CCZ (2015, 18,582 m^2 seabed area; Jones 2015; figure 3.5) using an autonomous underwater vehicle (AUV) (figure 3.1). Seafloor images were processed to improve visual quality following Morris et al.'s (2014) methodology, and at PAP-SO, they were mosaicked into ten-image tiles (c. 13 m^2 seabed area), whereas at CCZ, they were analysed individually (c. 1.7 m^2 seabed area). The AUV operated at a target altitude of 3.2 m above the seafloor at both sites, yielding images with a nominal seabed pixel resolution of c. 0.50 mm px^{-1} at PAP-SO and of c. 0.60 mm px^{-1} at CCZ.

6.2.2 Image data generation

Seafloor images were segregated into landscape types (i.e. topographic strata), as delimited using bathymetry data collected with the AUV during the photographic surveys. At PAP-SO, the hill (< 4840 m water depth) was categorised as distinct from the surrounding flat abyssal plain (c. 4850 m water depth) (Morris et al. 2016; appendix C). At CCZ, the plain (4100-4200

m water depth) was distinguished from the ridge (4000-4100 m), and from the trough (4200-4300 m) (Simon-Lledó et al. 2019a; appendix D). At each site, images were analysed to record of epibenthic invertebrate megafauna and demersal fish (count, taxonomic identification, body-size measurement) (Morris et al. 2016; Simon-Lledó et al. 2019a). All specimens, unitary and colonial forms, ≥ 1 cm in body length or in diameter, were retained in the analysis, with the exception of solitary tubicolous polychaetes (Sabellidae spp., Serpulidae spp.), bivalves, and gastropods, to avoid inclusion of empty tubes/shells. At PAP-SO, xenophyophores and demersal fish were observed (seen on imagery; personal observation; Lampitt 2017b, c; Stinchcombe 2017; Hartman 2019; Ruhl 2013, 2019), but not recorded in the present study. At both sites, specimens that could not be identified at the phylum level (i.e. referred to as indeterminate, < 1% total) were excluded from subsequent analysis.

6.2.3 Individual biomass estimation

6.2.3.1 Megabenthos (metazoan invertebrates and demersal fish)

The photographic dataset acquired at PAP-SO and at CCZ were analysed by independent image analysts for taxonomic assessment and individual body-size measurement of benthic specimens (Morris et al. 2016; Simon-Lledó et al. 2019a; appendices C and D). The PAP-SO is a 30-year time-series site where benthic trawling has been employed as a routine research tool (Billett et al. 2001, 2010), reporting between 60 and 80 megabenthos morphotypes. Durden et al. (2016a) accessed a database of some 47,000 specimens of trawl-caught megabenthos collected at PAP-SO to produce LWRs for 34 morphotypes, permitting indirect species-specific biomass (M_E in g wwt) estimation of the corresponding photographed morphotypes, from a single standard linear body-dimension measurement (SL) (chapter 4 equation 4.1; Durden et al. 2016a). At CCZ, the specimens were classified based on an existing morphotype catalogue (Amon et al. 2017a, b; Simon-Lledó et al. 2019a), however, the CCZ benthic megafauna has been little sampled and is typically poorly described (e.g. Glover et al. 2018), comprising many taxa that are new to science (Amon et al. 2016). Therefore, the generalised volumetric method (GVM) (Benoist et al. 2019b; chapter 4), based on geometric

considerations of individual body shape, was employed to estimate individual biovolume (V_E in mL; equation 4.3).

The CCZ photographic dataset was initially analysed prior to the start of this Ph.D. programme (Simon-Lledó et al. 2019a; appendix D), with the individual body-size measurement of specimens initially meant to be converted into biomass using LWRs, i.e. for each individual recorded, a standard linear (SL) body dimension was measured (see Durden et al. 2016a). To accelerate the process of GVM body-size measurements, a subset of the fauna assessed was re-measured to produce two dimensions per specimen, corresponding to an equivalent cylindrical diameter (ECD in mm) and to an equivalent cylindrical length (ECL in mm) (see details in chapter 4 section 4.3.2). For each metazoan morphotype identified, 50 individuals were randomly selected and measured according to the GVM approach, and those measurements were then extrapolated to the rest of the specimens, as follow:

$$ECD = SL \times ratio_a \quad \text{(equation 6.1a)}$$

$$ECL = SL \times ratio_b \quad \text{(equation 6.1b)}$$

where for each morphotype, $ratio_a = ECD/SL$, and $ratio_b = ECL/SL$, of the 50 individuals randomly selected. Estimated biovolume (V_E in mL) was determined using equation 4.3, and converted to biomass (M_E in g wwt) assuming tissue density of 1.056 g mL^{-1} (Benoist et al. 2019b; chapter 4). For Porifera, GVM-derived body volume (V_E) would greatly overestimate the actual proportion of organic content. Therefore, morphotype-specific corrections were applied to derive organic tissue biomass, ranging from 5% to 50% of V_E (Barthel 1995; Brey et al. 2010).

6.2.3.2 PAP-SO macrobenthos

Macrobenthos samples (macrofauna including all nematodes retained on the sieve; *n* = 492) were collected using a Megacorer at the PAP-SO central coring area, sorted on a 250-µm sieve, and identified to class level (chapter 3 section 3.3). Each specimen was observed using a stereomicroscope and manually sketched using a camera lucida, and photographed (figures 3.7 and 6.1). For estimation of individual biomass, the GVM (Benoist et al. 2019b; chapter 4) was employed. Two dimensions were measured for each individual: ECD (in mm) and ECL (in mm), which were representative of a cylinder of

equivalent volume. The body measurements were converted to estimated biovolume (V_E in mL) using the equation of a cylinder (equation 4.3), and converted to gram wet weight biomass (M_E in g wwt) assuming a tissue volumetric density of 1.056 (Benoist et al. 2019b; chapter 4).

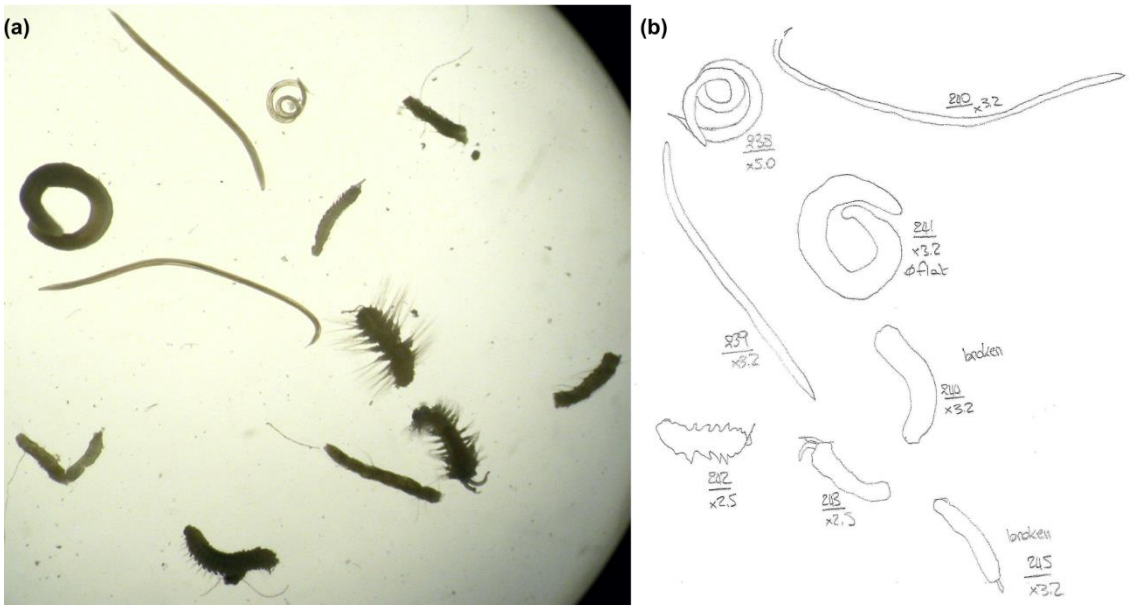

Figure 6.1. Macrobenthos specimens from the Porcupine Abyssal Plain sustained observatory. Example of macrobenthos samples (> 250 µm; 0-1 cm core-sediment horizon layer) of the phyla Annelida and Nematoda **(a)** as observed using a stereomicroscope, and **(b)** as manually sketched (i.e. body shape), for each specimen given individual identification number and the corresponding magnification of observation.

For incomplete polychaete specimens (i.e. only those fragments with a head; *n* = 59 out of 163 individuals), three methods were tested to estimate their complete body volume (V_{E-corr}):

(a) The V_{E-corr} of incomplete specimens (V_{E-corr_a}) was predicted based on the regression analysis of V_E on ECD of complete specimens as follows: $V_E = 0.0048 \times (ECD)^{2.4071}$ ($F_{1,109}$ = 375.85, p < 0.001, r^2 = 0.79). Then V_{E-corr} of incomplete specimens was estimated using that regression:

$$V_{E-corr\_a} = 0.0048 \times (ECD)^{2.4071} \qquad \text{(equation 6.2a)}$$

(b) The ECL of incomplete specimens (ECL_{corr_b}) was estimated by user judgement given the visible morphology of the specimen, in effect by applying a multiplication factor (i.e. 2, 3, 4, or 5) to the visible length of the fragment.

Then V_{E-corr} of incomplete specimens was estimated as:

$$V_{E-corr\_b} = \pi \times \left(\frac{ECD}{2}\right)^2 \times ECL_{corr\_b} \qquad \text{(equation 6.2b)}$$

(c) The ECL of incomplete specimens (ECL_{corr_c}) was estimated by assuming a constant multiplication factor of 10 between ECD and ECL; a similar approach to that adopted by Laguionie Marchais et al. (2020). Then V_{E-corr} of incomplete specimens was estimated as:

$$V_{E-corr\_c} = \pi \times \left(\frac{ECD}{2}\right)^2 \times ECD \times 10 \qquad \text{(equation 6.2c)}$$

Variation in median individual biovolume of incomplete polychaete specimens, as estimated by approaches (a-c), was illustrated by linear regression of biovolume-corrected (V_{E-corr_a-c}) on measured ECD, as performed in Minitab (V18.1, Minitab Inc.). Estimated biovolume (V_{E-corr} in mL) was then converted to biomass (M_{E-corr} in g wwt) assuming a tissue density of 1.056 g mL^{-1} (Benoist et al. 2019b; chapter 4).

6.2.3.3 CCZ xenophyophores (protozoan megabenthos)

Simon-Lledó et al. (2019a) identified 23 xenophyophore morphotypes. In this project, these protozoans were classified into four main categories based on overall morphological appearance: (i) hemispherical (e.g. *Syringammina* spp. grouped with morphotypes Reticulate 1-4, and Xenophyophore 2-4 and 6); (ii) plate like (e.g. morphotypes Plate 1, 2, 11, and Xenophyophore 8); (iii) tubular/branching (e.g. Plate 5, *Aschemonella* spp. grouped with Xenophyophore 1 and Tube 3); and (iv) undefined (e.g. Xenophyophore Other Form 2 type *Stannophyllum* spp.). In common with the GVM assessment of megabenthos metazoans (see section 6.2.3.1), 25 individuals per xenophyophore morphotype (yielding 100-125 individuals per morphological category; i-iv) were randomly selected and measured using the GVM approach (Benoist et al. 2019b; chapter 4). It was not possible to obtain GVM-derived estimates for three morphotypes (Other Form 3, Xenophyophore 10 and 11; c. 1.50% of the assemblage). For Xenophyophore 1 (type *Aschemonella* spp.), highly abundant (74%) in the protozoan assemblage, that covered two orders magnitude in ECD and one order magnitude in ECL, GVM-derived estimates were based upon a small percentage of randomly selected individuals (0.14%).

The GVM-estimated biovolume (V_E) of xenophyophores does not relate to the amount of living tissue (protoplasm) (Gooday et al. 2018); therefore, it was necessary to apply additional corrections (table 6.1):

(1) For hemispherical types (i) exhibiting a tightly or a loosely meshed, reticulated, test structure, comprising plate-like elements separated by open spaces, an 'envelop-to-structure' ratio was used to account only for the test structure volume (V_E), i.e. by discounting the open space of the outer, global, envelop body volume. The value of this ratio was visually gauged based upon the thickness of the test wall the compactness of the test structure, and it ranged from 50% (open structure) to 80% (compact structure).

(2) For all morphological categories (i-iv), a 'structure-to-cell' ratio was employed to estimate the amount of protoplasm (V_{E-corr}) comprising the test structure. Following table 2 in Levin and Gooday (1992), several values were tested, which represented a range of protoplasmic contributions to test volume (V_E): 0.01% (minimal; V_{E-corr_a}), 5% (maximal; V_{E-corr_b}), 0.8% (typical; V_{E-corr_c}), and taxon-specific values chosen to represent the closest relative in terms of physical structure (V_{E-corr_e}).

Recently, Gooday et al. (2018) performed micro-computed tomography (micro-CT; or 3-dimension x-ray imaging) to explore the internal structure of three CCZ species (*Psammina* spp. and *Galatheammina* sp.). The average value of their finding, 3.12% (table 1 in Gooday et al. 2018), was also tested to estimate protoplasmic contribution (V_{E-corr_d}) to test volume.

(3) Finally, for all categories (i-iv), a 'live-to-dead' ratio of 50% was applied, i.e. numerical density was reduced to one half of that recorded (Hughes and Gooday 2004; Professor A.J. Gooday, personal communication, February 27th 2018).

Variation in total xenophyophore standing stock estimates, as obtained using the different 'structure-to-cell' values (ratio 2), was assessed using Welch's ANOVA (Welch 1951), with subsequent pairwise comparisons made using the Games-Howell method (Games and Howell 1976). Data were $\log_{10}$-transformed prior to these analyses to account for the likely inhomogeneity of variance. Estimated (protoplasmic) biovolume (V_{E-corr}) was then converted to

biomass (M_{E-corr}) assuming a protoplasmic density of 1.056 g mL^{-1} (Benoist et al. 2019b; chapter 4).

Table 6.1. Summary table of the four main xenophyophore categories with the different correction-parameter values used to derive their biomass. The different steps to deriving xenophyophore protoplasm biomass (M_{E-corr}) from GVM-estimated body size (M_E) are detailed in section 6.2.3.3. **(1)** 'Envelop-to-structure' ratio applied to hemispherical specimens. **(2)** 'Structure-to-cell' ratio tested using different methods. **(3)** 'Live-to-dead' ratio (Hughes and Gooday 2004). Images of representative specimens for each category are also provided.

	Hemispherical	**Plate like**	**Tubular/branching**	**Undefined**
Main category			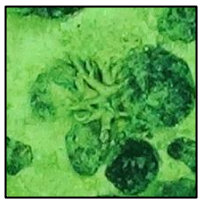	
	Reticulate 1	Xenophyophore 8	Plate 5	Undefined 2
(1)	50-80%	-	-	-
(2)	Five methods were tested across all categories: ***(a)*** 0.01% (minimal; Levin and Gooday 1992; M_{E-corr_a}); ***(b)*** 5% (maximal; Levin and Gooday 1992; M_{E-corr_b}); ***(c)*** 0.8% (typical; Levin and Gooday 1992; M_{E-corr_c}); ***(d)*** 3.12% (micro-CT average; Gooday et al. 2018; M_{E-corr_d}); ***(e)*** taxon-specific % value (Levin and Gooday 1992; M_{E-corr_e}).			
(3)	50%			

6.2.4 Standing stock analysis

Variation in epifaunal megabenthos (invertebrates) standing stock density and biomass at PAP-SO was analysed with water depth and terrain variables (bathymetric profile index, slope angle), as described by Morris et al. (2016). In their original assessment, the authors binned the image data into 12.5-m-depth intervals, and they assessed differences in stock variation using Welch's ANOVA (Welch 1951), with subsequent pairwise comparisons made using the Games-Howell method (Games and Howell 1976). In this Ph.D. thesis, data on infaunal macrobenthos was added to complement megabenthos stocks, and variation was assessed between the abyssal plain (c. 4850 m water depth) and the abyssal hill (< 4840 m water depth).

At CCZ, Simon-Lledó et al. (2019a) examined variation in epifaunal megabenthos (invertebrates + fish) standing stocks density (including

xenophyophores), and biomass (excluding xenophyophores), between the ridge, the trough, and the abyssal plain, areas (c. 4150 ± 150 m water depth), using a generalized linear model. In this thesis, variation in stocks (metazoan and including protozoan xenophyophores) between topographic strata was assessed using Welch's ANOVA (Welch 1951), with subsequent pairwise comparisons made using the Games-Howell method (Games and Howell 1976).

6.2.5 Body-size spectral analysis

Individual-based body-size spectra of abundance (N_i in ind. m^{-2}), biomass (W_i in g wwt m^{-2}), and estimated respiration flux (B_i in mg C m^{-2} d^{-1}), were constructed using $\sqrt{2}$ geometric body-size classes (M_i in g wwt) (appendix G). B_i was calculated from individual metabolic rate (I_i) using Hemmingsen's (1960) equation for standard metabolic rate of poikilotherms at 20 °C, with a site-specific temperature-correction (i.e. PAP, 2.5 °C; CCZ, 1.5 °C; Gillooly et al. 2001; details in chapter 3 section 3.5; equation 3.1), and multiplied by size-class abundance (N_i). In the present analysis, the normalisation constant employed in equation 3.1 converted to 0.0124 mg C d^{-1} at PAP, and to 0.0114 mg C d^{-1} at CCZ. A minimum number of ten individuals per size class was maintained by merging data between consecutive size classes where necessary. All variables are presented on $\log_{10}$ axes, where on the x-axis each class is c. 1.41 the size of the class above/below. Size spectra were produced for each site and for each topographic stratum (i.e. plain at both sites, hill at PAP-SO, ridge and trough at CCZ), with invertebrate data only (PAP-SO), and excluding/including demersal fish and xenophyophores (CCZ). The contribution of phyla overall to size-class abundance was calculated for both sites.

The right-hand side (Bett 2013, 2014) of abundance, biomass, and estimated respiration flux, spectra were compared against the MTE predictions using a linear regression model in Minitab (V18.1, Minitab Inc.). Body-size data of CCZ xenophyophores are presented in this thesis as an illustration of the method used to estimate their biomass; employing the GVM, and testing various corrections to derive protoplasmic contribution to estimated body size, are still at an exploratory phase. At PAP-SO, the distribution of abundance with body size of macrobenthos was compared to that of megabenthos by

general linear model (LM) analysis in Minitab, and variation in the slope constants and intercept coefficients was assessed. A similar assessment between metazoan and protozoan abundance distribution data was carried out at CCZ. For comparison of body-size spectra between topographic strata, regression analyses were performed with abundance data.

6.2.6 Sampling limitations

Differences in field operations, photographic-sample processing, and data acquisition (i.e. specimen detection, body-size measurement, and estimation of individual biomass) are fully presented in chapter 3 and briefly enumerated here; these will be discussed in more detail in the conclusion chapter. (1) The photographic samples at PAP-SO were analysed in the form of ten-image tiles, whereas at CCZ they were assessed individually, presenting disparity in the physical scale of photographic analysis. (2) Several image analysts assessed the two datasets, introducing the potential for individual analysis bias in terms of specimen detection, identification, and body-size measurement. (3) Morphotypes inhabiting tubes or shells were excluded from this analysis on the premise that it was impossible to determine whether they were alive or dead. (4) Two methods were employed to estimate individual biomass: the taxon-specific LWR approach; and the taxon-independent GVM approach. (5) At both sites, specimens that were observed partially or that were present above the seabed were allocated the mean individual biomass of their corresponding morphotype, leading to binning them into one resultant body-size bin. It was the case for four individuals only at CCZ. Similarly, at PAP-SO, taxa for which no LWRs were available in the literature, but for which biomass data had previously been obtained (i.e. from trawl-caught individuals), were allocated average individual biomass values (e.g. tunicates, Brisingida sea star, sponges). (6) PAP-SO infaunal macrobenthos samples were collected using a Megacorer, and each specimen was measured to estimate its individual body mass using the GVM. PAP-SO megabenthos were assessed using AUV photography, therefore targeting epifauna.

6.3 Results

6.3.1 Porcupine Abyssal Plain sustained observatory

6.3.1.1 Macrobenthos biomass estimates

The GVM was employed to estimate individual biomass of macrobenthos samples (250 µm mesh size; including all nematodes retained on the sieve). For incomplete polychaete specimens, three methods (a-c; section 6.2.3.2) were tested to estimate their complete body volume, yielding median individual biovolume (V_{E-corr}) values ranging from 4.55 × 10^{-5} mL (V_{E-corr_c}) to 8.91 × 10^{-5} mL ($V_{E-corr-b}$), by comparison to the median individual biovolume (V_E) of complete specimens 3.92 × 10^{-5} mL. Method (a), i.e. prediction of V_{E-corr_a} of incomplete specimens from regression analysis of V_E on ECD of complete specimens (equation 6.2a), gave estimates that were closer to those of the sampled intact-polychaete population. The V_{E-corr_a} estimates were notably less scattered around the regression line than those of method (b). Method (c) produced values similarly constrained as method (a), however, method (c) appeared to introduce a size-related bias (figure 6.2c), i.e. underestimation at low measured ECD, and overestimation at high measured ECD. Consequently, method (a) was selected as the optimal approach, and only data generated in that way (V_{E-corr_a}) were employed in subsequent analyses.

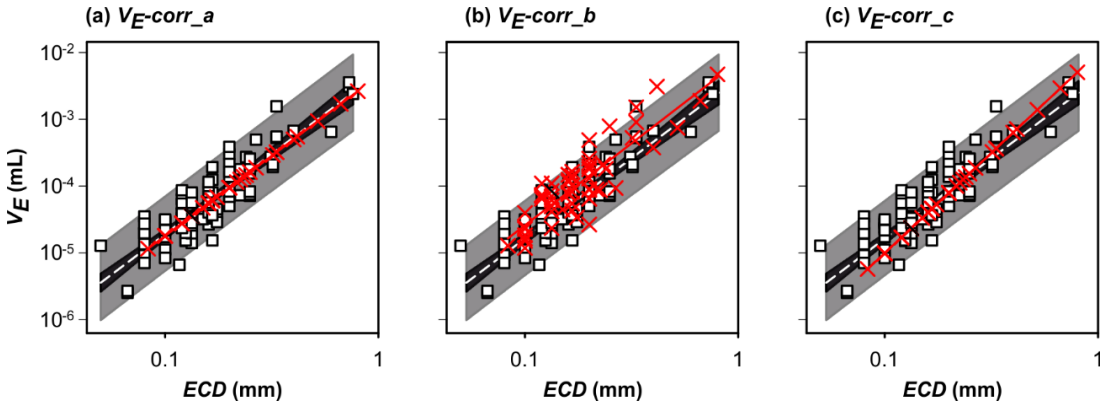

Figure 6.2. Estimation of individual GVM-derived biovolume of macrobenthic polychaetes from the Porcupine Abyssal Plain sustained observatory. Three methods were tested to estimate individual biovolume of incomplete polychaete specimens (V_{E-corr} in mL; see section 6.2.3.2). **(a)** V_{E-corr_a}, equation 6.2a. **(b)** V_{E-corr_b}, equation 6.2b. **(c)** V_{E-corr_c}, equation 6.2c. Estimated biovolume of incomplete specimens (V_{E-corr_a-c}, red cross) and its corresponding regression line (red) are overlaid on top of intact specimen data (V_E, white square) illustrated with regression line (dashed white) with corresponding 95% confidence intervals (black shade) and prediction intervals (grey shade).

6.3.1.2 Benthic assemblage description

The total megabenthic epifaunal abundance at PAP-SO was 0.62 ind. m^{-2} (figure 6.3), with Cnidaria and Echinodermata contributing 90% of the assemblage assessed. In particular, *Iosactis vagabunda* (Cnidaria sp. 2), Ophiuroidea, and Elpidiidae spp. (including *Amperima rosea*, *Ellipinion* spp., *Kolga* spp.), were the most abundant morphotypes observed, contributing 76% of the specimens. Standing stock density exhibited a statistically significant difference between topographic strata (Welch's ANOVA, $p < 0.001$), with the hill habitat having the higher density (0.64 ind. m^{-2}), and the surrounding abyssal plain the lower (0.56 ind. m^{-2}). The total macrobenthic infaunal abundance was 73 ind. m^{-2}, with Arthropoda, Annelida, and Nematoda, contributing 96% of the assemblage analysed. In particular, Copepoda (harpacticoids) and Polychaeta were the most abundant taxa analysed.

The total megabenthic epifaunal biomass, as estimated using LWRs, was 2.8 g wwt m^{-2} (figure 6.3), with Echinodermata and Cnidaria contributing 97% of the assemblage assessed. The biomass-dominant taxa were Elpidiidae spp., *Psychropotes longicauda*, *Pseudostichopus villosus*, and *Oneirophanta mutabilis*. Despite being a numerically dominant taxon, *I. vagabunda* contributed little (3.5%) to the total assemblage biomass. Standing stock biomass also varied significantly between topographic strata (Welch's ANOVA, $p < 0.001$), with the hill habitat having the higher biomass (5.7 g wwt m^{-2}), and the surrounding abyssal plain the lower (2.4 g wwt m^{-2}). The total macrobenthic infaunal biomass, as estimated using the GVM, was 0.02 g wwt m^{-2}, with Arthropoda, Annelida, and Mollusca, contributing 96% of the assemblage analysed. In particular, Isopoda, Polychaeta, and Bivalvia, were the biomass-dominant classes.

A total of 61 distinct morphotypes of epifaunal megabenthos in eight phyla were recorded, with almost all morphotypes observed in both the hill and the plain habitats. Five morphotypes were rare (i.e. $n \leq 5$ ind. recorded in total). Macrobenthos infauna were identified to class level and were represented by 12 classes in five phyla, plus an indeterminate specimen.

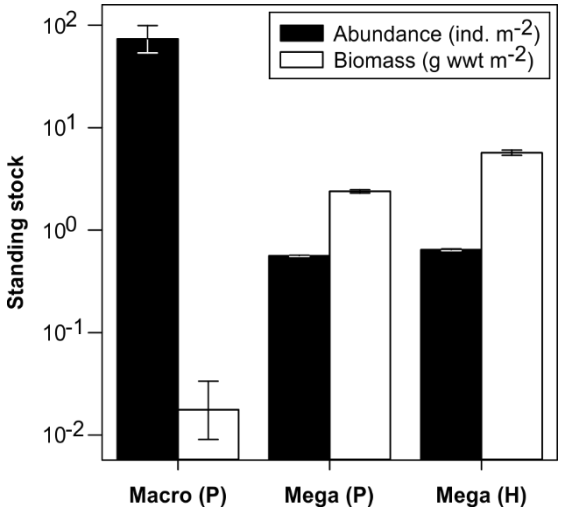

Figure 6.3. Standing stocks of macro- and megabenthic invertebrates at the Porcupine Abyssal Plain sustained observatory. Total faunal abundance (N in ind. m^{-2}) and biomass (W in g wwt m^{-2}) of macro- (250 µm sieve mesh) in abyssal 'PAP central' (Macro P) plain and megabenthic (≥ 1 cm) invertebrates in the plain (Mega P) and on the hill (Mega H), illustrated as geometric mean values with corresponding 95% confidence intervals.

6.3.1.3 Body-size spectra at PAP-SO

For macrobenthos, individual biomass ranged from 4.8 × 10^{-4} mg wwt (Nematoda) to 9.0 mg wwt (Bivalvia) (figure 6.4a). Although note the presence of an exceptionally large isopod (0.12 g wwt) that was collected opportunistically from a sediment core and retained in this analysis for illustration purpose (see chapter 3 section 3.5; figures 3.8 and 3.9). Arthropoda (Copepoda [Harpacticoida], Isopoda) body sizes were spread almost throughout the entire macrobenthos spectrum. Nematodes were principally restricted to the smaller body-size classes < 1.5 × 10^{-1} mg wwt, and dominated the smallest classes < 6.7 × 10^{-3} mg wwt. Annelida (Polychaeta) were mainly recorded in larger size classes > 1.4 × 10^{-2} mg wwt, where they were the dominant taxon in almost all cases. Mollusca (mostly bivalves) were largely restricted to the larger size classes > 8.6 × 10^{-1} mg wwt, where they were major contributors to size-class biomass. A single occurrence of Echinodermata (Ophiuroidea) was recorded at c. 5 mg wwt.

For megabenthos invertebrates, individual biomass ranged from 0.02 g wwt (Ophiuroidea) to 2.9 kg wwt (*P. longicauda*) (figure 6.4b). Cnidaria and Echinodermata were the major contributors to both abundance and biomass standing stocks, and they were found in all body-size classes (Cnidaria ≤ 320

g wwt). Polychaeta were spread in small classes ≤ 10 g wwt, similarly to Arthropoda that comprised Pycnogonida (around 0.1 g wwt) and squat lobsters. Tunicata and Porifera were all binned into the size class 0.63 g wwt as a result of the allocation of average individual biomass values (i.e. from trawl-caught specimens) to all the individuals recorded. A few occurrences of large Cephalopoda were observed in size class c. 160 g wwt.

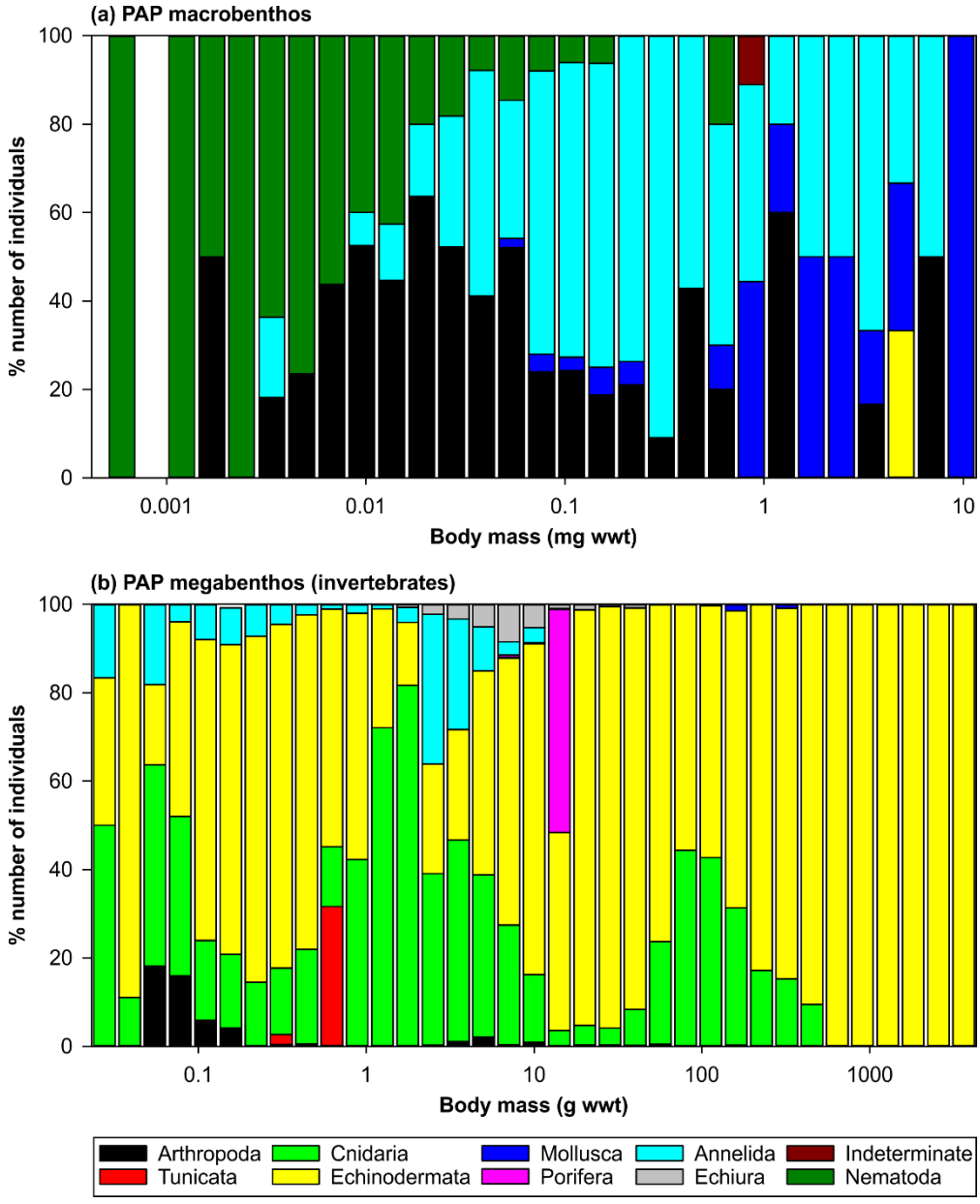

Figure 6.4. Contribution of phyla to total size-class abundance at the Porcupine Abyssal Plain sustained observatory. (a) Macrobenthic invertebrates (250 µm sieve mesh). **(b)** Megabenthic invertebrates (≥ 1 cm). Note different body mass units between macro- (mg) and megabenthos (g).

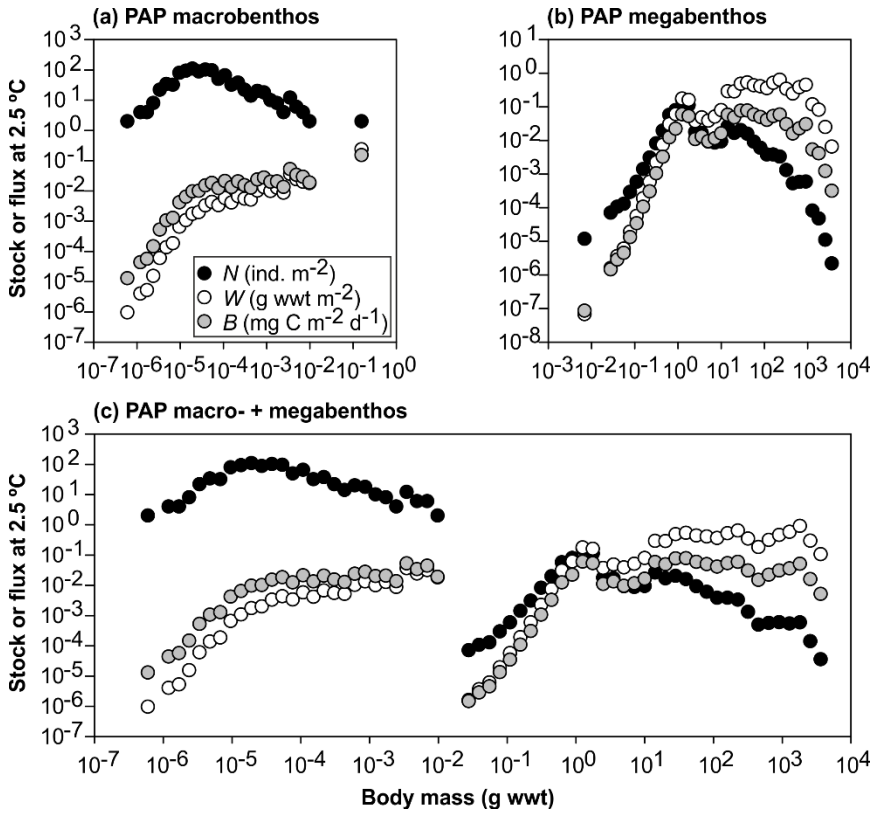

Figure 6.5. Macrobenthos and megabenthos body-size spectra at the Porcupine Abyssal Plain sustained observatory. Body-size distribution of abundance (N_i in ind. m^{-2}), biomass (W_i in g wwt m^{-2}), and estimated respiration flux (B_i in mg C m^{-2} d^{-1}) against body size (M_i in g wwt) at PAP-SO at in situ temperature (i.e. 2.5 °C). **(a)** Macrobenthic invertebrates (250 µm sieve mesh). **(b)** Megabenthic invertebrates (≥ 1 cm). **(c)** Combined macro- and megabenthic body-size spectra.

The individual-based body-size spectrum span 29 classes for macrobenthos, and 35 classes for megabenthos invertebrates (figure 6.4), and exhibited peaks at 1.91 × 10^{-2} mg wwt and 1.25 g wwt, respectively (figure 6.5), marking the starting point of the respective right-hand sides of the spectra (figure 6.6) . In the megabenthos, the numerically dominant taxa *I. vagabunda* and Ophiuroidea (60% of the assemblage) were principally found around the peak-abundance size class, with 85% of *I. vagabunda* and 30% of Ophiuroidea present in classes 1.25-1.80 g wwt. A trough is evident between size classes 5-10 g wwt, with an abrupt decline in abundance of these two morphotpyes, and of Polychaete sp. 1, Cnidaria spp. 5 and 12, followed by a secondary peak abundance between 14-40 g wwt related to high abundances of Elpidiidae spp. and Porifera. All *Umbellula* sp. 1 were binned into size class 3.5 g wwt, and all Porifera into class 14 g wwt, as a result of the allocation of single average individual biomass values (i.e. from trawl-caught specimens) to

all the individuals recorded. Similarly, for the different morphotypes of Tunicata (2.5 g wwt), Brisingida and Crinoidea (5.0 g wwt), Asteroid sp. 3 (Pterasterid; 28 g wwt).

6.3.1.4 Abundance, biomass, and respiration flux against MTE predictions at PAP-SO

Data at PAP were summarized well by the MTE predictions, both in the macrobenthos and in the megabenthos size fraction, and when combined (figure 6.6; table 6.2). Invertebrate abundance decreased with body size with slopes of -0.57 (macrobenthos) and -0.73 (megabenthos), not significantly different from the MTE prediction of -0.75 in the case of the megabenthos. Biomass increased with body size with slopes of 0.39 (macrobenthos) and 0.27 (megabenthos), not significantly different from the MTE prediction of 0.25 in the case of the megabenthos. Respiration flux varied with body size with slopes ranging between 0.18 (macrobenthos) and 0.02 (megabenthos), not significantly different from the MTE prediction of 0.00 in the case of megabenthos. Intercept values (related to resource supply) for abundance, biomass, and respiration flux, ranged between 0.0282 and 0.2710 across both size fractions, with the macrobenthos intercepts generally higher than those for the megabenthos (one order magnitude in the case of abundance and biomass).

Results of the general linear model analysis revealed no statistically significant difference in intercept between macro- and megabenthos body-size distribution of abundance ($F_{1,34}$ = 2.5, p = 0.124), nor in slope coefficient ($F_{1,34}$ = 3.31, p = 0.078). Abundance across the two size fractions (i.e. macro- + megabenthos) decreased with a slope of -0.70; not significantly different from the MTE prediction. Biomass and respiration flux across the two size fractions increased with slopes of 0.28 and of 0.03, respectively, neither being significantly different from the corresponding MTE predictions.

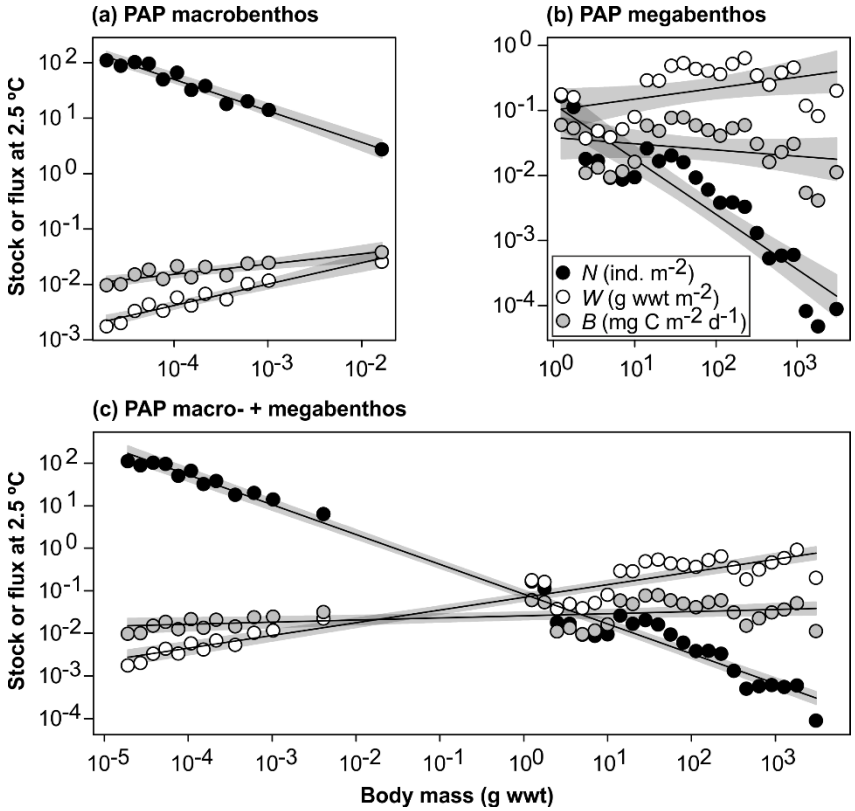

Figure 6.6. Macrobenthos and megabenthos right-hand side body-size spectra at the Porcupine Abyssal Plain sustained observatory. Body-size distribution of abundance (N_i in ind. m^{-2}), biomass (W_i in g wwt m^{-2}), and estimated respiration flux (B_i in mg C m^{-2} d^{-1}) against body size (M_i in g wwt) at PAP-SO at in situ temperature (i.e. 2.5 °C). **(a)** Macrobenthic invertebrates (250 µm sieve mesh). **(b)** Megabenthic invertebrates (≥ 1 cm). **(c)** Combined macro- and megabenthic body-size spectrum. Shaded areas are 95% confidence intervals. See table 6.2 for the corresponding regression equations.

Table 6.2. Spectral analyses of stocks and flux at the Porcupine Abyssal Plain sustained observatory. Regression analysis for abundance (N_i in ind. m^{-2}), biomass (W_i in g wwt m^{-2}), and estimated respiration flux (B_i in mg C m^{-2} d^{-1}) against body size (M_i in g wwt) of macrobenthic invertebrates (250 µm sieve mesh; Macro) and megabenthic invertebrates (≥ 1 cm; Mega) at PAP-SO at in situ temperature (i.e. 2.5 °C). See figure 6.6 for corresponding plots. *p < 0.05, **p < 0.01, ***p < 0.001, ns: not significant.

Regression	Equation	Slope 95% CI	N	F	r²
Abundance (ind. m^{-2})					
Macrobenthos	$N_i = 0.2710\ M_i^{-0.57}$	-0.64, -0.49	12	268.03***	0.96
Megabenthos	$N_i = 0.0943\ M_i^{-0.73}$	-0.87, -0.59	23	126.11***	0.86
Macro + mega	$N_i = 0.0840\ M_i^{-0.70}$	-0.74, -0.65	35	1147.47***	0.97
Biomass (g wwt m^{-2})					
Macrobenthos	$W_i = 0.1449\ M_i^{0.39}$	0.31, 0.47	12	114.23***	0.92
Megabenthos	$W_i = 0.0790\ M_i^{0.27}$	0.13, 0.41	23	16.50**	0.44
Macro + mega	$N_i = 0.0699\ M_i^{0.28}$	0.23, 0.32	35	189.65***	0.85
Respiration (mg C m^{-2} d^{-1})					
Macrobenthos	$B_i = 0.0910\ M_i^{0.18}$	0.11, 0.26	12	28.25***	0.74
Megabenthos	$B_i = 0.0317\ M_i^{0.02}$	-0.11, 0.16	23	0.10 ns	0.00
Macro + mega	$N_i = 0.0282\ M_i^{0.03}$	0.00, 0.07	35	4.19*	0.11

6.3.1.5 Habitat-specific body-size distribution of megabenthos abundance at PAP-SO

The body-size distribution of megabenthos abundance at PAP-SO was similar between the hill and the plain habitats, and data were summarized well by the MTE prediction in both habitats (figure 6.7; table 6.3). Invertebrate abundance decreased with body size with a slope of -0.72 on the hill, and of -0.68 on the plain, not significantly different from the MTE prediction of -0.75 in the case of the hill. The intercept value was slightly higher on the plain (0.0924) than on the hill (0.0791).

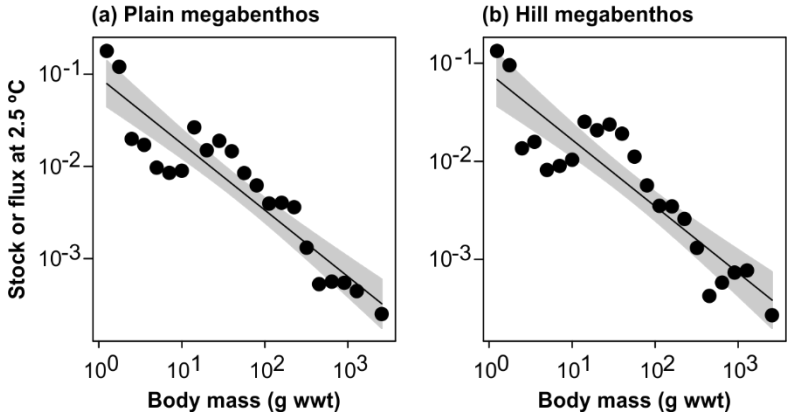

Figure 6.7. Megabenthos right-hand side body-size spectra at the Porcupine Abyssal Plain sustained observatory by habitat type. Body-size distribution of abundance (N_i in ind. m^{-2}) against body size (M_i in g wwt) at PAP-SO at in situ temperature (i.e. 2.5 °C). **(a)** Plain habitat (c. 4850 m water depth). **(b)** Hill habitat (< 4840 m water depth). Shaded areas are 95% confidence intervals. See table 6.3 for the corresponding regression equations.

Table 6.3. Spectral analyses of megabenthos abundance at the Porcupine Abyssal Plain sustained observatory by habitat type. Regression analysis for abundance (N_i in ind. m^{-2}) against body size (M_i in g wwt) for megabenthic invertebrates (≥ 1 cm) at PAP-SO at in situ temperature (i.e. 2.5 °C) between the plain habitat (c. 4840 m water depth) and the hill habitat (< 4840 m water depth). See figure 6.7 for corresponding plots. ***p < 0.001.

Regression	Equation	Slope 95% CI	N	F	r^2
Plain	$N_i = 0.0924\, M_i^{-0.72}$	-0.86, -0.77	22	123.44***	0.86
Hill	$N_i = 0.0791\, M_i^{-0.68}$	-0.83, -0.53	22	93.31***	0.82

6.3.2 Clarion-Clipperton Zone

6.3.2.1 Xenophyophore biomass estimates

The GVM was employed to estimate the body size of xenophyophores, with individual biovolume estimates (V_E) subsequently corrected to derive the outer test volume into living protoplasm biomass (M_{E-corr}), using different correction ratios obtained from literature (Levin and Gooday 1992; Gooday et al. 2018) (table 6.1; figure 6.8). Mean individual 'corrected' protoplasmic estimates ranged from 7.2 × 10^{-5} g wwt (M_{E-corr_a}; minimal volumetric protoplasmic contribution to V_E, 0.01%) to 3.6 × 10^{-2} g wwt (M_{E-corr_b}; maximal, 5%). Standing stock 'corrected' protoplasmic biomass estimates ranged from 1.2 × 10^{-4} g wwt m^{-2} (M_{E-corr_a}) to 6.1 × 10^{-2} g wwt m^{-2} (M_{E-corr_b}). Using the typical amount of protoplasm calculated from Levin and Gooday (1992) (i.e. 0.8%), and the morphotype-specific values estimated by the same authors, corrected standing stock biomass were estimated at 9.2 × 10^{-3} g wwt m^{-2} (M_{E-corr_c}), and at 7.3 × 10^{-2} g wwt m^{-3} (M_{E-corr_e}), respectively, i.e. very close between these two methods. Method (a; 0.01%) yielded very low biomass estimates by comparison to the other methods. Methods (d; 3.12%) and (e; taxon-specific %) were the most 'sophisticated' but may be difficult to implement generally. Method (c; 0.8%) may be a good compromise between realistically representative and practically implementable. Consequently, method (c) was selected to derive protoplasmic biomass, and only data generated in that way (M_{E-corr_c}) were employed in subsequent analyses.

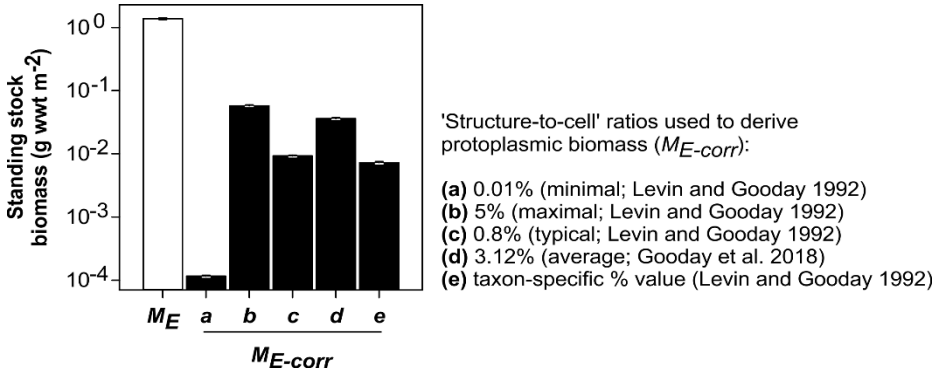

Figure 6.8. Xenophyophore GVM-derived biomass estimates at the Clarion-Clipperton Zone study site. The amount of living protoplasm (M_{E-corr}) in proportion to GVM-derived biomass (M_E) was estimated using different 'structure-to-cell' correction values (see section 6.2.3.3; table 6.1). Illustrated as geometric mean values with corresponding 95% confidence intervals.

6.3.2.2 Megabenthic assemblage description

The total megabenthos (metazoan) abundance at the CCZ study site was 0.41 ind. m^{-2} (figure 6.9a), with Cnidaria (mostly Anthozoa) dominating the assemblage assessed (41% total assemblage), especially in the plain (50%) and in the ridge (43%) habitats. Porifera was the second most abundant taxon (17%), and contributed the most to the fauna of the trough habitat (36%). Bryozoa, Annelida, and Echinodermata, were equitably present (9-10% total), similar to Mollusca and Arthropoda (6%). Among the Echinodermata, Ophiuroidea and Echinoidea, were the most abundant classes recorded, particularly on the ridge. Mollusca were mainly represented by Bivalvia, also most abundant on the ridge. Demersal fish were among the least abundant taxa (1%), and in equitable proportion between habitats. Combined with xenophyophores (protozoan; assuming one half of the individuals recorded were dead; see section 6.2.3.3; Hughes and Gooday 2004), the total megabenthic abundance at the survey site was 1.69 ind. m^{-2}. Xenophyophores dominated (75%) the epifauna megabenthos observed in all three landscape types assessed, and were particularly abundant on the ridge habitat. Metazoan invertebrate and demersal fish standing stock density exhibited a statistically significant difference between habitats (Welch's ANOVA, $p < 0.001$), with the plain and the ridge habitats having the higher density (0.27 ind. m^{-2}), and the trough habitat the lower (0.18 ind. m^{-2}). All pairwise comparisons were significant (Games-Howell, $p < 0.001$), except between the plain and the ridge habitat (Games-Howell, $p = 0.964$). Including xenophyophore data, standing stock density increased between three and five times between habitats, and exhibited a statistically significant difference between all habitat types (Welch's ANOVA, $p < 0.001$), with the ridge having the higher density (0.55 ind. m^{-2}), and the trough the lower (0.28 ind. m^{-2}); all pairwise comparisons were statistically significant (Games-Howell, $p < 0.001$).

Metazoan and protozoan biomass was estimated using the GVM (Benoist et al. 2019b; chapter 4), based on GVM-derived assessment of a sub-sample of the fauna that was extrapolated to the rest of the population (sections 6.2.3.1 and 6.2.3.3; equation 6.1). The total megabenthic (metazoan) biomass at CCZ was 1.24 g wwt m^{-2} (figure 6.9b), with Echinodermata (48%) and Fish (29%) the main contributors. The biomass-dominant invertebrate

taxa were Echinoid sp. 3 and the holothurians *Benthodytes typica* and *Peniagone* sp. 1, despite their low numerical abundance. Even though numerically dominant, Cnidaria and Porifera contributed little to the total metazoan biomass (8.7% and 0.15%, respectively). Annelida, Bryozoa, and Porifera, were the least contributors to total biomass. Metazoan standing stock biomass exhibited a statistically significant difference between habitats (Welch's ANOVA, $p < 0.001$), with the plain and the ridge habitats having the higher biomass (1.0×10^{-1} g wwt m^{-2}), and the trough habitat the lower (3.8×10^{-3} g wwt m^{-2}). All pairwise comparisons were significant (Games-Howell, $p < 0.001$), except between the plain and the ridge habitat (Games-Howell, $p = 0.821$). Including xenophyophore data (M_{E-corr_c}), standing stock biomass exhibited a statistically significant difference between all landscape types (Welch's ANOVA, $p < 0.001$), with the plain and the ridge having the higher biomass (3.4×10^{-2} g wwt m^{-2} and 5.7×10^{-2} g wwt m^{-2}, respectively), and the trough the lower (8.8×10^{-3} g wwt m^{-2}). All pairwise comparisons were significant (Games-Howell, $p < 0.001$), except between the ridge and the plain (Games-Howell, $p = 0.035$).

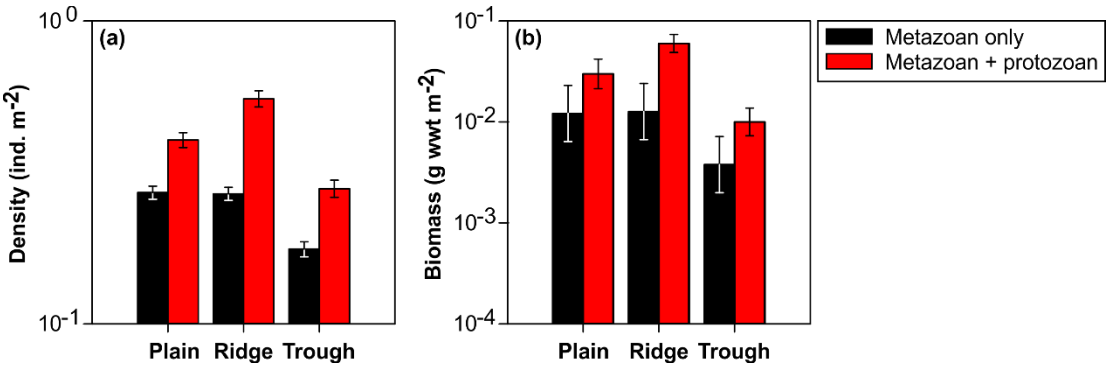

Figure 6.9. Standing stocks of megabenthic metazoan and xenophyophores at the Clarion-Clipperton Zone study site by habitat. (a) Total faunal abundance (N in ind. m^{-2}) and **(b)** total biomass (W in g wwt m^{-2}) of megabenthic (≥ 1 cm) invertebrates and demersal fish excluding/including xenophyophores, illustrated as geometric mean values with corresponding 95% confidence intervals. For xenophyophores, biomass (M_{E-corr_c})was derived using a 'typical' value of 0.8% for deriving protoplasmic contribution to GVM-derived body size (see section 6.2.3.3; table 6.1).

About 130 megabenthos metazoan morphotypes (invertebrates and demersal fish) were recorded in nine phyla, including 57 that were rare (i.e. $n \leq 5$ ind. recorded in total), and 20 singletons. The xenophyophore (protozoan)

morphotypes, previously identified by Simon-Lledó et al. (2019a), were grouped into four main morphological categories: (i) hemispherical, (ii) plate like, (iii) tubular/branching, and (iv) undefined (see example specimens in table 6.1).

6.3.2.3 Body-size spectra at CCZ

Metazoan invertebrates and demersal fish megabenthos. Individual biomass ranged from 0.06 mg wwt (Demosponge sp. 5) to 5.6 kg wwt (*Coryphaenoides* spp.) (figure 6.10a). Porifera and Cnidaria, which were the two most abundant phyla recorded, were spread through the smallest (mainly ≤ 0.01 g wwt) and the intermediate (≤ 3.5 g wwt) body-size classes, respectively, with only a few occurrences of larger individuals. Bryozoa, Annelida, and Mollusca, were mostly recorded in the smallest classes < c. 1 g wwt, and Echinodermata were principally found in classes ≥ 2.5 g wwt. The individual-based body-size metazoan spectrum spanned 49 classes, and revealed a peak abundance at 0.11 g wwt (figure 6.11a, b), marking the starting point of the right-hand side of the spectra (figure 6.14 a, b) (Bett 2013; 2014). A first smaller peak abundance is evident at size class 2.4×10^{-3} g wwt, associated with a high number of Porifera sp. 5, gradually decreasing in the next classes. The most abundant metazoan taxa were Alcyonacea sp. 1 (18%) and Porifera sp. 5 (11%). Most classes ≥ 160 g wwt comprised few individuals, mainly Echinoid sp. 3, the large holothurians *Peniagone* spp., *Benthodytes typica*, and *Benthothuria* sp. 1, Echinoid sp. 3, and the fish *Bathysaurus* sp. and *Coryphaenoides* spp. The addition of demersal fish data to the megabenthos spectrum did not change its overall shape, nonetheless the body-size distribution including fish was less scattered at the right-hand end, with most fish recorded in the classes 2.5 g wwt to 7.0 g wwt, and fewer occurrences in the largest classes.

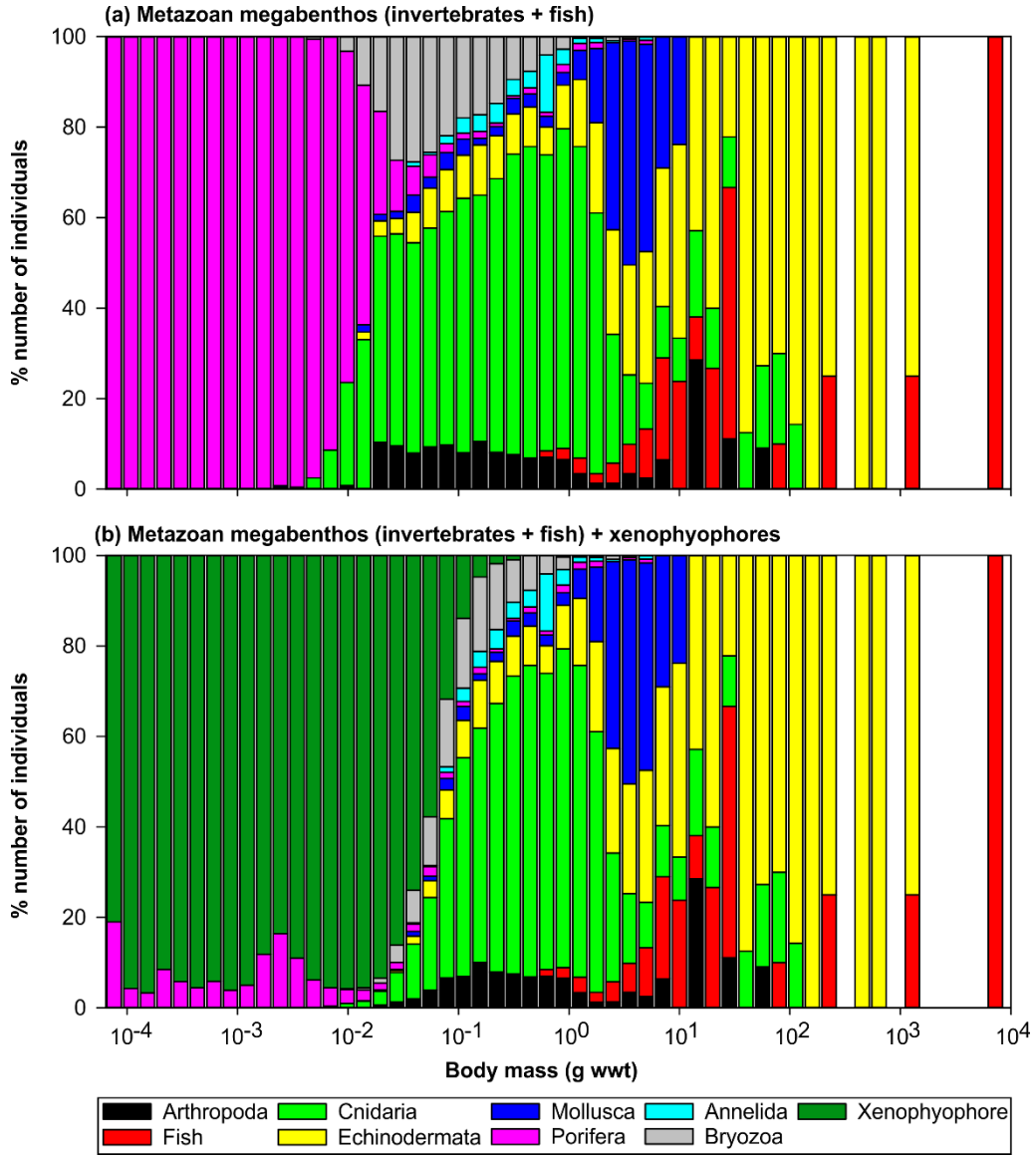

Figure 6.10. Contribution of phyla to total size-class abundance at the Clarion-Clipperton Zone study site. (a) Metazoan megabenthic invertebrates and demersal fish (≥ 1 cm). **(b)** Combined metazoan megabenthos (invertebrates + fish) and protozoan xenophyophores. For xenophyophores, biomass ($M_{E-corr\_c)}$ was derived using a 'typical' value of 0.8% for deriving protoplasmic contribution to GVM-derived body size (see sections 6.2.3.3 and 6.3.2.1; table 6.1; figure 6.8).

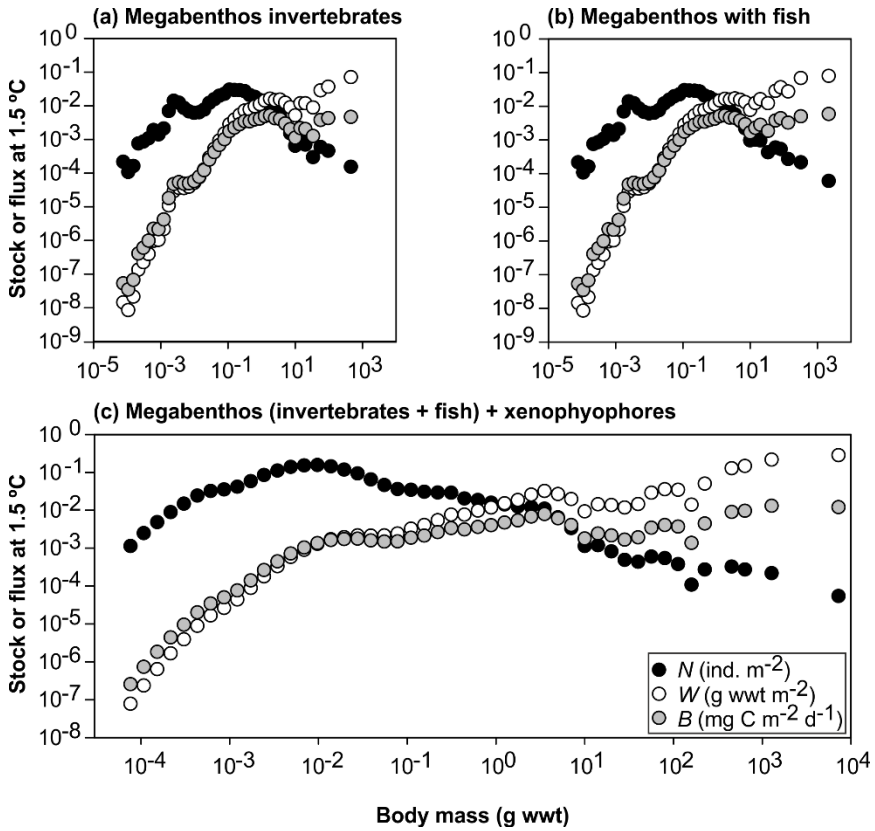

Figure 6.11. Megabenthos body-size spectra at the Clarion-Clipperton Zone study site. Body-size distribution of abundance (N_i in ind. m^{-2}), biomass (W_i in g wwt m^{-2}), and estimated respiration flux (B_i in mg C m^{-2} d^{-1}), against body size (M_i in g wwt) at CCZ at in situ temperature (i.e. 1.5 °C). **(a)** Metazoan megabenthic invertebrates (≥ 1 cm). **(a)** Combined metazoan invertebrates and demersal fish. **(c)** Combined metazoan megabenthos (invertebrates + fish) and protozoan xenophyophores. For xenophyophores, biomass (M_{E-corr_c})was derived using a 'typical' value of 0.8% for deriving protoplasmic contribution to GVM-derived body size (see sections 6.2.3.3 and 6.3.2.1; table 6.1; figure 6.8).

Xenophyophore fauna. The body-size distributions of xenophyophore abundance varied substantially between the different methods employed to derive protoplasmic contribution (M_{E-corr}) to GVM-derived test volume V_E, using different correction values ranging from 0.01% to 5% of V_E (sections 6.2.3.3 and 6.3.2.1; table 6.1; figure 6.12). They are illustrated in figure 6.12 for visual comparison, but the subsequent body-size spectral assessments were based on M_{E-corr_c} data (see results in section 6.3.2.1; figure 6.8). With protoplasmic biomass contributing 0.8% of their test volume, xenophyophore specimens ranged across 28 body size classes, from 5.4 × 10^{-5} g wwt to 0.63 g wwt (figure 6.10b). Without correction (i.e. considering test size V_E), xenophyophores were numerically more abundant than metazoans in the same size classes, whereas considering protoplasmic biomass, xenophyophores are more abundant in smaller size classes before the

metazoan peak abundance. M_{E-corr_c} estimates returned the xenophyophore body-size distribution in the smallest megabenthos size classes, with peak abundance at 4.9 × 10^{-3} g wwt, similarly to M_{E-corr_e}, and between M_{E-corr_a}, and M_{E-corr_b} and M_{E-corr_d} (figure 6.12a). Protozoans shared individuals of similar body range as metazoans across 18 body-size classes, i.e. the largest protozoan classes post peak abundance and the smallest metazoan classes prior peak abundance (1.7 × 10^{-3} – 6.3 × 10^{-1} g wwt). Combined metazoan and xenophyophore data showed a consistent decrease in abundance with body size (figure 6.12b). The most abundant morphological category was tubular/branching xenophyophores, between size classes 1.5 × 10^{-4} g wwt and 2.2 × 10^{-1} g wwt, which shared the same body-size range of hemispherical and of undefined-shape categories. Plate-like specimens were spread in the smallest classes ≤ 9.8 × 10^{-3}.

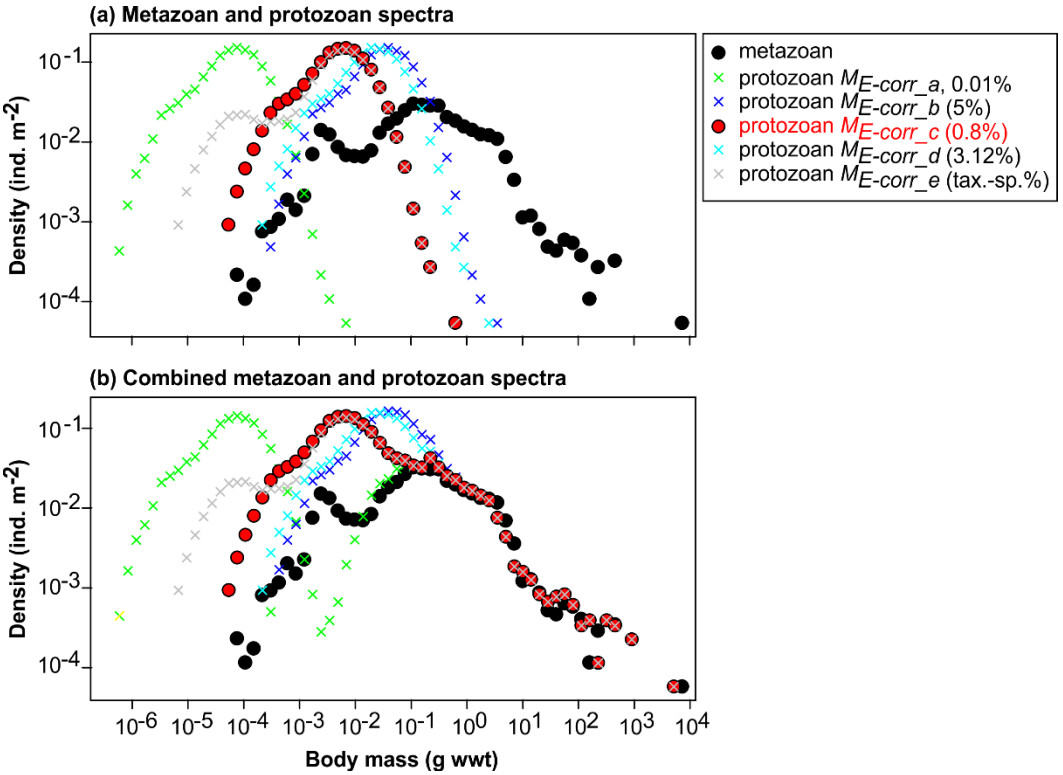

Figure 6.12. Protozoan megabenthos right-hand side body-size spectra at the Clarion-Clipperton Zone study site. Body-size distribution of abundance (N_i in ind. m^{-2}) against body size (M_i in g wwt) of metazoan (invertebrates and demersal fish; ≥ 1 cm) and protozoan (xenophyophores) megabenthos at CCZ at in situ temperature (i.e. 1.5 °C). **(a)** Metazoan and protozoan spectra plotted separately. **(b)** Combined metazoan and protozoan spectra. The amount of living protoplasm (M_{E-corr}) in proportion to GVM-derived biomass (M_E) was estimated using different 'structure-to-cell' correction values (see sections 6.2.3.3 and 6.3.2.1; table 6.1; figure 6.8).

6.3.2.4 Abundance, biomass, and respiration flux against MTE predictions at CCZ

Xenophyophore spectrum. Protoplasmic biomass data (M_{E-corr_c}) were used to compare the body-size distribution of protozoan and metazoan (invertebrates + fish) abundance, and of combined protozoans and metazoans. Results of the general linear model analysis revealed a statistically significant difference in slope coefficients between the protozoan (-1.96) and the metazoan (-0.71) spectra ($F_{1,30}$ = 85.22, p < 0.001; figure 6.13a; see metazoan assessment in the sub-section below and corresponding equation in table 6.4). The intercepts were also significantly different ($F_{1,30}$ = 36.29, p < 0.001; protozoans, 2.4 × 10^{-5}; metazoans, 9.7 × 10^{-3}). The spectrum combining data of both the protozoan and the metazoan assemblages was visually similar to the spectrum of the metazoans only (figure 6.13b). LM analysis indicated no significant difference between the slope coefficient of the combined data (-0.66) and that of metazoans only ($F_{1,53}$ = 85.22, p = 0.052). There was also no significant difference between the intercept value of the combined assemblages (1.0 × 10^{-2}) and that of metazoans only ($F_{1,53}$ = 1.37, p = 0.247).

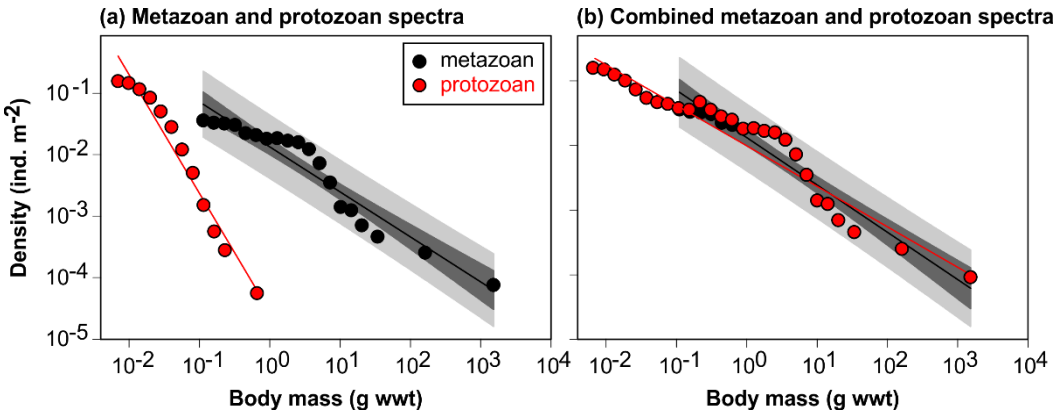

Figure 6.13. Protozoan megabenthos right-hand side body-size spectra at the Clarion-Clipperton Zone study site. Body-size distribution of abundance (N_i in ind. m^{-2}) against body size (M_i in g wwt) of metazoan (invertebrates and demersal fish; ≥ 1 cm) and protozoan (xenophyophores) megabenthos at CCZ at in situ temperature (i.e. 1.5 °C). **(a)** Metazoan and protozoan spectra plotted separately. **(b)** Combined metazoan and protozoan spectra. For xenophyophores, biomass (M_{E-corr_c})was derived using a 'typical' value of 0.8% for deriving protoplasmic contribution to GVM-derived body size (see sections 6.2.3.3 and 6.3.2.1; table 6.1; figure 6.8). The linear regression line for metazoan data is also presented (see table 6.4), with corresponding 95% confidence intervals (dark shade) and prediction intervals (light shade).

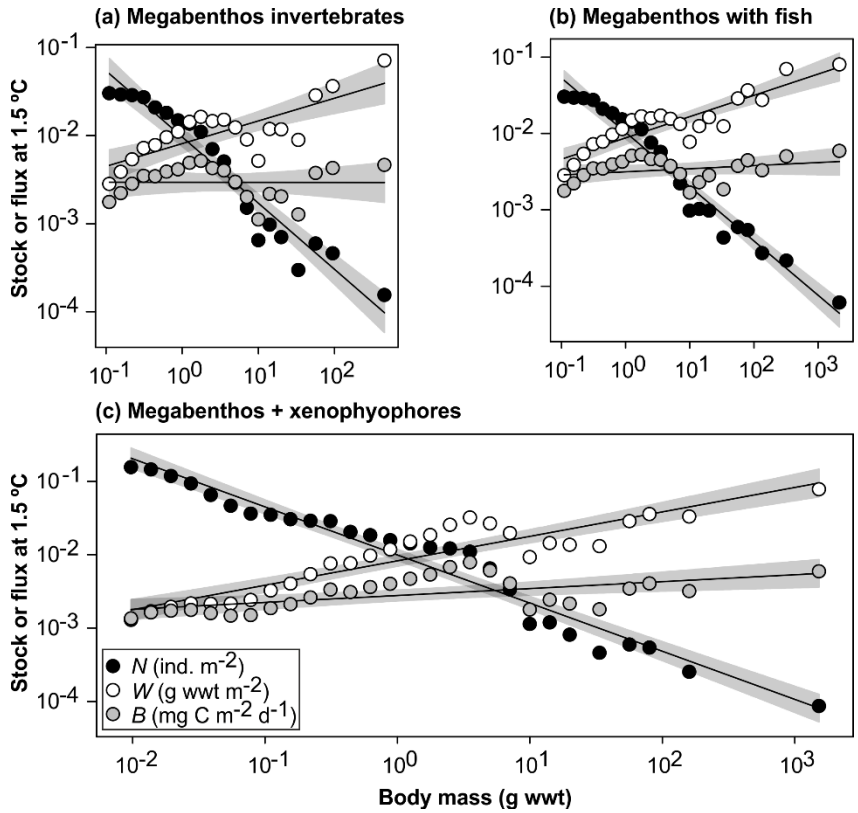

Figure 6.14. Megabenthos right-hand side body-size spectra at the Clarion-Clipperton Zone study site. Body-size distribution of abundance (N_i in ind. m^{-2}), biomass (W_i in g wwt m^{-2}), and estimated respiration flux (B_i in mg C m^{-2} d^{-1}) against body size (M_i in g wwt) at CCZ at in situ temperature (i.e. 1.5 °C). **(a)** Metazoan megabenthic invertebrates (≥ 1 cm). **(a)** Combined metazoan invertebrates and demersal fish. **(c)** Combined metazoan megabenthos and protozoan xenophyophores. For xenophyophores, biomass ($M_{E-corr_c)}$was derived using a 'typical' value of 0.8% for deriving protoplasmic contribution to GVM-derived body size (see sections 6.2.3.3 and 6.3.2.1; table 6.1; figure 6.8). Shaded areas are 95% confidence intervals. See table 6.4 for the corresponding regression equations.

Metazoan megabenthos and xenophyophore spectra. Data at CCZ were summarized well by the MTE predictions, both in the megabenthos metazoan and including protozoan xenophyophores (figure 6.14; table 6.4). Metazoan abundance decreased with body size with slopes of -0.75 (invertebrates only) and of -0.71 (including demersal fish), not significantly different from the MTE prediction of -0.75. Biomass increased with body size with slopes of 0.26 (invertebrates only) and 0.28 (including demersal fish), not significantly different from 0.25. Respiration flux was invariant with body size with slopes ranging between 0.00 (invertebrates only) and 0.04 (including demersal fish), not significantly different from 0.00.

Including xenophyophore data (M_{E-corr_c}), the combined protozoan and metazoan megabenthos body-size spectra followed the same trends as for the

metazoans only, although the slope coefficients were generally higher, i.e. abundance decreased with a slope of -0.66, biomass increased with a slope of 0.33, and respiration flux showed a slight increase with body-size (slope of 0.09). The relationships between these variables and the range of body sizes considered were statistically significant across the two assemblages combined, nonetheless, they departed slightly from the MTE predictions. Intercept values (i.e. related to resource supply) for abundance, biomass, and respiration flux, ranged between 0.0029 and 0.0201.

Table 6.4. Spectral analyses of stocks and flux at the Clarion-Clipperton Zone study site. Regression analysis for abundance (N_i in ind. m^{-2}), biomass (W_i in g wwt m^{-2}), and estimated respiration flux (B_i in mg C m^{-2} d^{-1}) against body size (M_i in g wwt) of metazoan megabenthic invertebrates and demersal fish, and combined metazoan and protozoan xenophyophores, at CCZ at in situ temperature (i.e. 1.5 °C). For xenophyophores, biomass ($M_{E-corr_c)}$was derived using a 'typical' value of 0.8% for deriving protoplasmic contribution to GVM-derived body size (see sections 6.2.3.3 and 6.3.2.1; table 6.1; figure 6.8). See figure 6.14 for corresponding plots. $^{**}p < 0.01$, $^{***}p < 0.001$, ns: not significant.

Regression	Equation	Slope 95% CI	N	F	r^2
Abundance (ind. m^{-2})					
Metazoan invertebrates	$N_i = 0.0097\ M_i^{-0.75}$	-0.85, -0.65	20	265.03***	0.94
Metazoan invertebrates + demersal fish	$N_i = 0.0103\ M_i^{-0.71}$	-0.77, -0.65	22	559.02***	0.97
Metazoan + protozoan	$N_i = 0.0100\ M_i^{-0.66}$	-0.71, -0.60	27	587.14***	0.96
Biomass (g wwt m^{-2})					
Metazoan invertebrates	$W_i = 0.0081\ M_i^{0.26}$	0.16, 0.36	20	29.92***	0.62
Metazoan invertebrates + demersal fish	$N_i = 0.0088\ M_i^{0.28}$	0.21, 0.34	22	83.11***	0.81
Metazoan + protozoan	$N_i = 0.0083\ M_i^{0.33}$	0.28, 0.39	27	149.52***	0.85
Respiration (mg C m^{-2} d^{-1})					
Metazoan invertebrates	$B_i = 0.0029\ M_i^{0.00}$	-0.10, 0.10	20	0.00 ns	0.00
Metazoan invertebrates + demersal fish	$N_i = 0.0032\ M_i^{0.04}$	-0.02, 0.10	22	1.78 ns	0.08
Metazoan + protozoan	$N_i = 0.0028\ M_i^{0.09}$	0.04, 0.15	27	12.20**	0.32

6.3.2.5 Habitat-specific body-size distribution of abundance at CCZ

The body-size distribution of abundance was fairly similar between the three landscape types at CCZ, although the body-size scaling of abundance was generally less steep when including xenophyophore fauna (figure 6.15; table 6.5). Data of metazoan megabenthos (invertebrates and demersal fish) were summarized well by the MTE prediction in all habitats, with abundance decreasing with body size with slopes between -0.68 (trough) to -0.73 (plain), not significantly different from the MTE prediction of -0.75. Including

xenophyophores, abundance decreased significantly with slopes between -0.53 (trough) to -0.62 (ridge), yet they differed to the MTE prediction, even though the lower 95% CI was very close to -0.75. Whether excluding or including xenophyophores, the intercept values were generally higher on the plain and on the ridge by comparison to the trough habitat.

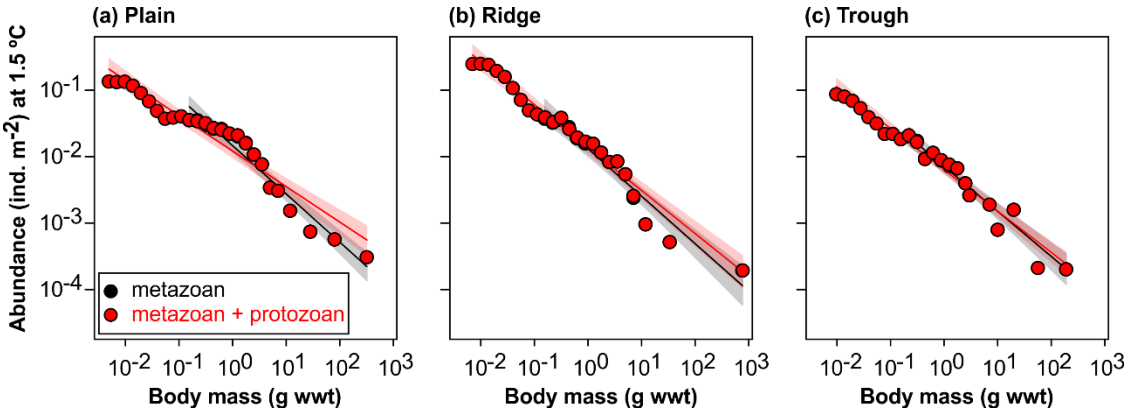

Figure 6.15. Megabenthos right-hand side body-size spectra at the Clarion-Clipperton Zone study site by habitat type. Body-size distribution of abundance (N_i in ind. m^{-2}) against body size (M_i in g wwt) at CCZ at in situ temperature (i.e. 1.5 °C) between **(a)** the plain (c. 4150 m water depth), **(b)** the ridge (< 4150 m water depth), and **(c)** the trough (> 4150 m water depth) habitats. Metazoan megabenthic invertebrates and demersal fish (≥ 1 cm; black circles). Combined metazoan megabenthos and protozoan xenophyophores (red circles). For xenophyophores, biomass ($M_{E-corr_c)}$was derived using a 'typical' value of 0.8% for deriving protoplasmic contribution to GVM-derived body size (see sections 6.2.3.3 and 6.3.2.1; table 6.1; figure 6.8). Shaded areas are 95% confidence intervals. See table 6.5 for the corresponding regression equations.

Table 6.5. Spectral analyses of megabenthos abundance at the Clarion-Clipperton Zone study site by habitat type. Regression analysis for abundance (N_i in ind. m^{-2}) against body size (M_i in g wwt) of metazoan megabenthic invertebrates and demersal fish, and combined metazoan and protozoan xenophyophore fauna, at CCZ *at* in situ *te*mperature (i.e. 1.5 °C). For xenophyophores, biomass ($M_{E-corr_c)}$was derived using a 'typical' value of 0.8% for deriving protoplasmic contribution to GVM-derived body size (see sections 6.2.3.3 and 6.3.2.1; table 6.1; figure 6.8). See figure 6.15 for corresponding plots. ***p < 0.001.

Regression	Equation	Slope 95% CI	N	F	r^2
Metazoan megabenthos invertebrates + fish					
Plain	$N_i = 0.0147\ M_i^{-0.73}$	-0.82, -0.63	16	275.64***	0.95
Ridge	$N_i = 0.0132\ M_i^{-0.72}$	-0.82, -0.60	15	196.72***	0.94
Trough	$N_i = 0.0072\ M_i^{-0.68}$	-0.78, -0.57	12	194.00***	0.95
Metazoan megabenthos + xenophyophores					
Plain	$N_i = 0.0122\ M_i^{-0.53}$	-0.61, -0.46	24	233.38***	0.91
Ridge	$N_i = 0.0136\ M_i^{-0.65}$	-0.72, -0.56	24	350.86***	0.94
Trough	$N_i = 0.0064\ M_i^{-0.62}$	-0.68, -0.56	24	459.42***	0.95

6.4 Discussion

6.4.1 General description

The two deep-sea sites surveyed were the Porcupine Abyssal Plain sustained observatory (c. 4850 m water depth) in the NE Atlantic, and the APEI-6 in the Clarion-Clipperton Zone study area (c. 4150 m water depth) in the NE Pacific. The PAP-SO is a 30-year time-series study site of international significance, which has been the subject of extensive sampling throughout the water column, from the surface of the ocean to the seafloor, expanding the understanding of biogeochemical fluxes across the pelagic and the benthic systems, and their role in the carbon cycle (Hartman et al. 2012). The seafloor at PAP-SO is little affected by anthropogenic activities, nonetheless litter has often been observed (collected during trawl surveys or seen on imagery; Lampitt 2017b, c; Stinchcombe 2017; Hartman 2019; Ruhl 2013, 2019), and studies have shown an accumulation of microplastic particles in the sediments (van Cauwenberghe et al. 2013; see also Maximenko et al. 2019). The megabenthos at PAP-SO has been studied during trawl surveys (Billett et al. 2001, 2010), and by towed-camera and by time-lapse camera assessments (Durden et al. 2015a, b). In 2012, the AUV *Autosub6000* collected seafloor imagery over a much larger area (> 100 km^2) (Ruhl 2013), increasing the ability to quantify megabenthic epifaunal biodiversity and standing stocks (invertebrates, Morris et al. 2014, 2016; appendix C; demersal fish, Milligan et al. 2016), and permitting morphometric assessment of about half of the morphotypes usually trawl-caught in the study area (Durden et al. 2016a).

The CCZ is a vast area targeted for industrial seafloor activity, particularly for mining of polymetallic nodules that are rich in metals such as manganese, cobalt, and nickel (Wedding et al. 2013; Glover et al. 2018). Over the entire six million km^2 CCZ extending across the northern Pacific Ocean, various zones have been designated for conducting industrial or research activity with various country contractors. These include areas of particular environmental interest where most ecological research has taken place in the last decade. Small-size benthic fauna (meio-, macrobenthos, including Foraminifera) has been fairly well studied (see Jones et al. 2017 and references therein). Seafloor imagery surveys have provided essential

knowledge of the benthic system, delivering valuable in situ information of the ecology of the megabenthos (Tilot 2006; Amon et al. 2016; 2017a, b; Tilot et al. 2018; Simon-Lledó et al. 2019a, b, d). Nonetheless, despite intense exploration effort in the CCZ, taxonomic (and morphometric) studies of the fauna are lacking, with most species new to science (Glover et al. 2015, 2018; Amon et al. 2016). In 2015, the APEI-6 study site was the object of a baseline environmental survey that aimed at describing the seafloor habitats and its constituent fauna across landscape types (Jones 2015). AUV photographic assessment aimed to provide ecological information as a barometer of change associated with mining activity in the CCZ (Simon-Lledó et al. 2019a; appendix D).

The deep seabed at these two sites is characterised by significant topographic variation, ranging hundreds of metres above and below the background abyssal plain: hills at PAP-SO, and ridges and troughs at the CCZ. Photographic assessment of these two remote study areas using AUV technology provided a uniform field- and data-analysis methodology. This ability to resolve ecologically significant information, at landscape scale, that addresses the topographic variation, suggests that the AUV-based photographic survey was an effective and efficient practical monitoring tool in the present case (Wynn et al. 2014).

The seafloor at both sites comprises primarily muddy sediments, though hard substrata (up to decimetre scale) also occur at both sites: PAP-SO, clinker and iceberg drop stones (Durden et al. 2015a, 2016a), CCZ, polymetallic nodules (Simon-Lledó et al. 2019a). Those 'islands' of hard substrata provide habitat and refuge for the benthic fauna observed at both sites. At PAP-SO, these hard substrata occur mainly on the hill, where Durden et al. (2015a) described assemblages dominated by suspension feeders, by comparison to the plain area where most specimens, such as *I. vagabunda*, are free-living and demonstrate intense burrowing activity. At the CCZ study site, Simon-Lledó et al. (2019a) noted that nodules were particularly abundant in the plain area, and made a connection between faunal diversity and the areal coverage of polymetallic nodules at the sediment surface (Simon-Lledó et al. 2019b). The authors also recorded larger hard-substratum structures (> 60 cm^2) such as cobbles, boulders, and whale bones (see Amon et al.

2017c), particularly in the ridge area. The authors determined the megafauna assemblages across the three landscape types notably comprised hard-substrata obligate specimens, with a high proportion of suspension feeders on the plain, and of deposit feeders on the ridge. From a topographic point of view, this is opposite to what Durden et al. (2015a, 2017) observed at PAP-SO; suspension feeding dominating the hill, and deposit feeding the plain. The AUV surveys at PAP-SO and at CCZ have shown substantial ecological variation at the landscape scale, and in both cases the presence of even modest occurrences of hard substrata introduce additional variation. Such environmental heterogeneity is thought to be a key driver of species richness (Stein et al. 2014; Yang et al. 2015), as was the case at the two study sites (PAP-SO, Morris et al. 2014; CCZ, Simon-Lledó et al. 2019a).

The benthic assemblages observed at PAP-SO comprised well-known taxa (Billett and Rice 2001; Billett et al. 2001, 2010; Durden et al. 2015a, b, 2016a) by comparison to the rather poorly-known taxa at the CCZ site (Amon et al. 2016). Morris et al. (2016) demonstrated the influence of seafloor topography in shaping the megabenthos at PAP-SO, with hill environments supporting greater faunal density than the surrounding abyssal plain, resulting from higher concentrations of particulate organic matter laterally advected in the water column (appendix C).

In the present analysis, data on the smaller benthos (macrofauna) from the PAP-SO central abyssal plain was analysed in complement, showing higher assemblage standing stock abundance (about two orders magnitude) than the megabenthos, however, their biomass was substantially lower, by almost three orders of magnitude (figure 6.3). At the CCZ study site, Simon-Lledó et al. (2019a) related variation of faunal standing stocks and composition with the local ecology of the elevated ridge and of the depressed trough in comparison to the level, flat, abyssal plain (appendix D). A high proportion of the CCZ megabenthos was attributed to xenophyophores, giant unicellular protozoans that can reach up to 20 cm in body size (Kamenskaya et al. 2015, 2016; Gooday et al. 2017a, b, 2018). It is unclear how many of these xenophyophore tests were alive at the time of observation (Hughes and Gooday 2004). For the present analysis, one half of the xenophyophore fauna was assumed to be alive. On that basis, standing stock density was

significantly higher including xenophyophores in all landscape types, by c. 300% overall (figure 6.9). Though, assuming that protoplasm biomass (M_{E-corr_c}) contributes 0.8% of xenophyophore test volume (see section below), standing stock biomass were not significantly different and increased by c. 1%.

6.4.2 Body-size structure

Quantitative individual biomass data of megabenthic assemblages were obtained from photographic analysis using two methods, and were used to assess the body-size distribution of abundance, biomass, and estimated respiration flux. At PAP-SO, species-specific length-weight relationships were employed (Morris et al. 2016; appendix C), as obtained from Durden et al.'s (2016a) morphometric analysis of corresponding specimens trawl-caught between 2002 and 2006. Despite how well known the PAP-SO megabenthos taxa are, LWRs are subject to temporal (and spatial) variability. For example, Benoist et al. (2019b; chapter 4) showed that the individual biomass of *P. longicauda*, a biomass-dominant holothurian at PAP-SO, can vary ±15% dependant on the year the LWR data were obtained in (see section 4.4.1.2; figure 4.6), potentially in response to variation in resource supply (e.g. Bett et al. 2001).

In the case of smaller benthos, volumetric-based methods have long been established (e.g. Alcaraz et al. 2003; Baguley et al. 2004; Mustard and Anderson 2005; Di Mauro et al. 2011; Jung et al. 2012; Moore et al. 2013; Mazurkiewicz et al. 2016), as the principal way of estimating individual biovolume; therefore, the GVM (Benoist et al. 2019b; chapter 4) was employed for PAP-SO macrobenthos samples. For incomplete polychaete specimens, individual biomass was best estimated from regression analysis of estimated biomass and measured equivalent cylindrical diameter of intact specimens (method a; equation 6.2a; figure 6.2). In their polychaete size-structure assessment of the deep-sea benthic system at Station M, NE Pacific, Laguionie Marchais et al. (2020) adopted a somewhat similar approach to deal with the high frequency of incomplete specimens (97%) encountered.

At the CCZ study site, where the fauna was poorly known in terms of taxonomy or morphometry, the GVM was preferred to species-specific LWRs,

eliminating likely systematic, taxonomic, temporal, and spatial, bias (Simon-Lledó et al. 2019a). In this Ph.D. thesis, the method was also tested on protozoan xenophyophore specimens, and adapted to derive protoplasmic biomass in proportion to GVM-derived body volume (figure 6.8). Five different 'structure-to-cell' correction values were tested, ranging from 0.01% to 5%, or representative of a morphological category (Levin and Gooday 1992; Gooday et al. 2018) (table 6.1; figure 6.8). Method (c) assumed a typical protoplasmic contribution of 0.8% to test volume (Levin and Gooday 1992), and it was found to be a good compromise between realistically representative xenophyophore biomass data, and practically implementable across the different morphotypes observed. Xenophyophore protoplasmic biomass represents very little by comparison to metazoan biomass; megabenthos total seafloor standing stock biomass including xenophyophores was estimated at c. 1% higher than without the protozoan fauna (figure 6.9). Xenophyophores occupied the lower end of the megabenthos body-size spectrum, mainly before the metazoan megabenthos range, although sharing a few body-size classes (figures 6.10 and 6.12).

Overall, the body-size spectra of macrobenthos (PAP-SO), megabenthos invertebrates (both sites), including demersal fish and xenophyophore fauna (CCZ), at the two deep-sea sites assessed were broadly represented by unimodal distributions of abundance (figures 6.5, 6.11, and 6.12), with some secondary peaks either side that may reflect true increase/decrease in abundance of some taxa, or be the result of potential annotator biases (Durden et al. 2016b, c). For example, at PAP-SO, high numbers of small specimens of *I. vagabunda* and Ophiuroidea were recorded at size class 1.25 g wwt (c. 14 mm in column and in disk diameter, respectively), where the megabenthos peak abundance occurs. These two taxa were likely under-recorded as a result of their small body and translucent appearance.

Similarly, some specimens considered as infauna were nonetheless often visible on images, such as echiurians, for which true total abundance was therefore underestimated. Echiurans are abundant and may play a significant role in carbon cycling at the seafloor (Bett and Rice 1993; Bett et al. 1995). In addition, some specimens that were observed partially (not contained fully within an image), or off the seabed, were allocated the mean body mass of

their corresponding morphotype, potentially generating spikes in the overall body-size distribution as a result of bulk assignment to a single size class. This was principally the case for Porifera, tunicates, and Brinsingida sea stars, for which morphometric data were lacking given the rarity of intact specimens in trawl catches.

The distribution of taxa among body-size classes was fairly similar between the two study sites, although the invertebrate megabenthos recorded at CCZ were overall somewhat smaller than at PAP-SO (c. 0.08 mg wwt to 1.3 kg, c. 0.3 g wwt to 3.6 kg, respectively) (figures 6.4 and 6.10). Note, however, that the smaller megabenthos at CCZ, < 0.1 g wwt, were represented mostly by Porifera and Annelida, their biomass individually estimated using the GVM (and corrected in the case of Porifera to derive organic tissue biomass), as opposed to the PAP-SO Porifera that were bulk assigned to size class 14 g wwt. Cnidaria were spread throughout the spectra at both study sites, dominating numerically both assemblages. Echinodermata were overall less abundant in numerical density at CCZ than at PAP-SO, with mostly Ophiuroidea and Crinoidea occupying the smallest body-size classes < 10 g wwt, and larger Holothuroidea recorded up to 160 g wwt. Mollusca were virtually absent at PAP-SO, with the exception of large Cephalopoda, whereas at CCZ, Bivalvia were high contributors of size classes 1-10 g wwt. This conceivably represents taxonomic or lifestyle variations influencing visibility in seabed photographs. The addition of macrobenthos data at PAP-SO, and of xenophyophore data at CCZ, provided a much-expanded view of the benthic body-size spectra, up to eleven orders of magnitude at PAP-SO, and appeared to indicate a continuous progression of stocks and flux with body size (figures 6.5 and 6.11). Body-size data on the smaller benthos (e.g. meio- and macrobenthos), would greatly enhance our understanding of benthic system at the CCZ study site, in terms of seafloor biomass distribution across a more complete assemblage.

6.4.3 Body-size distributions and MTE predictions

The body-size distribution[1] of the macrobenthos and of the megabenthos assemblages observed at the two deep-sea sites assessed broadly matched the predictions of the metabolic theory of ecology (Brown et al. 2004) (figures 6.6 and 6.13; tables 6.2 and 6.5). As noted in chapter 5, the addition/removal of fish from the assessment had little impact on the spectra, other than right-side extension, suggesting that a simple MTE-type model may be adequate. Body mass was a strong predictor of abundance distribution, with mass scaling approaching -0.75 at both sites, between habitats, and between and across the faunal fractions observed (macro-, megabenthos), indicating an equivalent distribution of resources within the body-size range studied, referred to as the 'energy equivalence rule' (EER) (Damuth 1981; White et al. 2007). Recently, Durden et al. (2019) showed that ingestion rates among abyssal deposit feeders (PAP-SO and Station M) exhibited a mass scaling close to the MTE prediction (0.75), revealing size-dependency of resource acquisition among these taxa, consistent with other studies on benthic detritivores (Cammen 1979; Pihl 1985). The consistent biomass partitioning observed across macro- and megabenthos at PAP-SO suggests that the two faunal fractions may be driven by similar factors in terms of their body-size distribution. Similarly, at the CCZ study site between metazoan megabenthos and protozoan xenophyophores, the results obtained in this analysis indicate consistent body-size scaling across the two benthic assemblage fractions.

The results obtained in this Ph.D. thesis are consistent with those from other environments. Kelly-Gerreyn et al. (2014), Górska and Włodarska-Kowalczuk (2017), and Laguionie Marchais et al. (2020), determined that the body-size distribution of small benthos invertebrates (meio-, macrobenthos) from contrasted environments in terms of water depth and seafloor temperature, were potentially linked to resource supply. Similarly, Vanreusel

[1] As noted in chapters 3 and 5, the maximum likelihood estimate (MLE) method (Edwards et al. 2017) was also tested for each site using the right-side slopes of abundance spectra, including and excluding demersal fish (except at PAP-SO), and including xenophyophores at CCZ. The MLE method considers the effect of data type (body mass or length) and resolution, and the effect of binning that data for conducting body-size spectral analyses. The MLE results (i.e. *b* exponent) showed no difference to those presented in the present thesis. They are not shown in this thesis, but will be the object of a future publication in a relevant journal.

et al. (1995) observed that nematodes from PAP-SO were more abundant, and generally larger at the individual level, than at an oligotrophic site off the Cape Verdes.

Górska and Włodarska-Kowalczuk (2017) studied meio- and macrobenthos from three Arctic coastal areas differing in resource supply and glacial disturbance, and found that these two factors may have controlled the body-size class partitioning of biomass. These Arctic body-size spectra nevertheless exhibited a similar shape to those obtained in this Ph.D. thesis (see chapter 1 section 1.3; figure 1.3). Laguionie Marchais et al. (2020) also studied the influence of seasonality on the partitioning of benthic polychaetes biomass at Station M, concluding that intra-annual variation in resource supply led to seasonally variable resource acquisition rates (metabolism), affecting principally the intercept parameter of the spectrum, but not the overall shape of spectrum, with the mass scaling coefficient estimated at -0.74. Similarly, Durden et al (2020) used time-lapse photography at PAP-SO and at Station M, to study the impact of seasonal detritus inputs on resource acquisition of megabenthos fauna. The authors' results suggested that deposit feeding rates were not particularly correlated to seasonality in particle flux, but rather to the natural history of the key taxa.

Biomass and respiration flux distribution with body size showed greater departures from the MTE predictions. Photographic acquisition of individual biomass data is subjected to many sources of errors. In some cases, the measured body dimension, first step to the estimation of body mass, may misrepresent the true body dimension of the specimen. For example, echiurians at PAP-SO are never fully visible with some portion of their body buried in the sediment (Bett and Rice 1993), some soft-bodied specimens (e.g. Elpidiidae spp., *Peniagone* spp. *Benthothuria* spp.) are often observed curved or retracted, from a lateral aspect (rather than dorsal), when attached to hard substrata (e.g. anemones), or partially buried in the sediment (e.g. sea stars, ophiuroids), resulting in under-/over-estimation of their body mass. In addition, subtle differences in some specimens' altitude over the seabed may produce slight over-estimation of their biomass, e.g. individuals colonising the upper end of tube worms, corals, or sponges. Also, the use of an inappropriate LWR in the calculation of individual body mass, i.e. in the

case of specimens identified to morphotype level, despite careful selection of the most representative known species (in terms of shape and body-size range), may produce poor estimates of individual body mass. Using the body volume of a specimen as a proxy for biomass, as tested with the GVM dataset, provided robust quantitative individual body-mass data over the full range of specimens observed without the need to omit some taxa/specimens (Benoist et al. 2019b; Simon-Lledó et al. 2019a; chapter 4).

Finally, as for the two shelf-sea datasets (chapter 5.B), the application of a single equation (chapter 1 equation 1.1), with a temperature-corrected normalisation coefficient obtained from Hemmingsen's (1960) data, to calculate all specimens' individual metabolism within a size class is attractive from a modelling perspective but may be overly simplistic (see chapter 7 where individual metabolism was calculated using a range of temperature-corrected normalisation coefficients found in the literature, in order to estimate seafloor carbon stocks and flows) (see also Laguionie Marchais et al. (2020)). Though Childress (1995), and more recently McClain et al. (2012), showed that marine benthic groups showed lesser or no decline in their metabolic rate in relation to depth alone (see also Childress et al. 1990; Drazen and Seibel 2007; Brey 2010; Seibel and Drazen 2007), and that shallow- and deep-water benthic organisms could be well represented by a single metabolic rate model. Brown et al. (2018) measured in situ metabolic rates of holothurians from shallow to bathyal environments, and found that metabolism did not differ between the two environments, however it was lower in abyssal holothurians (> 4000 m water depth). Individual metabolic rates do, however, exhibit a wide range of species-specific factors (Brey 2010; McClain et al. 2012).

At abyssal depths, fish are numerically low representatives of the benthos by comparison to invertebrates, and at the CCZ study site, their inclusion in the megabenthos body-size spectra did not alter the shape of the standing stocks and flux distributions (figures 6.11a, b and 6.14a, b; table 6.4). Most demersal fish observed were *Ipnops* spp. between 1-7 g wwt, and single occurrences of larger fish (*Bassozetus* sp., *Bathysaurus* sp., *Coryphaenoides* sp.) were recorded > 225 g wwt. Fish at PAP-SO were not included in the present analysis; however, they were previously quantified at 7.6×10^{-4} ind.

m^{-2} by AUV survey (Milligan et al. 2016), that is much lower than at the CCZ study site: 3.0×10^{-2} ind. m^{-2} (Simon-Lledó et al. 2019a; present study). In their AUV photographic assessment, Milligan et al. (2016) characterised the fish fauna as dominated by macrourids, *Coryphaenoides* spp., and eels, *Histiobranchus bathybius*.

The GVM of individual biomass estimation was tested on xenophyophores, and the results presented in this chapter should be interpreted with caution given the assumptions made. Nonetheless, using previous work from Levin and Gooday (1992) and Gooday et al. (2018), who attempted to estimate protoplasmic contribution to xenophyophore test volume, and considering half of the specimens to be alive (Hughes and Gooday 2004), the results of this analysis showed a consistent distribution of xenophyophore body size with that of the metazoan megabenthos (figures 6.11c, 6.12-6.14c; tables 6.4 and 6.5). Xenophyophores play a significant role in structuring benthic assemblages; their tests serving as colonisation space, refuge from predators, or reproduction areas, for various foraminifera, meio,- and macrofauna, species (Levin and Gooday 1992; Hughes and Gooday 2004; Laureillard et al. 2004). Xenophyophores are considered as detritivorous, suspension or surface-deposit feeders (Levin and Gooday 1992), and bacterivorous (Laureillard et al. 2004); as for the metazoan benthos, these taxa are almost exclusively reliant on the amount of particulate organic matter that circulates at the seafloor.

The MTE model was well represented by both the PAP-SO and the CCZ macro- and megabenthos assemblages, at site-scale and between the different habitat types assessed (plain, hill, ridge, and trough). In all cases, intercept values were slightly higher at PAP-SO than at CCZ, however it will be necessary to correct for the minor difference in temperature between the two sites in order to better assess the influence of resource supply in shaping deep-sea megabenthos body-size spectra (examined further in chapter 7).

6.4.4 Concluding remarks

In the context of climate change, the PAP-SO site is an ideal test ground for time-series monitoring of the benthos, where changes in the fauna have been observed in response to inter- and intra-annual drivers (e.g. seasonality

patterns) (Billett et al. 2001, 2010). In view of future mining activities, the APEI-6 at the CCZ was a good candidate for establishing a reference understanding of faunal distribution between landscape types. Jones et al. (2017) evaluated the effect of deep-sea nodule mining on benthic faunal assemblages from multiple surveys in the Pacific over a 26-year period following disturbance. Their results indicated that mining disturbance had major negative effects on faunal density and diversity, and these were more severe immediately after mining. They noted that small-sized and mobile fauna were less impacted over the long term, often recovering within one year, to the contrary of most other faunal groups that did not show signs of recovery even after 20 years. Similarly, Simon-Lledó et al. (2019c) assessed the effect of seabed mining 26 years following a simulated event in the DISCOL experimentation area in the Peru Basin. The authors found that deposit feeders were less affected by mining disturbance than suspension feeders, as a result of the resuspension of sediment plumes, and that biodiversity was generally lower in disturbed areas, even two decades later. Polymetallic nodule mining is planned to happen in the near future, over large areas in the CCZ, and it is expected to impact substantially the benthic system (Jones et al. 2017; Simon-Lledó et al. 2019c), in terms of changes to faunal composition and functional biodiversity, and in the re-distribution of standing stocks across faunal classes.

Taxon-based ecosystem approaches are needed for sustainable management of the deep sea (e.g. Glover et al. 2018), however, understanding of the stocks and flows of carbon and energy in the system, at the community level and at large scale, is equally important, particularly in the context of the "blue economy" (Smith-Godfrey 2016). The use of individual body size can be of great value for assessing ecosystem services, where body-size spectral analyses, in the form of a service-oriented framework, may improve our understanding of the response of benthic organisms in the face of climate change and other anthropogenic pressures (Blanchard et al. 2004, 2005, 2009; Petchey and Delgrano 2010; Rees et al. 2012; Godbold et al. 2013; Datta and Blanchard 2016; Henseler et al. 2019).

Chapter 7

Body-Size Distribution of Contrasting Benthic Assemblages

7.1 Introduction

The study areas assessed in this Ph.D. thesis were two multi-habitat-type shelf-sea sites in the Celtic Sea—the Greater Haig Fras (GHF) marine conservation zone and the UK-NERC Shelf-Sea Biogeochemistry (SSB) study area, and two deep-sea locations that featured topographic features tens (hills) to hundreds (ridge, trough) of metres above/below the surrounding abyssal plain at the Porcupine Abyssal Plain sustained observatory (PAP-SO) in the NE Atlantic, and at the Clarion-Clipperton Zone (CCZ) in the NE Pacific (see chapter 2 for sites description; figure 7.1). The main environmental characteristics of each benthic site showed distinct features in terms of water depth (c. 100-4850 m), seafloor temperature (1.5-10 °C annual mean) (Locarcini et al. 2018; Thomson et al. 2017), POC flux to the seabed (0.25-12.5 g C m^{-2} yr^{-1}) (Lutz et al. 2007), and seabed substratum type (muddy to coarse mobile sediments and rocks). These sites were primarily assessed using a photographic approach that consisted of continuous seafloor images acquired using an autonomous underwater vehicle (AUV), with ecological data extracted using standardised image processing and analysis techniques (Morris et al. 2014; Durden et al. 2016b, c; chapter 3).

At each site, the seafloor was characterised visually in terms of its substratum type (i.e. mobile sediments and/or hard substrata nature and areal cover), and the fauna was described (i.e. benthic invertebrates and demersal fish ≥ 1 cm; enumerated, taxonomically identified, and individually measured) (GHF, Benoist et al. 2019a; Ferguson et al. in prep.; SSB, Thomson et al. 2017; PAP-SO, Morris et al. 2016; CCZ, Simon-Llédo et al. 2019a). Additional data on macrobenthos and on protozoan xenophyophores were also included in the PAP and in the CCZ analyses, respectively. Individual body-size

measurements were converted to wet weight biomass units using two methods, namely a traditional, species-specific, length-weight relationship (LWR) approach, and a taxon-independent generalised volumetric method (GVM) that was developed during the course of this Ph.D. thesis (Benoist et al. 2019b; chapter 4). The benthic assemblages were evaluated in the form of spectral analyses, and the resultant body-size distributions were related to local environmental characteristics, and by reference to the numerical framework provided by the metabolic theory of ecology framework (MTE) (Brown et al. 2004) (shelf-sea sites, chapter 5; deep-sea sites, chapter 6).

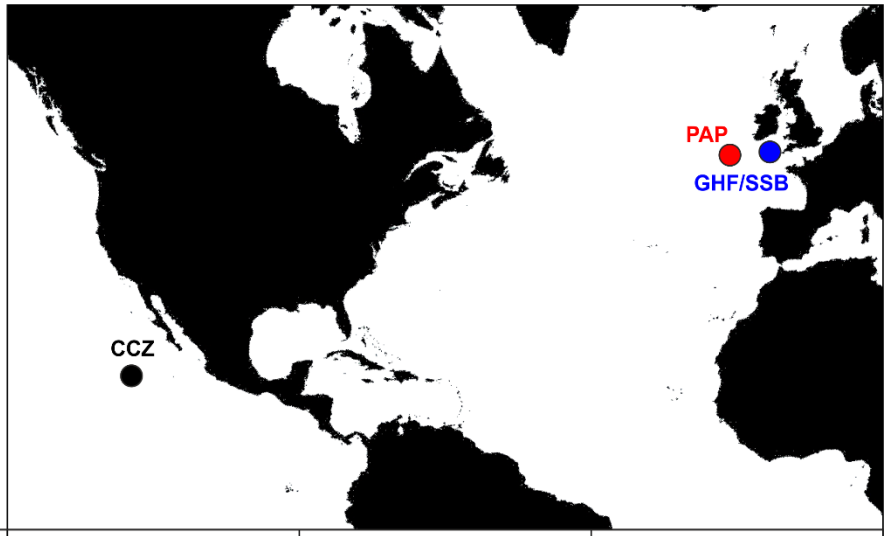

Study site	Clarion-Cliperton Zone (CCZ)	Porcupine Abyssal Plain (PAP)	Greater Haig Fras (GHF) Shelf-Sea Biogeochemistry study site (SSB)
Water depth (m)	4150	4850	100
Seafloor temperature (°C)	1.5	2.5	10
POC flux (g C m^{-2} yr^{-1})	0.25	2.5	12.5

Figure 7.1. General location of the study sites assessed. Greater Haig Fras (GHF) marine conservation zone; UK-NERC Shelf-Sea Biogeochemistry (SSB) study site; Porcupine Abyssal Plain sustained observatory (PAP-SO); Clarion-Clipperton Zone study site. Basic environmental information is given: mean water depth, mean annual seafloor temperature (GHF, SSB, Thomson et al. 2017; PAP-SO, CCZ, Locarcini et al. 2018), mean annual particulate organic carbon (POC) flux to the seafloor estimated from Lutz et al. (2007).

Based on the primary equation for individual metabolic rate (chapter 1 equation 1.1), the MTE can be extended to higher levels of organisation to predicting population and assemblage dynamics (Brown et al. 2004; Savage et al 2004a; Lewis et al. 2008; Yvon-Durocher and Allen 2012; Schramski et al. 2015). At steady state, and under 'energetic equivalence' (EER) (Damuth

1981; White et al. 2007), the density of individuals can be modelled from two variables: the local environmental temperature and the local resource supply (Damuth 1981; Brown and Gillooly 2003; Brown et al. 2004; Savage et al 2004a; Lewis et al. 2008) (equation 1.2). In the benthic environment, various studies from contrasting environments have shown consistency with the MTE predictions, but have been generally limited to small invertebrates: meio- and macrofauna (Kelly-Gerreyn et al. 2014; Laguionie Marchais et al. 2020; McClain et al. 2012), because of a historical limitation on quantitative sampling of large fauna.

The present study deals primarily with the larger fauna (megabenthos) from four contrasting sites, as analysed from AUV seabed imagery. In chapters 5 and 6, the body-size scaling of faunal density, biomass, and estimated respiration flux, were compared to the MTE predictions, i.e. consistency in trend (slope) and difference in elevation (intercept). The analyses were also made using demersal fish data at the two shelf-sea sites and at CCZ, and using xenophyophore data at the CCZ site. In all cases, the body-size distributions of megabenthic abundance appeared to be generally consistent with the simple prediction of the MTE (i.e. slope of -0.75). Additional data on macrobenthos at PAP-SO revealed a consistent trend in body-size scaling between the smaller (macro-) and the larger invertebrates (mega-). This is a reflection that the EER (Damuth 1981; White et al. 2007) may hold across the two faunal fractions considered (see figure 1.1a).

Benthic carbon stocks and flows models usually rely on data on the smaller benthos, typically at a small physical scale (e.g. box core, 0.1 m^2) (Hessler and Jumars 1974). For example, Timmermann et al. (2012) and Ehrnsten et al. (2019a, b) examined the individual, and the combined, effects of hypoxia and nutrient loading on benthic biomass in the Baltic Sea using data on macrobenthos that represented five main functional groups, and Yool et al. (2017) investigated the effect of future variations in seasonality on global patterns in benthic biomass using data on meio- to macrobenthos. Global budgets of benthic standing stocks and cycling of carbon across the full benthos body-size range are sparse, with data on larger fauna generally semi-quantified as a result of sampling limitations. Such datasets have been employed by Rowe et al. (2008) and by Wei et al. (2010) to study carbon

stocks and flows in benthic food webs, and by Jones et al. (2014) to make predictions of benthic biomass change, and thus ecosystem functioning, in the face of climate change. However, global datasets that rely on a multitude of data types potentially introduce methodological bias in terms of the mismatches in both the spatial scale observed, and the body sizes and the taxonomic groups assessed (see section on the evaluation of current methods in chapter 4; Benoist et al. 2019b).

In the present Ph.D. thesis, the MTE numerical framework was employed to investigate its potential in the modelling of carbon stocks and flows at the seafloor, and the model was well represented by the shelf- and the deep-sea benthic assemblages considered, at site-scale and between the different habitat types assessed (chapters 5.B and 6). Firstly, this chapter aims to compare the body-size distributions of the contrasted assemblages assessed, using the MTE numerical framework, and so attempt to link those observations to environmental factors, primarily temperature and resource supply (thesis main objective 3). Given the temperature-dependence of metabolism and its effect on population abundance (Gillooly et al. 2001; Brown et al. 2004), the abundance-size spectra of each assemblage were standardized, i.e. temperature-corrected (equation 1.5), to account for the substantial difference in temperature between the study sites (c. 10 °C range). The shelf-sea standing stocks are expected to be higher than the deep-sea stocks with respect to higher POC flux to the Celtic-Shelf seafloor. Deviations from the model may reflect the influence of uncontrolled environmental variables and/or anthropogenic impacts. Notably, the two shelf-sea sites differ in their exposure to human activities; this is likely to impact the benthos (chapter 5).

Secondly, on the assumption that benthic assemblages can be represented as a ‘single trophic level’ with respect to the EER (Damuth 1981; White et al. 2007), the MTE framework was used for modelling carbons stocks and flows at the seafloor (thesis main objective 4). The 'single trophic level' phrase is of course an abbreviation for a community where the food web/food chain is not dominated by a strong predator:prey body size relationship. As discussed in chapters 5.B and 6, the application of Hemmingsen’s (1960) temperature-corrected equation (equation 3.1), to calculate specimens’ individual metabolism for estimating respiration flux, may be seen as simplistic

for deep-sea invertebrates. However, studies have shown that marine benthic groups showed lesser or no decline in their metabolic rate in relation to depth alone (Childress et al. 1990; Childress 1995; Drazen and Seibel 2007; Brey 2010; McClain et al. 2012; Seibel and Drazen 2007), and that shallow- and deep-water benthic organisms could be appropriately represented by a single metabolic rate equation. To evaluate the model presented in this Ph.D. thesis, individual metabolic rate was estimated using different equations found in the literature, which were based on the study of benthic invertebrates (Brey 2010; McClain et al. 2012; Laguionie Marchais et al. 2020). The outcome of this demonstration is placed in the context of our current understanding of benthic biogeochemical modelling, in particular the physical scale of observation required to generate and interpret global budget data.

7.2 Methods

Detailed descriptions of the field methodology employed to collect seafloor imagery data, of the photographic processing applied to the raw photographic sampling units, and of the subsequent image analysis steps, are provided in chapter 3 section 3.2, and metadata are summarised in table 3.1. Indirect estimation of individual biomass data of directly sampled macrobenthos specimens, and of photographed megabenthos specimens, are described fully in chapters 3 sections 3.3 and 3.4, respectively, and in chapter 4. For CCZ xenophyophores, protoplasmic biomass data was assumed to contribute 0.8% of the protozoans' test volume (see chapter 6 section 6.3.2.) (Levin and Gooday 1992). The analytical methods followed to assess the body-size distribution of the assemblage studied are defined in sections 3.5 to 3.7. The sections below provide details on the application of the MTE numerical framework for comparing the body-size structure of contrasted benthic assemblages, and for modelling benthic carbon stocks and flows.

7.2.1 Body-size spectral analysis of contrasted benthic assemblages

7.2.1.1 Temperature-correction of body-size spectra

The right-hand side (Bett 2013, 2014) distributions of abundance, biomass, and estimated respiration flux, with body size, at in situ temperature, at the four study sites, were compared against the MTE predictions using a linear regression model[1] in Minitab (v18.1, Minitab Inc.) in chapters 5 (shelf-sea sites; tables 5.B.1 and 5.B.3) and 6 (deep-sea sites; tables 6.1 and 6.4), and the corresponding regression equations are recapitulated in table 7.1. As discussed in chapters 5.B and 6, biomass and respiration flux distributions with body size showed greater variability ('noise') than found in the abundance data, this potentially results in greater compounding of errors in these derived parameters. Therefore, the following analyses are focussed on the numerical abundance data alone.

Seafloor temperature varied substantially between the four study sites, complicating direct comparison of the body-size distributions of abundance. To simplify these comparisons, abundance data were corrected to a 1.5 °C equivalent, i.e. using CCZ as the reference site (equation 1.5) (Gillooly et al. 2001). Temperature-correction permitted direct comparison of the influence of other local environmental variables (e.g. POC flux to the seabed) in structuring the four benthic assemblages studied. Variation between sites was considered using a general linear model (LM). Homogeneity of the body-size distribution slopes was assessed using an interaction term between 'site' (factor) and 'body size' (covariate). In the present assessment, data on invertebrate megabenthos, demersal fish (except at PAP-SO), and xenophyophores (at CCZ) are presented. Additional data on macrobenthos at PAP-SO are also presented.

[1] The maximum likelihood estimate (MLE) method (Edwards et al. 2017) was also tested for each site using the right-side slopes of abundance spectra. The MLE method considers the effect of data type (body mass or length) and resolution, and the effect of binning that data for conducting body-size spectral analyses. The MLE results (i.e. *b* exponent) showed no difference to those presented in the present thesis. They are not shown in this thesis, but will be the object of a future publication in a relevant journal.

Table 7.1. Regression equations of megabenthos abundance with body size at the four study sites. Regression analysis for abundance (N_i in ind. m^{-2}) against body size (M_i in g wwt) of **(a)** megabenthic (≥ 1 cm) invertebrates and **(b)** combined with demersal fish, at the Greater Haig Fras (GHF) marine conservation zone (2012, GHF-1; 2015, GHF-2), the UK-NERC Shelf-Sea Biogeochemistry (SSB) study site, the Porcupine Abyssal Plain sustained observatory (PAP-SO), and the Clarion-Clipperton Zone (CCZ) study site, at in situ temperature (chapters 5 and 6). Results including smaller fauna (macrobenthos) at PAP-SO and xenophyophores at CCZ are also presented. *p < 0.05, **p < 0.01, ***p < 0.001, ns: not significant.

(a) Invertebrates

Site	Equation	Slope 95% CI	N	F	r^2
GHF-1 at 10 °C	$N_i = 0.0959\ M_i^{-0.72}$	-0.88, -0.56	17	91.12***	0.86
GHF-2 at 10 °C	$N_i = 0.0872\ M_i^{-0.74}$	-1.13, -0.36	11	19.37**	0.68
SSB at 10 °C	$N_i = 0.0323\ M_i^{-0.62}$	-0.70, -0.54	16	286.33***	0.95
PAP-SO at 2.5 °C	$N_i = 0.0943\ M_i^{-0.73}$	-0.87, -0.59	23	126.11***	0.86
PAP-SO at 2.5 °C (including macrobenthos)	$N_i = 0.0840\ M_i^{-0.70}$	-0.74, -0.65	35	1147.47***	0.97
CCZ at 1.5 °C	$N_i = 0.0097\ M_i^{-0.75}$	-0.85, -0.65	20	265.03***	0.94
CCZ at 1.5 °C (including xenophyophores)	$N_i = 0.0095\ M_i^{-0.66}$	-0.73, -0.61	25	557.35***	0.96

(b) Invertebrates + demersal **fish**

Site	Equation	Slope 95% CI	N	F	r^2
GHF-1 at 10 °C	$N_i = 0.0995\ M_i^{-0.66}$	-0.84, -0.64	18	58.63***	0.79
GHF-2 at 10 °C	$N_i = 0.0804\ M_i^{-0.71}$	-1.06, -0.36	12	20.11**	0.67
SSB at 10 °C	$N_i = 0.0478\ M_i^{-0.59}$	-0.73, -0.46	16	92.37***	0.87
CCZ at 1.5 °C	$N_i = 0.0103\ M_i^{-0.71}$	-0.77, -0.65	22	559.02***	0.97
CCZ at 1.5 °C (including xenophyophores)	$N_i = 0.0100\ M_i^{-0.66}$	-0.71, -0.60	27	587.14***	0.96

7.2.1.2 Evaluation of temperature-corrected standing stocks

To examine the effect of temperature at the four study sites, faunal abundance was illustrated at in situ temperature and at temperature corrected to a 1.5 °C equivalent, and the sites were identified in terms of their annual mean resource supply (Lutz et al. 2007) (see figure 7.1). The comparison of standing stock was completed using invertebrate megabenthos abundance data, within a selected body-size range across all sites, i.e. from 3.5 g wwt to 450 g wwt. This ensured fair evaluation of comparable stocks between the datasets. At GHF, the right-hand side distribution of abundance covered more body-size classes in 2012 (GHF-1) than in 2015 (GHF-2), and no significant difference was observed between the two spectra. Thus, only data from GHF-1 were employed in this analysis. The strength of the relationship between abundance and POC flux to the seafloor was assessed by linear regression.

7.2.2 Estimation of seafloor carbon stocks and flows

The PAP study was used as an example to evaluate the practical use of the MTE numerical model in estimating seafloor carbon stocks and flows. Considering the deep-sea fauna to rely exclusively on the POC flux produced in surface waters, and because in this area, mega-invertebrate primary consumers are found across all body-size classes (e.g. *Psychropotes longicauda*, 3.5 kg wwt, deposit feeder), as a first approximation it is reasonable to model the whole benthic community as a 'single-level-trophic system'. Clearly this is not realistic (e.g. see Iken et al. 2001; Durden et al. 2015b). However, this is not a strict requirement of the underlying model, it simply implies that trophic levels are not uniformly ordered by body mass, i.e. there are both large and small primary consumers, and there are both large and small predators—a condition common among benthic invertebrate assemblages (see discussion in section 7.4.2).

Using the regression equation of PAP-SO abundance with body size (table 7.1), the abundance-size spectrum was modelled from the smallest (nanobenthos and bacteria, geometric mean mass c. 1 fg C) to the largest fauna size class encountered in the field (i.e. megabenthos, c. 235 g C), in a similar fashion to Laguionie Marchais et al.'s (2020) study of the benthos at Station M in the NE Pacific. Body-size data (M_i) were converted to carbon (C) units using the conversion factors for dry/wet mass (0.2152), and for carbon/dry mass (0.3587) provided by Brey et al. (2010). To conform to the 'simple' MTE model, the slope of abundance scaling with body (carbon) mass was fixed at -0.75, i.e. assuming 'energetic equivalence' that conforms to Damuth's rule (Damuth 1981; White et al. 2007). This yielded size-class abundance (N_i in ind. m^{-2}) calculation as:

$$N_i = 2.34\, M_i^{3/4} \qquad \text{(equation 7.1)}$$

Size-class biomass (W_i in mg C m^{-2}) was calculated as:

$$W_i = N_i \times M_i \qquad \text{(equation 7.2)}$$

And size-class respiration flux (B_i in mg C m^{-2} d^{-1}) was calculated as the product of individual metabolic rate (I_i) and size-class abundance (N_i) as:

$$B_i = N_i \times I_i \qquad \text{(equation 7.3)}$$

To this point in the thesis, I_i was estimated using Hemmingsen's (1960) equation for standard metabolic rate of poikilotherms at 20 °C (equation 3.1),

with a site-specific temperature-correction (i.e. PAP, 2.5 °C) (equation 1.5; chapter 6 section 6.2.5) (Gillooly et al. 2001) as:

$$I_i = 0.0124\, {M_i}^{3/4} \qquad \text{(equation 7.4a)}$$

However, more recent studies have reported varying normalisation constants for individual metabolic rate. Brey (2010) produced a model for estimating aquatic invertebrate respiration that comprised empirical data across c. 900 species and their main life style (i.e. sessile or free living, diet, vision, starvation), and that also included both temperature and water depth as factors. Set to PAP environmental conditions (i.e. 2.5 °C, 4850 m water depth), the author's equation was:

$$I_i = 0.074\, {M_i}^{3/4} \qquad \text{(equation 7.4b)}$$

Similarly, McClain et al. (2012) compiled global data on diverse shallow and deep-sea organisms; set to PAP site temperature, their equation converts to:

$$I_i = 0.008\, {M_i}^{3/4} \qquad \text{(equation 7.4c)}$$

Recently, Laguionie Marchais et al. (2020) based their study of the benthos at Station M in the NE Pacific, on total sediment community oxygen consumption (SCOC) rates and polychaete body-mass spectra, and obtained the following equation (set to PAP site temperature):

$$I_i = 0.036\, {M_i}^{3/4} \qquad \text{(equation 7.4d)}$$

To assess the sensitivity of the MTE model to individual metabolic rate, I_i was calculated using equations 7.4a-d, and seafloor standing stocks and flows at PAP were evaluated.

In addition, the potential impact of the physical scale of study on the estimation of stocks and flows was also examined. To do so, the physical scale of study was estimated as the inverse of size-class numerical abundance (N_i):

$$A = 1/N_i \qquad \text{(equation 7.5)}$$

with A as indicative seafloor area in m^2, i.e. the seafloor area in which one individual of that body mass might be expected to be found. Abundance (N), biomass (W), and respiration flux (B), data were then accumulated across increasing body sizes (increasing seabed areas). Carbon residence time (rt in days, d) in the benthic system was then calculated as:

$$rt = W/B \qquad \text{(equation 7.6)}$$

The contribution of the conventional benthic faunal size fractions (i.e. micro-, nano-, meio-, macro-, and megabenthos) to seafloor stocks and flux is then presented, and discussed in comparison to the results obtained by Laguionie Marchais et al. (2020) in their study of the benthos at Station M, NE Pacific.

7.3 Results

7.3.1 Comparison of body-size spectra between sites

7.3.1.1 Temperature-corrected abundance-size distribution

Abundance data standardized to 1.5 °C permitted the direct comparison of standing stocks with body size between the contrasting sites assessed (figure 7.2). General linear model analysis indicated the slopes were homogeneous (invertebrates: $F_{1,133}$ = 1.22, p = 0.294, r^2 = 0.98; invertebrates + fish: $F_{1,133}$ = 0.69, p = 0.68, r^2 = 0.98). Site-specific slopes were, necessarily, unchanged to the slopes at in situ temperature (see table 7.1). However, to the contrary, the intercept values did change (with the exception of CCZ the reference temperature site) as a result of the application of temperature correction to the abundance data (equation 1.5) (Gillooly et al. 2001). The intercept values were significantly different between the four sites (invertebrates only: $F_{1,133}$ = 3440.9, p < 0.001, r^2 = 0.98; including fish: $F_{1,133}$ = 3098.01, p < 0.001, r^2 = 0.98), with CCZ being the lowest, and GHF-1 the highest. The range of temperature-corrected intercept values (0.01-0.20) increased about two-fold by comparison to the range of intercept values at in situ temperatures (0.01-0.10). Whether including or excluding fish data, no significant differences were detected between the two GHF datasets, PAP-SO and GHF-2, and PAP-SO and SSB.

7.3.1.2 Temperature-corrected standing stocks

The effect of temperature-correction of standing stock between sites, which also differed in resource supply (see figure 7.1), was highlighted by comparison of invertebrate abundance data, of the selected body-size range 3.5-450 g wwt, at in situ temperature and at temperature standardized to 1.5 °C (figure 7.3). The impact of temperature correction is readily seen by

the increase in the range of abundance from 0.01-0.16 ind. m^{-2} at in situ temperature to 0.01-0.36 ind. m^{-2} when standardised to 1.5 °C. This two-fold increase is consistent with an approximate doubling in metabolic rate with the c. 10 °C rise in temperature between CCZ and the Celtic Sea sites, GHF and SSB ($Q_{10} \approx 2$) (e.g. Gillooly et al. 2001). Note, however, that (i) invertebrate standings stocks at the SSB site were almost half those at GHF, despite the two shelf-sea sites likely receiving very similar resource flux given their close proximity, and that (ii) the PAP-SO stocks exceeded that of the SSB site.

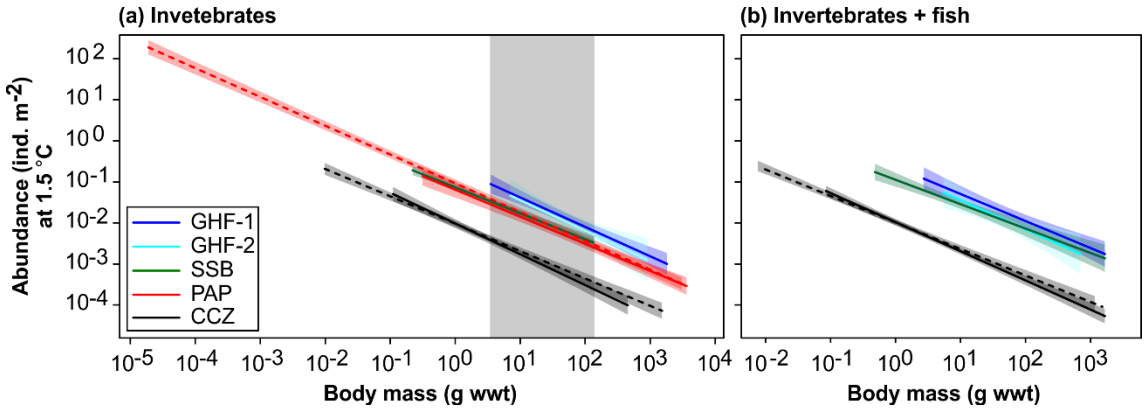

Figure 7.2. Temperature-corrected body-size spectra by study site. Right-hand side regression lines of the body-size distribution of abundance (N_i in ind. m^{-2}) against body size (M_i in g wwt) at the Greater Haig Fras (GHF) marine conservation zone (2012, GHF-1; 2015, GHF-2), the UK-NERC Shelf-Sea Biogeochemistry (SSB) study site, the Porcupine Abyssal Plain sustained observatory (PAP-SO), and the Clarion-Clipperton Zone study site. **(a)** Invertebrates. The shaded area indicates the body-size range selected for comparison of standing stock between sites (see figure 7.3). **(b)** Combined invertebrates and demersal fish. The dashed lines (a, b) at PAP-SO and at CCZ include data on macrobenthos and of xenophyophores, respectively.

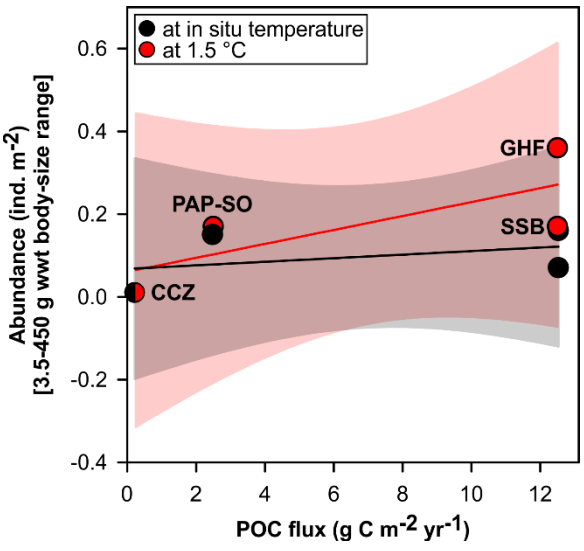

Figure 7.3. Effect of environmental temperature and POC flux to the seafloor on benthic assemblages. Standing stock of megabenthos (3.5-450 g wwt body-size range) abundance at the four study sites (GHF, Greater Haig Fras marine conservation zone; SSB, UK-NERC Shelf-Sea Biogeochemistry study site; PAP-SO, Porcupine Abyssal Plain sustained observatory; CCZ, Clarion-Clipperton Zone) characterized in terms of their resource supply (Lutz et al. 2007), at in situ temperature (R^2 = 0.16, p = 0.604) and at a reference temperature standardized to 1.5 °C (R^2 = 0.58, p = 0.237).

7.3.2 Seafloor carbon stocks and flows model at PAP-SO

7.3.2.1 Application of the MTE framework to the PAP benthos

Seafloor carbon stocks and flows at PAP-SO were estimated based on the assumption that the entire benthic assemblage could be well represented by the 'simple' MTE model for predicting abundance, biomass, and respiration flux (table 7.1; figure 7.4). In other words, it was assumed that the total benthos was under 'energetic equivalence', consistent with Damuth's rule (Damuth 1987; White et al. 2007). The PAP invertebrate megabenthos (geometric mean mass from c. 7 mg C to 235 g C) abundance data showed a body-size scaling that was close to the MTE model (i.e. slope of -0.75); therefore, under the EER, it is reasonable to assume that biomass and respiration flux were consistent with the MTE predictions (i.e. slope of 0.25 and of 0.00, respectively) (figure 7.4a). The model was expanded to the smallest benthic size class (nanobenthos and bacteria; c. 1 fg C), in a similar fashion to Laguionie Marchais et al. (2020) (figure 7.4b), permitting indirect estimation of total seafloor carbon stocks and flows (see next section).

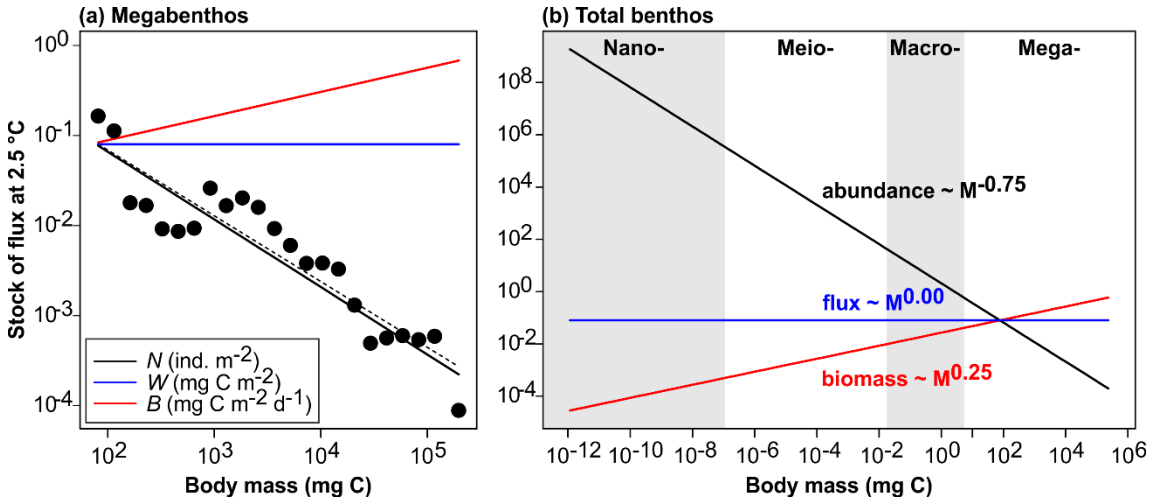

Figure 7.4. Seafloor carbon stocks and flows at PAP-SO. (a) Metabolic theory of ecology (MTE) predictions for megabenthos invertebrates standing stock abundance and biomass, and respiration flux with body size (solid lines). Field data (black circles) and corresponding linear regression (dashed line) are presented. **(b)** Expansion of the MTE model to the total benthic body-size spectrum, assuming energetic equivalence. Shaded areas indicate the different benthic faunal fractions: nano- (micro- and nano-), meio-, macro-, and megabenthos (table 7.2).

7.3.2.2 Carbon stocks and flows partitioning between faunal fractions

Seafloor carbon stocks and flows at PAP were modelled under the MTE numerical framework, using the regression equation of PAP-SO abundance with body-size (table 7.1), as applied to the entire benthic body-size range, i.e. from micro- to megabenthos (figure 7.4b). Respiration flux was calculated from individual metabolic rate, though several values for standard metabolic rate of aquatic invertebrates are reported in the literature. To assess the present model's sensitivity to metabolic rate, the normalisation constants for individual metabolic rate obtained by Hemmingsen (1960), Brey (2010), McClain et al. (2012), and Laguionie Marchais et al. (2020), temperature-corrected to match PAP conditions (equations 7.a-d, respectively) were used to further compare the derived respiration flux estimates (table 7.2). This yielded total benthos respiration to from 2.8 mg C m^{-2} d^{-1}, based McClain et al.'s (2012) equation, to 25.8 mg C m^{-2} d^{-1}, based on Brey's (2010) equation.

Laguionie Marchais et al. (2020) obtained their value for individual metabolic rate using sediment community oxygen demand data and polychaetes body-mass spectra from Station M, NE Pacific (equation 7.4d). Using their value in the present analysis generated total benthos respiration at 12.6 mg C m^{-2} d^{-1}. On the premise that Station M is comparable to the PAP site with regards to water depth (4050 m), temperature (1.5 °C), and resource supply to the seafloor (c. 1 g C m^{-2} yr^{-1}) (Lutz et al. 2007), respiration flux as derived from the Laguionie Marchais et al. (2020) value (equation 7.4d) was employed in the subsequent analysis.

Following the MTE simple predictions, i.e. assuming that the EER held throughout the entire range of body-size classes considered in the model, total respiration remained relatively invariant between faunal fractions, with nanobenthos and bacteria, meiobenthos, and megabenthos, each contributing 27-28% of the total carbon flux estimated. Macrobenthos contributed lesser as a result of fewer body-size classes comprising this fraction. On the other hand, total standing stock carbon biomass increased substantially between the nanobenthos and bacteria (0.1% total benthos biomass) to the megabenthos (c. 93%).

Table 7.2. Estimated seafloor carbon stocks and flows at PAP-SO based on the MTE model. Energetic equivalence was assumed throughout the complete benthic body-size spectrum. Biomass and respiration flux were calculated using equations 7.2 and 7.3, with different parameters tested for metabolic activity, obtained from the literature: (a) Hemmingsen (1960); (b) Brey (2010); (c) McClain et al. (2012); (d) Laguionie Marchais et al. (2020) (equations 7.a-7.d).

Benthos size category	Mass range (C)	Biomass		Respiration					Residence time			
		(mg C m^{-2})	(%)	(mg C m^{-2} d^{-1})				(%)	(d)			
				a	b	c	d		a	b	c	d
Nanobenthos and bacteria	1 fg-80 pg	0.6	0.1	1.2	7.3	0.8	3.6	28	0.5	0.1	0.7	0.2
Meiobenthos	80 pg-10 µg	10	1.2	1.2	7.3	0.8	3.6	28	8.0	1.3	12	3
Macrobenthos	10 µg-7 mg	44	5.5	0.7	4.2	0.5	2.1	16	62	10	94	21
Megabenthos	7 mg-235 g	743	93.2	1.2	6.9	0.8	3.4	27	643	108	976	222
Total	1 fg-235 g	798		4.3	25.8	2.8	12.6		184	31	280	64

7.3.2.3 MTE-based modelling of carbon stocks and flows at PAP

Results of stocks and flux partitioning between the benthic faunal fractions were obtained by accumulating the estimated values across the complete body-size range considered in the model (table 7.2). This also allowed an assessment of apparent stocks and flows at PAP against an indicative seafloor area surveyed, and so to evaluate the results obtained at the physical scale of conventional samplers and observations (figure 7.5).

Under the EER assumption, estimated respiration flux was found to be near-constant across benthos size categories, varying only as a result of the differing numbers of geometric size classes comprising each conventional benthos size category, i.e. macrobenthos 19 classes and 2.1 mg C m^{-2} d^{-1}; micro- and nanobenthos, meiobenthos, 33 classes and 3.6 mg C m^{-2} d^{-1}; megabenthos 31 classes and 3.4 mg C m^{-2} d^{-1}. Evaluated against seafloor area surveyed, total respiration flux was 6 mg C m^{-2} d^{-1} at the scale of a multiple-core sampler (c. 2.5×10^{-3} m^{-2}) (e.g. Barnett et al. 1984), and about two-fold higher at the scale of a seabed mass-imagery survey (c. 1×10^{3} m^{-2}). In contrast, carbon biomass substantially increased until the largest organisms were sampled, from c. 10 mg C m^{-2} at 0.1 m^2 seabed area (i.e. meio-/macrobenthos scale), to c. 800 mg C m^{-2} at the scale of the total area surveyed. These results illustrate both (i) the dominance of megabenthos in terms of benthic standing stock carbon biomass, and (ii) the potential scale-

dependence of stocks and flow estimates for the benthic ecosystem as a whole.

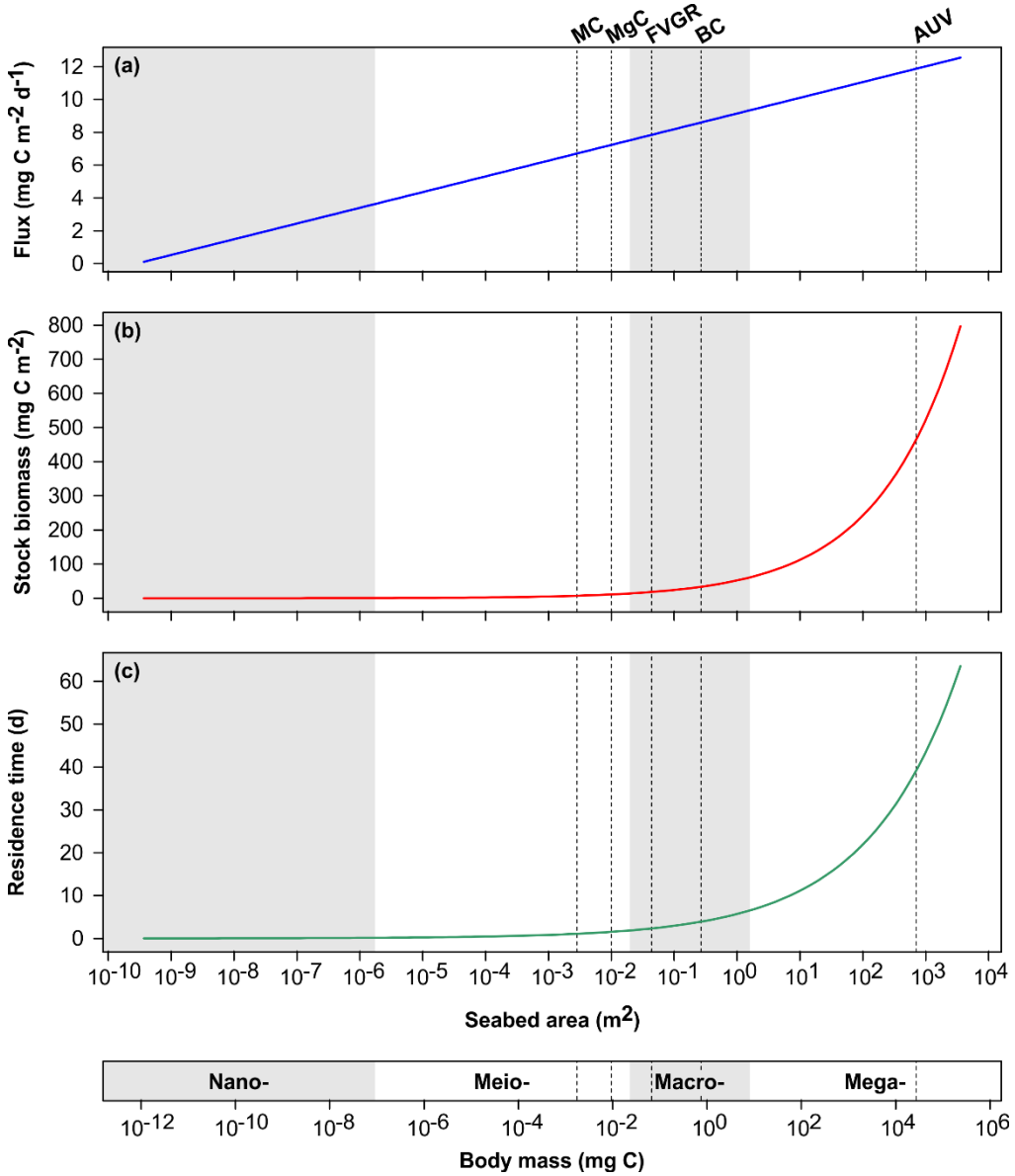

Figure 7.5. Estimated seafloor carbon stocks and flows at PAP-SO based on the MTE model. Cumulative plots of size-class **(a)** respiration flux as derived from individual metabolic rate (equation 7.4d) (Laguionie Marchais et al. 2020); **(b)** standing stock of carbon biomass; and **(c)** carbon residence time. Two x-axes are presented for assessment against seabed area, and against body mass. Shaded areas indicate the different benthic faunal fractions: nano- (micro- and nano-), meio-, macro-, and megabenthos (table 7.2).The vertical lines indicate the physical scale of conventional samplers and observations: MC, multiple corer (e.g. Barnett et al. 1984); MgC, Megacorer (e.g. Gage and Bett 2005); FVGR, flux chamber (e.g. Smith et al. 2001); BC, box corer (e.g. Hessler and Jumars 1974); AUV, mass imagery using towed camera and autonomous underwater vehicle (e.g. Durden et al. 2015a; Morris et al. 2016; Benoist et al. 2019a).

7.4 Discussion

7.4.1 Quantitative assessment of the benthos from contrasting environments

Benthic ecology necessarily relies upon remote investigation of the seafloor and its constituent organisms, and the most appropriate sampling methods depend upon the type of taxon/group of taxa of interest, in terms of body size (or the fraction separating micro-, nano-, meio-, macro-, and megabenthos) and of the environment they inhabit (e.g. infauna and epifauna in sedimentary habitats, sessile fauna on hard substrata, or mobile demersal fauna). Quantitative assessment ultimately relies upon the type of gear used for the collection of seafloor ecological data, and requires accurate information on the scale at which the data were acquired. As such, quantitative study of the benthos has typically been limited to the smaller fauna, mainly because of the spatial constraint (time and cost of field sampling and data analysis) inherent in surveys of the larger benthos (e.g. McIntyre 1956; Uzmann et al. 1977; Bett et al. 2001; Gage and Bett 2005). Further, where habitat-type-dependant field methods are employed, direct comparisons become difficult because of mismatches in both the spatial scale observed, and in the corresponding body sizes and taxonomic groups assessed. The underlying sampling limitation associated to the study of a size fraction, i.e. linked to the type of gear (sediment sampler for small fauna, trawl and seafloor photography for larger fauna), the spatial scale (tube core, 0.01 m^2; grab/box core, 0.1-0.2 m^2; individual photograph, 2 m^2; trawl, 2000 m^2), and the resolution (e.g. sieve- and trawl-mesh size, image pixel size), at which the data were collected, is essential to the coherent assessment of the resulting information.

In particular, the body-size range assessed cannot be reliably examined across its entirety, as a result of such practical limitations to obtaining consistent data from the smallest end of the body-size spectrum considered, and the spatial limitations on data at the largest sizes as a result of the positive allometric scaling of body mass and an organism's use of physical space (e.g. Peters 1983; Jetz et al. 2004). The potential impact of sampling artefacts also needs to be considered (e.g. Bett 2013, 2014), i.e. the need to

exclude specimens below some minimum reliably detected ('optimum') body size. The use of seafloor photography to study the megabenthos (Durden et al. 2016c), along with the development of autonomous underwater vehicles (Wynn et al. 2014; Jones et al. 2019), has enabled the acquisition of data at large spatial scale and across multiple habitat types, in a consistent and non-destructive manner (e.g. Morris et al. 2014, 2016; Marzinelli et al. 2015; Milligan et al. 2016; Benoist et al. 2019a; Simon-Lledó et al. 2019a). In the present Ph.D. thesis, data from four assemblages located in the Celtic Shelf at the Greater Haig Fras marine conservation zone and at the Shelf-Sea Biogeochemistry study site, and in the deeper regions of the Porcupine Abyssal Plain sustained observatory, NE Atlantic, and of the Clarion-Clipperton Zone, NE Pacific, were obtained using AUV-derived seafloor images.

Body size is a key physiological predictor of metabolism (e.g. Peters 1983), and the body-size structure of faunal assemblages is linked to ecosystem functioning by way of regulating stocks and flows of mass and energy in the environment (e.g. secondary productivity) (Banse and Mosher 1980). The metabolic theory of ecology is a framework based on metabolism at the organism (individual) level, and it can be used for modelling ecological processes at the ecosystem level (Brown et al. 2004; Yvon-Durocher and Allen 2012; Schramski et al. 2015). The simple interpretation of the MTE relies upon the 'energetic equivalence rule', which implies that energetic resources are proportionately acquired by each geometric size class along the body-size spectrum, assuming that organisms of similar size respond similarly to environmental constraints (Damuth 1981; Allen et al. 2002; Brown et al. 2003, 2004; White et al. 2007; Lewis et al. 2008; Isaac et al. 2012; Sewall et al. 2013). To address a key objective of this thesis, individual biomass data were generated indirectly using photogrammetric techniques, and the body-size distribution of standing stocks and flux of carbon were compared to the MTE predictions.

The benthic megafauna (invertebrates and demersal fish) of the Celtic Shelf and of PAP-SO are relatively well-known, enabling the use of species-specific allometric estimation of individual body size, through various morphometric datasets from which length-weight conversion factors were derived (Coull et al. 1989; Robinson et al. 2010; McCully et al. 2012; Silva et

al. 2013; Durden et al. 2016a). However, such information was not available for the fauna at the CCZ study site, leading to the development of a taxon-independent generalised volumetric method that was based solely on the general body size of the individual specimens observed (Benoist et al. 2019b; chapter 4).

7.4.2 Body-size structure of megabenthos assemblages linked to seafloor temperature and resource supply

Individual-based analysis of the body-size structure of contrasting assemblages, as assessed using the MTE framework, can provide insights into ecosystem functioning between environments that differ in temperature and/or in resource availability. Ultimately, this can help evaluate the contribution of different marine habitats to global ecosystem functionality, and the provision and maintenance of essential goods and services (Rees et al. 2012). The two shelf-sea sites investigated in the Celtic Sea exhibit moderate seabed annual temperature (c. 10 °C), and are subject to relatively high primary productivity (POC flux 12.5 g C m^{-2} yr^{-1}) (Lutz et al. 2007) and seasonality (e.g. Davis et al. 2019). By comparison, the deep-sea sites are exposed to rather low temperature and are meso- to oligotrophic (PAP-SO, 2.5 °C, 2.5 g C m^{-2} yr^{-1}; CCZ, 1.5 °C, 0.25 g C m^{-2} yr^{-1}) (Lutz et al. 2007).

Nonetheless, high seasonal and inter-annual variation in the quantity and quality of POC flux from surface waters are apparent at the abyssal seafloor at PAP-SO (Lampitt et al. 2001, 2010b), and time-series studies have revealed shifts in assemblage composition and biomass (Billett et al. 2001, 2010; Ruhl et al. 2014). As demonstrated in chapters 5.B (shelf-sea sites) and 6 (deep-sea sites), the body-size distribution of abundance and biomass, and of flows of carbon, as analysed using data on the megabenthos (invertebrates and combined with demersal fish), were consistent with the simple MTE model, i.e. consistency of slopes, indicating a broadly equivalent distribution of resources across the body-size range studied (table 7.1). As noted in chapters 5.B and 6, the addition/removal of fish from the assessment had little impact on the spectra, other than right-side extension, suggesting that a simple MTE-type model may be adequate; in general, simple models are to be preferred (parsimony). Notably, abundance (N_i) across the four megabenthic

assemblages was inversely related to their body size (M_i) such that $N_i \propto M_i^{-0.75}$, reflective of an underlying power-law distribution of individual body mass (Newman 2005).

The faunal fraction studied (megabenthos; 0.22 g wwt-3.2 kg wwt across study sites, up to 16 kg including demersal fish data) can, in effect, be represented as a 'single trophic level' with respect to the EER (Damuth 1981; White et al. 2007). This is, of course, a simplistic representation of the true food web structure, and it is not required by the MTE numerical framework, which does not exclude the presence of multiple trophic levels. Only that, trophic level is not body-size controlled, i.e. there are very small predators (e.g. nematodes), and very large surface deposit feeders (e.g. holothurians), forming an assemblage that is not dominated by a strong predator:prey body size relationship. At PAP-SO, Iken et al. (2001) identified at least three trophic levels from isotopic studies across the full benthic assemblage, with most macro- and megabenthic invertebrates classed as deposit feeders, and the remainder as suspension feeders and predators/scavengers; confirming a rather more complex system comprised of taxa exhibiting different levels of mixotrophy and competition for food. For example, Durden et al. (2015b) showed that the most abundant anemone, *Iosactis vagabunda*, one of the smallest representatives of the megabenthos, is typically a deposit-feeder, yet is also capable of capturing suprabenthic prey (e.g. polychaete) up to six times larger than itself.

Additional data on the macrobenthos at the PAP-SO revealed consistency in the trends of the body-size distribution of standing stocks and flows with those of the megabenthos, i.e. the elevation of the two slopes was consistent, indicating that the effective 'single trophic level' concept holds between the two body-size fractions observed. A similar observation was made between the protozoan xenophyophore and the metazoan megabenthos fractions at the CCZ study site. Laureillard et al. (2004) analysed the diet of xenophyophores (*Syringammina corbicula*) at three deep-sea study sites in the tropical NE Atlantic, which differed in trophic regime, and revealed that in addition to particle trapping ("suspension feeding"), the giant foraminifera also fed on bacteria obtained from the surrounding sediments ("deposit feeding").

In the present chapter, abundance data at each site were temperature-corrected to account for the substantial difference in bottom water temperature at the study sites, and to permit direct comparison of the influence of other local environmental variables (e.g. POC flux to the seabed). The results obtained were in accordance with the MTE predictions; the benthic assemblages were ordered by temperature-corrected abundance with resource supply (figures 7.2 and 7.3). GHF is located in a temperate area where high primary productivity, and increased habitat complexity, promote standing stocks and species diversity (Benoist et al. 2019a). By comparison, the CCZ benthos is representative of an oligotrophic zone, consistent with standing stocks that are very substantially lower than at all other sites.

The two shelf-sea sites studied are in close proximity (c. 110 km apart), and share similar environmental conditions (water depth, temperature, primary productivity). However, the temperature-corrected abundance with body-size distribution of invertebrate megabenthos at the SSB study site was markedly lower than that of the GHF site, and approximately level with that of the contrasting deep-sea PAP-SO site. This may reflect intensive demersal trawling in the SSB area, potentially removing a substantial fraction of benthic biomass (ICES 2008; Thomson et al. 2017). This observation aligns with other studies that have shown the impact of fishing pressure on benthic body-size spectra (Blanchard et al. 2004, 2005, 2009; Petchey and Delgrano 2010; Godbold et al. 2013; Mindel et al. 2017; Villnas et al. 2018), thus reinforcing the value of individual-based analysis and of temperature correction of the data. Regardless of relatively high resource supply to the Celtic Shelf seafloor, fishing impacts may have a substantial effect on benthic standing stocks.

It is evident from figure 7.3, accepting the premise that benthic stocks at the SSB study site have been negatively impacted, that the linear relationship between temperature-corrected abundance and POC flux to the seafloor would effectively be improved by removing the SSB data point. In demonstrations of the practical use of size-based assessment of benthic invertebrates and demersal fish assemblages in the NE Atlantic, Blanchard et al. (2004, 2005, 2009) and Mindel et al. (2017) have indicated the substantial effect of fishing pressure in restructuring body-size spectra, likely as a result of the direct removal of larger fish, and the consequent promotion of the development of

smaller-sized taxa. Villnas et al. (2018) investigated body-size as a key ecological indicator of ecosystem functioning for the benthos of the Baltic Sea, on the premise that size regulates sediment bioturbation, and that body-size structure reflects assemblage stability (i.e. mature communities include large and long-lived taxa), thus contributing to the resilience/recovery potential of the benthos in the face of climate change. The authors determined that changes in body-size patterns ultimately reshape food-web structures and stability, by affecting predator-prey interactions (see also Law et al. 2012).

The utility of considering the effect of environmental temperature when assessing total seafloor standing stocks and their linkage to resource supply, e.g. POC flux to the seafloor, was well demonstrated (figure 7.3). These results indicate the clear need to consider the long-understood effects of temperature on metabolism (e.g. Gillooly et al. 2001), in both the comparison of standing stocks, and in their potential prediction from resource supply parameters. The observations of the present study are consistent with similar studies on meio- and macrobenthos assemblages (Kelly-Gerreyn et al. 2014; Labra et al. 2015; Górska and Włodarska-Kowalczuk 2017; Yool et al. 2017; Joydas et al. 2018; Laguionie Marchais et al. 2020). This outcome highlights how global warming, and/or anthropogenic disturbance, can substantially alter ecosystem patterns and processes.

Increases in bottom water temperature with resource supply rate set constant, or decreased, will impose a reduction in benthic standing stocks. Jones et al. (2014) estimated a global 5% decrease in seafloor standing stock biomass associated with decreasing carbon flux export to the benthos in response to climate change. The joint effects of climate change and anthropogenic disturbance (e.g. fishing) will affect marine ecosystems differently around the planet, with deep-seas stocks more likely to be substantially reduced as a result of higher relative change in seafloor temperature, resource supply, and oxygen availability (Jones et al. 2014; Sweetman et al. 2017). Generally, the speed at which change is occurring is limiting the ability of the marine biota to persist, leading to changes in assemblage structure and distribution (Jones et al. 2014; Rutterford et al. 2015). Recently, Antão et al. (2019) showed that global warming has a much

more pronounced effect in the marine realm by comparison to the terrestrial environment.

7.4.3 Using the MTE model to estimate benthic carbon stocks and flows

The simple numerical framework provided by the metabolic theory of ecology indicates that while the largest organisms present in an assemblage may be rare, they can make an overwhelming contribution to total assemblage biomass, as demonstrated in this thesis. On the basis that the benthos can be reasonably represented by a 'single trophic level' concept, with primary consumers found across all body-size classes, and that abundance body-size distributions are broadly consistent with the EER (Damuth 1981; White et al. 2007), then the addition of quantitative megabenthos data is likely to have a significant impact on, and substantially improve, the modelling of benthic biogeochemical cycles.

Benthic carbon stocks and flows parameters are frequently only estimated at small physical scales: 0.05–0.20 m^2 seabed area. In this project, total respiration flux varied markedly as derived from individual metabolic rate using different equations found in the literature (table 7.2). McClain et al.'s (2012) study on diverse shallow and deep-sea organisms reported a low metabolic rate (0.008 mg C d^{-1}), by comparison to Brey's (2010) data that described higher metabolic rates (0.074 mg C d^{-1}). Laguionie Marchais et al.'s (2020) value of 0.036 mg C d^{-1}, derived from a study of the benthos in the abyssal NE Pacific, was of an intermediate rate and likely the most appropriate in the present case.

At the scale of the PAP-SO survey (c. 8.5 ha), the total community respiration estimated using the MTE model was 12.6 mg C m^{-2} d^{-1}, higher than previously reported values obtained from sediment-traps (3.3 mg C m^{-2} d^{-1} at 3000 m water depth) (Lampitt et al. 2001), and sediment community oxygen consumption direct measurements (5.4 mg C m^{-2} d^{-1}) (Witbaard et al. 2000). This may be understandable given the general ineffectiveness of sediment-trap-based estimation of POC flux to depth (Smith et al. 2013), because of in situ contamination of the samples (bacteria, swimming zooplankton), and of

the inability of capturing rarer yet substantial sources of carbon (e.g. fish or jelly-fish fall) (Higgs et al. 2014; Smith et al. 2016).

van Oevelen et al. (2012) and Durden et al. (2017) employed a linear inverse modelling (LIM) approach for indirectly assessing carbon flows in the benthic food web at PAP, which integrated carbon stock estimates and processing rates. The authors estimated total respiration at 6.7 mg C m^{-2} d^{-1} on the abyssal plain (van Oevelen et al. 2012), and between 6.2 mg C m^{-2} d^{-1} on the plain and 13.2 mg C m^{-2} d^{-1} on an abyssal hill (Durden et al. 2017). Note, however, that in these two LIM-based studies, the partitioning of stocks and flux between the conventional benthos size fractions was very different to that found in the present MTE-based model (i.e. ecosystem metabolism was dominated by bacteria). A similar observation was made by Laguionie Marchais et al. (2020) when comparing their MTE-based result to the LIM-based results of Dunlop et al. (2016) at Station M in the abyssal NE Pacific.

It is evident that relying on physically small samples in the estimation of ecosystem-level benthic carbon stocks, and residence time, at the seafloor can be problematic, e.g. underestimating carbon residence time by orders of magnitude (figure 7.5). These results generally reflect the potential importance of large organisms that are usually long-lived, and thus represent a substantial portion of the living carbon residing in the benthic compartment (e.g. Pershing et al. 2010). Similar results were obtained by Laguionie Marchais et al. (2020) in their study of resource partitioning between faunal body-size fractions at the abyssal Station M site in the NE Pacific.

The simplicity of a single body-size spectrum representing the entire benthic assemblage is very appealing, not least from a computational consideration when attempting to make global assessments (e.g. Jones et al. 2014; Yool et al. 2017). The results of the present investigation of megabenthos, macrobenthos, and xenophyophores, taken together with those of Kelly-Gerreyn et al. (2014) and Laguionie Marchais et al. (2020) concerning meio- and macrobenthos, suggest that this simple representation may have practical value and application in many benthic studies.

The use of a ‘single-trophic level’ construction from bacteria (see Arandia-Gorostidi et al. 2017) to megafauna is clearly a very major assumption, however, it is important to note that it does not exclude the

presence of multiple trophic levels, only that they are distributed throughout the spectrum, i.e. small predators and very large detritivores co-exist. This can be usefully contrasted with the body-size spectra of pelagic systems that may have a 'flat' biomass spectrum (Sheldon et al. 1972; Blanchard et al. 2004, 2005, 2009; Cuesta et al. 2018) (chapter 1 figure 1.1), through a body-size structured arrangement of trophic levels. In practical terms, a detailed knowledge of body-size spectra does appear to offer a significant improvement in the characterisation of benthic biogeochemical cycles. Jennings et al. (2008) employed a similar approach using primary productivity and ocean temperature data to model the relative contributions of different consumer groups in the pelagic open ocean, based on life-history theory and food-web ecology. The authors concluded that simple ecological theories can be synthesized to set baselines and monitor any change related to natural/induced variation at the global scale. Taxon-based ecosystem approaches for sustainable management of the seas are needed (e.g. Glover et al. 2018), nonetheless, understanding of the stocks and flows of carbon and energy in the system, at the assemblage level and at large scale, is equally important, particularly in the context of the "blue economy" (Smith-Godfrey 2016).

7.5 Conclusion

The metabolic theory of ecology is a mathematical model that predicts ecological processes at all levels of organisation. It is mechanistic in its approach in assuming that the body-size scaling of whole-organism resting metabolism is determined by the fractal geometry of resource distribution networks level, and that temperature has a role in controlling the rate of biological activities. In other words, it describes how the first principles of biology, physics, and chemistry govern the uptake and transport rates of energy and materials within organisms, and between organisms and their environments.

The results of this project revealed consistent ecological patterns in the distribution of benthic assemblages, which could largely be explained with two variables: individual body size and local environmental temperature. In science, patterns do not happen at random, and those observed in the present

contribution, call for further research to better understanding the mechanistic basis of MTE. The theoretical prospect that metabolism can drive high-level ecological processes needs to be further explored and tested empirically, in order to use this framework for predicting ecosystem processes, particularly in view of climate change.

In conclusion, photographic samples of contrasting shallow- and deep-sea benthic megafauna permitted the construction of high-quality, individual-based, body-size spectra. In doing so, this work enabled the assessment of the sampling effort required, informing on the need for close control over data quality, particularly when comparing datasets generated by different researchers and methodologies. The body-size spectra revealed were consistent with the MTE numerical framework, i.e. controlled by both seafloor temperature and resource supply, and demonstrated the use of a simple, universal, framework, for detailed assessment of benthic standing stocks. In its simple form, the MTE does not provide a mechanistic understanding of how individual metabolism responds to particular environmental conditions other than temperature and resource supply, however, it provides a useful framework to describe patterns, and it establishes a baseline against which to assess and interpret change. The present Ph.D. thesis demonstrated the potential of MTE modelling for (a) interpreting differences in benthic biomass distribution, on the basis of allometric scaling and temperature-dependence of metabolism at the organism level, and for (b) improving our understanding of 'total' stocks and flows of carbon in benthic ecosystems.

Chapter 8

Thesis conclusions

The purpose of this Ph.D. thesis was to advance the state-of-the-art in the quantitative ecology of the marine megabenthos by (a) adopting and further developing the use of mass photography by autonomous underwater vehicle, and (b) extending size-based analysis of ecosystem structure and functioning to the largest size fraction of the benthos. The body-size structure of environmentally contrasted marine benthic communities was examined in order to investigate the effects of seafloor temperature and resource supply on the stocks and flows of mass and energy, using the metabolic theory of ecology framework (MTE) (Brown et al. 2004). The main objectives presented in chapter 1 were met, allowing successful assessment of seafloor carbon stocks and flows based on spectral analysis. The present chapter summarises the core research outcomes, and their implications for future monitoring of the benthos, as well as for research in benthic biogeochemical modelling.

8.1 Can we construct quantitative body-size spectra of megabenthic assemblages using seafloor photography?

Objective 1:

- **Construction of quantitative abundance, biomass, and estimated respiration flux, body-size spectra for benthic assemblages.**

The results obtained in this project demonstrate the practical advantage of mass photographic surveys of the megabenthos (≥ 1 cm body size) using autonomous technology. Seafloor assemblages across four contrasted study sites (in terms of water depth and temperature, and habitat type; chapter 2) (Morris et al. 2016; Thomson et al. 2017; Benoist et al. 2019a; Simon-Lledó et al. 2019a) were investigated using high-quality seafloor images obtained with an underwater vehicle (AUV) (field methods and sample processing;

chapter 3). This approach allowed the generation of quantitative ecological data in a consistent manner, and over landscape-scale areas encompassing multiple habitat types (chapter 5.A) (Wynn et al. 2014; Durden et al. 2016c; Benoist et al. 2019a; Jones et al. 2019).

Individual-based assessment of the body-size structure of the benthos required indirect estimation of the body size of specimens, which was achieved using two photogrammetric approaches: (i) a taxon-specific length-weight relationship (LWR) method where morphometric data were available from the literature, and (ii) a generalised volumetric method developed during the course of this project (GVM) (chapter 4; Benoist et al. 2019b), where such information was unavailable. Chapter 4 describes the GVM that is based on the morphology of individual specimens, and provides a methodological comparison of the advantages of this method over LWRs, given the likely taxonomic, temporal, and spatial, dependencies of morphometric assessments.

Subsequent spectral analyses of the body-size distribution of abundance, biomass, and estimated respiration flux (Peters 1983), showed a remarkable uniformity of the shape of the spectra across the four assemblages (chapters 5.B and 6). At all sites, the distribution of abundance with body size adopted a dome-like pattern, with a prominent peak representing the lower limit of body size reliably recorded for the megafaunal fraction in these studies, i.e. reflecting the practical resolution of the photographic approach. Additional data on the macrobenthos, collected from sediment cores at one study site, was analysed in complement, and the data revealed similar patterns to those of the corresponding megabenthos data. Individual-based body-size spectral analyses proved beneficial to the uniform assessment of the sampling effort allocated to the generation of biomass data at the assemblage level, and it served as the foundation for the subsequent assessment of benthic standing stocks and flows at the four study sites.

8.2 Can we model benthic standing stocks and flows using the MTE numerical framework?

Objectives 2 and 3:

- **Evaluation of the reliable size spectra of the megabenthos: assessment of consistency in slope between environmentally contrasted assemblages, and of uniformity in intercept with corresponding data of smaller benthos (at one study site only), subsequent comparison with the MTE predictions.**
- **Investigation of the effect of environmental temperature and resource supply on the distribution of benthic assemblages: application of temperature-correction to standardize standing stock data, and comparison of the elevation between the slopes.**

In heterotrophic populations, individual biological units (organisms) represent particular energy flow systems–within and between units–that act together by using, storing, and re-distributing energy and materials in the environment (Brown et al. 2004; Savage et al. 2004a; Allen and Gillooly 2007). As presented in chapter 1, the MTE is based on the body-mass allometry and the temperature-dependence of individual metabolic rate, and the theory makes predictions about ecological processes at higher biological levels of organisation (e.g. assemblage).

The right-hand side of the body-size spectra, assumed to be the quantitatively reliable component (Bett 2013, 2014), were assessed in the MTE framework (Brown et al. 2004). The project results matched well with the model's predictions, with abundance (N_i) across the four megabenthic assemblages inversely related to their body size (M_i) such that $N_i \propto {M_i}^{-0.75}$, reflective of an underlying power-law distribution of individual body mass (Newman 2005). Accepting that individual metabolic rate scales with body mass as $B_i \propto {M_i}^{0.75}$, these findings are consistent with the 'energetic equivalence rule' (EER) (Damuth 1981). This work adds to a small body of literature that suggests that Damuth's rule (White et al. 2007) may be of value in assessing the stocks and flows of mass and energy in the marine benthos (Kelly-Gerreyn et al. 2014; Labra et al. 2015; Górska and Włodarska-Kowalczuk 2017; Laguionie Marchais et al. 2020).

At the Porcupine Abyssal Plain sustained observatory site, additional data for smaller invertebrates (macrobenthos) were generated and analysed, and the distribution of standing stocks revealed consistency between the macro- and the megabenthos assemblages. This outcome suggested that the full metazoan benthic assemblage could potentially be modelled as a single unit. Clearly, this is a simplistic representation of the benthos, nonetheless, its simplicity is mathematically attractive for incorporation in global modelling efforts, see for example Yool et al. (2017).

The four study sites were contrasted in terms of seafloor temperature and resource supply, with the shelf-sea sites in the Celtic Sea representing comparatively warm and eutrophic environments, as opposed to the deep-sea sites in the NE Atlantic and in the NE Pacific that are relatively cold and oligotrophic (chapter 2). As a result of the major effect of environmental temperature on individual metabolism, it was important to apply a temperature correction (Gillooly et al. 2001) to standardize the data between the study sites prior to comparison (Laguionie Marchais et al. 2020). Although the shape of the body-size spectra was similar between sites, temperature-corrected standing stocks illustrated the link to resource supply availability.

Although temporal comparisons of body-size spectra were not possible within the constraints of this project, other studies, e.g. Labra et al. (2015) and Laguionie Marchais et al. (2020), have shown that if benthic assemblages respond to annual and inter-annual variability by the means of shifts in the abundance of some taxa (Billett et al. 2001, 2010; Ruhl et al. 2014), the shape (slope) of the spectra remain approximately constant in time, while the elevation (intercept) may vary in response to resource supply. Jones and Lawton (1995) noted that "species biomasses fluctuate considerably in time and space, while total biomass remains far more constant", suggesting an ecological equilibrium regulating the use of natural resources in space and in time, and highlighting the natural resilience of the biota to fluctuation in food supply.

Various broad-scale ecological patterns have been observed to follow simple mathematical functions (e.g. Lawton 1999; Newman 2005), indicating a basic process with the potential for deeper, mechanistic, understanding. Individual-based assessment of the body-size structure of faunal assemblages

can be used as a complement to taxon-based methodologies, for quantifying fluctuations in standing stocks across environmental gradients. In light of the results of this project, the MTE numerical framework seems to be a useful tool for the study of the benthos, providing a baseline against which to evaluate, or predict, change in stocks and flows of carbon at the seafloor, based on simple bio-energetic assumptions of individual metabolism.

8.3 Can we use the MTE framework to improve modelling of benthic carbon stocks and flows?

Objective 4:

- **Use the MTE framework for modelling carbon stocks and flows at the seafloor, as illustrated using the deep-sea dataset from the NE Atlantic.**

The MTE framework was employed in a modelling exercise to indirectly estimate seafloor carbon stocks and flows, as illustrated using the deep-sea dataset from the Porcupine Abyssal Plain sustained observatory (PAP-SO) in the NE Atlantic (chapter 7). Field data were consistent with the MTE framework, and revealed a uniform relationship in standing stock scaling across eight orders of magnitude in body mass (i.e. from macro- to megabenthos; chapter 6 section 6.3.1), characteristic of a relatively 'simple' benthic food web, where all the constituent organisms rely on the particulate organic matter produced in surface waters (Etter and Grassle 1992; Johnson et al. 2007).

A singular size spectrum provides a useful summary of the benthic system, and application of the MTE numerical framework can provide a better understanding of the benthic system. The assumption of a 'single trophic level' system extending from bacteria to megafauna was applied at PAP-SO, although it does not exclude the presence of multiple trophic levels, only that the first trophic level is present across all size classes. Thus, seafloor carbon stocks and flows were estimated assuming that the EER (Damuth 1981; White et al. 2007) held throughout the complete benthic size spectrum. Individual metabolic rate was estimated using different equations found in the literature (Hemmingsen 1960; Brey 2010; McClain et al. 2012; Laguionie Marchais et al.

2020), in order to assess the model's sensitivity to individual metabolic activity in the modelling of ecosystem metabolism.

In this project, the addition of megabenthos data considerably changed the current biogeochemical estimates (typically measured at 0.01 m^2), highlighting a gradual increase of energy flux with seabed area assessed, and a very substantial increase in carbon biomass and residence time in the benthos, at large scales of seafloor area surveyed. Field data matched well the model's prediction, revealing that in a system where faunal abundance seems to follow a power-law distribution (Newman 2005), seafloor stocks of carbon (and residence time) estimates keep increasing until the largest organisms (i.e. megabenthos) are effectively quantified. Similar observations were made by Laguionie Marchais et al. (2020) at the Station M study site in the deep NE Pacific, using polychaete body-size spectra. For biogeochemical modelling purposes, this critical observation emphasizes the importance of sampling the largest specimens which dominate faunal assemblages in terms of carbon storage and life expectancy (i.e. 93% contribution) (e.g. Pershing et al. 2010). It also redefines the contribution of the different faunal fractions to ecosystem processes such as carbon cycling (e.g. see Laguionie Marchais et al. 2020; see also van Oevelen et al. 2012 and Durden et al. 2017). Using the MTE approach provided new insights into potential resource partitioning in the benthic ecosystem as a whole.

8.4 Limitations and improvements to this study

Differences in field operations, photographic-sample processing, and data acquisition (i.e. specimen detection, body-size measurement, and estimation of individual biomass) can potentially introduce systematic bias between sampling and analysis methods. This can be prevented by following rigorous quality control and assessment of the data generated. For example, differences in the physical scale of observation (associated to sampling gear), and in the resolution of observation (i.e. seafloor image pixel size in photographic work), introduce bias in taxonomic identification and in 'optimal' body-size detection. Thus, fair comparison of assemblages should be made based upon a selected body-size range. Also, because specimens are not homogeneously distributed in space, assessments should be made on a

minimum number of individuals rather than a fixed physical sample size (e.g. Benoist et al. 2019a; Simon-Lledó et al. 2019a).

Individual-based body-size spectra analysis necessarily relies upon individual biomass data. As discussed in chapter 4, the use of species-specific length-weight relationship to acquire that data can be limiting because of systematic taxonomic, temporal, and spatial, dependencies known to impact morphometric assessments. The generalised volumetric method developed in this Ph.D. thesis was a good alternative for estimating the biomass of photographically surveyed benthic megafauna, macrobenthos, and also protozoan xenophyophores (chapter 6), highlighting the benefits of a taxon-independent approach. Nonetheless, whichever method is employed, a direct estimate of individual mass should be made for every specimen. This also applies to the organisms that are observed partially or above the seabed; allocating the mean individual biomass of the corresponding morphotype leads to the generation of 'spikes' in the overall body-size distribution as a result of their bulk assignment to single size classes.

8.5 Implication for future research and conservation of the benthos

The results of this project add to an emerging set of observations in the fields of benthic conservation and management, and of carbon stocks and flows modelling, both in shelf seas and in the wider deep ocean. This section addresses the implications of the Ph.D. thesis findings, and draws a series of suggestions for benthic ecologists and modellers, and for conservation practitioners.

This study has provided state-of-the art insights on the body-size distributions of megabenthic invertebrate and demersal fish assemblages from contrasted environments, and their potential links to seafloor temperature and resource supply. The patterns revealed in this Ph.D. thesis were broadly consistent with the simple predictions of the metabolic theory of ecology (MTE) (Brown et al. 2004). The body-size distribution of benthic assemblages appears to be stable in time (i.e. slope), as observed in previous studies (Labra et al. 2015; Laguionie Marchais et al. 2020). This provides the basis for further examinations of these apparently consistent ecological patterns across

the entire benthic size spectrum, and in a wider range of environmental settings, perhaps particularly those where natural stressors and/or anthropogenic disturbance are key drivers that may modify body-size spectra. Further data is needed to investigate the effect of seasonal flux of particulate organic matter to the seafloor and the response of the various benthic faunal fractions.

Empirical sampling across the entire benthic spectrum is required to further verify the assumptions made in this project, and to directly determine the contribution of the different faunal fractions to biogeochemical processes at the seafloor. This would increase understanding about how body-size spectra respond to varying conditions, in terms of the resulting body-size range and structure, and would call for further research on the mechanism(s) underlying metabolism from individual to ecosystem scales. For evaluation of standing stocks, in the name of management and conservation of natural resources, and for modelling purposes, body-size spectra analysis could be made in reference to broad-scale patterns of specimens' distribution, using the MTE predictions as a baseline for assessing change.

Given the rapidly increasing volume of data, particularly from seabed mass imagery, it will be necessary to standardize sampling effort (in terms of taxonomy, body-size range considered and subsequent individual measurement, physical scale of sampling/observation), in order to quantify the contribution of specimens in the environment. Body-size-based assessments are likely to be a valuable complement to more conventional taxon-based approaches, and the two might usefully be combined to reduce the potential for systematic bias between sampling methods.

8.6 Conclusion

This Ph.D. project demonstrated (i) the use of mass photography by AUV in generating high-quality, quantitative, ecological data in a consistent manner, and over landscape-scale areas encompassing multiple habitat types, and (ii) the potential of the MTE numerical framework for investigating benthic assemblages, and for modelling carbon stocks and flows at the seafloor under simple bio-energetic assumptions of individual metabolism. The results revealed consistent ecological patterns in the distribution of benthic

assemblages, which could largely be explained with two variables: individual body size and local environmental temperature. In science, patterns do not happen at random, and those observed in this project call for further research to better understanding the mechanistic basis of the MTE. The theoretical prospect that metabolism can drive high-level ecological processes needs to be further explored and tested empirically in order to use the framework to predict ecosystem processes, particularly in view of climate change.

References

Alcaraz M, Saiz E, Calbet A, Trepat I, Broglio E. 2003. Estimating zooplankton biomass through image analysis. Marine Biology **143**(2), 307-315. DOI: 10.1007/s00227-003-1094-8

Allen DM. 1971. Mean Square Error of Prediction as a Criterion for Selecting Variables. Technometrics **13**(3), 469-475. DOI: 10.2307/1267161

Allen AP, Brown JH, Gillooly JF. 2002. Global Biodiversity, Biochemical Kinetics, and the Energetic-Equivalence Rule. Science **297**, 1545-1548.

Allen AP, Gillooly JF. 2007. The mechanistic basis of the metabolic theory of ecology. Oikos **116**(6), 1073-1077. DOI: 10.1111/j.2007.0030-1299.16079.x

Althaus F, Hill N, Ferrari R, Edwards L, Przeslawski R, Schonberg CH, Stuart-Smith R, Barrett N, Edgar G, Colquhoun J, Tran M, Jordan A, Rees T, Gowlett-Holmes K. 2015. A Standardised Vocabulary for Identifying Benthic Biota and Substrata from Underwater Imagery: The CATAMI Classification Scheme. PLoS ONE **10**(10), e0141039. DOI: 10.1371/journal.pone.0141039

Amon DJ, Ziegler AF, Dahlgren TG, Glover AG, Goineau A, Gooday AJ, Wiklund H, Smith CR. 2016. Insights into the abundance and diversity of abyssal megafauna in a polymetallic-nodule region in the eastern Clarion-Clipperton Zone. Scientific Reports **6**, 30492. DOI: 10.1038/srep30492

Amon DJ, Ziegler AF, Kremenetskaia A, Mah CL, Mooi R, O'Hara T, Pawson DL, Roux M, Smith CR. 2017a. Megafauna of the UKSRL exploration contract area and eastern Clarion-Clipperton Zone in the Pacific Ocean: Echinodermata. Biodiversity Data Journal **5**, e11794. DOI: 10.3897/BDJ.5.e11794

Amon DJ, Ziegler AF, Drazen JC, Grischenko AV, Leitner AB, Lindsay DJ, Voight JR, Wicksten MK, Young CM, Smith CR. 2017b. Megafauna of the UKSRL exploration contract area and eastern Clarion-Clipperton Zone in the Pacific Ocean: Annelida, Arthropoda, Bryozoa, Chordata, Ctenophora, Mollusca. Biodiversity Data Journal **5**, e14598. DOI: 10.3897/BDJ.5.e14598

Amon DJ, Hilario A, Arbizu PM, Smith CR. 2017c. Observations of organic falls from the abyssal Clarion-Clipperton Zone in the tropical eastern Pacific Ocean. Marine Biodiversity **47**(2), 311-321. DOI: 10.1007/s12526-016-0572-4

Anderson K, Gaston KJ. 2013. Lightweight unmanned aerial vehicles will revolutionize spatial ecology. Frontiers in Ecology and the Environment **11**(3), 138-146. DOI: 10.1890/120150

Anderson MJ, Santana-Garcon J. 2015. Measures of precision for dissimilarity-based multivariate analysis of ecological communities. Ecology Letters **18**(1), 66-73. DOI: 10.1111/ele.12385

Antão LH, Bates AE, Blowes SA, Waldock C, Supp SR, Magurran AE, Dornelas M, Schipper AM. 2019. Temperature-related biodiversity change across

temperate marine and terrestrial systems, pre-print. DOI: 10.1101/841833

Arandia-Gorostidi N, Huete-Stauffer TM, Alonso-Saez L, XA GM. 2017. Testing the metabolic theory of ecology with marine bacteria: different temperature sensitivity of major phylogenetic groups during the spring phytoplankton bloom. Environmental Microbiology **19**(11), 4493-4505. DOI: 10.1111/1462-2920.13898

Ardron JA, Simon-Lledó E, Jones DOB, Ruhl HA. 2019. Detecting the Effects of Deep-Seabed Nodule Mining: Simulations Using Megafaunal Data From the Clarion-Clipperton Zone. Frontiers in Marine Science **6**, 604. DOI: 10.3389/fmars.2019.00604

Baguley JG, Hyde LJ, Montagna PA. 2004. A semi-automated digital microphotographic approach to measure meiofaunal biomass. Limnology and Oceanography-Methods **2**(6), 181-190. DOI: 10.4319/lom.2004.2.181

Banse K, Mosher S. 1980. Adult Body-Mass and Annual Production-Biomass Relationships of Field Populations. Ecological Monographs **50**(3), 355-379. DOI: 10.2307/2937256

Barnett PR, Watson J, Connelly D. 1984. The multiple corer for taking virtually undisturbed samples from shelf, bathyal and abyssal sediments. Oceanologica Acta **7**(4), 339-408.

Bar-On YM, Phillips R, Milo R. 2018. The biomass distribution on Earth. Proceedings of the National Academy of Sciences of the United States of America **115**(25), 6506-6511. DOI: 10.1073/pnas.1711842115

Barrio Froján C, Diesing M, Curtis M. 2015. Mapping of the Haig Fras Site of Community Importance (SCI) JNCC/Cefas Partnership (Report Serie. No. 4.). Peterborough, UK: JNCC/Cefas. pp. 25.

Barthel D. 1995. Tissue composition of sponges from the Weddell Sea, Antarctica: not much meat on the bones. Marine Ecology Progress Series **123**, 149-153.

Basset A, Sangiorgio F, Pinna M. 2004. Monitoring with benthic macroinvertebrates: advantages and disadvantages of body size descriptors. Aquatic Conservation: Marine and Freshwater Ecosystems **14**(S1), S43-S58. DOI: 10.1002/aqc.649

Basset A, Cozzoli F, Paparella F. 2012. A unifying approach to allometric scaling of resource ingestion rates under limiting conditions. Ecosphere **3**(1), 1-14. DOI: 10.1890/Es11-00249.1

Baum KA, Haynes KJ, Dillemuth FP, Cronin JT. 2004. The matric enhances the effectiveness of corridors and stepping stones. Ecology **85**, 2671-2676.

Benoist NMA, Morris KJ, Bett BJ, Durden JM, Huvenne VAI, Le Bas TP, Wynn RB, Ware SJ, Ruhl HA. 2019a. Monitoring mosaic biotopes in a marine conservation zone by autonomous underwater vehicle. Conservation Biology **33**(5), 1174-1186. DOI: 10.1111/cobi.13312

Benoist NMA, Bett BJ, Morris KJ, Ruhl HA. 2019b. A generalised volumetric method to estimate the biomass of photographically surveyed benthic

megafauna. Progress in Oceanography - Special Issue VIS: Northeast Atlantic PAP-SO **178**, 102188. DOI: 10.1016/j.pocean.2019.102188

Bergstad OA. 2009. Fish: demersal fish (life histories, behavior, adaptations). JH Steele (Ed.) In Encyclopedia of Ocean Sciences. Elsevier, Massachusetts, USA, pp. 458-466.

Bertness MD, Gaines SD, Hay ME. 2001. Marine Community Ecology. Sinauer Associates Sunderland: Massachusetts, USA. pp. 550.

Bertness MD, Bruno J, Silliman B, Stachowick J. 2014. Marine Community Ecology and Conservation. Sinaeur Associates Sunderland: Oxford University Press, UK. pp. 560.

Bett BJ, Rice AL. 1993. The feeding behaviour of an abyssal echiuran revealed by in situ time-lapse photography Deep Sea Research I **40**(9), 1767-1779.

Bett BJ, Rice AL, Thurston MH. 1995. A Quantitative Photographic Survey of Spoke-Burrow Type Lebensspuren on the Cape-Verde Abyssal-Plain. Internationale Revue Der Gesamten Hydrobiologie **80**(2), 153-170. DOI: 10.1002/iroh.19950800204

Bett BJ. 2001. UK Atlantic Margin Environmental Survey: Introduction and overview of bathyal benthic ecology. Continental Shelf Research **21**(8-10), 917-956. DOI: 10.1016/S0278-4343(00)00119-9

Bett BJ, Malzone MG, Narayanaswamy BE, Wigham BD. 2001. Temporal variability in phytodetritus and megabenthic activity at the seabed in the deep Northeast Atlantic. Progress in Oceanography **50**(1-4), 349-368. DOI: 10.1016/S0079-6611(01)00066-0

Bett BJ. 2013. Characteristic benthic size spectra: potential sampling artefacts. Marine Ecology Progress Series **487**, 1-6. DOI: 10.3354/meps10441

Bett BJ. 2014. Macroecology and meiobenthos: Reply to Warwick (2014). Marine Ecology Progress Series **505**, 299-302. DOI: 10.3354/meps10831

Bett BJ. 2019. Megafauna. In: Cochran JK, HJ Bokuniewicz and PL Yager (Editors) Encyclopedia of Ocean Sciences, 3rd edition, pp. 735-741. Volume 2). Elsevier Inc.

Billett DSM, Rice AL. 2001. The BENGAL programme: introduction and overview. Progress in Oceanography **50**(1-4), 13-25. DOI: 10.1016/S0079-6611(01)00046-5

Billett DSM, Bett BJ, Rice AL, Thurston MH, Galéron J, Sibuet M, Wolff GA. 2001. Long-term change in the megabenthos of the Porcupine Abyssal Plain (NE Atlantic). Progress in Oceanography **50**(1-4), 325-348. DOI: 10.1016/S0079-6611(01)00060-X

Billett DSM, Bett BJ, Reid WDK, Boorman B, Priede IG. 2010. Long-term change in the abyssal NE Atlantic: The '*Amperima* Event' revisited. Deep Sea Research Part II: Topical Studies in Oceanography **57**(15), 1406-1417. DOI: 10.1016/j.dsr2.2009.02.001

Blanchard JL, LeLoc'h F, Hily C, Boucher J. 2004. Fishing effects on diversity, size and community structure of the benthic invertebrate and fish megafauna on the Bay of Biscay coast of France. Marine Ecology Progress Series 280, 249-260.

Blanchard JL, Dulvy NK, Jennings S, Ellis JR, Pinnegar JK, Tidd A, Kell LT. 2005. Do climate and fishing influence size-based indicators of Celtic Sea fish community structure? ICES Journal of Marine Science **62**(3), 405-411. DOI: 10.1016/j.icesjms.2005.01.006

Blanchard JL, Jennings S, Law R, Castle MD, McCloghrie P, Rochet MJ, Benoit E. 2009. How does abundance scale with body size in coupled size-structured food webs? Journal of Animal Ecology **78**(1), 270-280. DOI: 10.1111/j.1365-2656.2008.01466.x

Brey T. 2010. An empirical model for estimating aquatic invertebrate respiration. Methods in Ecology and Evolution **1**(1), 92-101. DOI: 10.1111/j.2041-210X.2009.00008.x

Brey T, Müller-Wiegmann C, Zittier ZMC, Hagen W. 2010. Body composition in aquatic organisms — A global data bank of relationships between mass, elemental composition and energy content. Journal of Sea Research **64**(3), 334-340. DOI: 10.1016/j.seares.2010.05.002

Brown JH, Carrillo L, Fernand L, Horsburgh KJ, Hill AE, Young EF, Medler KJ. 2003. Observations of the physical structure and seasonal jet-like circulation of the Celtic Sea and St. George's Channel of the Irish Sea. Continental Shelf Research **23**(6), 533-561. DOI: 10.1016/S0278-4343(03)00008-6

Brown JH, Gillooly JF. 2003. Ecological food webs: high-quality data facilitate theoretical unification. Proceedings of the National Academy of Sciences of the United States of America **100**(4), 1467-1468. DOI: 10.1073/pnas.0630310100

Brown JH, Gillooly JF, Allen AP, Savage VM, West GB. 2004. Toward a Metabolic Theory of Ecology. Ecology **85**(7), 1771-1789.

Brown JH, Sibly RM. 2012. The Metabolic Theory of Ecology and its Central Equation. In: Sibly RM, JH Brown and A Kodric-Brown (Editors) Metabolic Ecology - A Scaling Approach, 1st edition, pp. 21-33. John Wiley & Sons, Ltd.

Brown A, Hauton C, Stratmann T, Sweetman A, van Oevelen D, Jones DOB. 2018. Metabolic rates are significantly lower in abyssal Holothuroidea than in shallow-water Holothuroidea. Royal Society Open Science **5**(5), 172162. DOI: 10.1098/rsos.172162

Buhl-Mortensen L, Buhl-Mortensen P, Dolan MFJ, Dannheim J, Bellec V, Holte B. 2012. Habitat complexity and bottom fauna composition at different scales on the continental shelf and slope of northern Norway. Hydrobiologia **685**(1), 191-219. DOI: 10.1007/s10750-011-0988-6

Calow P. 1977. Ecology, Evolution and Energetics: A Study in Metabolic Adaptation. Advances in Ecological Research **10**, 1-62. DOI: 10.1016/s0065-2504(08)60233-0

Cammen LM. 1979. Ingestion rate: An empirical model for aquatic deposit feeders and detritivores. Oecologia **44**(3), 303-310. DOI: 10.1007/BF00545232

Childress JJ, Cowles DL, Favuzzi JA, Mickel TJ. 1990. Metabolic rates of benthic deep-sea decapod crustaceans decline with increasing depth primarily

due to the decline in temperature. Deep Sea Research Part A. Oceanographic Research Papers **37**(6), 929-949. DOI: 10.1016/0198-0149(90)90104-4

Childress JJ. 1995. Are there physiological and biochemical adaptations of metabolism in deep-sea animals? TRENDS in Ecology and Evolution **10**(1), 30-36.

Clarke KR, Warwick RM. 1994. Changes in Marine Communities: An Approach to Statistical Analysis and Interpretation. PRIMER-E: Plymouth.

Clarke A. 2017. The Metabolic Theory of Ecology. In Principles of Thermal Ecology (Chapter 12). Oxford University Press, Oxford, UK, pp. 267-284. DOI: 10.1093/oso/9780199551668.001.0001

Colwell RK, Chao A, Gotelli NJ, Lin SY, Mao CX, Chazdon RL, Longino JT. 2012. Models and estimators linking individual-based and sample-based rarefaction, extrapolation and comparison of assemblages. Journal of Plant Ecology **5**(1), 3-21. DOI: 10.1093/jpe/rtr044

Colwell RK. 2013. EstimateS: Statistical estimation of species richness and shared species from samples. Version 9 and earlier. User's Guide and application. Retrieved from http://purl.oclc.org/estimates (Accessed 06.04.2017).

Constable AJ, Costa DP, Schofield O, Newman L, Urban ER, Fulton EA, Melbourne-Thomas J, Ballerini T, Boyd PW, Brandt A, de la Mare WK, Edwards M, Eléaume M, Emmerson L, Fennel K, Fielding S, Griffiths H, Gutt J, Hindell MA, Hofmann EE, Jennings S, La HS, McCurdy A, Mitchell BG, Moltmann T, Muelbert M, Murphy E, Press AJ, Raymond B, Reid K, Reiss C, Rice J, Salter I, Smith DC, Song S, Southwell C, Swadling KM, van de Putte A, Willis Z. 2016. Developing priority variables ("ecosystem Essential Ocean Variables" — eEOVs) for observing dynamics and change in Southern Ocean ecosystems. Journal of Marine Systems **161**, 26-41. DOI: 10.1016/j.jmarsys.2016.05.003

Costello MJ. 2009. Distinguishing marine habitat classification concepts for ecological data management. Marine Ecology Progress Series **397**, 253-268. DOI: 10.3354/meps08317

Coull KA, Jermyn AS, Newton AW, Henderson GI, Hall WB. 1989. Length-weight relationships for 88 species of fish encountered in the North East Atlantic. Scottish Fisheries Research Report 43. Aberdeen: Department of Agriculture and Fisheries for Scotland. pp. 81.

Cuesta JA, Delius GW, Law R. 2018. Sheldon spectrum and the plankton paradox: two sides of the same coin-a trait-based plankton size-spectrum model. Journal of Mathematical Biology **76**(1-2), 67-96. DOI: 10.1007/s00285-017-1132-7

Damuth J. 1981. Population-Density and Body Size in Mammals. Nature **290**(5808), 699-700. DOI: 10.1038/290699a0

Damuth J. 1987. Interspecific allometry of population density in mammals and other animals: the independence of body mass and population energy-use. Biological Journal of the Linnean Society **31**(3), 193-246. DOI: 10.1111/j.1095-8312.1987.tb01990.x

Datta S, Blanchard JL. 2016. The effects of seasonal processes on size spectrum dynamics. Canadian Journal of Fisheries and Aquatic Sciences **73**(4), 598-610. DOI: 10.1139/cjfas-2015-0468

Dauvin JC. 2015. History of benthic research in the English Channel: From general patterns of communities to habitat mosaic description. Journal of Sea Research **100**, 32-45. DOI: 10.1016/j.seares.2014.11.005

Davis CE, Blackbird S, Wolff G, Woodward M, Mahaffey C. 2019. Seasonal organic matter dynamics in a temperate shelf sea. Progress in Oceanography **177**, 101925. DOI: 10.1016/j.pocean.2018.02.021

Davison AC, Hinkley DV. 1997. Bootstrap Methods and Their Application. Cambridge University Press. pp. 592.

De Cáceres M, Legendre P. 2009. Associations between species and groups of sites: indices and statistical inference. Ecology **90**(12), 3566-3574.

de Haas H, van Weering TCE, de Stigter H. 2002. Organic carbon in shelf seas: sinks or sources, processes and products. Continental Shelf Research **22**(5), 691-717. DOI: 10.1016/s0278-4343(01)00093-0

Di Mauro R, Cepeda G, Capitanio F, Viñas MD. 2011. Using ZooImage automated system for the estimation of biovolume of copepods from the northern Argentine Sea. Journal of Sea Research **66**(2), 69-75. DOI: 10.1016/j.seares.2011.04.013

Diesing M, Kröger S, Parker R, Jenkins C, Mason C, Weston K. 2017. Predicting the standing stock of organic carbon in surface sediments of the North–West European continental shelf. Biogeochemistry **135**(1-2), 183-200. DOI: 10.1007/s10533-017-0310-4

Donald PF, Evans AD. 2006. Habitat connectivity and matrix restoration: the wider implications of agri-environment schemes. Journal of Applied Ecology **43**(2), 209-218. DOI: 10.1111/j.1365-2664.2006.01146.x

Drazen JC, Seibel BA. 2007. Depth-related trends in metabolism of benthic and benthopelagic deep-sea fishes. Limnology and Oceanography **52**(5), 2306-2316.

Dunlop KM, van Oevelen D, Ruhl HA, Huffard CL, Kuhnz LA, Smith KL. 2016. Carbon cycling in the deep eastern North Pacific benthic food web: Investigating the effect of organic carbon input. Limnology and Oceanography **61**(6), 1956-1968. DOI: 10.1002/lno.10345

Duplisea DE, Drgas A. 1999. Sensitivity of a benthic, metazoan, biomass size spectrum to differences in sediment granulometry. Marine Ecology Progress Series **177**, 73-81. DOI: 10.3354/meps177073

Durden JM, Bett BJ, Jones DOB, Huvenne VAI, Ruhl HA. 2015a. Abyssal hills – hidden source of increased habitat heterogeneity, benthic megafaunal biomass and diversity in the deep sea. Progress in Oceanography **137**, 209-218. DOI: 10.1016/j.pocean.2015.06.006

Durden JM, Bett BJ, Ruhl HA. 2015b. The hemisessile lifestyle and feeding strategies of *Iosactis vagabunda* (Actiniaria, Iosactiidae), a dominant megafaunal species of the Porcupine Abyssal Plain. Deep Sea Research Part I: Oceanographic Research Papers **102**, 72-77. DOI: 10.1016/j.dsr.2015.04.010

Durden JM, Bett BJ, Horton T, Serpell-Stevens A, Morris KJ, Billett DSM, Ruhl HA. 2016a. Improving the estimation of deep-sea megabenthos biomass: dimension to wet weight conversions for abyssal invertebrates. Marine Ecology Progress Series **552**, 71-79. DOI: 10.3354/meps11769

Durden JM, Bett BJ, Schoening T, Morris KJ, Nattkemper TW, Ruhl HA. 2016b. Comparison of image annotation data generated by multiple investigators for benthic ecology. Marine Ecology Progress Series **552**, 61-70. DOI: 10.3354/meps11775

Durden JM, Schoening T, Althaus F, Friedman A, Garcia R, Glover AG, Greinert J, Stout NJ, Jones DOB, Jordt A, Kaeli JW, Koser K, Kuhnz LA, Lindsay D, Morris KJ, Nattkemper TW, Osterloff J, Ruhl HA, Singh H, Tran M, Bett BJ. 2016c. Perspectives in Visual Imaging for Marine Biology and Ecology: From Acquisition to Understanding. Oceanography and Marine Biology: An Annual Review, **54**, 1-72. DOI: 10.1201/9781315368597

Durden JM, Ruhl HA, Pebody C, Blackbird SJ, van Oevelen D. 2017. Differences in the carbon flows in the benthic food webs of abyssal hill and plain habitats. Limnology and Oceanography **62**(4), 1771-1782. DOI: 10.1002/lno.10532

Durden JM, Lallier LE, Murphy K, Jaeckel A, Gjerde K, Jones DOB. 2018. Environmental Impact Assessment process for deep-sea mining in 'the Area'. Marine Policy **87**, 194-202. DOI: 10.1016/j.marpol.2017.10.013

Durden JM, Bett BJ, Huffard CL, Ruhl HA, Smith KL. 2019. Abyssal deposit-feeding rates consistent with the metabolic theory of ecology. Ecology **100**(1), e02564. DOI: 10.1002/ecy.2564

Durden JM, Bett BJ, Huffard CL, Pebody C, Ruhl HA, Smith KL. 2020. Response of deep-sea deposit-feeding rates to detrital inputs: A comparison of two abyssal time-series sites. Deep Sea Research Part II: Topical Studies in Oceanography **173**, 104677. DOI: 10.1016/j.dsr2.2019.104677

Edwards AM, Robinson JPW, Plank MJ, Baum JK, Blanchard JL. 2017. Testing and recommending methods for fitting size spectra to data. Methods in Ecology and Evolution **8**(1), 57-67. DOI: 10.1111/2041-210x.12641

Edwards AM, Robinson JPW, Blanchard JL, Baum JK, Plank MJ. 2020. Accounting for the bin structure of data removes bias when fitting size spectra. Marine Ecology Progress Series **636**, 19-33. DOI: 10.3354/meps13230

Ehrnsten E, Bauer B, Gustafsson BG. 2019. Combined Effects of Environmental Drivers on Marine Trophic Groups – A Systematic Model Comparison. Frontiers in Marine Science **6**, 492. DOI: 10.3389/fmars.2019.00492

Ehrnsten E, Norkko A, Timmermann K, Gustafsson BG. 2019. Benthic-pelagic coupling in coastal seas – Modelling macrofaunal biomass and carbon processing in response to organic matter supply. Journal of Marine Systems **196**, 36-47. DOI: 10.1016/j.jmarsys.2019.04.003

Ellis JR, Rogers SI, Freeman SM. 2000. Demersal assemblages in the Irish Sea, St George's Channel and Bristol Channel. Estuarine Coastal and Shelf Science **51**(3), 299-315. DOI: 10.1006/ecss.2000.0677

Ellis JR, Martinez I, Burt GJ, Scott BE. 2013. Epibenthic assemblages in the Celtic Sea and associated with the Jones Bank. Progress in Oceanography **117**, 76-88. DOI: 10.1016/j.pocean.2013.06.012

Etter RJ, Grassle JF. 1992. Patterns of Species-Diversity in the Deep-Sea as a Function of Sediment Particle-Size Diversity. Nature **360**(6404), 576-578. DOI: 10.1038/360576a0

Forcino FL, Leighton LR, Twerdy P, Cahill JF. 2015. Reexamining Sample Size Requirements for Multivariate, Abundance-Based Community Research: When Resources are Limited, the Research Does Not Have to Be. PLoS ONE **10**(6), e0128379. DOI: 10.1371/journal.pone.0128379

Foster SD, Hosack GR, Hill NA, Barrett NS, Lucieer VL. 2014. Choosing between strategies for designing surveys: autonomous underwater vehicles. Methods in Ecology and Evolution **5**(3), 287-297. DOI: 10.1111/2041-210x.12156

Froese R. 2006. Cube law, condition factor and weight-length relationships: history, meta-analysis and recommendations. Journal of Applied Ichthyology **22**(4), 241-253. DOI: 10.1111/j.1439-0426.2006.00805.x

Gage JD, Tyler P. 1991. Deep-Sea Biology - A Natural History of Organisms at the Deep-Sea Floor. Cambridge University Press: Cambridge, UK. pp. 524.

Gage JD, Hughes DJ, Vecino JLG. 2002. Sieve size influence in estimating biomass, abundance and diversity in samples of deep-sea macrobenthos. Marine Ecology Progress Series **225**, 97-107. DOI: 10.3354/meps225097

Gage JD, Bett BJ. 2005. Deep-Sea Benthic Sampling. In: Eleftheriou A and A McIntyre (Editors) Methods for the study of marine benthos, 3rd edition, pp. 273-325. Blackwell Science: Oxford.

Galparsoro I, Connor DW, Borja A, Aish A, Amorim P, Bajjouk T, Chambers C, Coggan R, Dirberg G, Ellwood H, Evans D, Goodin KL, Grehan A, Haldin J, Howell K, Jenkins C, Michez N, Mo G, Buhl-Mortensen P, Pearce B, Populus J, Salomidi M, Sanchez F, Serrano A, Shumchenia E, Tempera F, Vasquez M. 2012. Using EUNIS habitat classification for benthic mapping in European seas: present concerns and future needs. Marine Pollution Bulletin **64**(12), 2630-2638. DOI: 10.1016/j.marpolbul.2012.10.010

Games P, Howell J. 1976. Pairwise Multiple Comparison Procedures with Unequal N's and/or Variances: A Monte Carlo Study. Journal of Educational and Behavioural Statistics **1**(2), 113-125.

Garcia HE, Weathers K, Paver CR, Smolyar I, Boyer AG, Locarcini RA, Zweng MM, Mishonov AV, Baranova OK, Seidov D, Reagan JR. 2018. World Ocean Atlas 2018, Volume 3: Dissolved Oxygen, Apparent Oxygen Utilization, and Oxygen Saturation. A. Mishonov Technical Ed. NOAA Atlas NESDIS 83, 38 pp.

Gates AR, Benfield MC, Booth DJ, Fowler AM, Skropeta D, Jones DOB. 2017. Deep-sea observations at hydrocarbon drilling locations: Contributions from the SERPENT Project after 120 field visits. Deep-Sea Research Part Ii-Topical Studies in Oceanography **137**, 463-479. DOI: 10.1016/j.dsr2.2016.07.011

GEO BON. 2011. Adequacy of Biodiversity Observation Systems to Support the CBD 2020 Targets. Group on Earth Observations Biodiversity Observation Network. http://www.earthobservations.org/documents/cop/bi_geobon/2011_cbd_adequacy_report.pdf.

Gerlach SA, Hahn AE, Schrage M. 1985. Size Spectra of Benthic Biomass and Metabolism. Marine Ecology Progress Series **26**(1-2), 161-173. DOI: 10.3354/meps026161

Gillooly JF, Brown JH, West GB, Savage VM, Charnov EL. 2001. Effects of size and temperature on metabolic rate. Science **293**(5538), 2248-2251. DOI: 10.1126/science.1061967

Glover A, Dahlgren T, Wiklund H, Mohrbeck I, Smith C. 2015. An End-to-End DNA Taxonomy Methodology for Benthic Biodiversity Survey in the Clarion-Clipperton Zone, Central Pacific Abyss. Journal of Marine Science and Engineering **4**(1). DOI: 10.3390/jmse4010002

Glover AG, Wiklund H, Chen C, Dahlgren TG. 2018. Managing a sustainable deep-sea 'blue economy' requires knowledge of what actually lives there. eLife **7**, e41319. DOI: 10.7554/eLife.41319

Godbold JA, Bailey DM, Collins MA, Gordon JDM, Spallek WA, Priede IG. 2013. Putative fishery-induced changes in biomass and population size structures of demersal deep-sea fishes in ICES Sub-area VII, Northeast Atlantic Ocean. Biogeosciences **10**(1), 529-539. DOI: 10.5194/bg-10-529-2013

Godbold JA, Hale R, Wood CL, Solan M. 2017. Vulnerability of macronutrients to the concurrent effects of enhanced temperature and atmospheric pCO2 in representative shelf sea sediment habitats. Biogeochemistry **135**(1-2), 89-102. DOI: 10.1007/s10533-017-0340-y

Gooday AJ, Holzmann M, Caulle C, Goineau A, Kamenskaya O, Weber AAT, Pawlowski J. 2017a. Giant protists (xenophyophores, Foraminifera) are exceptionally diverse in parts of the abyssal eastern Pacific licensed for polymetallic nodule exploration. Biological Conservation **207**, 106-116. DOI: 10.1016/j.biocon.2017.01.006

Gooday AJ, Holzmann M, Caulle C, Goineau A, Jones DOB, Kamenskaya O, Simon-Lledó E, Weber AAT, Pawlowski J. 2017b. New species of the xenophyophore genus *Aschemonella* (Rhizaria: Foraminifera) from areas of the abyssal eastern Pacific licensed for polymetallic nodule exploration. Zoological Journal of the Linnean Society **182**(3), 479-499. DOI: 10.1093/zoolinnean/zlx052

Gooday AJ, Sykes D, Goral T, Zubkov MV, Glover AG. 2018. Micro-CT 3D imaging reveals the internal structure of three abyssal xenophyophore species (Protista, Foraminifera) from the eastern equatorial Pacific Ocean. Scientific Reports **8**(1), 12103. DOI: 10.1038/s41598-018-30186-2

Górska B, Włodarska-Kowalczuk M. 2017. Food and disturbance effects on Arctic benthic biomass and production size spectra. Progress in Oceanography **152**, 50-61. DOI: 10.1016/j.pocean.2017.02.005

Gray A, Elliott J. 2009. Ecology of marine sediments: from science to management. Oxford University Press: Oxford, UK. pp. 225.

Griffiths JR, Kadin M, Nascimento FJA, Tamelander T, Tornroos A, Bonaglia S, Bonsdorff E, Bruchert V, Gardmark A, Jarnstrom M, Kotta J, Lindegren M, Nordstrom MC, Norkko A, Olsson J, Weigel B, Zydelis R, Blenckner T, Niiranen S, Winder M. 2017. The importance of benthic-pelagic coupling for marine ecosystem functioning in a changing world. Global Change Biology **23**(6), 2179-2196. DOI: 10.1111/gcb.13642

"Guest Editors". Introduction/Overview article. Progress in Oceanography, Porcupine Abyssal Plain Special Issue.

Harris P. 2012. Biogeography, benthic ecology, and habitat classification schemes. In: Harris PT and EK Baker (Editors) Seafloor Geomorphology as Benthic Habitat, 1st edition, pp. 61-91. Elsevier: London, UK.

Harris PT, Macmillan-Lawler M, Rupp J, Baker EK. 2014. Geomorphology of the oceans. Marine Geology **352**, 4-24. DOI: 10.1016/j.margeo.2014.01.011

Hartman SE, Larkin KE, Lampitt RS, Lankhorst M, Hydes DJ. 2010. Seasonal and inter-annual biogeochemical variations in the Porcupine Abyssal Plain 2003–2005 associated with winter mixing and surface circulation. Deep Sea Research Part II: Topical Studies in Oceanography **57**(15), 1303-1312. DOI: 10.1016/j.dsr2.2010.01.007

Hartman SE, Lampitt RS, Larkin KE, Pagnani M, Campbell J, Gkritzalis T, Jiang ZP, Pebody CA, Ruhl HA, Gooday AJ, Bett BJ, Billett DSM, Provost P, McLachlan R, Turton JD, Lankester S. 2012. The Porcupine Abyssal Plain fixed-point sustained observatory (PAP-SO): variations and trends from the Northeast Atlantic fixed-point time-series. ICES Journal of Marine Science **69**(5), 776-783. DOI: 10.1093/icesjms/fss077

Hartman S. 2019. RRS Discovery Cruise D103, 21 June-10 July 2019. Water column and seafloor time-series studies at the Porcupine Abyssal Plain Sustained Observatory (Report No. 61). Southampton, UK: National Oceanography Centre. pp. 146.

Hemmingsen AM. 1960. Energy metabolism as related to body size and respiratory surface, and its evolution. Reports of the Steno Memorial Hospital and the Nordisk Insulinlaboratorium. **9**, 1-110.

Henseler C, Nordstrom MC, Tornroos A, Snickars M, Pecuchet L, Lindegren M, Bonsdorff E. 2019. Coastal habitats and their importance for the diversity of benthic communities: A species- and trait-based approach. Estuarine Coastal and Shelf Science **226**, 106272. DOI: 10.1016/j.ecss.2019.106272

Hessler RR, Jumars PA. 1974. Abyssal community analysis from replicate box cores in the central North Pacific. Deep-Sea Research 21, 185-209.

Higgs ND, Gates AR, Jones DO. 2014. Fish food in the deep sea: revisiting the role of large food-falls. PLoS ONE **9**(5), e96016. DOI: 10.1371/journal.pone.0096016

Hillebrand H, Durselen CD, Kirschtel D, Pollingher U, Zohary T. 1999. Biovolume calculation for pelagic and benthic microalgae. Journal of Phycology **35**(2), 403-424. DOI: 10.1046/j.1529-8817.1999.3520403.x

Hiscock K, Langmead O, Warwick R, Smith A. 2005. Identification of seabed indicator species to support implementation of the EU Habitats and Water

Framework Directives. Report to the Joint Nature Conservation Committee and the Environment Agency from the Marine Biological Association. Marine Biological Association: Plymouth, UK. JNCC Contract F90-01-705. pp. 77.

Hosking B. in prep. Classification of benthic megafauna using Convolutional Neural Networks. Progress in Oceanography, Porcupine Abyssal Plain Special Issue.

Hughes JA, Gooday AJ. 2004. Associations between living benthic foraminifera and dead tests of *Syringammina fragilissima* (Xenophyophorea) in the Darwin Mounds region (NE Atlantic). Deep Sea Research Part I: Oceanographic Research Papers **51**(11), 1741-1758. DOI: 10.1016/j.dsr.2004.06.004

Huvenne VA, Tyler PA, Masson DG, Fisher EH, Hauton C, Huhnerbach V, Le Bas TP, Wolff GA. 2011. A picture on the wall: innovative mapping reveals cold-water coral refuge in submarine canyon. PLoS ONE **6**(12), e28755. DOI: 10.1371/journal.pone.0028755

Huvenne VAI. 2016. RRS James Cook Cruise 124-125-126, 09 Aug - 12 Sept, CODEMAP2015 Habitat mapping and ROV vibrocorer trials around Whittard Canyon and Haig Fras (Report No. 36). Southampton, UK: National Oceanography Centre. pp. 223.

Huvenne VAI, Bett BJ, Masson DG, Le Bas TP, Wheeler AJ. 2016. Effectiveness of a deep-sea cold-water coral Marine Protected Area, following eight years of fisheries closure. Biological Conservation **200**, 60-69. DOI: 10.1016/j.biocon.2016.05.030

Huvenne VA, Furlong M. 2019. RRS James Cook Cruise JC166-167, 19 June-6 July 2018. CLASS - Climate-linked Atlantic System Science Haig Fras Marine Conservation Zone AUV habitat monitoring, Equipment trials and staff training (Report No. 56). Southampton, UK: National Oceanography Centre. pp. 152.

ICES. 2008. Report of the Working Group for Regional Ecosystem Description (WGRED), 25–29 February 2008 (Report No. ICES CM 2008/ACOM:47). Copenhagen, Denmark: ICES. pp. 203.

ICES. 2016. ICES Advice 2016, Book 5. Celtic Seas Ecoregion – Ecosystem overview. pp. 16.

Iken K, Brey T, Wand U, Voigt J, Junghans P. 2001. Food web structure of the benthic community at the Porcupine Abyssal Plain (NE Atlantic): a stable isotope analysis. Progress in Oceanography **50**(1-4), 383-405. DOI: 10.1016/S0079-6611(01)00062-3

Isaac NJB, Carbone C, McGill B. 2012. Population and Community Ecology. In: Sibly RM, JH Brown and A Kodric-Brown (Editors) Metabolic Ecology: A Scaling Approach, 1st edition, pp. 77-85. John Wiley & Sons, Ltd.

Iversen MH, Nowald N, Ploug H, Jackson GA, Fischer G. 2010. High resolution profiles of vertical particulate organic matter export off Cape Blanc, Mauritania: Degradation processes and ballasting effects. Deep-Sea Research Part I-Oceanographic Research Papers **57**(6), 771-784. DOI: 10.1016/j.dsr.2010.03.007

Jennings S, Warr KJ, Mackinson S. 2002. Use of size-based production and stable isotope analyses to predict trophic transfer efficiencies and predator-prey body mass ratios in food webs. Marine Ecology Progress Series **240**, 11-20. DOI: 10.3354/meps240011

Jennings S, Melin F, Blanchard JL, Forster RM, Dulvy NK, Wilson RW. 2008. Global-scale predictions of community and ecosystem properties from simple ecological theory. Proceedings of the Royal Society of Biological Sciences **275**(1641), 1375-1383. DOI: 10.1098/rspb.2008.0192

Jetz W, Carbone C, Fulford J, Brown JH. 2004. The scaling of animal space use. Science **306**(5694), 266-268. DOI: 10.1126/science.1102138

Jiménez F, Rodriguez J, Bautista B, Rodriguez V. 1987. Relations between Chlorophyll, Phytoplankton Cell Abundance and Biovolume during a Winter Bloom in Mediterranean Coastal Waters. Journal of Experimental Marine Biology and Ecology **105**(2-3), 161-173. DOI: 10.1016/0022-0981(87)90169-9

Johnson NA, Campbell JW, Moorre TS, Rex MA, Etter RJ, McClain CR, Dowell MD. 2007. The relationship between the standing stock of deep-sea macrobenthos and surface production in the western North Atlantic. Deep-Sea Research Part I-Oceanographic Research Papers **54**(8), 1350-1360. DOI: 10.1016/j.dsr.2007.04.011

Joint Nature Conservation Committee. 2018. Greater Haig Fras MPA. Retrieved from http://archive.jncc.gov.uk/default.aspx?page=7135 (Accessed 24 January 2020).

Jones CG, Lawton JH. 1995. Linking species and ecosystem. Jones CG and JH Lawton (Editors). Springer US: New York, USA.

Jones DOB, Bett BJ, Tyler PA. 2007. Megabenthic ecology of the deep Faroe–Shetland channel: A photographic study. Deep Sea Research Part I: Oceanographic Research Papers **54**(7), 1111-1128. DOI: 10.1016/j.dsr.2007.04.001

Jones DO, Yool A, Wei CL, Henson SA, Ruhl HA, Watson RA, Gehlen M. 2014. Global reductions in seafloor biomass in response to climate change. Global Change Biology **20**(6), 1861-1872. DOI: 10.1111/gcb.12480

Jones DOB. 2015. RRS James Cook Cruise JC120, 15 Apr - 19 May 2015. Manzanillo to Manzanillo, Mexico. Managing Impacts of Deep-seA resource exploitation (MIDAS): Clarion-Clipperton Zone, North Eastern Area of Particular Environmental Interest (Report No. 32). Southampton, UK: National Oceanography Centre. pp. 117.

Jones DO, Kaiser S, Sweetman AK, Smith CR, Ménot L, Vink A, Trueblood D, Greinert J, Billett DS, Arbizu PM, Radziejewska T, Singh R, Ingole B, Stratmann T, Simon-Lledo E, Durden JM, Clark MR. 2017. Biological responses to disturbance from simulated deep-sea polymetallic nodule mining. PLoS ONE **12**(2), e0171750. DOI: 10.1371/journal.pone.0171750

Jones DOB, Gates AR, Huvenne VAI, Phillips AB, Bett BJ. 2019. Autonomous marine environmental monitoring: Application in decommissioned oil fields. Science of the Total Environment **668**, 835-853. DOI: 10.1016/j.scitotenv.2019.02.310

Joydas TV, Qurban MA, Ali SM, Albarau JF, Rabaoui L, Manikandan KP, Ashraf M, Papadopoulos VP, Giacobbe S, Krishnakumar PK. 2018. Macrobenthic community structure in the deep waters of the Red Sea. Deep-Sea Research Part I-Oceanographic Research Papers **137**, 38-56. DOI: 10.1016/j.dsr.2018.05.004

Jung J, Nakajima M, Kojima M, Ooe K, Fukuda T. 2012. Microchip device for measurement of body volume of C. elegans as bioindicator application. Journal of Micro-Nano Mechatronics **7**(1-3), 3-11. DOI: 10.1007/s12213-011-0036-7

Kamenskaya OE, Gooday AJ, Tendal OS, Melnik VF. 2015. Xenophyophores (Protista, Foraminifera) from the Clarion-Clipperton Fracture Zone with description of three new species. Marine Biodiversity **45**(3), 581-593. DOI: 10.1007/s12526-015-0330-z

Kamenskaya OE, Gooday AJ, Tendal OS, Melnik VF. 2016. Xenophyophores (Rhizaria, Foraminifera) from the Russian license area of the Clarion-Clipperton Zone (eastern equatorial Pacific), with the description of three new species. Marine Biodiversity **47**(2), 299-306. DOI: 10.1007/s12526-016-0595-x

Kelly-Gerreyn BA, Martin AP, Bett BJ, Anderson TR, Kaariainen JI, Main CE, Marcinko CJ, Yool A. 2014. Benthic biomass size spectra in shelf and deep-sea sediments. Biogeosciences **11**(22), 6401-6416. DOI: 10.5194/bg-11-6401-2014

Kimmerer W, Avent SR, Bollens SM, Feyrer F, Grimaldo LF, Moyle PB, Nobriga M, Visintainer T. 2005. Variability in Length–Weight Relationships Used to Estimate Biomass of Estuarine Fish from Survey Data. Transactions of the American Fisheries Society **134**(2), 481-495. DOI: 10.1577/t04-042.1

Kissling WD, Walls R, Bowser A, Jones MO, Kattge J, Agosti D, Amengual J, Basset A, van Bodegom PM, Cornelissen JHC, Denny EG, Deudero S, Egloff W, Elmendorf SC, Alonso Garcia E, Jones KD, Jones OR, Lavorel S, Lear D, Navarro LM, Pawar S, Pirzl R, Ruger N, Sal S, Salguero-Gomez R, Schigel D, Schulz KS, Skidmore A, Guralnick RP. 2018. Towards global data products of Essential Biodiversity Variables on species traits. Nature Ecology & Evolution **2**(10), 1531-1540. DOI: 10.1038/s41559-018-0667-3

Kooijman SALM. 2000. Dynamic Energy and Mass Budgets in Biological Systems. Cambridge University Press: Cambridge, pp. 424.

Labra FA, Hernandez-Miranda E, Quinones RA. 2015. Dynamic relationships between body size, species richness, abundance, and energy use in a shallow marine epibenthic faunal community. Ecology and Evolution **5**(2), 391-408. DOI: 10.1002/ece3.1343

Laguionie Marchais C, Bett BJ, Paterson GLJ, Smith KL, Ruhl HA. 2020. Using metabolic theory to assess structure and function in the deep-sea benthos, including microbial and metazoan dominance. Deep Sea Research Part II: Topical Studies in Oceanography **173**. DOI: 10.1016/j.dsr2.2020.104762

Lalli C, Parsons TR. 1997. Biological Oceanography: An Introduction. Butterworth-Heinemann. pp. 320.

Lampert W. 1984. The measurement of respiration. In: Downing JA and FH Rigler (Editors) A manual on methods for the assessment of secondary productivity in fresh waters, 2nd edition, pp. 413–468. Blackwell: Oxford, UK.

Lampitt RS, Billett DSM, Rice AL. 1986. Biomass of the Invertebrate Megabenthos from 500 to 4100-M in the Northeast Atlantic-Ocean. Marine Biology **93**(1), 69-81. DOI: 10.1007/Bf00428656

Lampitt RS, Bett BJ, Kiriakoulakis K, Popova EE, Ragueneau O, Vangriesheim A, Wolff G. 2001. Material supply to the abyssal seafloor in the Northeast Atlantic. Progress in Oceanography **50**, 27-63.

Lampitt RS, Billett DSM, Martin AP. 2010a. The sustained observatory over the Porcupine Abyssal Plain (PAP): Insights from time series observations and process studies Preface. Deep-Sea Research Part Ii-Topical Studies in Oceanography **57**(15), 1267-1271. DOI: 10.1016/j.dsr2.2010.01.003

Lampitt RS, Salter I, de Cuevas BA, Hartman S, Larkin KE, Pebody CA. 2010b. Long-term variability of downward particle flux in the deep northeast Atlantic: Causes and trends. Deep Sea Research Part II: Topical Studies in Oceanography **57**(15), 1346-1361. DOI: 10.1016/j.dsr2.2010.01.011

Lampitt RS. 2017a. RV Meteor Cruise 108, 06-24 Jul 2014. Cruise to the Porcupine Abyssal Plain sustained observatory (Report No. 42). Southampton, UK: National Oceanography Centre. pp. 127.

Lampitt RS. 2017b. RRS Discovery Cruise DY032, 20 Jun - 07 Jul 2015. Cruise to the Porcupine Abyssal Plain sustained observatory (Report No. 43). Southampton, UK: National Oceanography Centre. pp. 143.

Lampitt RS. 2017c. RRS Discovery Cruise DY077, 14 Apr-01 May 2017. Cruise to the Porcupine Abyssal Plain sustained observatory (Report No. 46). Southampton, UK: National Oceanography Centre. pp. 193.

Langenkämper D, Zurowietz M, Schoening T, Nattkemper TW. 2017. BIIGLE 2.0 - Browsing and Annotating Large Marine Image Collections. Frontiers in Marine Science **4**(83). DOI: 10.3389/fmars.2017.00083

Langenkämper D, Nattkemper TW. 2017. COATL - A learning architecture for online real-time detection and classification assistance for environmental data, in. Proceedings of the Proceedings of the 23rd International Conference on Pattern Recognition, ICPR, Cancún, México. 597–602 pp.

Laureillard J, Mejanelle L, Sibuet M. 2004. Use of lipids to study the trophic ecology of deep-sea xenophyophores. Marine Ecology Progress Series **270**, 129-140. DOI: 10.3354/meps270129

Law R, Plank MJ, Kolding J. 2012. On balanced exploitation of marine ecosystems: results from dynamic size spectra. ICES Journal of Marine Science **69**(4), 602-614. DOI: 10.1093/icesjms/fss031

Lawton JH. 1999. Are there general laws in ecology? Oikos **84**(117-192).

Legendre P. 1993. Spatial Autocorrelation - Trouble or New Paradigm. Ecology **74**(6), 1659-1673. DOI: 10.2307/1939924

Legendre P, Legendre L. 1998. Numerical ecology. In Developments in Environmental Modelling. Elsevier: Amsterdam. pp. 1006.

Legendre P. 2018. lmodel2: Model II Regression. R package version 1.7-3. Retrieved from https://CRAN.R-project.org/package=lmodel2).

Levin LA, Gooday AJ. 1992. Possible Roles for Xenophyophores in Deep-Sea Carbon Cycling. In: Rowe GT and V Pariente (Editors) Deep-Sea Food Chains and the Global Carbon Cycle, pp. 93-104. (Volume 360). Springer: Dordrecht, Netherlands.

Levin LA, Bett BJ, Gates AR, Heimbach P, Howe BM, Janssen F, McCurdy A, Ruhl HA, Snelgrove P, Stocks KI, Bailey D, Baumann-Pickering S, Beaverson C, Benfield MC, Booth DJ, Carreiro-Silva M, Colaco A, Eble MC, Fowler AM, Gjerde KM, Jones DOB, Katsumata K, Kelley D, Le Bris N, Leonardi AP, Lejzerowicz F, Macreadie PI, McLean D, Meitz F, Morato T, Netburn A, Pawlowski J, Smith CR, Sun S, Uchida H, Vardaro MF, Venkatesan R, Weller RA. 2019. Global Observing Needs in the Deep Ocean. Frontiers in Marine Science **6**, 241. DOI: 10.3389/fmars.2019.00241

Lewis HM, Law R, McKane AJ. 2008. Abundance-body size relationships: the roles of metabolism and population dynamics. Journal of Animal Ecology **77**(5), 1056-1062. DOI: 10.1111/j.1365-2656.2008.01405.x

Lewis LS, Smith JE, Eynaud Y. 2018. Comparative metabolic ecology of tropical herbivorous echinoids on a coral reef. PLoS ONE **13**(1), e0190470. DOI: 10.1371/journal.pone.0190470

Lindstrom E, Gunn J, Fischer A, McCurdy A, Glover L. 2012. A Framework for Ocean Observing. By the Task Team for an Integrated Framework for Sustained Ocean Observing. UNESCO. IOC/INF-1284. Paris, France.

Locarcini RA, Mishonov AV, Baranova OK, Boyer TP, Zweng MM, Garcia HE, Reagan JR, Seidov D, Weathers K, Paver CR, Smolyar I. 2018. World Ocean Atlas 2018, Volume 1: Temperature. A. Mishonov Technical Ed. NOAA Atlas NESDIS 81, 52 pp.

Lodge M, Johnson D, Le Gurun G, Wengler M, Weaver P, Gunn V. 2014. Seabed mining: International Seabed Authority environmental management plan for the Clarion–Clipperton Zone. A partnership approach. Marine Policy **49**, 66-72. DOI: 10.1016/j.marpol.2014.04.006

Luisetti T, Turner RK, Andrews JE, Jickells TD, Kröger S, Diesing M, Paltriguera L, Johnson MT, Parker ER, Bakker DCE, Weston K. 2019. Quantifying and valuing carbon flows and stores in coastal and shelf ecosystems in the UK. Ecosystem Services **35**, 67-76. DOI: 10.1016/j.ecoser.2018.10.013

Lutz MJ, Caldeira K, Dunbar RB, Behrenfeld MJ. 2007. Seasonal rhythms of net primary production and particulate organic carbon flux to depth describe the efficiency of biological pump in the global ocean. Journal of Geophysical Research-Oceans **112**, 26. DOI: 10.1029/2006jc003706

Magurran AE. 2004. Measuring Biological Diversity. Wiley-Blackwell, pp. 256.

Maino JL, Kearney MR, Nisbet RM, Kooijman SA. 2014. Reconciling theories for metabolic scaling. Journal of Animal Ecology **83**(1), 20-29. DOI: 10.1111/1365-2656.12085

Mahé K, Bellamy E, Delpech JP, Lazard C, Salaun M, Vérin Y, Coppin F, Travers-Trolet M. 2016. Evidence of a relationship between weight and

total length of marine fish in the North-eastern Atlantic Ocean: physiological, spatial and temporal variations. Journal of the Marine Biological Association of the United Kingdom **98**(3), 617-625. DOI: 10.1017/s0025315416001752

Mare MF. 1942. A study of a marine benthic community with special reference to the micro-organisms. Journal of the Marine Biological Association of the United Kingdom **25**(3), 517-554.

Marsay CM, Sanders RJ, Henson SA, Pabortsava K, Achterberg EP, Lampitt RS. 2015. Attenuation of sinking particulate organic carbon flux through the mesopelagic ocean. Proceedings of the National Academy of Sciences of the United States of America **112**(4), 1089-1094. DOI: 10.1073/pnas.1415311112

Martin JH, Knauer GA, Karl DM, Broenkow WW. 1987. Vertex - Carbon Cycling in the Northeast Pacific. Deep-Sea Research Part a-Oceanographic Research Papers **34**(2), 267-285. DOI: 10.1016/0198-0149(87)90086-0

Marzinelli EM, Williams SB, Babcock RC, Barrett NS, Johnson CR, Jordan A, Kendrick GA, Pizarro OR, Smale DA, Steinberg PD. 2015. Large-scale geographic variation in distribution and abundance of Australian deep-water kelp forests. PLoS ONE **10**(2), e0118390. DOI: 10.1371/journal.pone.0118390

Maximenko N, Corradi P, Law KL, Van Sebille E, Garaba SP, Lampitt RS, Galgani F, Martinez-Vicente V, Goddijn-Murphy L, Veiga JM, Thompson RC, Maes C, Moller D, Löscher CR, Addamo AM, Lamson MR, Centurioni LR, Posth NR, Lumpkin R, Vinci M, Martins AM, Pieper CD, Isobe A, Hanke G, Edwards M, Chubarenko IP, Rodriguez E, Aliani S, Arias M, Asner GP, Brosich A, Carlton JT, Chao Y, Cook A-M, Cundy AB, Galloway TS, Giorgetti A, Goni GJ, Guichoux Y, Haram LE, Hardesty BD, Holdsworth N, Lebreton L, Leslie HA, Macadam-Somer I, Mace T, Manuel M, Marsh R, Martinez E, Mayor DJ, Le Moigne M, Molina Jack ME, Mowlem MC, Obbard RW, Pabortsava K, Robberson B, Rotaru A-E, Ruiz GM, Spedicato MT, Thiel M, Turra A, Wilcox C. 2019. Toward the Integrated Marine Debris Observing System. Frontiers in Marine Science **6**. DOI: 10.3389/fmars.2019.00447

Mazurkiewicz M, Górska B, Jankowska E, Włodarska-Kowalczuk M. 2016. Assessment of nematode biomass in marine sediments: A semi-automated image analysis method. Limnology and Oceanography-Methods **14**(12), 816-827. DOI: 10.1002/lom3.10128

McClain CR. 2004. Connecting species richness, abundance and body size in deep-sea gastropods. Global Ecology and Biogeography **13**(4), 327-334. DOI: 10.1111/j.1466-822X.2004.00106.x

McClain CR, Boyer AG. 2009. Biodiversity and body size are linked across metazoans. Proceedings of the Roayl Society of Biological Sciences **276**(1665), 2209-2215. DOI: 10.1098/rspb.2009.0245

McClain CR, Allen AP, Tittensor DP, Rex MA. 2012. Energetics of life on the deep seafloor. Proceedings of the National Academy of Sciences of the United States of America **109**(38), 15366-15371. DOI: 10.1073/pnas.1208976109

McCully SR, Scott F, Ellis JR. 2012. Lengths at maturity and conversion factors for skates (Rajidae) around the British Isles, with an analysis of data in the literature. ICES Journal of Marine Science **69**(10), 1812-1822. DOI: 10.1093/icesjms/fss150

McIntyre A. 1956. The use of trawl, grab and camera in estimating marine benthos. Journal of the Marine Biological Association of the United Kingdom **35**, 419-429.

McPhail S, Furlong M, Pebody M, Perret J, Stevenson J, Webb A, White D. 2009. Exploring beneath the PIG Ice Shelf with the Autosub3 AUV in. Proceedings of the OCEANS 2009-EUROPE: Bergen, Germany, 8 pp.

Méthot G, Hudon C, Gagnon P, Pinel-Alloul B, Armellin A, Poirier A-MT. 2012. Macroinvertebrate size–mass relationships: how specific should they be? Freshwater Science **31**(3), 750-764. DOI: 10.1899/11-120.1

Meyer E. 1989. The Relationship between Body Length Parameters and Dry Mass in Running Water Invertebrates. Archiv für Hydrobiologie **117**(2), 191-203.

Milligan RJ. 2015. Natural and anthropogenic drivers of deep-sea fish populations. Ph.D. thesis (pp. 312), University of Glasgow.

Milligan RJ, Morris KJ, Bett BJ, Durden JM, Jones DO, Robert K, Ruhl HA, Bailey DM. 2016. High resolution study of the spatial distributions of abyssal fishes by autonomous underwater vehicle. Scientific Reports **6**, 26095. DOI: 10.1038/srep26095

Miloslavich P, Bax NJ, Simmons SE, Klein E, Appeltans W, Aburto-Oropeza O, Andersen Garcia M, Batten SD, Benedetti-Cecchi L, Checkley DM, Jr., Chiba S, Duffy JE, Dunn DC, Fischer A, Gunn J, Kudela R, Marsac F, Muller-Karger FE, Obura D, Shin YJ. 2018. Essential ocean variables for global sustained observations of biodiversity and ecosystem changes. Global Change Biology **24**, 1354-1013. DOI: 10.1111/gcb.14108

Minitab. 2013. Multiple Regression Analysis: Use Adjusted R-Squared and Predicted R-Squared to Include the Correct Number of Variables. Retrieved from http://blog.minitab.com/blog/adventures-in-statistics-2/multiple-regession-analysis-use-adjusted-r-squared-and-predicted-r-squared-to-include-the-correct-number-of-variables (Accessed 25 Sept. 2017).

Monk J, Barrett N, Bridge T, Carroll A, Friedman A, Ierodiaconou D, Jordan A, Kendrick G, Lucieer V. 2018. Marine sampling field manual for autonomous underwater vehicles (AUVs). In: Przeslawski R and S Foster (Editors) In Field Manuals for Marine Sampling to Monitor Australian Waters, pp. 65-81.

Moore BT, Jordan JM, Baugh LR. 2013. WormSizer: high-throughput analysis of nematode size and shape. PLoS ONE **8**(2), e57142. DOI: 10.1371/journal.pone.0057142

Morris KJ, Bett BJ, Durden JM, Huvenne VAI, Milligan R, Jones DOB, McPhail S, Robert K, Bailey DM, Ruhl HA. 2014. A new method for ecological surveying of the abyss using autonomous underwater vehicle photography. Limnology and Oceanography-Methods **12**(11), 795-809. DOI: 10.4319/lom.2014.12.795

Morris KJ, Bett BJ, Durden JM, Benoist NM, Huvenne VA, Jones DO, Robert K, Ichino MC, Wolff GA, Ruhl HA. 2016. Landscape-scale spatial heterogeneity in phytodetrital cover and megafauna biomass in the abyss links to modest topographic variation. Scientific Reports **6**, 34080. DOI: 10.1038/srep34080

Muller-Karger FE, Miloslavich P, Bax NJ, Simmons S, Costello MJ, Pinto IS, Canonico G, Turner W, Gill M, Montes E, Best BD, Pearlman J, Halpin P, Dunn D, Benson A, Martin CS, Weatherdon LV, Appeltans W, Provoost P, Klein E, Kelble CR, Miller RJ, Chavez FP, Iken K, Chiba S, Obura D, Navarro LM, Pereira HM, Allain V, Batten S, Benedetti-Checchi L, Duffy JE, Kudela RM, Rebelo LM, Shin Y, Geller G. 2018. Advancing Marine Biological Observations and Data Requirements of the Complementary Essential Ocean Variables (EOVs) and Essential Biodiversity Variables (EBVs) Frameworks. Frontiers in Marine Science **5**. DOI: 10.3389/fmars.2018.00211

Mustard AT, Anderson TR. 2005. Use of spherical and spheroidal models to calculate zooplankton biovolume from particle equivalent spherical diameter as measured by an optical plankton counter. Limnology and Oceanography-Methods **3**, 183-189. DOI: 10.4319/lom.2005.3.183

Narayanaswamy BE, Bett BJ, Lamont PA, Rowden AA, Bell EM, Ménot L. 2016. Corers and Grabs. In: Clark MR, M Consalvey and AA Rowden (Editors) Biological Sampling in the Deep Sea, pp. 207-227. Wiley-Blackwell: Hoboken, New Jersey.

Newman MEJ. 2005. Power laws, Pareto distributions and Zipf's law. Contemporary Physics **46**(5), 323-351. DOI: 10.1080/00107510500052444

Novack-Gottshall PM. 2008. Using simple body-size metrics to estimate fossil body volume: Empirical validation using diverse paleozoic invertebrates. Palaios **23**(3-4), 163-173. DOI: 10.2110/palo.2007.p07-017r

Nussbaum BD, Gilbert RO. 2001. Editorial: Special issue on composite sampling. Environmental and Ecological Statistics **8**(2), 89-90. DOI: 10.1023/A:1011337029268

Odum EP, Barrett GW. 2005. Fundamentals of Ecology. Thomson Brooks / Cole: Belmont.

Olds AD, Connolly RM, Pitt KA, Pittman SJ, Maxwell PS, Huijbers CM, Moore BR, Albert S, Rissik D, Babcock RC, Schlacher TA. 2016. Quantifying the conservation value of seascape connectivity: a global synthesis. Global Ecology and Biogeography **25**(1), 3-15. DOI: 10.1111/geb.12388

Pereira HM, Ferrier S, Walters M, Geller GN, Jongman RH, Scholes RJ, Bruford MW, Brummitt N, Butchart SH, Cardoso AC, Coops NC, Dulloo E, Faith DP, Freyhof J, Gregory RD, Heip C, Hoft R, Hurtt G, Jetz W, Karp DS, McGeoch MA, Obura D, Onoda Y, Pettorelli N, Reyers B, Sayre R, Scharlemann JP, Stuart SN, Turak E, Walpole M, Wegmann M. 2013. Ecology. Essential biodiversity variables. Science **339**(6117), 277-278. DOI: 10.1126/science.1229931

Perkins NR, Foster SD, Hill NA, Marzloff MP, Barrett NS. 2017. Temporal and spatial variability in the cover of deep reef species: Implications for

monitoring. Ecological Indicators **77**, 337-347. DOI: 10.1016/j.ecolind.2017.02.030

Pershing AJ, Christensen LB, Record NR, Sherwood GD, Stetson PB. 2010. The impact of whaling on the ocean carbon cycle: why bigger was better. PLoS ONE **5**(8), e12444. DOI: 10.1371/journal.pone.0012444

Petchey OL, Belgrano A. 2010. Body-size distributions and size-spectra: universal indicators of ecological status? Biology Letters **6**(4), 434-437. DOI: 10.1098/rsbl.2010.0240

Peters RH. 1983. The Ecological Implications of Body Size. Cambridge University Press. pp. 333.

Pihl L. 1985. Food Selection and Consumption of Mobile Epibenthic Fauna in Shallow Marine Areas. Marine Ecology Progress Series **22**(2), 169-179. DOI: 10.3354/meps022169

Pineda J, Cho W, Starczak V, Govindarajan AF, Guzman HM, Girdhar Y, Holleman RC, Churchill J, Singh H, Ralston DK. 2016. A crab swarm at an ecological hotspot: patchiness and population density from AUV observations at a coastal, tropical seamount. PeerJ **4**, e1770. DOI: 10.7717/peerj.1770

Post AL, Beaman RJ, O'Brien PE, Eleaume M, Riddle MJ. 2011. Community structure and benthic habitats across the George V Shelf, East Antarctica: Trends through space and time. Deep-Sea Research Part Ii-Topical Studies in Oceanography **58**(1-2), 105-118. DOI: 10.1016/j.dsr2.2010.05.020

Primavera JH, Parado-Estepa FD, Lebata JL. 1998. Morphometric relationship of length and weight of giant tiger prawn Penaeus monodon according to life stage, sex and source. Aquaculture **164**(1-4), 67-75. DOI: 10.1016/S0044-8486(98)00177-X

R Core Team. 2016. "R: A Language and Environment for Statistical Computing." In. R Foundation for Statistical Computing, Vienna, Austria.

Radziejewska T. 2014. Characteristics of the Sub-equatorial North-Eastern Pacific Ocean's Abyss, with a Particular Reference to the Clarion-Clipperton Fracture Zone. In: SpringerBriefs (Editor) Meiobenthos in the Sub-equatorial Pacific Abyss, pp. 13-28. Springer-Verlag Berlin Heidelberg.

Raffaelli D, Bell E, Weithoff G, Matsumoto A, Cruz-Motta JJ, Kershaw P, Parker R, Parry D, Jones M. 2003. The ups and downs of benthic ecology: considerations of scale, heterogeneity and surveillance for benthic–pelagic coupling. Journal of Experimental Marine Biology and Ecology **285-286**, 191-203. DOI: 10.1016/s0022-0981(02)00527-0

Rees HL, Pendle MA, Waldcock R, Limpenny DS, Boyd SE. 1999. A comparison of benthic biodiversity in the North Sea, English Channel, and Celtic Seas. ICES Journal of Marine Science **56**(2), 228-246. DOI: 10.1006/jmsc.1998.0438

Rees SE, Austen MC, Attrill MJ, Rodwell LD. 2012. Incorporating indirect ecosystem services into marine protected area planning and management. International Journal of Biodiversity Science, Ecosystem

Services & Management **8**(3), 273-285. DOI: 10.1080/21513732.2012.680500

Reynoldson TB, Metcalfe-Smith JL. 1992. An overview of the assessment of aquatic ecosystem health using benthic invertebrates. Journal of Aquatic Ecosystem Health **1**(4), 295-308. DOI: 10.1007/bf00044171

Rice AL, Thurston MH, Bett BJ. 1994. The Iosdl Deepseas Program - Introduction and Photographic Evidence for the Presence and Absence of a Seasonal Input of Phytodetritus at Contrasting Abyssal Sites in the Northeastern Atlantic. Deep-Sea Research Part I-Oceanographic Research Papers **41**(9), 1305-1320. DOI: 10.1016/0967-0637(94)90099-X

Richardson AJ, Lamberts C, Isaacs G, Moloney CL, Gibbons MJ. 2000. Length-Weight Relationships of Some Important Forage Crustaceans from South Africa. Naga, The ICLARM Quarterly **23**(2), 29-33.

Robinson CJ, Anislado V, Lopez A. 2004. The pelagic red crab (Pleuroncodes planipes) related to active upwelling sites in the California Current off the west coast of Baja California. Deep-Sea Research Part II-Topical Studies in Oceanography **51**(6-9), 753-766. DOI: 10.1016/j.dsr2.2004.05.018

Robinson LA, Greenstreet SPR, Reiss H, Callaway R, Craeymeersch J, de Boois I, Degraer S, Ehrich S, Fraser HM, Goffin A, Kröncke I, Jorgenson LL, Robertson MR, Lancaster J. 2010. Length–weight relationships of 216 North Sea benthic invertebrates and fish. Journal of the Marine Biological Association of the United Kingdom **90**(1), 95-104. DOI: 10.1017/s0025315409991408

Rowe GT, Wei C, Nunnally C, Haedrich R, Montagna P, Baguley JG, Bernhard JM, Wicksten M, Ammons A, Briones EE, Soliman Y, Deming JW. 2008. Comparative biomass structure and estimated carbon flow in food webs in the deep Gulf of Mexico. Deep Sea Research Part II: Topical Studies in Oceanography **55**(24-26), 2699-2711. DOI: 10.1016/j.dsr2.2008.07.020

Ruhl HA. 2013. RRS Discovery Cruise 377 & 378, 05-27 Jul 2012, Southampton to Southampton. Autonomous ecological surveying of the abyss: understanding mesoscale spatial heterogeneity at the Porcupine Abyssal Plain (Report No. 23). Southampton, UK: National Oceanography Centre. pp. 73.

Ruhl HA. 2016. RRS Discovery Cruise DY034, 06 Aug-02 Sep 2015, Southampton to Southampton. Shelf sea biogeochemistry (Report No. 39). Southampton, UK: National Oceanography Centre. pp. 121.

Ruhl HA. 2019. RRS James Cook Cruise JC165, 19 May-12 June 2018. Water column and seafloor time-series studies at the Porcupine Abyssal Plain Sustained Observatory (Report No. 57). Southampton, UK: National Oceanography Centre. pp. 158.

Rutterford LA, Simpson SD, Jennings S, Johnson MP, Blanchard JL, Schoen PJ, Sims DW, Tinker J, Genner MJ. 2015. Future fish distributions constrained by depth in warming seas. Nature Climate Change **5**(6), 569-+. DOI: 10.1038/nclimate2607

Salas F, Marcos C, Neto JM, Patrício J, Pérez-Ruzafa A, Marques JC. 2006. User-friendly guide for using benthic ecological indicators in coastal and

marine quality assessment. Ocean & Coastal Management **49**(5-6), 308-331. DOI: 10.1016/j.ocecoaman.2006.03.001

Sanders H. 1968. Marine benthic diversity: a comparative study. The American Naturalist **102**, 243-282.

Savage VM, Gillooly JF, Brown JH, Charnov EL. 2004a. Effects of body size and temperature on population growth. American Naturalist **163**(3), 429-441. DOI: 10.1086/381872

Savage VM, Gillooly JF, Woodruff WH, West GB, Allen AP, Enquist BJ, Brown JH. 2004b. The predominance of quarter-power scaling in biology. Functional Ecology **18**(2), 257-282. DOI: 10.1111/j.0269-8463.2004.00856.x

Savage VM, West GB. 2006. Biological Scaling and Physiological Time: Biomedical Applications. In: T.S. D and K J.Y. (Editors) Complex Systems Science in Biomedicine. Topics in Biomedical Engineering International Book Series, pp. 141-163. Springer: Boston, Massachusetts.

Schmitz OJ, Raymond PA, Estes JA, Kurz WA, Holtgrieve GW, Ritchie ME, Schindler DE, Spivak AC, Wilson RW, Bradford MA, Christensen V, Deegan L, Smetacek V, Vanni MJ, Wilmers CC. 2013. Animating the Carbon Cycle. Ecosystems **17**(2), 344-359. DOI: 10.1007/s10021-013-9715-7

Schneck F, Melo AS. 2010. Reliable sample sizes for estimating similarity among macroinvertebrate assemblages in tropical streams. Annales De Limnologie-International Journal of Limnology **46**(2), 93-100. DOI: 10.1051/limn/2010013

Schoening T, Bergmann M, Ontrup J, Taylor J, Dannheim J, Gutt J, Purser A, Nattkemper TW. 2012. Semi-automated image analysis for the assessment of megafaunal densities at the Arctic deep-sea observatory HAUSGARTEN. PLoS ONE **7**(6), e38179. DOI: 10.1371/journal.pone.0038179

Schoening T, Kuhn T, Jones DOB, Simon-Lledo E, Nattkemper TW. 2016. Fully automated image segmentation for benthic resource assessment of poly-metallic nodules. Methods in Oceanography **15-16**, 78-89. DOI: 10.1016/j.mio.2016.04.002

Schoening T, Jones DOB, Greinert J. 2017. Compact-Morphology-based poly-metallic Nodule Delineation. Scientific Reports **7**(1), 13338. DOI: 10.1038/s41598-017-13335-x

Schramski JR, Dell AI, Grady JM, Sibly RM, Brown JH. 2015. Metabolic theory predicts whole-ecosystem properties. Proceedings of the National Academy of Sciences of the United States of America **112**(8), 2617-2622. DOI: 10.1073/pnas.1423502112

Schwinghamer P. 1981. Characteristic Size Distributions of Integral Benthic Communities. Canadian Journal of Fisheries and Aquatic Sciences **38**(10), 1255-1263. DOI: 10.1139/f81-167

Schwinghamer P. 1983. Generating Ecological Hypotheses from Biomass Spectra Using Causal-Analysis - a Benthic Example. Marine Ecology Progress Series **13**(2-3), 151-166. DOI: 10.3354/meps013151

Schwinghamer P. 1985. Observations on size-structure and pelagic coupling of some shelf and abyssal benthic communities, in Gibbs P (Ed.). Proceedings of the 19th European Marine Biology Symposium, Plymouth, UK, 16-21 September 1984. 347-360 pp.

Schwinghamer P. 1988. Influence of Pollution Along a Natural Gradient and in a Mesocosm Experiment on Biomass-Size Spectra of Benthic Communities. Marine Ecology Progress Series **46**(1-3), 199-206. DOI: 10.3354/meps046199

Seguro I, Marca AD, Painting SJ, Shutler JD, Suggett DJ, Kaiser J. 2019. High-resolution net and gross biological production during a Celtic Sea spring bloom. Progress in Oceanography **177**. DOI: 10.1016/j.pocean.2017.12.003

Seibel BA, Drazen JC. 2007. The rate of metabolism in marine animals: environmental constraints, ecological demands and energetic opportunities. Philosophical Transactions of the Royal Society B **362**(1487), 2061-2078. DOI: 10.1098/rstb.2007.2101

Sewall BJ, Freestone AL, Hawes JE, Andriamanarina E. 2013. Size-energy relationships in ecological communities. PLoS ONE **8**(8), e68657. DOI: 10.1371/journal.pone.0068657

Sharples J, Holligan PM. 2006. Interdisciplinary studies in the Celtic Seas (19,E). In: Robinson AR and KH Brink (Editors) The Sea - The Global Coastal Ocean: Interdisciplinary Regional Studies and Syntheses, Part 2, pp. 1003-1031. Volume 14, Part B). Cambridge, MA.

Sheldon RW, Parsons TR. 1967. A continuous size spectrum for particulate matter in the sea. Journal of the Fisheries Research Board of Canada **24**, 900-925. DOI: 10.1139/f67-081

Sheldon RW, Prakash A, Sutfcliffe WH. 1972. The Size Distribution of Particles in the Ocean. Limnology and Oceanography **17**(3), 327-340.

Silva JF, Ellis JR, Ayers RA. 2013. Length-weight relationships of marine fish collected from around the British Isles. Science Series Technical Report no. 150. Cefas, Lowestoft. pp. 109.

Simon-Lledó E, Bett BJ, Huvenne VAI, Schoening T, Benoist NMA, Jeffreys RM, Durden JM, Jones DOB. 2019a. Megafaunal variation in the abyssal landscape of the Clarion Clipperton Zone. Progress in Oceanography **170**, 119-133. DOI: 10.1016/j.pocean.2018.11.003

Simon-Lledó E, Bett BJ, Huvenne VAI, Schoening T, Benoist NMA, Jones DOB. 2019b. Ecology of a polymetallic nodule occurrence gradient: Implications for deep-sea mining. Limnology and Oceanography **64**(5), 1883-1894. DOI: 10.1002/lno.11157

Simon-Lledó E, Bett BJ, Huvenne VAI, Koser K, Schoening T, Greinert J, Jones DOB. 2019c. Biological effects 26 years after simulated deep-sea mining. Scientific Reports **9**(1), 8040. DOI: 10.1038/s41598-019-44492-w

Simon-Lledó E, Thompson S, Yool A, Flynn A, Pomee C, Parianos J, Jones DOB. 2019d. Preliminary Observations of the Abyssal Megafauna of Kiribati. Frontiers in Marine Science **6**. DOI: 10.3389/fmars.2019.00605

Smith KJL, Kaufmann RS, Baldwin RJ, Carlucci AF. 2001. Pelagic—benthic coupling in the abyssal eastern North Pacific: An 8-year time-series study of food supply and demand. Limnology and Oceanography **46**(3), 543-556. DOI: 10.4319/lo.2001.46.3.0543

Smith KL, Jr., Ruhl HA, Kahru M, Huffard CL, Sherman AD. 2013. Deep ocean communities impacted by changing climate over 24 y in the abyssal northeast Pacific Ocean. Proceedings of the National Academy of Sciences of the United States of America **110**(49), 19838-19841. DOI: 10.1073/pnas.1315447110

Smith KL, Huffard CL, Sherman AD, Ruhl HA. 2016. Decadal Change in Sediment Community Oxygen Consumption in the Abyssal Northeast Pacific. Aquatic Geochemistry **22**(5-6), 401-417. DOI: 10.1007/s10498-016-9293-3

Smith-Godfrey S. 2016. Defining the Blue Economy. Maritime Affairs: Journal of the National Maritime Foundation of India **12**(1), 58-64. DOI:: 10.1080/09733159.2016.1175131

Sousa T, Domingos T, Poggiale JC, Kooijman SA. 2010. Dynamic energy budget theory restores coherence in biology. Philosophical Transactions of the Royal Society Biological Sciences **365**(1557), 3413-3428. DOI: 10.1098/rstb.2010.0166

Stein A, Gerstner K, Kreft H. 2014. Environmental heterogeneity as a universal driver of species richness across taxa, biomes and spatial scales. Ecology Letters **17**(7), 866-880. DOI: 10.1111/ele.12277

Stinchcombe M. 2017. RRS Discovery Cruise DY050, 18 Apr - 08 May 2016. Cruise to the Porcupine Abyssal Plain sustained observatory (Report No. 45). Southampton, UK: National Oceanography Centre. pp. 189.

Stoffels RJ, Karbe S, Paterson RA. 2003. Length-mass models for some common New Zealand littoral-benthic macroinvertebrates, with a note on within-taxon variability in parameter values among published models. New Zealand Journal of Marine and Freshwater Research **37**(2), 449-460. DOI: 10.1080/00288330.2003.9517179

Stratmann T, Lins L, Purser A, Marcon Y, Rodrigues CF, Ravara A, Cunha MR, Simon-Lledo E, Jones DOB, Sweetman AK, Koser K, van Oevelen D. 2018. Abyssal plain faunal carbon flows remain depressed 26 years after a simulated deep-sea mining disturbance. Biogeosciences **15**(13), 4131-4145. DOI: 10.5194/bg-15-4131-2018

Sun J, Liu DY. 2003. Geometric models for calculating cell biovolume and surface area for phytoplankton. Journal of Plankton Research **25**(11), 1331-1346. DOI: 10.1093/plankt/fbg096

Tamburello N, Cote IM, Dulvy NK. 2015. Energy and the Scaling of Animal Space Use. American Naturalist **186**(2), 196-211. DOI: 10.1086/682070

Thompson CEL, Silburn B, Williams ME, Hull T, Sivyer D, Amoudry LO, Widdicombe S, Ingels J, Carnovale G, McNeill CL, Hale R, Marchais CL, Hicks N, Smith HEK, Klar JK, Hiddink JG, Kowalik J, Kitidis V, Reynolds S, Woodward EMS, Tait K, Homoky WB, Kroger S, Bolam S, Godbold JA, Aldridge J, Mayor DJ, Benoist NMA, Bett BJ, Morris KJ, Parker ER, Ruhl HA, Statham PJ, Solan M. 2017. An approach for the identification of

exemplar sites for scaling up targeted field observations of benthic biogeochemistry in heterogeneous environments. Biogeochemistry **135**(1-2), 1-34. DOI: 10.1007/s10533-017-0366-1

Thornton B, Bodenmann A, Pizarro O, Williams SB, Friedman A, Nakajima R, Takai K, Motoki K, Watsuji T, Hirayama H, Matsui Y, Watanabe H, Ura T. 2016. Biometric assessment of deep-sea vent megabenthic communities using multi-resolution 3D image reconstructions. Deep-Sea Research Part I-Oceanographic Research Papers **116**(200-219), 200-219. DOI: 10.1016/j.dsr.2016.08.009

Tilot V. 2006. Biodiversity and distribution of megafauna. Vol. 2: Annotated photographic atlas of the echinoderms of the Clarion-Clipperton fracture zone. Paris, France: UNESCO/IOC. pp. 62.

Tilot V, Ormond R, Moreno Navas J, Catalá TS. 2018. The Benthic Megafaunal Assemblages of the CCZ (Eastern Pacific) and an Approach to their Management in the Face of Threatened Anthropogenic Impacts. Frontiers in Marine Science **5**. DOI: 10.3389/fmars.2018.00007

Timmermann K, Norkko J, Janas U, Norkko A, Gustafsson BG, Bonsdorff E. 2012. Modelling macrofaunal biomass in relation to hypoxia and nutrient loading. Journal of Marine Systems **105-108**, 60-69. DOI: 10.1016/j.jmarsys.2012.06.001

Tolimieri N, Clarke ME, Singh H, Goldfinger C. 2008. Evaluating the SeaBED AUV for monitoring groundfish in untrawlable habitat, in: Reynolds, J.R., Greene, H.G. (Eds.), Marine Habitat Mapping Technology for Alaska. Alaska Sea Grant College Program, University of Alaska Fairbanks, Fairbanks, Alaska. 129-141. DOI::10.4027/mhmta.2008.09

Tomlinson S, Arnall SG, Munn A, Bradshaw SD, Maloney SK, Dixon KW, Didham RK. 2014. Applications and implications of ecological energetics. Trends in Ecology and Evolution **29**(5), 280-290. DOI: 10.1016/j.tree.2014.03.003

Tsai CH, Hsieh Ch, Nakazawa T, Lusseau D. 2016. Predator–prey mass ratio revisited: does preference of relative prey body size depend on individual predator size? Functional Ecology **30**(12), 1979-1987. DOI: 10.1111/1365-2435.12680

UNEP-WCMC, IUCN. 2019. Marine Protected Planet. Retrieved from www.protectedplanet.net (Accessed Feb. 2020).

United Nations General Assembly. 2015. Transforming our world: The 2030 agenda for sustainable development. pp. 35.

Uzmann JR, Cooper RA, Wigley RL. 1977. Synoptic comparison of three sampling techniques for estimating abundance and distribution of selected megafauna: submersible vs camera sled vs otter trawl. Marine Fisheries Review **39**(12), 11-19.

van Cauwenberghe L, Vanreusel A, Mees J, Janssen CR. 2013. Microplastic pollution in deep-sea sediments. Environmental Pollution **182**, 495-499. DOI: 10.1016/j.envpol.2013.08.013

van der Meer J. 2006. Metabolic theories in ecology. Trends in Ecology and Evolution **21**(3), 136-140. DOI: 10.1016/j.tree.2005.11.004

van Oevelen D, Soetaert K, Heip C. 2012. Carbon flows in the benthic food web of the Porcupine Abyssal Plain: The (un)importance of labile detritus in supporting microbial and faunal carbon demands. Limnology and Oceanography **57**(2), 645-664. DOI: 10.4319/lo.2012.57.2.0645

van Rein HB, Brown CJ, Quinn R, Breen J. 2009. A review of sublittoral monitoring methods in temperate waters: a focus on scale. Underwater Technology **28**(3), 99-113. DOI: 10.3723/ut.28.099

Vanreusel A, Vincx M, Bett BJ, Rice AL. 1995. Nematode Biomass Spectra at Two Abyssal Sites in the NE Atlantic with a Contrasting Food Supply. Internationale Revue Der Gesamten Hydrobiologie **80**(2), 287-296.

Villnas A, Hewitt J, Snickars M, Westerbom M, Norkko A. 2018. Template for using biological trait groupings when exploring large-scale variation in seafloor multifunctionality. Ecological Application **28**(1), 78-94. DOI: 10.1002/eap.1630

Warton DI, Wright IJ, Falster DS, Westoby M. 2006. Bivariate line-fitting methods for allometry. Biological Reviews Cambridge Philosophical Society **81**(2), 259-291. DOI: 10.1017/S1464793106007007

Warton DI, Duursma RA, Falster DS, Taskinen S. 2012. smatr 3-an R package for estimation and inference about allometric lines. Methods in Ecology and Evolution **3**(2), 257-259. DOI: 10.1111/j.2041-210X.2011.00153.x

Warwick RM. 1984. Species size distributions in marine benthic communities. Oecologia **61**(1), 32-41. DOI: 10.1007/BF00379085

Wedding LM, Friedlander AM, Kittinger JN, Watling L, Gaines SD, Bennett M, Hardy SM, Smith CR. 2013. From principles to practice: a spatial approach to systematic conservation planning in the deep sea. Proceedings of the Royal Society of Biological Sciences **280**(1773), 20131684. DOI: 10.1098/rspb.2013.1684

Wei CL, Rowe GT, Escobar-Briones E, Boetius A, Soltwedel T, Caley MJ, Soliman Y, Huettmann F, Qu F, Yu Z, Pitcher CR, Haedrich RL, Wicksten MK, Rex MA, Baguley JG, Sharma J, Danovaro R, MacDonald IR, Nunnally CC, Deming JW, Montagna P, Levesque M, Weslawski JM, Wlodarska-Kowalczuk M, Ingole BS, Bett BJ, Billett DS, Yool A, Bluhm BA, Iken K, Narayanaswamy BE. 2010. Global patterns and predictions of seafloor biomass using random forests. PLoS ONE **5**(12), e15323. DOI: 10.1371/journal.pone.0015323

Welch B. 1951. On the comparison of several mean values: An alternative approach. Biometrika **38**, 330-336.

West GB, Brown JH, Enquist BJ. 1997. A general model for the origin of allometric scaling laws in biology. Science **276**(5309), 122-126. DOI: 10.1126/science.276.5309.122

West GB, Brown JH, Enquist BJ. 1999. The fourth dimension of life: fractal geometry and allometric scaling of organisms. Science **284**(5420), 1677-1679. DOI: 10.1126/science.284.5420.1677

West GB, Brown JH. 2005. The origin of allometric scaling laws in biology from genomes to ecosystems: towards a quantitative unifying theory of

biological structure and organization. Journal of Experimental Biology **208**(Pt 9), 1575-1592. DOI: 10.1242/jeb.01589

White EP, Ernest SK, Kerkhoff AJ, Enquist BJ. 2007. Relationships between body size and abundance in ecology. Trends in Ecology and Evolution **22**(6), 323-330. DOI: 10.1016/j.tree.2007.03.007

Whittaker RJ, Willis KJ, Field R. 2001. Scale and species richness: towards a general, hierarchical theory of species diversity. Journal of Biogeography **28**(4), 453-470. DOI: 10.1046/j.1365-2699.2001.00563.x

Witbaard R, Duineveld GCA, Van der Weele JA, Berghuis EM, Reyss JP. 2000. The benthic response to the seasonal deposition of phytopigments at the Porcupine Abyssal Plain in the North East Atlantic. Journal of Sea Research **43**(1), 15-31. DOI: 10.1016/s1385-1101(99)00040-4

Wollast R. 1998. Evaluation and Comparison of the Global Carbon Cycle in the Coastal Zone and in the Open Ocean. In: Brink KH and AR Robinson (Editors) The Sea, pp. 213-253. Volume 10). Wiley: New York, USA.

Woodcock P, O'Leary BC, Kaiser MJ, Pullin AS. 2017. Your evidence or mine? Systematic evaluation of reviews of marine protected area effectiveness. Fish and Fisheries **18**(4), 668-681. DOI: 10.1111/faf.12196

Wynn RB, Huvenne VAI, Le Bas TP, Murton BJ, Connelly DP, Bett BJ, Ruhl HA, Morris KJ, Peakall J, Parsons DR, Sumner EJ, Darby SE, Dorrell RM, Hunt JE. 2014. Autonomous Underwater Vehicles (AUVs): Their past, present and future contributions to the advancement of marine geoscience. Marine Geology **352**, 451-468. DOI: 10.1016/j.margeo.2014.03.012

Yang Z, Liu X, Zhou M, Ai D, Wang G, Wang Y, Chu C, Lundholm JT. 2015. The effect of environmental heterogeneity on species richness depends on community position along the environmental gradient. Scientific Reports **5**(15723), 15723. DOI: 10.1038/srep15723

Yool A, Martin AP, Anderson TR, Bett BJ, Jones DOB, Ruhl HA. 2017. Big in the benthos: Future change of seafloor community biomass in a global, body size-resolved model. Global Change Biology **23**(9), 3554-3566. DOI: 10.1111/gcb.13680

Yvon-Durocher G, Allen AP. 2012. Linking community size structure and ecosystem functioning using metabolic theory. Philosophical Transactions of the Royal Society Biological Sciences **367**(1605), 2998-3007. DOI: 10.1098/rstb.2012.0246

Zelada Leon A, Huvenne VAI, Benoist NMA, Ferguson M, Bett BJ, Wynn RB. 2020. Assessing the Repeatability of Automated Seafloor Classification Algorithms, with Application in Marine Protected Area Monitoring. Remote Sensing 12(10), 1572. DOI: 10.3390/rs12101572

Zilli F, del Barco J, Vanzetti A. 2017. Biometry of neotropical invertebrates inhabiting floodplain rivers: unravelling bionomy. Iheringia Serie Zoologia **107**, e2017014. DOI: 10.1590/1678-4766e2017014

Appendices

Appendix A:

Monitoring mosaic biotopes in a marine conservation zone by autonomous underwater vehicle

Benoist NMA[a,b], Morris KJ[a], Bett BJ[a], Durden JM[a,b,c], Huvenne VAI[a], Le Bas TP[a], Wynn RB[a], Ware SJ[d], Ruhl H[a]

[a] National Oceanography Centre, Southampton SO14 3ZH, UK
[b] University of Southampton, Southampton SO14 3ZH, UK
[c] University of Hawaii, Honolulu HI 96822, USA
[d] Centre for Environment Fisheries and Aquaculture Science, Lowestoft NR33 0HT, UK

Published in Conservation Biology*, March 2019, **33**(5), 1174-1186. DOI: 10.1111/cobi.13312*

Acknowledgements

We are grateful to the crew and science party of RRS Discovery cruise D377/D378 and the Marine Autonomous and Robotic Systems group at the National Oceanography Centre. This work was supported in part by the Department for Environment, Food and Rural Affairs funded project Investigating the Feasibility of Utilizing AUV and Glider Technology for Mapping and Monitoring of the UK MPA Network (MB0118), the Natural Environment Research Council (NERC) project Autonomous Ecological Surveying of the Abyss (AESA) (funding grant number NE/H021787/1), and the NERC Marine Environmental Mapping Programme (MAREMAP). This study is a contribution to the Climate Linked Atlantic Sector Science (CLASS) project and was supported by U.K. NERC National Capability funding (NE/R015953/1). A. Gates (NOC) and A. Callaway (Cefas) kindly assisted with faunal identifications.

Appendix A.1

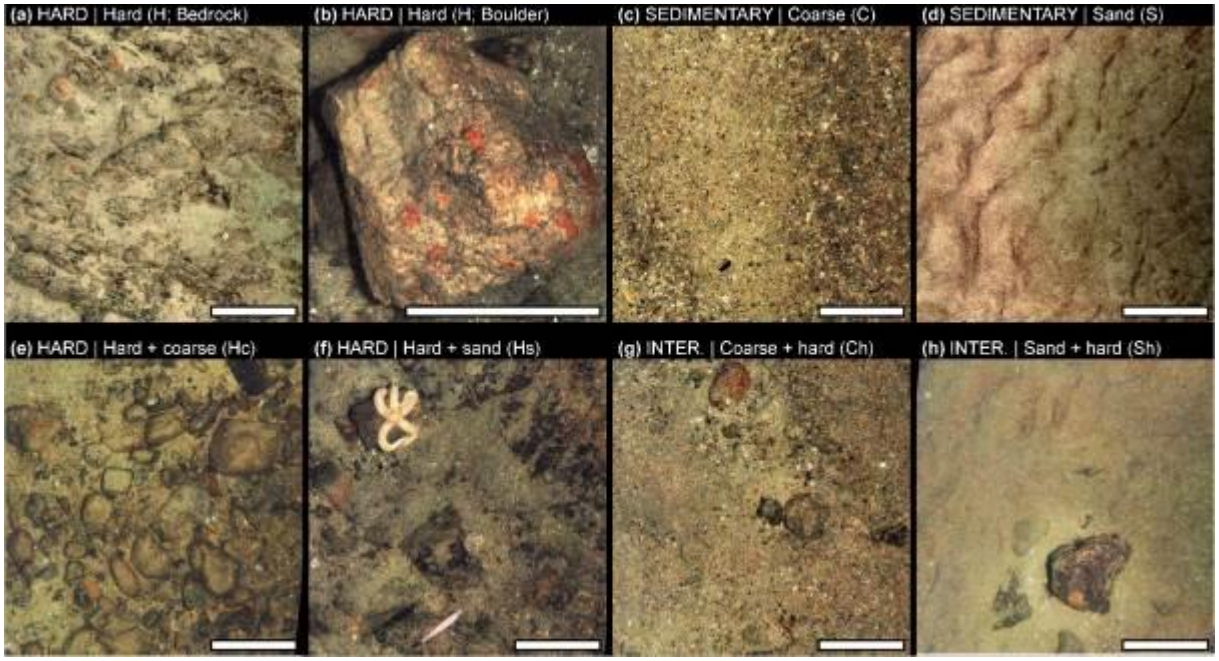

Figure A.1-1. Examples of substratum types. The top pane shows the three main substratum types identified: Hard substrata with **(a)** bedrock and **(b)** boulder, **(c)** Coarse, and **(d)** Sand. The bottom pane shows mixed (mosaic) substratum categories with hard as primary substratum type: **(e)** hard + coarse, **(f)** hard + sand, and hard as secondary substratum type: **(g)** coarse + hard, **(h)** sand + hard. The categories with hard as the only or primary substratum type are referred to as "Hard habitats" (a, b, e, f), those where it was secondary as "Intermediate habitats" (c, g), and those where it was absent as "Sedimentary habitats" (d, h). Scale bars represent 30 cm.

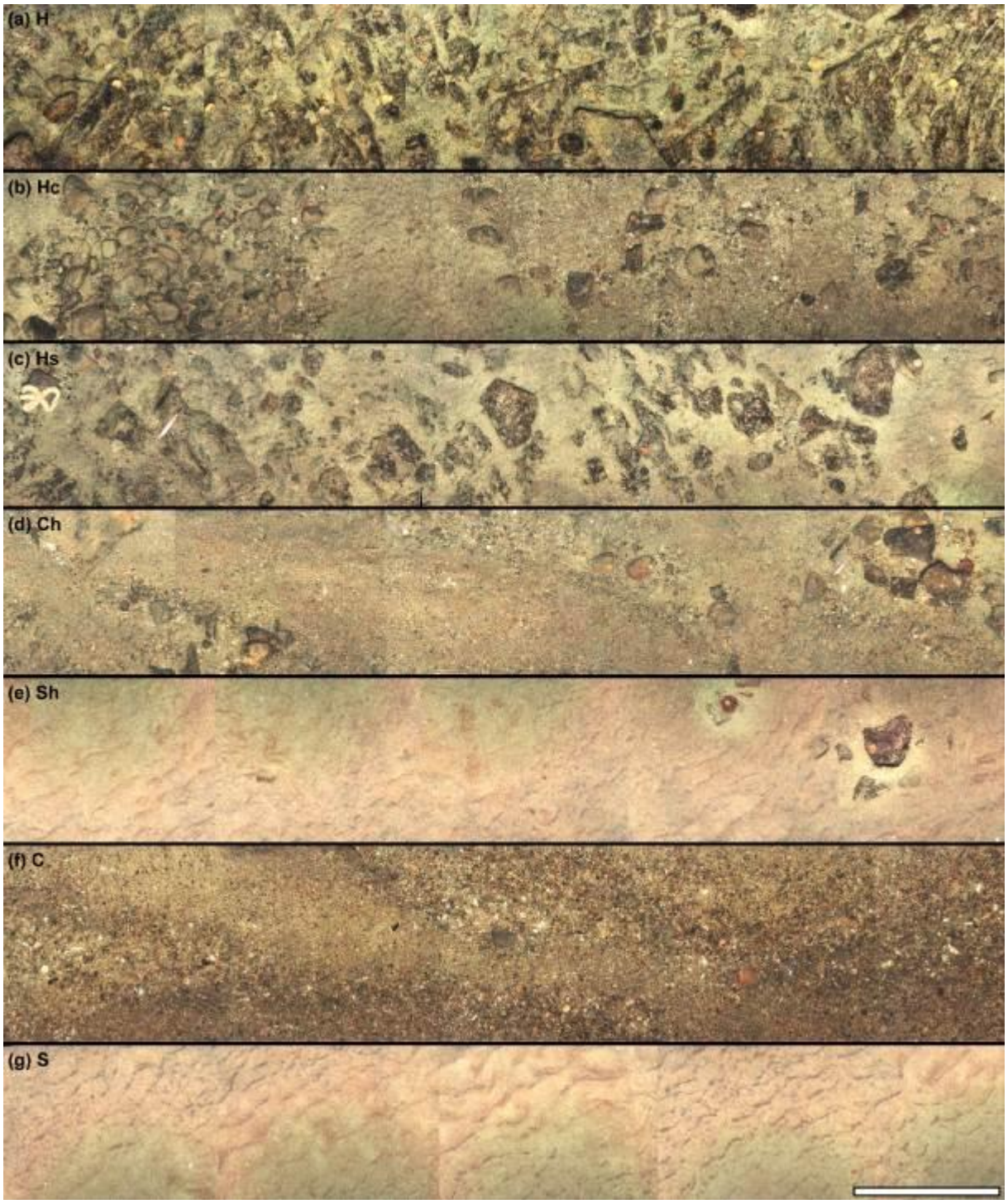

Figure A.1-2. Examples of tile-scale substratum type classification. **(a)** Hard, **(b)** Hard + coarse, **(c)** Hard + sand, **(d)** Coarse + hard, **(e)** Sand + hard, **(f)** Coarse, **(g)** Sand. The categories with hard as the sole or primary substratum type are referred to as Hard habitats (a-c), those where it was secondary as Intermediate habitats (d, e), and those where it was absent as Sedimentary habitats (f, g). Scale bar represents 50 cm.

Appendix A.2

Figure A.2. Examples of close spatial association between distinct taxa **(a-g)**, anthropogenic debris **(h-j)**, and **(k)** rarities [*Galeus* ?*melastomus*]. **(a)** Axinellidae spp. and *Parazoanthus* sp.; **(b)** *Bolocera* sp. and natant decapods; **(c)** *Parazoanthus* sp. and *Porella* sp.; (d) *Parazoanthus* sp. growing on anthropogenic item; **(e)** *Bolocera* sp., *Lithodes maja*, and Axinellidae spp.; **(f)** *Bolocera* sp. and *Lithodes maja*; **(g)** *Salmacina dysteri* and *Munida* sp.; **(h)** trawl net section; **(i-j)** plastic bag / debris.

Appendix A.3

Table S3. Specimen body-size measurements were converted from image pixel to seabed units (mm) by trigonometry (Morris et al., 2014). Individual wet weight (g wwt) was estimated from length-weight relationships in the form $W = a\ L^b$, W, wet weight (g wwt), L, length (mm), and a and b are coefficients gathered from the literature for each morphotype (or near approximation by taxon and body form). Where a specimen was obscured such that a measurement could not be made, it was assigned the mean individual body weight of the corresponding taxon / morphotype. The body weight of 55 of the 74 morphotypes was estimated, corresponding to 34% of the specimens observed. The unquantified taxa were predominantly colonial or encrusting forms. This table lists all taxa / morphotypes encountered in the Greater Haig Fras marine conservation zone survey, the number of specimens (n), the body dimension measured (Dim.), Range of measurements made, literature source (Ref.), reference taxon (Ref. taxon), coefficients a and b (Coeff.), and range of measurements in literature source (RRange).

Taxon / Morphotype			n	Dim.	Range (mm)		Ref.	Ref. taxon	Coeff. a	Coeff. b	RRange (mm)	
Annelida	Polychaeta	*Salmacina dysteri*	547	D	-	-	-	-	-	-	-	-
Arthropoda	Malacostraca	Inachidae 01 (?*Inachus* spp.)	39	Wc	14	34	[1]	*I. dorsettensis*	1.73·10-03	2.541	5	25
	Malacostraca	Inachidae 02 (?*Macropodia* spp.)*	3	Wc	-	-	-	-	-	-	-	-
	Malacostraca	*Liocarcinus* spp.	9	Wc	18	53	[1]	*L. depurator*	1.59·10-04	3.144	3	52
	Malacostraca	*Lithodes maja*	14	Wc	27	76	[2]	*L. murrayi*	5.95·10-04	3.009	4	11
	Malacostraca	*Munida* spp. (include *M. rugosa*)	480	Lc	9	62	[1]	*M. rugosa*	8.49·10-04	3.073	6	34
	Malacostraca	Paguridae 01 (*Pagurus* ?bernhardus)	14	Wc	29	64	[3]	*P. bouvieri*	4.60·10-01	1.055	10	27
	Malacostraca	Paguridae 02 (*Pagurus* ?prideaux)	625	Wc	16	70	[3]	*P. bouvieri*	4.60·10-01	1.055	10	27
	Malacostraca	Porcellanidae spp.	2	Wc	35	36	[1]	*L. depurator*	1.59·10-04	3.144	3	52
Bryozoa	Bryozoa	Bryozoa 01	777	D	-	-	-	-	-	-	-	-
	Gymnolaemata	*Pentapora foliacea*	11	D	-	-	-	-	-	-	-	-
	Gymnolaemata	*Porella* spp. (*P. ?compressa*)	1504	L	-	-	-	-	-	-	-	-
	Gymnolaemata	*Reteporella* spp.	130	D	-	-	-	-	-	-	-	-
Chordata	Actinopterii	*Callionymus* spp. (include *C. lyra*, *C. maticulatus*)	22	L	50	228	[1]	*C. lyra*	1.02·10-05	2.927	26	228
	Actinopterii	Fish 10	19	L	36	86	[1]	*D. bimaculata*	2.59·10-05	2.737	20	36
	Actinopterii	Gadidae spp.	514	L	124	578	[1]	*G. morhua*	1.21·10-07	3.819	50	550
	Actinopterii	Gadiforme 09 (?*Merluccius merluccius*)	2	L	340	340	[4]	*M. merluccius*	3.25·10-06	3.099	160	660
	Actinopterii	*Gadus morhua*	1	L	124	578	[1]	*G. morhua*	1.21·10-07	3.819	50	550
	Actinopterii	*Gaidropsarus vulgaris*	2	L	124	294	[1]	*G. vulgaris*	3.40·10-05	2.547	26	91
	Actinopterii	*Hippoglossoides platessoides*	13	L	102	274	[1]	*H. platessoides*	7.41·10-06	2.978	12	250
	Actinopterii	*Lepidorhombus whiffiagonis*	37	L	139	414	[1]	*L. whiffiagonis*	2.40·10-05	2.746	25	315
	Actinopterii	*Microchirus variegatus*	13	L	126	225	[1]	*M. variegatus*	5.75·10-06	3.141	22	155
	Elasmobranchii	*Galeus* sp. (*G. ?melastomus*)	1	L	727	727	[5]	*G. melastomus*	1.73·10-06	3.020	95	600
	Elasmobranchii	*Leucoraja naevus*	5	Lw	288	489	[4]	*R. naevus*	2.68·10-05	2.959	80	380
	Elasmobranchii	Rajidae sp. (?*Dipturus* sp.)	2	Lw	480	483	[4]	*R. naevus*	2.68·10-05	2.959	80	380
	Elasmobranchii	*Scyliorhinus canicula**	2	L	-	-	-	-	-	-	-	-
Cnidaria	Anthozoa	Anthozoa 01	35	CD	10	43	[6]	Cnidaria	2.60·10-03	2.360	5	80
	Anthozoa	Anthozoa 03	163	CD	10	68	[6]	Cnidaria	2.60·10-03	2.360	5	80
	Anthozoa	Anthozoa 05 (?*Sagartia* spp.)	14	CD	19	236	[6]	Cnidaria	2.60·10-03	2.360	5	80
	Anthozoa	Anthozoa 06	22	CD	17	39	[6]	Cnidaria	2.60·10-03	2.360	5	80
	Anthozoa	Anthozoa 07	1	CD	54	54	[6]	Cnidaria	2.60·10-03	2.360	5	80
	Anthozoa	Anthozoa 08	35	CD	8	38	[6]	Cnidaria	2.60·10-03	2.360	5	80
	Anthozoa	Anthozoa 11	35	CD	15	119	[6]	Cnidaria	2.60·10-03	2.360	5	80
	Anthozoa	Anthozoa 16	32	CD	12	43	[6]	Cnidaria	2.60·10-03	2.360	5	80
	Anthozoa	Anthozoa 19	2	CD	36	57	[6]	Cnidaria	2.60·10-03	2.360	5	80
	Anthozoa	Anthozoa 21	2	CD	17	17	[6]	Cnidaria	2.60·10-03	2.360	5	80
	Anthozoa	Anthozoa 24	6	CD	28	49	[6]	Cnidaria	2.60·10-03	2.360	5	80
	Anthozoa	Anthozoa 34	52	CD	12	54	[6]	Cnidaria	2.60·10-03	2.360	5	80
	Anthozoa	Anthozoa 39	26	CD	19	53	[6]	Cnidaria	2.60·10-03	2.360	5	80
	Anthozoa	*Bolocera* spp. (include *B. tuediae*)	251	CD	13	70	[6]	Cnidaria	2.60·10-03	2.360	5	80

Taxon / Morphotype			n	Dim.	Range (mm)		Ref.	Ref. taxon	Coeff. a	Coeff. b	RRange (mm)	
	Anthozoa	*Caryophyllia smithii**	379	CD	-	-	-	-	-	-	-	-
	Anthozoa	Cerianthid 01 (?*Arachnanthus* sp.)	181	CD	14	78	[6]	Cnidaria	2.60·10-03	2.360	5	80
	Anthozoa	Cerianthid 03 (?*Pachycerianthus* spp.)	16	CD	27	64	[6]	Cnidaria	2.60·10-03	2.360	5	80
	Anthozoa	Hormathiid 01 (?*Actinauge* spp.)	3	CD	23	44	[6]	Cnidaria	2.60·10-03	2.360	5	80
	Anthozoa	*Parazoanthus* (*P. ?anguicomus*)	1629	D	-	-	-	-	-	-	-	-
	Anthozoa	*Urticina* spp. (include *U. felina*)	27	CD	21	91	[6]	Cnidaria	2.60·10-03	2.360	5	80
	Hydrozoa	Hydroid 01 (?*Abietinaria* spp.)	16	L	-	-	-	-	-	-	-	-
Echinodermata	Asteroidea	*Asterias rubens*	16	L/D	46	122	[1]	*A. rubens*	3.59·10-04	2.509	1	280
	Asteroidea	Asteroid 01	17	L/D	15	38	[1]	*P. pulvillus*	3.15·10-04	2.706	8	101
	Asteroidea	Asteroid 02 (?*Henricia oculata*)	16	L/D	8	26	[1]	*H. sanguinolata*	3.99·10-04	2.350	7	127
	Asteroidea	*Astropecten irregularis*	5	L/D	68	99	[1]	*A. irregularis*	1.71·10-04	2.746	3	125
	Asteroidea	*Crossaster papposus*	1	L/D	111	111	[1]	*C. papposus*	2.85·10-05	3.144	8	167
	Asteroidea	*Luidia ciliaris*	25	D	58	260	[1]	*L. sarsii*	1.10·10-04	3.940	4	99
	Asteroidea	*Luidia sarsii*	3	D	53	77	[1]	*L. sarsii*	1.10·10-04	3.940	4	99
	Asteroidea	*Marthasterias glacialis*	2	L/D	119	119	[1]	*A. rubens*	3.59·10-04	2.509	1	280
	Asteroidea	*Porania pulvillus*	1124	L/D	9	73	[1]	*P. pulvillus*	3.15·10-04	2.706	8	101
	Asteroidea	*Stichastrella rosea*	139	L/D	12	114	[1]	*S. rosea*	3.36·10-04	2.437	14	112
	Crinoidea	Antedon spp. (includes *A. bifida*)	58	L/D	-	-	-	-	-	-	-	-
	Echinoidea	Echinoid 01	15	D	22	102	[1]	*E. acutus*	5.68·10-04	2.846	5	79
	Echinoidea	Echinoid 05	4	D	27	33	[1]	*E. acutus*	5.68·10-04	2.846	5	79
	Echinoidea	*Echinus esculentus*	128	D	32	124	[1]	*E. esculentus*	3.47·10-04	3.012	10	100
	Ophiuroidea	Ophiuroid 01 (include ?*Ophiura* spp.)	207	D	160	207	[1]	*O. sarsi*	4.52·10-03	2.216	4	31
	Ophiuroidea	Ophiuroid 02 (include ?*Ophiothrix fragilis*, ?*Ophiocomina nigra*)	13	D	54	102	[1]	*O. nigra*	5.73·10-03	2.220	5	11
Mollusca	Cephalopoda	*Eledone cirrhosa*	2	Lm	111	111	[1]	*E. cirrhosa*	1.95·10-03	2.672	37	96
	Cephalopoda	Eledone 02	3	Lm	57	140	[1]	*E. cirrhosa*	1.95·10-03	2.672	37	96
Porifera	Desmospongiae	Axinellidae spp. (include *Phakellia ventilabrum*, *Axinella infundibuliformis*)	2457	D	-	-	-	-	-	-	-	-
	Porifera	Porifera 02	403	L	-	-	-	-	-	-	-	-
	Porifera	Porifera 03	23	D	-	-	-	-	-	-	-	-
	Porifera	Porifera 13	26	L	-	-	-	-	-	-	-	-
	Desmospongiae	Porifera 20 (include ?*Suberites carnosus*)	116	D	-	-	-	-	-	-	-	-
	Desmospongiae	Porifera 22 (*?Quasillina* sp.)	2	D	-	-	-	-	-	-	-	-
	Desmospongiae	Porifera 23 (include ?*Polymastia boletiformis*)	362	D	-	-	-	-	-	-	-	-
	Desmospongiae	Porifera 24 (?*Polymastia* sp.)	7	D	-	-	-	-	-	-	-	-
	Desmospongiae	Porifera 25 (?*Myxilla* sp.)	3	D	-	-	-	-	-	-	-	-

Dimension measured (Dim.): Wc, width of carapace; D, 'longest diameter' of an individual or a colony; CD, column diameter; L, total length; Lc, carapace length; Lm, mantle length; L/D, longest arm to opposite edge of disc. * Partial observation(s) biomass not estimated.

[1] Robinson, L.A., Greenstreet, S.P.R., Reiss, H., Callaway, R., Craeymeersch, J., de Boois, J., Degraer, S., Ehrich, S., Fraser, H.M., Goffin, A., Kröncke, I., Lindal Jorgenson, L., Robertson, M.R., Lancaster, J., 2010. Length-weight relationships of 216 North Sea benthic invertebrates and fish. Journal of the Marine Biological Association of the United Kingdom **90**, 95-104.

[2] Arnaud, P.M., Do-Chi, T., 1977. Données biologiques et biométriques sur les lithodes *Lithodes murrayi* (Crustacea: Decapoda: Anomura) des îles Crozet (SW océan Indien). Marine Biology **39**, 147-159.

[3] Richardson, A.J., Lamberts, C., Isaacs, G., Moloney, C.L., Gibbons, M.J., 2000. Length-weight relationships of some important forage crustaceans from South Africa. Naga, The ICLARM Quarterly **23**, 29-33.

[4] Coull, K.A., Jermyn, A.S., Newton, A.W., Henderson, G.I., Hall, W.B., 1989. Length / weight relationships for 88 species of fish encountered in the North East Atlantic. Scottish Fisheries Research Report Number 43. Department of Agriculture and Fisheries for Scotland, Aberdeen. ISBN 0308 8022.

[5] Merella, P., Quetglas, A., Alemany, F., Carbonell, A., 1997. Length-weight relationship of fishes and cephalopods from the Balearic Islands (Western Mediterranean). Naga, The ICLARM Quarterly **20**, 66-68.

[6] Durden, J.M., Bett, B.J., Horton, T., Serpell-Stevens, A., Morris, K.J., Billett, D.S.M., Ruhl, H.A., 2016. Improving the estimation of deep-sea megabenthos biomass: dimension to wet weight conversions for abyssal invertebrates. Marine Ecology Progress Series **552**, 71-79.

Appendix A.4

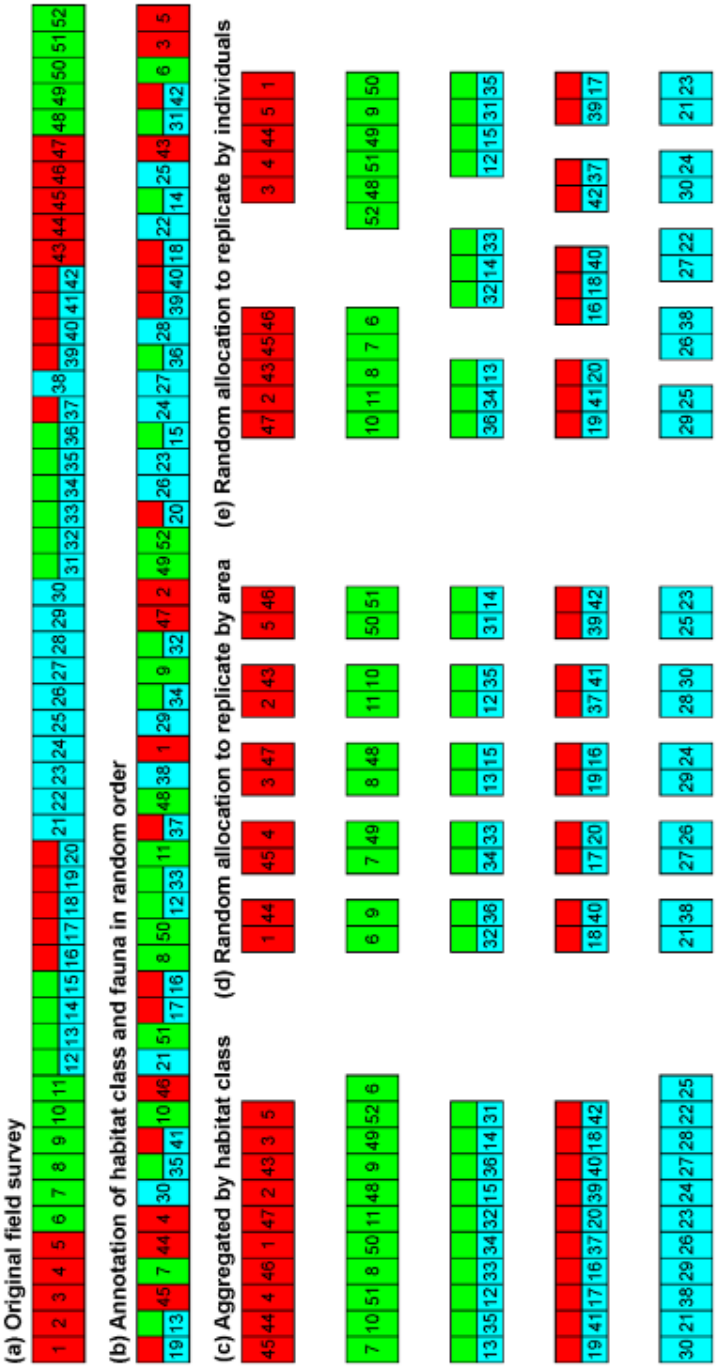

Figure A.4. Simplified 'cartoon' graphic representation of the visual survey methodology, note that the field survey comprised 2637 tiles, for clarity this graphic has only 52 tiles. **(a)** Original non-random spatial survey with substratum type classified by colour (e.g. red, sand; green, coarse; cyan, rock; two-colour, mosaic). **(b)** Tiles were examined and annotated for substratum type and faunal composition in random order to avoid (i) systematic temporal annotator bias in habitat classification or faunal identification, and (ii) unconscious annotator bias between spatially related images. **(c)** Subsequent aggregation of tiles by substratum type. Then final random allocation of tile data to replicate composite samples on the basis of: **(d)** approximately fixed seabed area (c. 150 m^2 in our study), or **(e)** approximately fixed number of individuals (c. 150 individuals in our study), to remove the spatial structure (autocorrelation) inherent in the original transect.

Appendix A.5

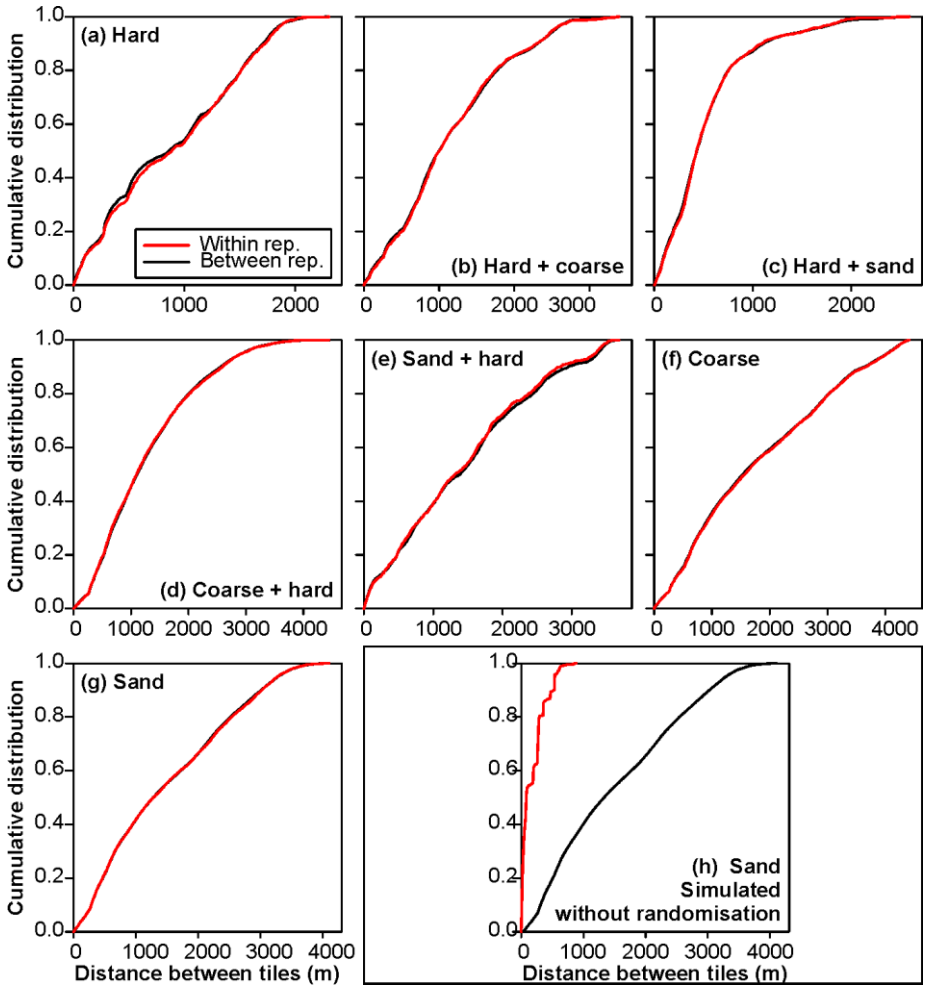

Figure A.5. Testing spatial randomisation of photographic tiles. Cumulative distributions of spatial distances between all pairs of tiles within (red) and between (black) replicates. **(a-g)** As analysed in the present study, tiles randomly selected to compose replicates of c. 150 m^2 (see Figure A.4). **(h)** A simulated version of the Sand dataset produced without randomisation, tiles selected in spatial order to composite replicates of c. 150 m^2. The very close correspondence of within and between replicate spatial distances indicates successful randomisation (a-g), as contrasted with the obvious disparity in spatial arrangement without randomisation (h). The correspondence of within and between replicate distance cumulative distributions was assessed by one-sided (within not greater than between) two-sample Kolmogorov-Smirnov tests (e.g. Siegel & Castellan, 1988), as implemented with the ks.test function in the R Stats Package (Version 3.5.0; R Core Team, 2017). Results: Hard, D^+ = 0.008, p = 0.783; Hard+coarse, 0.014, p = 0.241; Hard+sand, 0.007, p = 0.642; Coarse+hard, 0.011, p = 0.088; Sand+hard, 0.021, p = 0.202; Coarse, 0.002, p = 0.91; Sand, 0.004, p = 0.684. In all analysed cases (a-g), cumulative within was not significantly greater than cumulative between, in marked contrast to the simulated (non-randomised) Sand dataset where there was a highly significant difference (D^+ = 0.743, $p < 0.001$).

Siegel, S, Castellan, NJ, 1988. Nonparametric statistics for the behavioural sciences. New York: McGraw-Hill.

R Core Team, 2017. R: a language and environment for statistical computing. R Foundation for Statistical Computing, Vienna, Austria.

Appendix A.6

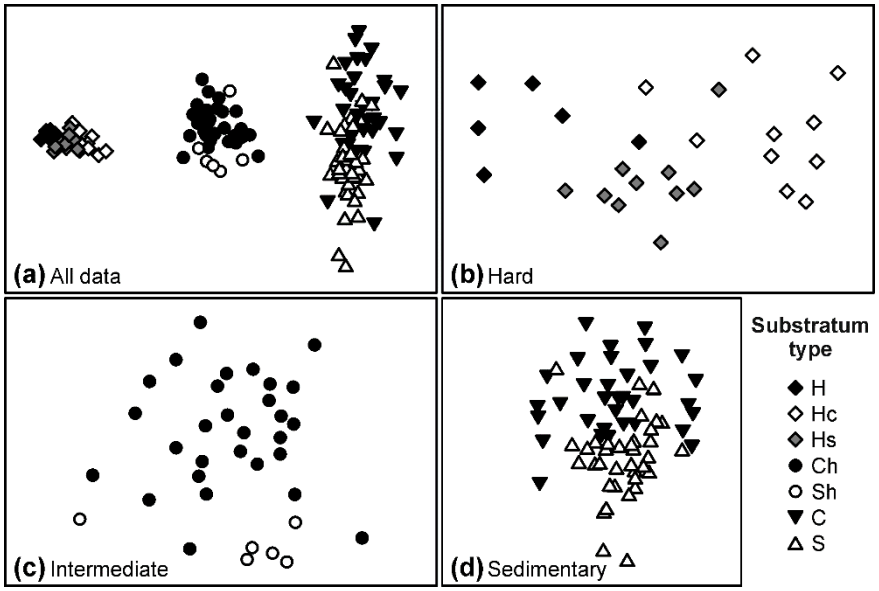

Figure A.6. Variation in faunal composition by substratum type in composite area samples, illustrated by 2D non-metric multidimensional scaling ordination of Bray-Curtis dissimilarity of log-transformed density. **(a)** All data. **(b)** Hard habitats. **(c)** Intermediate habitats **(d)** Sedimentary habitats. Primary substratum types are indicated (H)ard, (I)ntermediate, (C)oarse, and (S)and, with secondary substratum types indicated by corresponding lower case letters.

Table A.2. Pairwise comparisons of faunal composition between substratum types in composite area samples, lower left half-matrix details ANOSIM R values, upper right half-matrix details average faunal dissimilarity. Primary substratum types are indicated (H)ard, (I)ntermediate, (C)oarse, and (S)and, with secondary substratum types indicated by corresponding lower case letters.

Substratum type	Hard			Intermediate		Sedimentary	
	H	Hc	Hs	Ch	Sh	C	S
H	-	37.9	28.1	83.3	82.0	98.2	98.4
Hc	0.88**	-	29.1	72.1	68.9	95.4	94.8
Hs	0.68**	0.71**	-	78.9	76.5	96.8	96.7
Ch	1.00**	1.00**	1.00**	-	49.4	78.8	77.2
Sh	1.00*	1.00**	1.00**	0.45**	-	79.0	73.5
C	1.00**	1.00**	1.00**	0.94**	0.91**	-	59.2
S	1.00**	1.00**	1.00**	0.96**	0.91**	0.36**	-

* $p < 0.05$, ** $p < 0.001$

Appendix A.7

Table A.7. Indicator species analysis of composite area samples by summary substratum class (subs.): (H)ard, (I)ntermediate, (C)oarse, and (S)and. All taxa with an indicator value (IndVal[1]) adjusted[2] p-value (Adj-p) < 0.05 are listed, in each case, specificity (A parameter[1]), fidelity (B parameter[1]), and resultant indicator value are given, frequency of occurrence (fidelity) is also listed for each substratum class.

Subs.	Taxon	Specificity	Fidelity	IndVal	Adj-p	Frequency (%)			
						H	I	C	S
H	*Parazoanthus* sp.	0.9881	1.0000	0.994	0.0002	100.0	34.3	3.0	0.0
	Axinellidae spp.	0.9671	1.0000	0.983	0.0002	100.0	77.1	0.0	0.0
	Porella sp.	0.9552	1.0000	0.977	0.0002	100.0	74.3	0.0	0.0
	Porifera 20	0.9211	1.0000	0.960	0.0002	100.0	28.6	0.0	0.0
	Salmacina dysteri	0.9181	1.0000	0.958	0.0002	100.0	65.7	0.0	5.6
	Munida sp.	0.9036	1.0000	0.951	0.0002	100.0	74.3	3.0	5.6
	Echinus esculentus	0.9042	0.9615	0.932	0.0002	96.2	37.1	0.0	0.0
	Reteporella spp.	0.8543	1.0000	0.924	0.0002	100.0	40.0	0.0	5.6
	Stichastrella rosea	0.7002	1.0000	0.837	0.0002	100.0	60.0	27.3	19.4
	Antedon spp.	0.8078	0.8077	0.808	0.0002	80.8	28.6	3.0	2.8
	Caryophyllia smithii	1.0000	0.5385	0.734	0.0002	53.8	0.0	0.0	0.0
	Inachidae 01	0.8065	0.5769	0.682	0.0002	57.7	14.3	6.1	0.0
	Porifera 03	0.9673	0.4231	0.640	0.0002	42.3	2.9	0.0	0.0
	Lithodes maja	0.9453	0.4231	0.632	0.0002	42.3	2.9	0.0	0.0
	Porifera 13	0.9056	0.4231	0.619	0.0002	42.3	8.6	0.0	0.0
	Luidia ciliaris	0.6788	0.5000	0.583	0.0002	50.0	11.4	9.1	0.0
	Asterias rubens	0.9474	0.3462	0.573	0.0002	34.6	2.9	0.0	0.0
	Asteroid 07	0.8487	0.3462	0.542	0.0002	34.6	5.7	0.0	2.8
	Cerianthid 03	0.7294	0.3846	0.530	0.0002	38.5	8.6	3.0	2.8
	Asteroid 01	0.7030	0.3846	0.520	0.0004	38.5	8.6	0.0	2.8
	Pentapora foliacea	1.0000	0.2692	0.519	0.0002	26.9	0.0	0.0	0.0
	Hydroid 01	1.0000	0.2308	0.480	0.0002	23.1	0.0	0.0	0.0
	Ophiuroid 02	0.7443	0.2692	0.448	0.0024	26.9	8.6	0.0	2.8
	Echinoid 01	0.6523	0.2692	0.419	0.0062	26.9	11.4	3.0	0.0
	Porifera 24	0.7491	0.1923	0.380	0.0094	19.2	5.7	0.0	0.0
	Porifera 25	1.0000	0.1154	0.340	0.0137	11.5	0.0	0.0	0.0
I	Anthozoa 39	0.7116	0.4286	0.552	0.0002	7.7	42.9	12.1	2.8
C	Paguridae 01	0.6476	0.2121	0.371	0.0322	3.8	0.0	21.2	8.3
S	Fish 10	0.7306	0.3333	0.494	0.0006	0.0	5.7	6.1	33.3
	Liocarcinus spp.	0.7623	0.2500	0.437	0.0033	0.0	5.7	3.0	25.0
	Hippoglossoides platessoides	0.7593	0.1944	0.384	0.0094	3.8	2.9	0.0	19.4

[1] Notation as given by Dufrêne and Legendre (1997), calculated with the 'multipatt' function in the R 'indicspecies' package.

[2] Adjustment for multiple testing by method of Benjamini and Hochberg (1995), as implemented by the 'p.adjust' function in the R 'stats' package.

Benjamini, Y., Hochberg, Y., 1995. Controlling the false discovery rate: a practical and powerful approach to multiple testing. *Journal of the Royal Statistical Society Series B*, **57**, 289-300.

Dufrêne, M., Legendre, P., 1997. Species assemblages and indicator species: the need for a flexible asymmetrical approach. *Ecological Monographs*, **67**, 345-366.

Appendix B:

An approach for the identification of exemplar sites for scaling up targeted field observations of benthic biogeochemistry in heterogeneous environments

Thompson CEL[a,b], Silburn B[c], Williams ME[d], Hull T[c], Sivyer D[c], Amoudry LO[d], Widdicombe S[e], Ingels J[e], Carnovale G[e], McNeill CL[e], Hale R[a], Marchais CL[a], Hicks N, Smith HEK, Klar JK[a], Hiddink JG, Kowalik J, Kitidis V[e], Reynolds S, Woodward EMS[e], Tait K[e], Homoky WB, Kroger S[c], Bolam S[c], Godbold JA[a], Aldridge J[c], Mayor DJ[a], **Benoist NMA[a,b]**, Bett BJ[a], Morris KJ[a], Parker ER[c], Ruhl HA[a], Statham PJ[a], Solan M[a].

[a] National Oceanography Centre, Southampton SO14 3ZH, UK
[b] University of Southampton, Southampton SO14 3ZH, UK
[c] Centre for Environment Fisheries and Aquaculture Science, Lowestoft NR33 0HT, UK
[d] National Oceanography Centre, Liverpool L3 5DA, UK
[e] Plymouth Marine Laboratory, Plymouth PL1 3DH, UK
[f] Scottish Association for Marine Science, Oban, Argyll PA37 1QA, UK

Published in Biogeochemistry, *August 2017,* ***135****(1-2): 1-34. DOI: 10.1007/s10533-017-0366-1. The abstract is provided on the next page, and the complete publication is available online (https://link.springer.com/article/10.1007/s10533-017-0366-1).*

Abstract

Continental shelf sediments are globally important for biogeochemical activity. Quantification of shelf-scale stocks and fluxes of carbon and nutrients requires the extrapolation of observations made at limited points in space and time. The procedure for selecting exemplar sites to form the basis of this up-scaling is discussed in relation to a UK-funded research programme investigating biogeochemistry in shelf seas. A three-step selection process is proposed in which (1) a target area representative of UK shelf sediment heterogeneity is selected, (2) the target area is assessed for spatial heterogeneity in sediment and habitat type, bed and water column structure and hydrodynamic forcing, and (3) study sites are selected within this target area encompassing the range of spatial heterogeneity required to address key scientific questions regarding shelf scale biogeochemistry, and minimise confounding variables. This led to the selection of four sites within the Celtic Sea that are significantly different in terms of their sediment, bed structure, and macrofaunal, meiofaunal and microbial community structures and diversity, but have minimal variations in water depth, tidal and wave magnitudes and directions, temperature and salinity. They form the basis of a research cruise programme of observation, sampling and experimentation encompassing the spring bloom cycle. Typical variation in key biogeochemical, sediment, biological and hydro-dynamic parameters over a pre to post bloom period are presented, with a discussion of anthropogenic influences in the region. This methodology ensures the best likelihood of site-specific work being useful for up-scaling activities, increasing our understanding of benthic biogeochemistry at the UK-shelf scale.

Keywords: benthic biogeochemistry, continental shelf seas, ecosystem services, blue carbon, nutrient cycling

Appendix C:

Landscape-scale spatial heterogeneity in phytodetrital cover and megafauna biomass in the abyss links to modest topographic variation

Morris KJ[a], Bett BJ[a], Durden JM[a,b], **Benoist NMA[a,b]**, Huvenne VA[a], Jones DO[a], Robert K[a], Ichino MC[a,b], Wolff GA[c], Ruhl HA[a]

[a] National Oceanography Centre, Southampton SO14 3ZH, UK
[b] University of Southampton, Southampton SO14 3ZH, UK
[c] University of Liverpool, Liverpool L69 3BX, UK

Published in Scientific Reports, *September 2016, **6**: 34080. DOI: 10.1038/srep34080. The abstract is provided below, and the complete publication is available online (https://www.nature.com/articles/srep34080).*

Abstract

Sinking particulate organic matter (POM, phytodetritus) is the principal limiting resource for deep-sea life. However, little is known about spatial variation in POM supply to the abyssal seafloor, which is frequently assumed to be homogenous. In reality, the abyss has a highly complex landscape with millions of hills and mountains. Here, we show a significant increase in seabed POM% cover (by ~1.05 times), and a large significant increase in megafauna biomass (by ~2.5 times), on abyssal hill terrain in comparison to the surrounding plain. These differences are substantially greater than predicted by current models linking water depth to POM supply or benthic biomass. Our observed variations in POM% cover (phytodetritus), megafauna biomass, sediment total organic carbon and total nitrogen, sedimentology, and benthic boundary layer turbidity, all appear to be consistent with topographically enhanced current speeds driving these enhancements.The effects are detectable with bathymetric elevations of only 10 s of metres above the surrounding plain.These results imply considerable unquantified heterogeneity in global ecology.

Appendix D:

Megafaunal variation in the abyssal landscape of the Clarion-Clipperton Zone

Simon-Lledó E[a,b], Bett BJ[a], Huvenne VAI[a], Schoening T[c], **Benoist NMA[a,b]**, Jeffreys RM, Durden JM[a,b], Jones DOB[a]

[a] National Oceanography Centre, Southampton SO14 3ZH, UK
[b] University of Southampton, Southampton SO14 3ZH, UK
[c] GEOMAR Helmholtz Centre for Ocean Research, Kiel D-24148, Germany
[d] University of Liverpool, Liverpool L69 3BX, UK

Published in Progress in Oceanography, *January 2019, **170**, 119-133: 34080 DOI: 10.1016/j.pocean.2018.11.003. The abstract is provided on the next page, and the complete publication is available online (https://www.sciencedirect.com/science/article/pii/S0079661118301824).*

Abstract

The potential for imminent polymetallic nodule mining in the Clarion Clipperton Fracture Zone (CCZ) has attracted considerable scientific and public attention. This concern stems from both the extremely large seafloor areas that may be impacted by mining, and the very limited knowledge of the fauna and ecology of this region. The environmental factors regulating seafloor ecology are still very poorly understood. In this study, we focus on megafaunal ecology in the proposed conservation zone 'Area of Particular Environmental Interest 6' (study area centred 17°16'N, 122°55'W). We employ bathymetric data to objectively define three landscape types in the area (a level bottom Flat, an elevated Ridge, a depressed Trough; water depth 3950–4250 m) that are characteristic of the wider CCZ. We use direct seabed sampling to characterise the sedimentary environment in each landscape, detecting no statistically significant differences in particle size distributions or organic matter content. Additional seafloor characteristics and data on both the metazoan and xenophyophore components of the megafauna were derived by extensive photographic survey from an autonomous underwater vehicle. Image data revealed that there were statistically significant differences in seafloor cover by nodules and in the occurrence of other hard substrata habitat between landscapes. Statistically significant differences in megafauna standing stock, functional structuring, diversity, and faunal composition were detected between landscapes. The Flat and Ridge areas exhibited a significantly higher standing stock and a distinct assemblage composition compared to the Trough. Geomorphological variations, presumably regulating local bottom water flows and the occurrence of nodule and xenophyophore test substrata, between study areas may be the mechanism driving these assemblage differences. We also used these data to assess the influence of sampling unit

size on the estimation of ecological parameters. We discuss these results in the contexts of regional benthic ecology and the appropriate management of potential mining activities in the CCZ and elsewhere in the deep ocean.

Keywords: biodiversity, geomorphology, polymetallic nodules, deep-sea mining, abyssal plains, sample size, NE Pacific, CCZ, APEI

Appendix E:

A generalised volumetric method to estimate the biomass of photographically surveyed benthic megafauna

Benoist NMA[a,b], Bett BJ[a], Morris KJ[a], Ruhl HA[a,c]

[a] National Oceanography Centre, Southampton SO14 3ZH, UK
[b] University of Southampton, Southampton SO14 3ZH, UK
[c] Monterey Bay Aquarium Research Institute, California 95039, USA

Published in Progress in Oceanography*, September 2019, **178**: 102188. DOI: 10.1016/j.pocean.2019.102188*

Acknowledgements

We are grateful to the crews and science parties of the RRS Discovery cruises DY034, DY050, and DY077, and to Amanda Serpell-Stevens and Claire Laguionie Marchais for assisting in the taxonomic identification of specimen material. Our work was supported by two UK Natural Environment Research Council programmes: "Climate Linked Atlantic Section Science" (CLASS) National Capability funding (grant number NE/R015953/1), and "Shelf Sea Biogeochemistry" (SSB) (grant number NE/K001744/1) that was jointly funded by the UK Department for Environment, Food and Rural Affairs. The underlying research data is available online in the open research data repository Mendeley Data at http://dx.doi.org/10.17632/558fp8pb44.1.

Table E.1. Summary data of the benthic mega-invertebrates and demersal fish **(i)** trawl-caught at the Porcupine Abyssal Plain Sustained Observatory, northeast Atlantic, and **(ii)** observed from AUV images in the Celtic Sea.

Figure E.1. Photographic examples of the benthic mega-invertebrates and demersal fish trawl-caught at the Porcupine Abyssal Plain Sustained Observatory, northeast Atlantic, and observed from AUV images in the Celtic Sea.

Table E.1. Summary data of the benthic mega-invertebrates and demersal fish **(i)** trawl-caught at the Porcupine Abyssal Plain Sustained Observatory, northeast Atlantic, and **(ii)** observed from AUV images in the Celtic Sea. For each class and for total count, values indicate number of morphotypes [number of specimens]. Measured ($_M$) and estimated ($_E$) biomass (M_M, M_E; in g) and biovolume (V_M, V_E; in mL) are given as total. M_E was estimated using length-weight relationships available from literature. V_E was estimated using the generalised volumetric method. For the Celtic Sea training images dataset and for the inter-operator common images dataset, values indicate biomass or biovolume estimated by Operator 1/Operator 2.

		Porcupine Abyssal Plain (trawl catch)	Celtic Sea (AUV photography)		
Phylum	**Class**	**Validation with fresh specimens**	**Training images**	**Inter-operator variation common images**	**Full field trial images**
Annelida	Polychaeta	2 [6]	1 [2]	1 [1]	3 [17]
Arthropoda	Malacostraca	5 [24]	1 [21]	11 [41]	16 [472]
Arthropoda	Pycnogonida	1 [7]			
Arthropoda	Hexanauplia	1 [3]			
Bryozoa	Bryozoa		1 [7]	2 [9]	3 [126]
Bryozoa	Gymnolaemata			1 [6]	2 [48]
Chordata	Actinopterygii	1 [1]	1 [23]	11 [37]	18 [379]
Cnidaria	Anthozoa	8 [52]	1 [26]	8 [42]	19 [410]
Cnidaria	Cnidaria			3 [29]	3 [611]
Cnidaria	Hydrozoa		1 [1]		1 [24]
Echinodermata	Asteroidea	3 [23]	1 [20]	7 [40]	9 [522]
Echinodermata	Crinoidea		1 [10]	1 [1]	1 [38]
Echinodermata	Echinoidea		1 [6]	1 [1]	3 [10]
Echinodermata	Holothuroidea	10 [85]			
Echinodermata	Ophiuroidea	2 [2]	1 [11]	1 [11]	3 [170]
Mollusca	Bivalvia				1 [7]
Mollusca	Cephalopoda		1 [3]		3 [14]
Porifera	Desmospongiae			2 [3]	4 [13]
Porifera	Porifera				3 [35]
Sipuncula	Sipunculidea	1 [3]			
Total	Count	34 [206]	11 [130]	49 [221]	92 [2896]
	M_M (g fwwt)	16321	na	na	na
	V_M (mL)	15252	na	na	na
	M_E (g fwwt)	22115	na	1024 / 973	31927
	$V_{E\text{-}partial}$ (mL)	na	na	1099 / 1212	32599
	V_E (mL)	13697	47160* / 47953*	1279 / 1366	33352

* Note the training images set comprised six individuals > 1 kg that were not analysed in the full field trial images set.

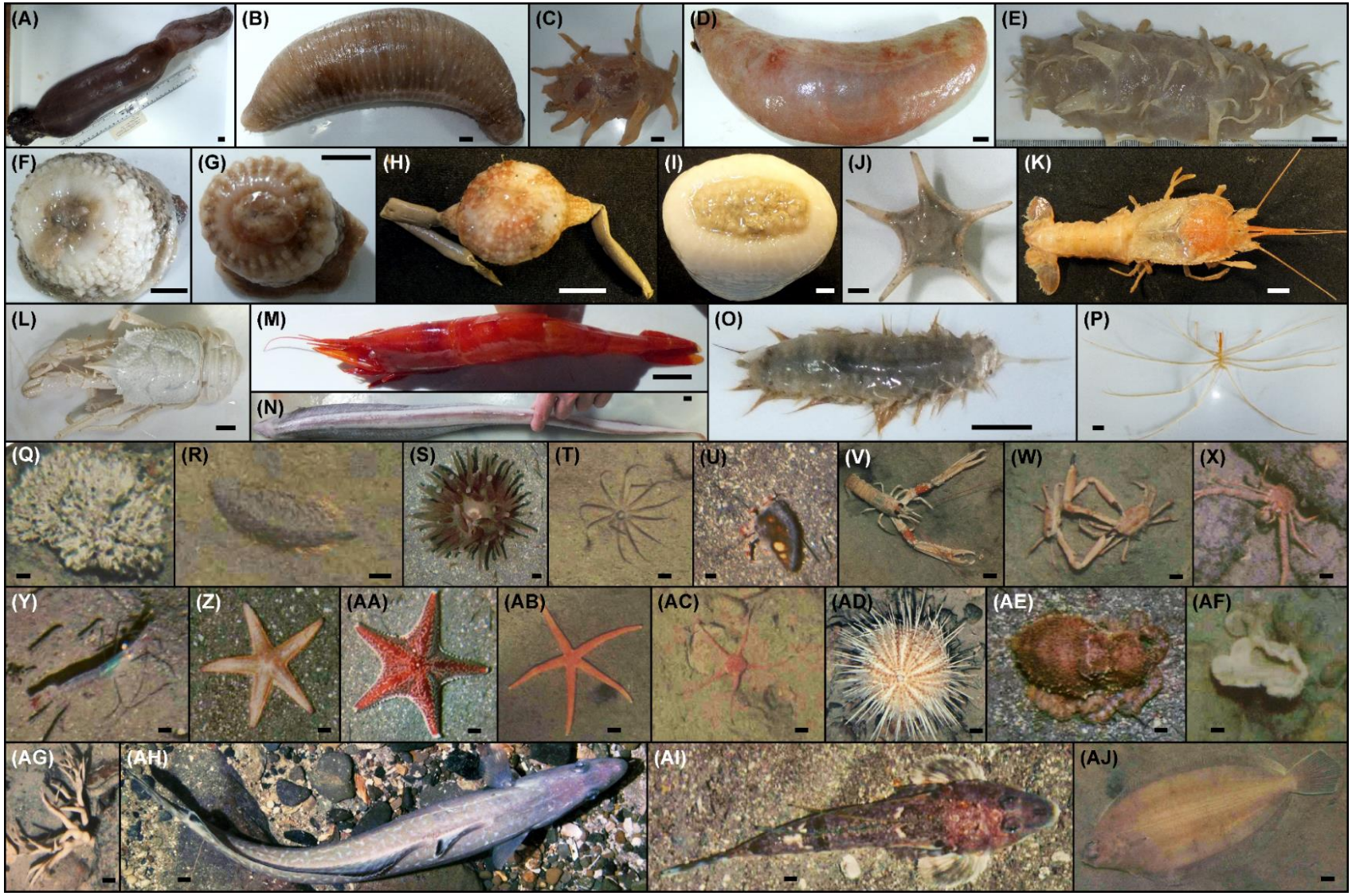

Fig. E.1. Photographic examples of the benthic mega-invertebrates and demersal fish (A-P) trawl-caught at the Porcupine Abyssal Plain Sustained Observatory, northeast Atlantic, and (Q-AJ) observed from AUV images in the Celtic Sea. **(A)** *Psychropotes longicauda*; **(B)** *Paroriza* sp.; **(C)** *Deima* sp.; **(D)** *Molpadiodemas villosus*; **(E)** *Oneirophanta mutabilis*; **(F)** *Kadosactis* sp.; **(G)** *Actinauge* sp.; **(H)** *Amphiantus* sp.; **(I)** *Parasicyonis biotrans*; **(J)** *Hyphalaster inermis*; **(K)** *Willemoesia leptodactyla*; **(L)** *Munidopsis crassa*; **(M)** *Cerataspis* sp.; **(N)** *Histiobranchus bathybius*; **(O)** *Laetmonice* sp; **(P)** *Colossendeis* sp.; **(Q)** *Salmacina dysteri*; **(R)** *Aphrodita aculeata*; **(S)** *Bolocera* sp.; **(T)** Anthozoa sp.34; **(U)** Paguridae sp.2; **(V)** *Nephrops norvegicus*; **(W)** *Goneplax rhomboides*; **(X)** *Munida* sp.; **(Y)** Caridea sp.1; **(Z)** *Astropecten irregularis*; **(AA)** *Porania pulvillus*; **(AB)** Asteroid sp.2; **(AC)** Ophiuroid sp.1; **(AD)** *Gracilechinus acutus*; **(AE)** *Eledone cirrhosa*; **(AF)** Axinellidae; **(AG)** *Porella* sp.; **(AH)** *Molva molva*; **(AI)** *Callionymus* sp.; **(AJ)** *Lepidorhombus whiffiagonis*. Scale bar is 1 cm.

Appendix F:

Taxon and morphotype catalogue

This appendix provides a list of megabenthos (≥ 1 cm body size) morphotypes (species/species groups/higher taxa; e.g. Althaus et al. 2015) as recorded visually from seafloor imagery at the two Celtic Shelf sites assessed in this Ph.D. thesis: the Greater Haig Fras (GHF) marine conservation zone and the UK-NERC Shelf-Sea Biogeochemistry (SSB) study area (c. 100 m water depth). Morphotypes were identified using various online field guides (last accessed November 2019) including: the Atlas of Benthic Invertebrates (http://atlasbenthal.ifremer.fr/), the Marine Life Information Network (MarLIN, https://www.marlin.ac.uk/), SeaLifeBase (www.sealifebase.org), FishBase (www.fishbase.org), the Encyclopedia of Marine Life of Britain and Ireland (http://www.habitas.org.uk/marinelife/), the DORIS database (https://doris.ffessm.fr/), the Marine Species Identification Portal (http://species-identification.org/).

This appendix also provides a list of trawl-caught specimens from the Porcupine Abyssal Plain sustained observatory (PAP-SO; NE Atlantic; 4850 m water depth) (see chapter 4). Amanda Serpell-Stevens (NOCS) participated in the identification of the specimens.

The authoritative classification of those taxa identified to genera or species level was verified using the World Register of Marine Species (http://www.marinespecies.org/).

F.1 Celtic Shelf sites

ANNELIDA	
Polychaeta	
Phyllodocida / Aphroditidae / ***Aphrodita* sp.** Likely to include *A. aculeate*. Flat, ovoid, scale worm that flushes with sediment. Iridescent body edge (setae) often visible. *n* (ind.): 2 (SSB) Range (mm): 61-76 (total length)	
Sabellida / **Sabellidae 2** Looks like *Myxicola infundibulum*. Tubeworm buried in sediment, crown of brown/purple tentacles visible, forming a characteristic funnel. Retracts when disturbed. *n* (ind.): 8 (SSB) Range (mm): 12-24 (crown diameter)	
Sabellida / **Serpulidae 1** Likely to include *Salmacina dysteri*, *Filograna implexa*. White (grey when dead), circular to ovoid, bushy colony of densely aggregated tubeworms (each 4-5 mm long, 0.5 mm diameter). *n* (ind.): 547 (GHF-1), 47 (GHF-2), 7 (SSB) Range (mm): 46-313 (colony diameter)	

ARTHROPODA	
Malacostraca / Decapoda / Anomura	
Cancridae / ***Cancer pagurus*** Wide crab with a smooth, reddish-brown, oval-shaped, 'piecrust'-edged, carapace, and two large black-tipped claw pincers. *n* (ind.): 1 (GHF-2) Range (mm): 173 (carapace width)	
Galatheidae / ***Munida* sp.** Likely to include *M. rugosa*, *M. sarsi*. Orange to reddish-brown lobster with two long white-tipped pincers. Abdomen held under the thorax. Close to rocks; may be hidden under rock or between crevices. *n* (ind.): 480 (GHF-1), 244 (GHF-2), 26 (SSB) Range (mm): 6-67 (carapace length)	
Lithodidae / ***Lithodes maja*** Large spiky crab with rather large and long legs around circular carapace. Close to rocks, often found beneath the tentacles of *Bolocera* sp. *n* (ind.): 14 (GHF-1), 3 (GHF-2) Range (mm): 27-76 (carapace width)	

Paguridae 1

Likely to include *Pagurus bernhardus*, *P. alatus*.
Reddish crab inhabiting a gastropod shell; body within the shell, head and large legs are visible at the free extremity.

n (ind.): 14 (GHF-1), 2 (GHF-2), 9 (SSB)
Range (mm): 16-64 (carapace width)

Paguridae 2

Likely to include *Pagurus prideaux*.
Crab inhabiting an anemone (*Adamsia palliata*); large head and legs are visible at the free extremity.

n (ind.): 625 (GHF-1), 47 (GHF-2), 63 (SSB)
Range (mm): 5-70 (carapace width)

Paguridae 3

Likely to include *Anapagurus laevis*, *A. hyndmanni*, *A. chiroacanthus*.
Very small crab inhabiting a small slender gastropod shell.

n (ind.): 144 (SSB)
Range (mm): 3-15 (carapace width)

Polybiidae / ***Liocarcinus* sp.**

Looks like *L. depurator*.
Small, light-orange crab, with tipped-black swimming legs at the posterior end of a carapace that is wider than long.

n (ind.): 9 (GHF-1), 3 (SSB)
Range (mm): 18-53 (carapace width)

Porcellanidae sp.

Looks like *Porcellana platycheles*.
Small crab with rather large pincer in comparison to body, round carapace, 5th pair of leg much reduced giving the appearance of only three pairs of walking legs.

n (ind.): 2 (GHF-1), 2 (SSB)
Range (mm): 19-36 (carapace width)

Malacostraca / Decapoda / Astacidea

Nephropidae / ***Nephrops norvegicus***

Slim orange-white lobster with two long and large pincers, two prominent black eyes, and at least two pairs of antennae often visible. Often buried in sediment; claws may be visible.

n (ind.): 4 (SSB)
Range (mm): 8-33 (carapace length)

Malacostraca / Decapoda / Brachyura

Goneplacidae / ***Goneplax rhomboides***

Orange crab with rectangular carapace. Males exhibit very long chelipeds with black-tipped pincers.

n (ind.): 45 (SSB)
Range (mm): 0-34 (carapace width)

Inachidae 1

Likely to include *Inachus dorsettensis*, *I. leptochirus*.
Small brownish spider crab with shorter legs than Inachidae 2, triangular-shaped carapace.

n (ind.): 39 (GHF-1), 1 (GHF-2)
Range (mm): 14-34 (carapace width)

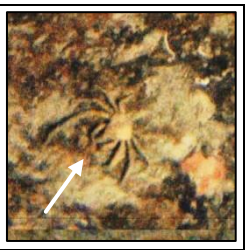

Inachidae 2

Likely to include *Macropodia linaresi*, *M. tenuirostris*.
Small brownish spider crab with longer, thinner, legs than Inachidae 1, triangular-shaped carapace.

n (ind.): 3 (GHF-1), 1 (GHF-2), 10 (SSB)
Range (mm): 8-21 (carapace width)

Leucosiidae / ***Ebalia* sp.**

Likely to include *E. granulosa*, *E. tumefacta*, *E. tuberosa*.
Small pinkish/orange diamond-shaped crab with rather long pincers by comparison to the body, carapace as wide as long.

n (ind.): 26 (SSB)
Range (mm): 6-18 (carapace width)

Brachyura 6

Likely a Pinnotheridae.
Small white crab with short pincers. Commensalism with various hosts, e.g. holothurians, urchins, molluscs. Note this may be a dead crab turned upside down; pea crabs are usually found on/in their host.

n (ind.): 2 (SSB)
Range (mm): 15-19 (carapace width)

Brachyura 7

Small crab with short slender legs.

n (ind.): 16 (SSB)
Range (mm): 5-23 (carapace width)

Malacostraca / Decapoda / Caridea

Caridea 1

Elongated, transparent to red shrimp with glowing eyes and long antennae.

n (ind.): 23 (SSB)
Range (mm): 36-79 (total length)

Caridea 2

Elongated, greyish small shrimp.

n (ind.): 97 (SSB)
Range (mm): 15-69 (total length)

BRYOZOA

Bryozoa 1

Likely to include *Parasmittina trispinosa*, *Escharoides coccinea*, *Schizomavella sarniensis*, *Cellepora pumicosa*.
Orange encrusting, irregular, patch growing on rocks.

n (ind.): 777 (GHF-1), 1423 (GHF-2), 110 (SSB)
Range (mm): 5-125 (colony diameter)

Bryozoa 5

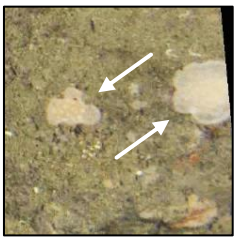

Looks like *Schizomavella linearis*.
White-pinkish (lightening in colour towards the edge) encrusting, circular but irregular, patch.

n (ind.): 6 (GHF-2), 11 (SSB)
Range (mm): 14-62 (colony diameter)

Bryozoa 6

Looks like *Cellaria* sp, *Omalosecosa ramulosa*.
Bushy yellowish branching colony, with short thick, dichotomic, branches, growing in all directions.

n (ind.): 23 (GHF-2), 5 (SSB)
Range (mm): 10-95 (colony diameter)

Gymnolaemata / Cheilostomatida

Bitectiporidae / ***Pentapora foliacea***

Orange-brownish (pale when dead), roundish, leaf-like colony. Honeycomb structure, with sheets wavy and convoluted. Often close to rocks.

n (ind.): 11 (GHF-1), 3 (GHF-2)
Range (mm): 24-303 (colony diameter)

Bryocryptellidae / ***Porella* sp.**

Looks like to include *P. compressa*.
Bushy colony with flattened branches growing in all dimensions, hard like a stony coral, variable in colour.

n (ind.): 1504 (GHF-1), 763 (GHF-2), 44 (SSB)
Range (mm): 9-203 (colony height)

Phidoloporidae / ***Reteporella* sp.**

Small white bushy colony formed by a very thin network of tiny zoids organised in fine reticulated, wavy, jagged-looking plates.

n (ind.): 1325 (GHF-2), 4 (SSB)
Range (mm): 9-101 (colony height)

CHORDATA	
Ascidiacea	
Aplousobranchia / Diazonidae / ***Diazona violacea*** Large globular colony composed of several transparent 'tubes' with visible white ring at the end. *n* (ind.): 2 (GHF-2) Range (mm): not measured	
Actinopterii / Clupeiforme	
Clupeiforme 2 Likely to include *Engraulis encrasicolus*. Slender, streamlined, fish, one dorsal fin, whitish-grey, reflective eyes on top of the head, apparent red mark behind eyes. *n* (ind.): 71 (GHF-2), 48 (SSB) Range (mm): 31-120 (total length)	
Clupeiforme 12 Likely to include *Sprattus sprattus*, *Clupea harengus*. Thin, silvery fish. *n* (ind.): 3 (SSB) Range (mm): 72-90 (total length)	
Actinopterii / Perciforme	
Perciforme 3 Looks like a Gobiidae. Elongated fish, whitish/pinkish to grey, eyes on the side of the head. *n* (ind.): 2 (GHF-2), 74 (SSB) Range (mm): 54-252 (total length)	
Perciforme 7 Very small fish, round head, eyes on top of head. *n* (ind.): 7 (SSB) Range (mm): 25-58 (total length)	
Perciforme 10 Small slender fish. *n* (ind.): 19 (GHF-1), 10 (SSB) Range (mm): 20-50 (total length)	

Callionymidae / ***Callionymus* sp.**

Likely to include *C. maculatus*,*C. reticulatus*, *C. lyra*.
Flattened fish, triangular-shaped head with eyes close together visible on top, slender towards the tail. Large pelvic fins. Small (juvenile) specimens may be confused with gobies.

n (ind.): 22 (GHF-1), 1 (GHF-2), 54 (SSB)
Range (mm): 22-297 (total length)

Labridae 6

Likely to include *Centrolabrus exoletus*, *Ctenolabrus rupestris*.
Small orange to reddish fish with slender body and pointed snout, relatively large eyes on the side.

n (ind.): 3 (GHF-2)
Range (mm): 80-150 (total length)

Actinopterii / Gadiforme

Gadidae sp.

Elongated pinkish fish, slender towards the tail, three obvious dorsal fins, and eyes on the side.

n (ind.): 514 (GHF-1), 53 (SSB)
Range (mm): 50-550 (total length)

Gadidae / ***Gadus morhua***

Large chunky fish, slender towards the tail, three dorsal fins.

n (ind.): 1 (GHF-1)
Range (mm): 427 (total length)

Gadidae 5

Likely to include *Melanogrammus aeglefinus*, *Merlangius merlangus*, *Trisopterus* sp.
Elongated fish, two black spots behind pectoral fins.

n (ind.): 1 (GHF-2), 5 (SSB)
Range (mm): 34-275 (total length)

Gadidae 9

Looks like *Merluccius merluccius*.
Large elongated fish, slender towards the tail, 2nd dorsal fin longer than 1st one, light in colour to grey, appears with stripes or uniform, eyes on the side of the head.

n (ind.): 2 (GHF-1), 3 (GHF-2), 3 (SSB)
Range (mm): 160-660 (total length)

Lotidae / ***Gaidropsarus vulgaris***

Elongated fish, yellow-beige with brown spots, round pectoral fins.

n (ind.): 2 (GHF-1)
Range (mm): 26-91 (total length)

Lotidae / ***Molva molva***

Large elongated fish, slender towards the tail, 2nd dorsal fin longer than 1st one, grey, 2 barbells in front of mouth.

n (ind.): 1 (SSB)
Range (mm): not measured

Actinopterii / Lophiiforme

Lophiidae / ***Lophius piscatorius***

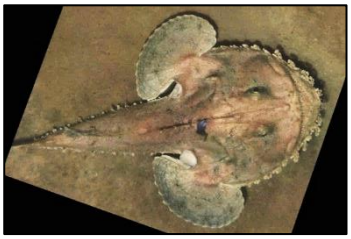

Large flattened fish; round body with slender tail, hemispherical pectoral fins, eyes on top of the head.

n (ind.): 4 (SSB)
Range (mm): 108-1046(total length)

Actinopterii / Scorpaeniforme

Triglidae 1

Likely to include *Chelidonichthys cuculus*, *Trigla lyra*.
Small elongated red fish, slender towards the tail, large round pectoral fins, barbells in front of pectoral fins, eyes on side of the head, stripes on the body.

n (ind.): 2 (GHF-2), 2 (SSB)
Range (mm): 114-460 (total length)

Triglidae 2

Looks like *Chelidonichthys obscurus*.
Small elongated reddish fish, slender towards the tail, large round blue-grey pectoral fins.

n (ind.): 1 (GHF-2)
Range (mm): 21-162 (total length)

Triglidae 3

Looks like *Eutriglia gurnardus*.
Small elongated fish, slender towards the tail, large round pectoral fins, barbells in front of pectoral fins, eyes on side of the head.

n (ind.): 2 (SSB)
Range (mm): 16-225 (total length)

Actinopterii / Pleuronectiforme

Pleuronectidae / ***Hippoglossoides platessoides***

Beige right-eyed flatfish, pectoral fins all around body, relatively straight lateral line.

n (ind.): 13 (GHF-1), 66 (SSB)
Range (mm): 12-471 (total length)

Pleuronectidae 5

Likely to include *Microstomus kitt*, *Limanda limanda*.
Large brownish right-eyed flatfish with small pointy head, pectoral fins all around body, round tail.

n (ind.): 2 (GHF-2), 4 (SSB)
Range (mm): 77-310 (total length)

Scophthalmidae / ***Lepidorhombus whiffiagonis***

Left-eyed flatfish with pointy head, pectoral fins all around body, large triangular tail, appears with either straps, spots, or somewhat uniform.

n (ind.): 37 (GHF-1), 3 (GHF-2), 3 (SSB)
Range (mm): 25-321 (total length)

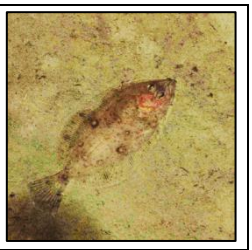

Soleidae / ***Microchirus variegatus***

Stripy beige slender flatfish, round tail.

n (ind.): 13 (GHF-1)
Range (mm): 22-155 (total length)

Elasmobranchii / Carcharhiniforme

Schyliorhinidae / ***Scyliorhinus canicula***

Long catshark, slender towards the tail, eyes on the side of round head, pointy pectoral fins with brown spots, brown spots on body.

n (ind.): 2 (GHF-1), 1 (GHF-2)
Range (mm): 75-421 (total length)

Pentanchidae / ***Galeus* sp.**

Looks like *G. melastomus*.

n (ind.): 1 (GHF-1)
Range (mm): 727 (total length)

Elasmobranchii / Rajiforme

Rajidae / ***Leucoraja naevus***

Beige ray with 2 obvious spots on top of the body.

n (ind.): 5 (GHF-1), 1 (GHF-2)
Range (mm): 80-380 (wings breadth)

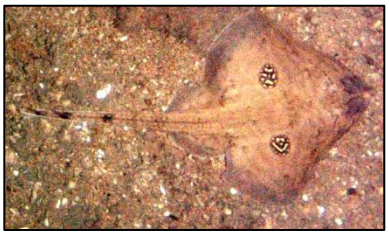

Rajidae sp.

Looks like *Dipturus* sp.

n (ind.): 2 (GHF-1)
Range (mm): 80-380 (wings breadth)

CNIDARIA	
Cnidaria 1 Looks like a hydroid. Plumose cnidarian; thin feather-like stalk. *n* (ind.): 173 (SSB) Range (mm): 11-118 (stalk height)	
Cnidaria 2 Looks like a pennatulid. Plumose cnidarian, transparent erect specimen, white central stalk may be visible. *n* (ind.): 374 (SSB) Range (mm): 3-84 (stalk height)	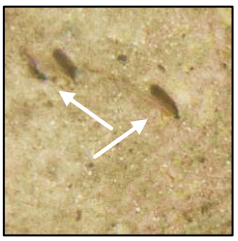
Cnidaria 3 Looks like a pennatulid. Plumose cnidarian with ≥ 2 thin erect stalks. *n* (ind.): 64 (SSB) Range (mm): 4-97 (stalk height)	
Anthozoa	
Anthozoa 1 Small brown anemone with multiple long tentacles. *n* (ind.): 35 (GHF-1), 2 (GHF-2), 7 (SSB) Range (mm): 3-43 (oral disc diameter)	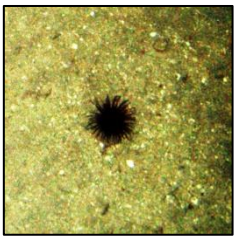
Anthozoa 3 Small flattened anemone with dark disc and white edges. *n* (ind.): 163 (GHF-1), 3 (GHF-2), 7 (SSB) Range (mm): 4-68 (oral disc diameter)	
Anthozoa 5 Looks like *Sagartia* sp., *Actinothoe sphyrodeta*. 'Flat' anemone with red disk and white tentacles (up to 100-200, 3-4 cm in length). *n* (ind.): 49 (GHF-1), 7 (GHF-2) Range (mm): 12-236 (oral disc diameter)	
Anthozoa 6 Light-coloured anemone with pinkish oral disk and translucent, chubby, tentacles. *n* (ind.): 22 (GHF-1) Range (mm): 17-39 (oral disc diameter)	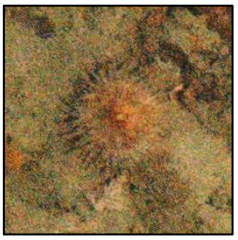

Anthozoa 8

Small anemone buried in sediment with eight long chunky, striped, tentacles.

n (ind.): 35 (GHF-1), 2 (SSB)
Range (mm): 8-38 (oral disc diameter)

Anthozoa 16

Small (cup coral?) anemone with white disc and brown tentacles.

n (ind.): 32 (GHF-1), 6 (SSB)
Range (mm): 1-43 (oral disc diameter)

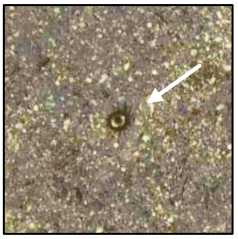

Anthozoa 19

Looks like *Capnea sanguinea*, *Aureliania* sp.
'Flat' red or orange anemone with very short tentacles.

n (ind.): 2 (GHF-1)
Range (mm): 36-57 (oral disc diameter)

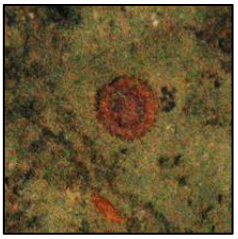

Anthozoa 24

Anemone with fine, long, tentacles.

n (ind.): 6 (GHF-1)
Range (mm): 28-49 (oral disc diameter)

Anthozoa 25

Bulbous transparent anemone with short tentacles.

n (ind.): 24 (SSB)
Range (mm): 3-19 (oral disc diameter)

Anthozoa 34

Looks like *Halcampoides* sp.
Small translucent anemone buried in sediment with 12 long tentacles.

n (ind.): 52 (GHF-1), 278 (SSB)
Range (mm): 1-54 (oral disc diameter)

Anthozoa 35

Small translucent anemone buried in sediment with very long, fine, tentacles.

n (ind.): 4 (SSB)
Range (mm): 2-13 (oral disc diameter)

Anthozoa 39 Anemone with defined edge and short tentacles, five white radii originating from the centre may be visible. *n* (ind.): 26 (GHF-1), 2 (SSB) Range (mm): 5-53 (oral disc diameter)	
Anthozoa 40 Looks like *Epizoanthus couchii*. Small, white, (solitary zoanthid?) with tentacles about as long as oral disc diameter. *n* (ind.): 4 (GHF-2) Range (mm): 12-14 (oral disc diameter)	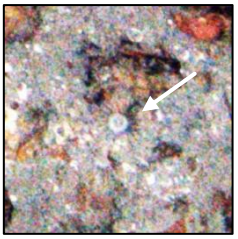
Anthozoa / Hexacorallia / Actinaria	
Actiniidae / ***Bolocera* sp.** Likely to include *B. tuediae*. Large red anemone with long, bulbous white-tipped tentacles. *n* (ind.): 251 (GHF-1), 67 (GHF-2), 3 (SSB) Range (mm): 11-118 (oral disc diameter)	
Actiniidae / ***Urticina* sp.** Likely to *U. felina*. Large anemone, pink-orange disc and transparent short tentacles with white base, radial striations visible. *n* (ind.): 27 (GHF-1), 4 (GHF-2) Range (mm): 21-116 (oral disc diameter)	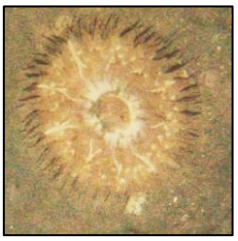
Hormathiidae / **Hormathiid sp.** Likely to include *Actinauge* sp. Anemone with short pinkish tentacles and bulbous column. *n* (ind.): 3 (GHF-1), 3 (GHF-2), 1 (SSB) Range (mm): 4-44 (oral disc diameter)	
Metridiidae / ***Metridium* sp.** Likely to include *M. senile* Very tall and large white anemone, fluffy appearance when tentacles extended. *n* (ind.): 1 (SSB) Range (mm): 79 (oral disc diameter)	
Anthozoa / Hexacorallia / Scleractinia	
Caryophylliidae / ***Caryophyllia smithii*** Small cup coral, rather ovoid, red-orange-yellow. *n* (ind.): 379 (GHF-1), 61 (GHF-2), 15 (SSB) Range (mm): 2-25 (oral disc diameter)	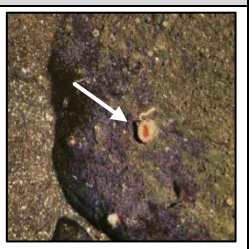

Anthozoa / Hexacorallia / Zoantharia	
Parazoanthidae / ***Parazoanthus* sp.** Likely to include *P. anguicomus*, *P. axinellae*. White colonial zoanthids (up to 25 mm in height). *n* (ind.): 1629 (GHF-1), 701 (SSB) Range (mm): 14-540 (colony diameter)	
Anthozoa / Ceriantharia	
Cerianthid 1 Looks like *Arachnanthus sarsi*. Tube anemone with (~30) long tentacles in single series. *n* (ind.): 181 (GHF-1), 10 (SSB) Range (mm): 3-42 (oral disc diameter)	
Cerianthid 3 Looks like *Pachycerianthus* sp. Tube anemone with long white tentacles in two series. *n* (ind.): 16 (GHF-1), 8 (GHF-2) Range (mm): 3-78 (oral disc diameter)	
Certianthid 7 Looks like *Cerianthus lloydii*. Small tube anemone buried in sediment with >1 row of long fine tentacles. *n* (ind.): 19 (SSB) Range (mm): 24-69 (oral disc diameter)	
Anthozoa / Octocorallia	
Alcyonacea / Alcyoniidae / ***Alcyonium digitatum*** White soft-coral colony with translucent polyps. *n* (ind.): 2 (SSB) Range (mm): 51-61 (colony height)	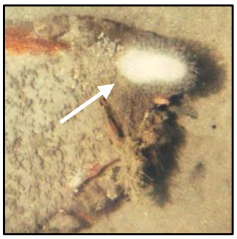
Alcyonacea / Plexauridae / ***Swiftia* sp.** Likely to include *S. pallida*. Small white-yellowish branching colony. *n* (ind.): 37 (GHF-2), 3 (SSB) Range (mm): 18-73 (colony height)	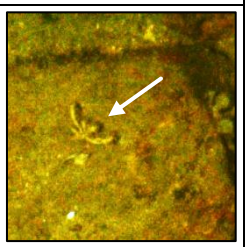
Pennatulacea / Virgulariidae / ***Virgularia* sp.** Likely to include *V. mirabilis*. Elongated pinkish colony with obvious white stalk. *n* (ind.): 7 (SSB) Range (mm): 12-37 (stalk height)	

Hydrozoa

Hydrozoa 1

Looks like *Abietinaria abietina*.
Brown branching hydroid.

n (ind.): 16 (GHF-1), 2 (GHF-2), 24 (SSB)
Range (mm): 4-222 (colony height)

ECHINODERMATA

Asteroidea

Asteroidea 1

Looks like *Peltaster placenta*, *Asterina gibbosa*.
White cushion star, red on the edge.

n (ind.): 17 (GHF-1)
Range (mm): 8-101 (longest arm to opposite edge of disc)

Asteroidea 2

Looks like *Henricia* sp.
Rather small orange to red sea star with 5 slender arms.

n (ind.): 21 (GHF-2), 9 (SSB)
Range (mm): 7-127 (longest arm to opposite edge of disc)

Asteroidea 7

Looks like *Leptasterias muelleri*.
Small asteroid with purple-coloured central disk and whitish arms.

n (ind.): 16 (GHF-1), 9 (GHF-2), 430 (SSB)
Range (mm): 1-280 (longest arm to opposite edge of disc)

Forcipulatida / Asteriidae / ***Asterias rubens***

Fat sea star, orangish in colour, striation from centre of the disc to tip of each arm often visible, disc often quite bulbous, arms tapering at the end.

n (ind.): 16 (GHF-1), 1 (GHF-2), 1 (SSB)
Range (mm): 1-280 (longest arm to opposite edge of disc)

Forcipulatida / Asteriidae / ***Marthasterias glacialis***

Five long arms around small disc, spines along arms, striation from centre of the disc to tip of each arm often visible.

n (ind.): 2 (GHF-1)
Range (mm): 1-280 (longest arm to opposite edge of disc)

Forcipulatida / Stichasteridae / ***Stichastrella rosea***

Five long tapering arms around small disc, spines along arms.

n (ind.): 139 (GHF-1), 14 (GHF-2), 11 (SSB)
Range (mm): 14-112 (longest arm to opposite edge of disc)

Paxillosida / Astropectinidae / ***Astropecten irregularis*** Flattened sea star with stiff angular arms, tip of the arms often visible as purple, spines may be visible on the edge of the arms. *n* (ind.): 5 (GHF-1), 4 (GHF-2), 49 (SSB) Range (mm): 3-125 (longest arm to opposite edge of disc)	
Valvatida / Solasteridae / ***Crossaster papposus*** 12 to 14 arms, mostly red, large disc. *n* (ind.): 1 (GHF-1), 2 (GHF-2), 1 (SSB) Range (mm): 6-167 (longest arm to opposite edge of disc)	
Valvatida / Poraniidae / ***Porania pulvillus*** Red cushion star. *n* (ind.): 1124 (GHF-1), 321 (GHF-2), 9 (SSB) Range (mm): 8-101 (longest arm to opposite edge of disc)	
Crinoidea	
Comatulida / Antedonidae / ***Antedon* sp.** Likely to include *A. bifida*, *A. petasus*. Long thin arms around very small body. *n* (ind.): 58 (GHF-1), 3 (GHF-2), 38 (SSB) Range (mm): 9-65 (longest arm to opposite edge of disc)	
Echinoidea	
Echinoidea 1 Likely to include *Acrocnida brachiate*, *Amphiura chiajei*, *Amphiura filiformis*. Rather small sea urchin, pink with long white spines. *n* (ind.): 15 (GHF-1), 2 (SSB) Range (mm): 5-79 (test diameter)	
Camarodonta / Echinidae / ***Echinus esculentus*** Rather big sea urchin, pink with white spines. *n* (ind.): 128 (GHF-1), 28 (GHF-2), 4 (SSB) Range (mm): 10-100 (test diameter)	
Spatangoida sp. Likely to include *Echinocardium flavescens, E. cordatum, Brissopsis lyrifera*. Flattened white heart-shaped sea urchin. *n* (ind.): 4 (SSB) Range (mm): 10-57 (test diameter)	
Holothuroidea	

Holothuroidea 1 Looks like *Mesothuria intestinalis*. Holothurian covered in sediment and small debris. *n* (ind.): 2 (GHF-2) Range (mm): 27-416 (total length)	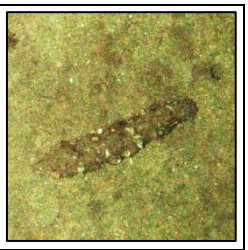
Ophiuroidea	
Ophiuroidea 1 Likely to includes *Ophiura ophiura*, *O. sarsii*, *O. albida*. Orange brittle star. *n* (ind.): 207 (GHF-1), 99 (GHF-2), 167 (SSB) Range (mm): 3-37 (longest arm to opposite edge of disc)	
Ophiuroidea 2 Likely to include *Ophiocomina nigra*, *Ophiothrix fragilis*. Black brittle star. *n* (ind.): 13 (GHF-1), 6 (GHF-2) Range (mm): 5-11 (longest arm to opposite edge of disc)	
Ophiuroidea 3 Small ophiuroid light in colour in very long thin arms. *n* (ind.): 1 (SSB) Range (mm): 2-14 (longest arm to opposite edge of disc)	

MOLLUSCA

Bivalvia

Pterioida / Pinidae / ***Atrina fragilis***

Buried bivalve, opened at the extremity above the sediment, showing two ovoid black holes.

n (ind.): 7 (SSB)
Range (mm): 40-91 (diameter of opening)

Cephalopoda / Octopoda

Octopodidae / ***Eledone cirrhosa***

Brown octopus with white spots.

n (ind.): 2 (GHF-1), 1 (SSB)
Range (mm): 51-111 (mantle length)

Octopodidae / ***Eledone* 2**

Uniform brown octopus.

n (ind.): 3 (GHF-1), 2 (GHF-2)
Range (mm): 42-140 (mantle length)

Cephalopoda / Teuthida

Teuthida sp.

Likely to include *Loligo vulgaris*, *Illex illecebrosus*, *I. coindetii*, *Alloteuthis subulata*, *A. media*, *Todaropsis eblanae*.
Transparent squid with long mantle.

n (ind.): 4 (GHF-2), 3 (SSB)
Range (mm): 37-102 (mantle length)

Cephalopoda / Sepiida

Sepiida sp.

Likely to include *Sepiola atlantica*, *Sepietta oweniana*, *Sepia officinalis*, *S. orbignyana*, *S. elegans*.
Small black-brown to pale cuttlefish. Mantle length up to 6 cm.

n (ind.): 4 (GHF-2), 3 (SSB)
Range (mm): 8-46 (mantle length)

PORIFERA	
Desmospongiae	
Axinellida / **Axinellidae sp.** Including *Phakellia ventilabrum*, *Axinella infundibuliformis*. Yellow cup sponge, comes in various shapes. *n* (ind.): 2457 (GHF-1), 715 (GHF-2), 9 (SSB) Range (mm): 8-184 (diameter of the cup)	
Porifera 2 Branching brown to grey sponge. *n* (ind.): 403 (GHF-1), 54 (GHF-2) Range (mm): 25-276 (longest axis)	
Porifera 3 Encrusting yellow-beige sponge. *n* (ind.): 23 (GHF-1), 9 (GHF-2) Range (mm): 46-250 (longest axis)	
Porifera 20 Looks like *Suberites* sp. Grey spherical sponge with visible holes. *n* (ind.): 116 (GHF-1), 15 (GHF-2), 2 (SSB) Range (mm): 14-82 (longest axis)	
Porifera 21 Looks like *Suberites* sp. White encrusting sponge. *n* (ind.): 3 (GHF-2), 1 (SSB) Range (mm): 29-85 (longest axis)	
Porifera 22 Looks like *Quasillina* sp. Small cylindrical sponge with visible hole at one end. *n* (ind.): 2 (GHF-1) Range (mm): 38-40 (longest axis)	
Porifera 23 Looks like *Polymastia* sp. Yellow spiny round sponge. *n* (ind.): 362 (GHF-1), 53 (GHF-2), 1 (SSB) Range (mm): 16-112 (longest axis)	

Porifera 24

Looks like *Polymastia* sp.
Grey spiny round sponge.

n (ind.): 7 (GHF-1), 1 (GHF-2)
Range (mm): 41-68 (longest axis)

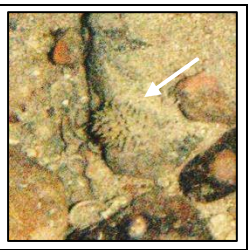

Porifera 25

Looks like *Myxilla* sp.
Encrusting beige sponge with multiple holes.

n (ind.): 3 (GHF-1)
Range (mm): 53-105 (longest axis)

Porifera 26

Encrusting yellow specimen.

n (ind.): 206 (GHF-2), 23 (SSB)
Range (mm): 8-104 (longest axis)

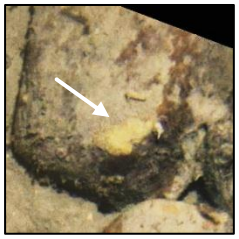

Porifera 27

Likely to include *Halicondria* sp., *Terpios fugax*.
Encrusting blue sponge.

n (ind.): 41 (GHF-2), 5 (SSB)
Range (mm): 7-191 (longest axis)

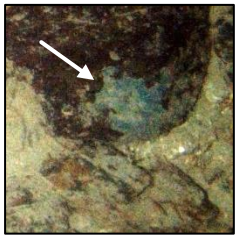

F.2 Porcupine Abyssal Plain sustained observatory

ANNELIDA	
Polychaeta	
Phyllodocida / Aphroditidae / ***Laetmonice* sp.** Flat, ovoid, scale worm with rather long chaetae, brown-grey in colour. *n* (ind.): 5 Range (mm): 38-57 (total length)	

ARTHROPODA	
Hexanauplia / Cirripedia	
Cirripedia sp. Highly modified crab with laterally flattened carapace attached to a peduncle. *n* (ind.): 3 Range (mm): 35-41 (rostral length)	
Pycnogonida	
Pantopoda / Family Collosendeidae / ***Colossendeis* sp.** Includes *C. colossea*, *C. minor*. Spider crab yellow-orange in colour with very fine long legs. *n* (ind.): 7 Range (mm): 107-145 mm (leg length)	
Malacostraca / Decapoda	
Munidopsidae / ***Munidopsis crassa*** White squat lobster with elongated thin rostrum, spiny tooth-edged carapace, large and long spiny legs, no hook on the tail. *n* (ind.): 9 Range (mm): 39-75 (carapace length)	
Munidopsidae / ***Munidopsis parfaiti*** White squat lobster with large-based rostrum, knobbly smooth-edged carapace, small smooth legs, hooks on tail. *n* (ind.): 2 Range (mm): 22-46 (carapace length)	

Aristeidae sp.

Includes *Cerataspis monstruosus*.
Red shrimp with prominent crenulated rostrum (adult stage).

n (ind.): 9
Range (mm): 47-92 (carapace length)

Polychelidae / ***Willemoesia leptodactyla***

Lobster-like crustacean, short rostrum.

n (ind.): 3
Range (mm): 45-112 (carapace length)

CNIDARIA

Anthozoa / Actinaria

Hormathiidae / ***Actinauge abyssorum***

Knobbly column (inconsistent pattern). Specimen attach to hard substrates (rock, clinker, litter, stalks, sponge spicules, etc.), yielding deformed pedal disk.

n (ind.): 14
Range (mm): 11-26 (column diameter)

Hormathiidae / ***Amphianthus bathybium***

Small white-pinkish specimen with knobbly column (vertical arrangement of small knobbles). Specimen attach to hard substrates (rock, clinker, litter, stalks, sponge spicules, tube worms, etc.), yielding deformed pedal disk.

n (ind.): 15
Range (mm): 9-15 (column diameter)

Iosactinidae / ***Iosactis vagabunda***

Small elongated specimen with smooth column.

n (ind.): 7
Range (mm): 4-8 (column diameter)

Kadosactinidae / ***Kadosactis sulcata***

Small white specimen with conical knobbly column.

n (ind.): 2
Range (mm): 22-30 (column diameter)

Actinostolidae / ***Parasicyonis biotrans***

Large white specimen with smooth, wrinkled column.

n (ind.): 5
Range (mm): 26-80 (column diameter)

Anthozoa / Pennatulacea

Umbellulidae / ***Umbellula monocephalus***

Light-colour branching stalk increasing in width with height, 8 branching arms.

n (ind.): 4
Range (mm): 137-507 (column diameter)

ECHINODERMATA

Asteroidea

Paxillosida / Porcellanasteridae / ***Dytaster grandis grandis***

Orange specimen, spiny arms longer than disk diameter.

n (ind.): 7
Range (mm): 56-161 (longest arm to opposite edge of disc)

Paxillosida / Porcellanasteridae / ***Hyphalaster inermis***

Light colour asteroid with five thin arms, no spines on the arms. Similar to *Styracaster* sp. which has spines along the arms (mostly towards the base).

n (ind.): 13
Range (mm): 19-81 (longest arm to opposite edge of disc)

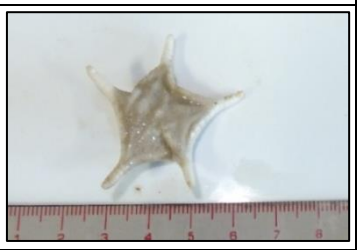

Holothuroidea

Elasipodida / Deimatidae / ***Deima validum validum***

Beige/light pink, body flattened oval in shape, 3 sets of large dorsal papilla along length of body, corresponding papillae extending to the side, a pair of papillae extend from the anterior and posterior.

n (ind.): 3
Range (mm): 99-106 (total length)

Molpadida / Molpadiidae/ ***Molpadia blakei***

Purple(ish) specimen, with a little spine at posterior end.

n (ind.): 3
Range (mm): 87-94 (total length)

Aspidochirotida / Synallactidae / ***Molpadiodemas villosus***

The small specimens can be similar to *Pseudostichopus aemulatus*; however, these are more 'colourful' on the underside, and depends on the tube feet arrangement.

n (ind.): 17
Range (mm): 49-228 (total length)

Elasipodida / Deimatidae / ***Oneirophanta mutabilis mutabilis***

White elongated specimen with several papillae on sides and at both extremities, as well as several mouth tentacles. Often in association with a gastropod parasite at the posterior end.

n (ind.): 21
Range (mm): 49-155 (total length)

Aspidochirotida / Synallactidae/ ***Paroriza prouhoi***

'Spiky' brownish specimen often found in association with *Sicyopus commensalis* (located at anterior end of the cucumber).

n (ind.): 7
Range (mm): 161-257 (total length)

Elasipodida / Psychropotidae / ***Psychropotes longicauda***

Purple holothuroid with tail at posterior end.

n (ind.): 22
Range (mm): 64-345 (total length)

Aspidochirotida / Synallactidae / ***Pseudostichopus aemulatus***

Generally small specimen often found in association with foraminifera. Similar to small specimens of *Molpadiodemas villosus* but more uniform in colour.

n (ind.): 7
Range (mm): 35-105 (total length)

Appendix G:

Abundance, biomass, and respiration flux data from the four study sites

This appendix contains tables body-size-class data of numerical density (N_i, number of ind. m^{-2}), estimated biomass- (W_i in g wwt m^{-2}), and estimated respiration flux (B_i in mg C m^{-2} d^{-1}) of benthic megafauna (≥ 1 cm body size) at the four study sites assessed in this Ph.D. thesis. The Greater Haig Fras (GHF) marine conservation zone and the UK-NERC Shelf-Sea Biogeochemistry (SSB) study area are two shelf-sea sites (c. 100 m water depth) located in the Celtic Sea, NE Atlantic. The Porcupine Abyssal Plain (PAP) sustained observatory and the Clarion-Clipperton Zone are two deep-sea sites (c. 4850 m and c. 4150 m water depth, respectively) located in the NE Atlantic and in the NE Pacific Ocean, respectively. Individual biomass data were obtained from photographic analysis using two approaches, a length-weight relationship (LWR) method and a generalised volumetric method (GVM), as indicated for each site in the table legend. Size-class respiration flux was calculated as described in the table legends. Similar data (N_i, W_i, B_i) on invertebrates macrobenthos (≥ 250 µm) at PAP, and on xenophyophores (‘giant’ protozoan Foraminifera) at CCZ, were also analysed. All the literature references cited can be found in the references list of the Ph.D. thesis. A list of data tables can be found on the following page.

List of tables

G.1 Greater Haig Fras marine conservation zone

Table G.1. Invertebrate megabenthos standing stocks at Greater Haig Fras marine conservation zone in 2012. Geometric size-class data of numerical density (N_i, number of ind. m^{-2}), estimated biomass- (W_i in g wwt m^{-2}), and estimated respiration flux (B_i in mg C m^{-2} d^{-1}). Individual biomass was derived from existing length-weight relationships (LWRs) available in literature (Benoist et al. 2019a and references therein; chapter 3 section 3.4; appendix A). Size-class estimated respiration flux was calculated from individual metabolic rate (chapter 1 equation 1.1) using Hemmingsen's (1960) equation for standard metabolic rate with site-specific temperature-correction (i.e. 10 °C; Gillooly et al. 2001), and multiplied by size-class abundance (N_i) (section 3.5). The asterisk indicates the start of the quantitative right-hand side of the spectrum (Bett 2013). Consecutive shaded rows indicate merged data to ensure a minimum of 10 individuals per body-size class. Total seabed area analysed was 19,223 m^2.

Size class	Geometric body size (g wwt)	N_i (ind. m^{-2})	W_i (g wwt m^{-2})	B_i (mg C m^{-2} d^{-1})
13	7.81×10^{-2}	1.04×10^{-4}	6.45×10^{-6}	1.04×10^{-5}
14	1.10×10^{-1}	1.04×10^{-4}	1.06×10^{-5}	1.34×10^{-5}
15	1.56×10^{-1}	2.60×10^{-4}	3.59×10^{-5}	4.36×10^{-5}
16	2.21×10^{-1}	3.12×10^{-4}	5.91×10^{-5}	6.78×10^{-5}
17	3.13×10^{-1}	5.20×10^{-4}	1.43×10^{-4}	1.47×10^{-4}
18	4.42×10^{-1}	8.32×10^{-4}	3.15×10^{-4}	3.04×10^{-4}
19	6.25×10^{-1}	2.18×10^{-3}	1.14×10^{-3}	1.04×10^{-3}
20	8.84×10^{-1}	2.29×10^{-3}	1.73×10^{-3}	1.41×10^{-3}
21	1.25×10^{0}	6.09×10^{-3}	6.58×10^{-3}	4.86×10^{-3}
22	1.77×10^{0}	1.13×10^{-2}	1.74×10^{-2}	1.17×10^{-2}
23	2.50×10^{0}	1.48×10^{-2}	3.13×10^{-2}	1.99×10^{-2}
24*	3.54×10^{0}	2.15×10^{-2}	6.36×10^{-2}	3.75×10^{-2}
25	5.00×10^{0}	1.52×10^{-2}	6.40×10^{-2}	3.44×10^{-2}
26	7.07×10^{0}	1.35×10^{-2}	8.01×10^{-2}	3.97×10^{-2}
27	1.00×10^{1}	1.41×10^{-2}	1.18×10^{-1}	5.37×10^{-2}
28	1.41×10^{1}	1.50×10^{-2}	1.82×10^{-1}	7.42×10^{-2}
29	2.00×10^{1}	2.11×10^{-2}	3.67×10^{-1}	1.35×10^{-1}
30	2.83×10^{1}	1.88×10^{-2}	4.42×10^{-1}	1.56×10^{-1}
31	4.00×10^{1}	1.25×10^{-2}	4.40×10^{-1}	1.35×10^{-1}
32	5.66×10^{1}	6.66×10^{-3}	3.16×10^{-1}	9.31×10^{-2}
33	8.00×10^{1}	4.94×10^{-3}	3.37×10^{-1}	8.97×10^{-2}
34	1.13×10^{2}	4.27×10^{-3}	4.07×10^{-1}	1.00×10^{-1}
35	1.60×10^{2}	3.23×10^{-3}	4.37×10^{-1}	9.85×10^{-2}
36	2.26×10^{2}	3.28×10^{-3}	6.27×10^{-1}	1.30×10^{-1}
37	3.20×10^{2}	1.98×10^{-3}	5.31×10^{-1}	1.02×10^{-1}
38	4.53×10^{2}	9.36×10^{-4}	3.74×10^{-1}	6.24×10^{-2}
39	6.40×10^{2}	6.76×10^{-4}	3.67×10^{-1}	5.85×10^{-2}
40	9.05 × 102	3.12×10^{-4}	2.25×10^{-1}	3.20×10^{-2}
41	1.28×10^{3}	2.60×10^{-4}	2.65×10^{-1}	3.46×10^{-2}
42	1.81×10^{3}	-	-	-
43	2.56×10^{3}	5.20×10^{-5}	1.12×10^{-1}	1.16×10^{-2}
44	3.62×10^{3}	1.04×10^{-4}	3.09×10^{-1}	3.02×10^{-2}

Table G.2. Invertebrate megabenthos and demersal fish standing stocks at Greater Haig Fras marine conservation zone in 2012. Geometric size-class data of numerical density (N_i, number of ind. m^{-2}), estimated biomass- (W_i in g wwt m^{-2}), and estimated respiration flux (B_i in mg C m^{-2} d^{-1}). Individual biomass was derived from existing length weight relationships (LWRs) available in literature (Benoist et al. 2019a and references therein; chapter 3 section 3.4; appendix A). Size-class estimated respiration flux was calculated from individual metabolic rate (chapter 1 equation 1.1) using Hemmingsen's (1960) equation for standard metabolic rate with site-specific temperature-correction (i.e. 10 °C; Gillooly et al. 2001), and multiplied by size-class abundance (N_i) (section 3.5). The asterisk indicates the start of the quantitative right-hand side of the spectrum (Bett 2013). Consecutive shaded rows indicate merged data to ensure a minimum of 10 individuals per body-size class. Total seabed area analysed was 19,223 m^2.

Size class	Geometric body size (g wwt)	N_i (ind. m^{-2})	W_i (g wwt m^{-2})	B_i (mg C m^{-2} d^{-1})
13	7.81×10^{-2}	1.04×10^{-4}	6.45×10^{-6}	1.04×10^{-5}
14	1.10×10^{-1}	1.04×10^{-4}	1.06×10^{-5}	1.34×10^{-5}
15	1.56×10^{-1}	2.60×10^{-4}	3.59×10^{-5}	4.36×10^{-5}
16	2.21×10^{-1}	3.12×10^{-4}	5.91×10^{-5}	6.78×10^{-5}
17	3.13×10^{-1}	5.20×10^{-4}	1.43×10^{-4}	1.47×10^{-4}
18	4.42×10^{-1}	8.32×10^{-4}	3.15×10^{-4}	3.04×10^{-4}
19	6.25×10^{-1}	2.24×10^{-3}	1.16×10^{-3}	1.06×10^{-3}
20	8.84×10^{-1}	2.39×10^{-3}	1.81×10^{-3}	1.47×10^{-3}
21	1.25×10^{0}	6.14×10^{-3}	6.63×10^{-3}	4.90×10^{-3}
22	1.77×10^{0}	1.15×10^{-2}	1.77×10^{-2}	1.20×10^{-2}
23	2.50×10^{0}	1.55×10^{-2}	3.27×10^{-2}	2.08×10^{-2}
24*	3.54×10^{0}	2.16×10^{-2}	6.40×10^{-2}	3.77×10^{-2}
25	5.00×10^{0}	1.53×10^{-2}	6.45×10^{-2}	3.46×10^{-2}
26	7.07×10^{0}	1.40×10^{-2}	8.29×10^{-2}	4.11×10^{-2}
27	1.00×10^{1}	1.44×10^{-2}	1.20×10^{-1}	5.48×10^{-2}
28	1.41×10^{1}	1.55×10^{-2}	1.87×10^{-1}	7.63×10^{-2}
29	2.00×10^{1}	2.22×10^{-2}	3.85×10^{-1}	1.42×10^{-1}
30	2.83×10^{1}	2.07×10^{-2}	4.87×10^{-1}	1.72×10^{-1}
31	4.00×10^{1}	1.55×10^{-2}	5.40×10^{-1}	1.67×10^{-1}
32	5.66×10^{1}	1.26×10^{-2}	6.05×10^{-1}	1.76×10^{-1}
33	8.00×10^{1}	1.19×10^{-2}	8.08×10^{-1}	2.15×10^{-1}
34	1.13×10^{2}	8.90×10^{-3}	8.41×10^{-1}	2.09×10^{-1}
35	1.60×10^{2}	7.96×10^{-3}	1.02×10^{0}	2.43×10^{-1}
36	2.26×10^{2}	4.47×10^{-3}	8.51×10^{-1}	1.77×10^{-1}
37	3.20×10^{2}	2.76×10^{-3}	7.35×10^{-1}	1.42×10^{-1}
38	4.53×10^{2}	1.35×10^{-3}	5.32×10^{-1}	9.02×10^{-2}
39	6.40×10^{2}	9.88×10^{-4}	5.24×10^{-1}	8.55×10^{-2}
40	9.05×10^{2}	6.76×10^{-4}	5.02×10^{-1}	7.59×10^{-2}
41	1.28×10^{3}	4.68×10^{-4}	4.97×10^{-1}	6.22×10^{-2}
42	1.81×10^{3}	5.20×10^{-5}	6.97×10^{-2}	8.97×10^{-3}
43	2.56×10^{3}	5.20×10^{-5}	1.12×10^{-1}	1.16×10^{-2}
44	3.62×10^{3}	1.04×10^{-4}	3.09×10^{-1}	3.02×10^{-2}

Table G.3. Invertebrate megabenthos at Greater Haig Fras marine conservation zone in 2015. Geometric size-class data of numerical density (N_i, number of ind. m^{-2}), estimated biomass- (W_i in g wwt m^{-2}), and estimated respiration flux (B_i in mg C m^{-2} d^{-1}). Individual biomass was derived from existing length weight relationships (LWRs) available in literature (Benoist et al. 2019a and references therein; chapter 3 section 3.4; appendix A). Size-class estimated respiration flux was calculated from individual metabolic rate (chapter 1 equation 1.1) using Hemmingsen's (1960) equation for standard metabolic rate with site-specific temperature-correction (i.e. 10 °C; Gillooly et al. 2001), and multiplied by size-class abundance (N_i) (section 3.5). The asterisk indicates the start of the quantitative right-hand side of the spectrum (Bett 2013). Consecutive shaded rows indicate merged data to ensure a minimum of 10 individuals per body-size class. Total seabed area analysed was 5142 m^2.

Size class	Geometric body size (g wwt)	N_i (ind. m^{-2})	W_i (g wwt m^{-2})	B_i (mg C m^{-2} d^{-1})
6	6.91×10^{-3}	1.17×10^{-3}	7.85×10^{-6}	1.72×10^{-5}
7	9.77×10^{-3}	2.33×10^{-3}	1.95×10^{-5}	4.45×10^{-5}
8	1.38×10^{-2}	2.33×10^{-3}	2.66×10^{-5}	5.77×10^{-5}
9	1.95×10^{-2}	2.53×10^{-3}	4.04×10^{-5}	8.11×10^{-5}
10	2.76×10^{-2}	2.14×10^{-3}	4.88×10^{-5}	8.91×10^{-5}
11	3.91×10^{-2}	1.36×10^{-3}	4.17×10^{-5}	7.35×10^{-5}
12	5.52×10^{-2}	9.72×10^{-4}	4.09×10^{-5}	6.81×10^{-5}
13	7.81×10^{-2}	7.78×10^{-4}	5.15×10^{-5}	7.07×10^{-5}
14	1.10×10^{-1}	3.89×10^{-4}	4.10×10^{-5}	4.59×10^{-5}
15	1.56×10^{-1}	3.89×10^{-4}	5.66×10^{-5}	5.95×10^{-5}
16	2.21×10^{-1}	7.78×10^{-4}	1.34×10^{-4}	1.54×10^{-4}
17	3.13×10^{-1}	5.83×10^{-4}	1.61×10^{-4}	1.50×10^{-4}
18	4.42×10^{-1}	1.94×10^{-4}	6.87×10^{-5}	6.50×10^{-5}
19	6.25×10^{-1}	4.47×10^{-3}	2.37×10^{-3}	1.94×10^{-3}
20	8.84×10^{-1}	8.75×10^{-3}	6.76×10^{-3}	4.92×10^{-3}
21	1.25×10^{0}	6.42×10^{-3}	6.87×10^{-3}	4.68×10^{-3}
22	1.77×10^{0}	6.81×10^{-3}	1.02×10^{-2}	6.44×10^{-3}
23	2.50×10^{0}	9.53×10^{-3}	2.02×10^{-2}	1.17×10^{-2}
24	3.54×10^{0}	1.50×10^{-2}	4.50×10^{-2}	2.38×10^{-2}
25	5.00×10^{0}	2.31×10^{-2}	9.78×10^{-2}	4.78×10^{-2}
26*	7.07×10^{0}	3.29×10^{-2}	1.88×10^{-1}	8.81×10^{-2}
27	1.00×10^{1}	2.24×10^{-2}	1.89×10^{-1}	7.77×10^{-2}
28	1.41×10^{1}	1.24×10^{-2}	1.47×10^{-1}	5.61×10^{-2}
29	2.00×10^{1}	6.81×10^{-3}	1.11×10^{-1}	3.98×10^{-2}
30	2.83×10^{1}	2.92×10^{-3}	6.95×10^{-2}	2.21×10^{-2}
31	4.76×10^{1}	1.65×10^{-3}	6.35×10^{-2}	1.85×10^{-2}
32	6.73×10^{1}	1.85×10^{-3}	1.07×10^{-1}	2.69×10^{-2}
33	9.51×10^{1}	5.64×10^{-3}	5.17×10^{-1}	1.06×10^{-1}
34	1.35×10^{2}	7.78×10^{-3}	8.58×10^{-1}	1.90×10^{-1}
35	1.90×10^{2}	4.08×10^{-3}	5.64×10^{-1}	1.30×10^{-1}
36	2.69×10^{2}	1.17×10^{-3}	2.53×10^{-1}	4.81×10^{-2}
37	3.81×10^{2}	5.83×10^{-4}	1.76×10^{-1}	3.12×10^{-2}
38	5.38×10^{2}	3.89×10^{-4}	1.74×10^{-1}	2.70×10^{-2}
39	7.61×10^{2}	4.86×10^{-4}	3.31×10^{-1}	4.37×10^{-2}
40	1.08×10^{3}	3.89×10^{-4}	3.23×10^{-1}	4.54×10^{-2}
41	1.52×10^{3}	1.94×10^{-4}	2.29×10^{-1}	2.94×10^{-2}
42	2.15×10^{3}	9.72×10^{-5}	1.34×10^{-1}	1.91×10^{-2}

Table G.4. Invertebrate megabenthos at Greater Haig Fras marine conservation zone in 2015. Geometric size-class data of numerical density (N_i, number of ind. m^{-2}), estimated biomass- (W_i in g wwt m^{-2}), and estimated respiration flux (B_i in mg C m^{-2} d^{-1}). Individual biomass was derived from existing length weight relationships (LWRs) available in literature (Benoist et al. 2019a and references therein; chapter 3 section 3.4; appendix A). Size-class estimated respiration flux was calculated from individual metabolic rate (chapter 1 equation 1.1) using Hemmingsen's (1960) equation for standard metabolic rate with site-specific temperature-correction (i.e. 10 °C; Gillooly et al. 2001), and multiplied by size-class abundance (N_i) (section 3.5). The asterisk indicates the start of the quantitative right-hand side of the spectrum (Bett 2013). Consecutive shaded rows indicate merged data to ensure a minimum of 10 individuals per body-size class. Total seabed area analysed was 5142 m^2.

Size class	Geometric body size (g wwt)	N_i (ind. m^{-2})	W_i (g wwt m^{-2})	B_i (mg C m^{-2} d^{-1})
6	6.91×10^{-3}	1.17×10^{-3}	7.85×10^{-6}	1.72×10^{-5}
7	9.77×10^{-3}	2.33×10^{-3}	1.95×10^{-5}	4.45×10^{-5}
8	1.38×10^{-2}	2.33×10^{-3}	2.66×10^{-5}	5.77×10^{-5}
9	1.95×10^{-2}	2.53×10^{-3}	4.04×10^{-5}	8.11×10^{-5}
10	2.76×10^{-2}	2.14×10^{-3}	4.88×10^{-5}	8.91×10^{-5}
11	3.91×10^{-2}	1.36×10^{-3}	4.17×10^{-5}	7.35×10^{-5}
12	5.52×10^{-2}	1.17×10^{-3}	5.05×10^{-5}	8.18×10^{-5}
13	7.81×10^{-2}	9.72×10^{-4}	6.38×10^{-5}	8.84×10^{-5}
14	1.10×10^{-1}	1.17×10^{-3}	1.12×10^{-4}	1.38×10^{-4}
15	1.56×10^{-1}	5.83×10^{-4}	7.87×10^{-5}	8.93×10^{-5}
16	2.21×10^{-1}	9.72×10^{-4}	1.66×10^{-4}	1.93×10^{-4}
17	3.13×10^{-1}	1.75×10^{-3}	4.67×10^{-4}	4.51×10^{-4}
18	4.42×10^{-1}	1.36×10^{-3}	4.57×10^{-4}	4.55×10^{-4}
19	6.25×10^{-1}	7.00×10^{-3}	3.83×10^{-3}	3.03×10^{-3}
20	8.84×10^{-1}	9.92×10^{-3}	7.61×10^{-3}	5.58×10^{-3}
21	1.25×10^{0}	7.78×10^{-3}	8.25×10^{-3}	5.67×10^{-3}
22	1.77×10^{0}	7.97×10^{-3}	1.20×10^{-2}	7.54×10^{-3}
23	2.50×10^{0}	1.09×10^{-2}	2.31×10^{-2}	1.34×10^{-2}
24	3.54×10^{0}	1.56×10^{-2}	4.68×10^{-2}	2.48×10^{-2}
25	5.00×10^{0}	2.41×10^{-2}	1.02×10^{-1}	4.98×10^{-2}
26*	7.07×10^{0}	4.08×10^{-2}	2.41×10^{-1}	1.09×10^{-1}
27	1.00×10^{1}	2.26×10^{-2}	1.90×10^{-1}	7.84×10^{-2}
28	1.41×10^{1}	1.24×10^{-2}	1.47×10^{-1}	5.61×10^{-2}
29	2.00×10^{1}	7.20×10^{-3}	1.18×10^{-1}	4.21×10^{-2}
30	2.83×10^{1}	4.08×10^{-3}	9.79×10^{-2}	3.10×10^{-2}
31	4.76×10^{1}	2.14×10^{-3}	7.20×10^{-2}	2.11×10^{-2}
32	6.73×10^{1}	1.94×10^{-3}	8.91×10^{-2}	2.48×10^{-2}
33	9.51×10^{1}	2.53×10^{-3}	1.64×10^{-1}	4.19×10^{-2}
34	1.35×10^{2}	9.33×10^{-3}	9.20×10^{-1}	2.01×10^{-1}
35	1.90×10^{2}	6.61×10^{-3}	8.34×10^{-1}	1.84×10^{-1}
36	2.69×10^{2}	1.75×10^{-3}	3.28×10^{-1}	6.33×10^{-2}
37	3.81×10^{2}	9.72×10^{-4}	2.60×10^{-1}	4.56×10^{-2}
38	5.38×10^{2}	3.89×10^{-4}	1.41×10^{-1}	2.37×10^{-2}
39	7.61×10^{2}	7.78×10^{-4}	4.40×10^{-1}	6.14×10^{-2}
40	1.08×10^{3}	9.72×10^{-4}	7.62×10^{-1}	9.96×10^{-2}
41	1.52×10^{3}	1.94×10^{-4}	1.90×10^{-1}	2.59×10^{-2}
42	2.15×10^{3}	1.94×10^{-4}	2.67×10^{-1}	3.35×10^{-2}

G.2 Shelf-Sea Biogeochemistry study area

Table G.5. Invertebrate megabenthos standing stocks at the UK-NERC Shelf-Sea Biogeochemistry study area in 2015. Geometric size-class data of numerical density (N_i, number of ind. m^{-2}), estimated biomass- (W_i in g wwt m^{-2}), and estimated respiration flux (B_i in mg C m^{-2} d^{-1}). Individual biomass was derived using a generalised volumetric method (GVM) (Benoist et al. 2019b; chapter 3 section 3.4; chapter 4). Size-class estimated respiration flux was calculated from individual metabolic rate (chapter 1 equation 1.1) using Hemmingsen's (1960) equation for standard metabolic rate with site-specific temperature-correction (i.e. 10 °C; Gillooly et al. 2001), and multiplied by size-class abundance (N_i) (section 3.5). The asterisk indicates the start of the quantitative right-hand side of the spectrum (Bett 2013). Consecutive shaded rows indicate merged data to ensure a minimum of 10 individuals per body-size class. Total seabed area analysed was 3876 m^2.

Size class	Geometric body size (g wwt)	N_i (ind. m^{-2})	W_i (g wwt m^{-2})	B_i (mg C m^{-2} d^{-1})
3	2.44×10^{-3}	1.03×10^{-3}	2.19×10^{-6}	6.95×10^{-6}
4	3.45×10^{-3}	1.03×10^{-3}	3.19×10^{-6}	9.02×10^{-6}
5	4.88×10^{-3}	2.84×10^{-3}	1.18×10^{-5}	3.22×10^{-5}
6	6.91×10^{-3}	2.84×10^{-3}	1.73×10^{-5}	4.17×10^{-5}
7	9.77×10^{-3}	5.16×10^{-3}	4.30×10^{-5}	9.84×10^{-5}
8	1.38×10^{-2}	8.00×10^{-3}	9.33×10^{-5}	1.98×10^{-4}
9	1.95×10^{-2}	1.34×10^{-2}	2.24×10^{-4}	4.31×10^{-4}
10	2.76×10^{-2}	1.96×10^{-2}	4.64×10^{-4}	8.17×10^{-4}
11	3.91×10^{-2}	2.50×10^{-2}	8.34×10^{-4}	1.35×10^{-3}
12	5.52×10^{-2}	2.97×10^{-2}	1.39×10^{-3}	2.08×10^{-3}
13	7.81×10^{-2}	4.52×10^{-2}	3.02×10^{-3}	4.10×10^{-3}
14	1.10×10^{-1}	4.90×10^{-2}	4.63×10^{-3}	5.78×10^{-3}
15	1.56×10^{-1}	4.98×10^{-2}	6.61×10^{-3}	7.62×10^{-3}
16*	2.21×10^{-1}	5.86×10^{-2}	1.09×10^{-2}	1.16×10^{-2}
17	3.13×10^{-1}	5.68×10^{-2}	1.51×10^{-2}	1.46×10^{-2}
18	4.42×10^{-1}	5.08×10^{-2}	1.87×10^{-2}	1.70×10^{-2}
19	6.25×10^{-1}	5.24×10^{-2}	2.78×10^{-2}	2.27×10^{-2}
20	8.84×10^{-1}	3.51×10^{-2}	2.59×10^{-2}	1.97×10^{-2}
21	1.25×10^{0}	2.73×10^{-2}	2.89×10^{-2}	1.99×10^{-2}
22	1.77×10^{0}	2.19×10^{-2}	3.20×10^{-2}	2.07×10^{-2}
23	2.50×10^{0}	2.06×10^{-2}	4.34×10^{-2}	2.53×10^{-2}
24	3.54×10^{0}	1.65×10^{-2}	4.98×10^{-2}	2.63×10^{-2}
25	5.00×10^{0}	1.11×10^{-2}	4.75×10^{-2}	2.29×10^{-2}
26	7.07×10^{0}	9.55×10^{-3}	5.78×10^{-2}	2.56×10^{-2}
27	1.00×10^{1}	1.16×10^{-2}	9.87×10^{-2}	4.04×10^{-2}
28	1.41×10^{1}	9.55×10^{-3}	1.16×10^{-1}	4.31×10^{-2}
29	2.00×10^{1}	4.90×10^{-3}	8.22×10^{-2}	2.87×10^{-2}
30	2.83×10^{1}	4.13×10^{-3}	9.70×10^{-2}	3.13×10^{-2}
31	4.00×10^{1}	2.32×10^{-3}	8.28×10^{-2}	2.29×10^{-2}
32	5.66×10^{1}	1.29×10^{-3}	5.68×10^{-2}	1.65×10^{-2}
33	8.00×10^{1}	1.03×10^{-3}	7.08×10^{-2}	1.71×10^{-2}
34	1.13×10^{2}	1.03×10^{-3}	1.04×10^{-1}	2.22×10^{-2}
35	1.60×10^{2}	-	-	-
36	2.26×10^{2}	-	-	-
37	3.20×10^{2}	-	-	-
38	4.53×10^{2}	2.58×10^{-4}	9.34×10^{-2}	1.57×10^{-2}

Table G.6. Invertebrate megabenthos and demersal fish standing stocks at the UK-NERC Shelf-Sea Biogeochemistry study area in 2015. Geometric size-class data of numerical density (N_i, number of ind. m^{-2}), estimated biomass- (W_i in g wwt m^{-2}), and estimated respiration flux (B_i in mg C m^{-2} d^{-1}). Individual biomass was derived using a generalised volumetric method (GVM) (Benoist et al. 2019b; chapter 3 section 3.4; chapter 4). Size-class estimated respiration flux was calculated from individual metabolic rate (chapter 1 equation 1.1) using Hemmingsen's (1960) equation for standard metabolic rate with site-specific temperature-correction (i.e. 10 °C; Gillooly et al. 2001), and multiplied by size-class abundance (N_i) (section 3.5). The asterisk indicates the start of the quantitative right-hand side of the spectrum (Bett 2013). Consecutive shaded rows indicate merged data to ensure a minimum of 10 individuals per body-size class. Total seabed area analysed was 3876 m^2.

Size class	Geometric body size (g wwt)	N_i (ind. m^{-2})	W_i (g wwt m^{-2})	B_i (mg C m^{-2} d^{-1})
3	2.44×10^{-3}	1.03×10^{-3}	2.19×10^{-6}	6.95×10^{-6}
4	3.45×10^{-3}	1.03×10^{-3}	3.19×10^{-6}	9.02×10^{-6}
5	4.88×10^{-3}	2.84×10^{-3}	1.18×10^{-5}	3.22×10^{-5}
6	6.91×10^{-3}	2.84×10^{-3}	1.73×10^{-5}	4.17×10^{-5}
7	9.77×10^{-3}	5.16×10^{-3}	4.30×10^{-5}	9.84×10^{-5}
8	1.38×10^{-2}	8.00×10^{-3}	9.33×10^{-5}	1.98×10^{-4}
9	1.95×10^{-2}	1.34×10^{-2}	2.24×10^{-4}	4.31×10^{-4}
10	2.76×10^{-2}	1.96×10^{-2}	4.64×10^{-4}	8.17×10^{-4}
11	3.91×10^{-2}	2.50×10^{-2}	8.34×10^{-4}	1.35×10^{-3}
12	5.52×10^{-2}	2.99×10^{-2}	1.40×10^{-3}	2.10×10^{-3}
13	7.81×10^{-2}	4.54×10^{-2}	3.04×10^{-3}	4.13×10^{-3}
14	1.10×10^{-1}	4.93×10^{-2}	4.66×10^{-3}	5.81×10^{-3}
15	1.56×10^{-1}	5.03×10^{-2}	6.68×10^{-3}	7.70×10^{-3}
16*	2.21×10^{-1}	5.99×10^{-2}	1.12×10^{-2}	1.19×10^{-2}
17	3.13×10^{-1}	5.70×10^{-2}	1.51×10^{-2}	1.47×10^{-2}
18	4.42×10^{-1}	5.39×10^{-2}	1.99×10^{-2}	1.80×10^{-2}
19	6.25×10^{-1}	6.04×10^{-2}	3.22×10^{-2}	2.62×10^{-2}
20	8.84×10^{-1}	4.00×10^{-2}	2.95×10^{-2}	2.25×10^{-2}
21	1.25×10^{0}	3.15×10^{-2}	3.34×10^{-2}	2.30×10^{-2}
22	1.77×10^{0}	2.61×10^{-2}	3.83×10^{-2}	2.47×10^{-2}
23	2.50×10^{0}	2.53×10^{-2}	5.29×10^{-2}	3.10×10^{-2}
24	3.54×10^{0}	3.28×10^{-2}	9.96×10^{-2}	5.22×10^{-2}
25	5.00×10^{0}	1.47×10^{-2}	6.26×10^{-2}	3.04×10^{-2}
26	7.07×10^{0}	1.42×10^{-2}	8.53×10^{-2}	3.80×10^{-2}
27	1.00×10^{1}	1.39×10^{-2}	1.19×10^{-1}	4.84×10^{-2}
28	1.41×10^{1}	1.08×10^{-2}	1.32×10^{-1}	4.89×10^{-2}
29	2.00×10^{1}	1.91×10^{-2}	2.95×10^{-1}	1.12×10^{-1}
30	2.83×10^{1}	6.19×10^{-3}	1.47×10^{-1}	4.70×10^{-2}
31	4.00×10^{1}	4.39×10^{-3}	1.51×10^{-1}	4.32×10^{-2}
32	5.66×10^{1}	1.47×10^{-2}	6.73×10^{-1}	1.88×10^{-1}
33	8.00×10^{1}	1.29×10^{-3}	9.01×10^{-2}	2.14×10^{-2}
34	1.13×10^{2}	2.06×10^{-3}	1.99×10^{-1}	4.44×10^{-2}
35	1.60×10^{2}	5.16×10^{-4}	7.98×10^{-2}	1.44×10^{-2}
36	2.26×10^{2}	2.58×10^{-4}	4.75×10^{-2}	9.33×10^{-3}
37	3.20×10^{2}	1.55×10^{-3}	3.94×10^{-1}	7.27×10^{-2}
38	4.53×10^{2}	5.16×10^{-4}	1.98×10^{-1}	3.14×10^{-2}
39	6.40×10^{2}	-	-	-
40	9.05×10^{2}	1.03×10^{-3}	7.07×10^{-1}	1.06×10^{-1}
41	1.28×10^{3}	1.03 × 10-3	1.21 × 100	1.37 × 10-1
42	1.81×10^{3}	-	-	-
43	2.56×10^{3}	-	-	-
44	3.62×10^{3}	-	-	-
45	5.12×10^{3}	-	-	-
46	7.24×10^{3}	-	-	-
47	1.02×10^{4}	-	-	-
48	1.45×10^{4}	-	-	-
49	2.05×10^{4}	2.58×10^{-4}	4.18×10^{0}	2.75×10^{-1}

G.3 Porcupine Abyssal Plain sustained observatory

Table G.7. Invertebrate macrobenthos standing stocks at the Porcupine Abyssal Plain study area between 2014 and 2015. Geometric size-class data of numerical density (N_i, number of ind. m^{-2}), estimated biomass- (W_i in g wwt m^{-2}), and estimated respiration flux (B_i in mg C m^{-2} d^{-1}). Individual biomass was derived using a generalised volumetric method (GVM) (Benoist et al. 2019b; chapter 3 section 3.4; chapter 4). Size-class estimated respiration flux was calculated from individual metabolic rate (chapter 1 equation 1.1) using Hemmingsen's (1960) equation for standard metabolic rate with site-specific temperature-correction (i.e. 2.5 °C; Gillooly et al. 2001), and multiplied by size-class abundance (N_i) (section 3.5). The asterisk indicates the start of the quantitative right-hand side of the spectrum (Bett 2013). Consecutive shaded rows indicate merged data to ensure a minimum of 10 individuals per body-size class. Total seabed area analysed was 0.503 m^2.

Size class	Geometric body size (g wwt)	N_i (ind. m^{-2})	W_i (g wwt m^{-2})	B_i (mg C m^{-2} d^{-1})
-21	5.96×10^{-4}	1.99×10^{0}	9.56×10^{-7}	1.29×10^{-5}
-20	8.43×10^{-7}	-	-	-
-19	1.19×10^{-3}	3.98×10^{0}	3.99×10^{-6}	4.35×10^{-5}
-18	1.69×10^{-3}	3.98×10^{0}	5.24×10^{-6}	5.64×10^{-5}
-17	2.38×10^{-3}	7.96×10^{0}	1.55×10^{-5}	1.46×10^{-4}
-16	3.37×10^{-3}	2.19×10^{1}	6.03×10^{-5}	5.22×10^{-4}
-15	4.77×10^{-3}	3.38×10^{1}	1.36×10^{-4}	1.05×10^{-3}
-14	6.74×10^{-3}	3.18×10^{1}	1.85×10^{-4}	1.28×10^{-3}
-13	9.54×10^{-3}	7.96×10^{1}	6.48×10^{-4}	4.14×10^{-3}
-12	1.35×10^{-2}	9.35×10^{1}	1.07×10^{-3}	6.32×10^{-3}
-11*	1.91×10^{-2}	1.09×10^{2}	1.73×10^{-3}	9.59×10^{-3}
-10	2.70×10^{-2}	8.75×10^{1}	1.99×10^{-3}	9.95×10^{-3}
-9	3.81×10^{-2}	1.01×10^{2}	3.29×10^{-3}	1.50×10^{-2}
-8	5.39×10^{-2}	9.55×10^{1}	4.31×10^{-3}	1.83×10^{-2}
-7	7.63×10^{-2}	4.97×10^{1}	3.32×10^{-3}	1.23×10^{-2}
-6	1.08×10^{-1}	6.57×10^{1}	5.73×10^{-3}	2.11×10^{-2}
-5	1.53×10^{-1}	3.18×10^{1}	4.11×10^{-3}	1.33×10^{-2}
-4	2.16×10^{-1}	3.78×10^{1}	6.66×10^{-3}	2.05×10^{-2}
-3	3.05×10^{-1}	2.19×10^{1}	5.52×10^{-3}	1.54×10^{-2}
-2	4.32×10^{-1}	1.39×10^{1}	5.07×10^{-3}	1.27×10^{-2}
-1	6.10×10^{-1}	1.99×10^{1}	1.01×10^{-2}	2.35×10^{-2}
0	8.63×10^{-1}	1.79×10^{1}	1.32×10^{-2}	2.75×10^{-2}
1	1.22×10^{0}	9.95×10^{0}	9.88×10^{-3}	1.98×10^{-2}
2	1.73×10^{0}	7.96×10^{0}	1.25×10^{-2}	2.06×10^{-2}
3	2.44×10^{0}	3.98×10^{0}	8.60×10^{-3}	1.33×10^{-2}
4	3.45×10^{0}	1.19×10^{1}	3.64×10^{-2}	5.19×10^{-2}
5	4.88×10^{0}	5.97×10^{0}	2.41×10^{-2}	3.37×10^{-2}
6	6.91×10^{0}	3.98×10^{0}	1.98×10^{-2}	2.91×10^{-2}
7	9.77×10^{0}	1.99×10^{0}	1.80×10^{-2}	1.89×10^{-2}
8	1.38×10^{-2}	-	-	-
9	1.95×10^{-2}	-	-	-
10	2.76×10^{-2}	-	-	-
11	3.91×10^{-2}	-	-	-
12	5.52×10^{-2}	-	-	-
13	7.81×10^{-2}	-	-	-
14	1.10×10^{-1}	-	-	-
15	1.56×10^{2}	1.99×10^{0}	2.35×10^{-1}	1.51×10^{-1}

Table G.8. Invertebrate megabenthos standing stocks at the Porcupine Abyssal Plain study area in 2012. Geometric size-class data of numerical density (N_i, number of ind. m^{-2}), estimated biomass- (W_i in g wwt m^{-2}), and estimated respiration flux (B_i in mg C m^{-2} d^{-1}). Individual biomass was derived from existing length weight relationships (LWRs) available in literature (Durden et al. 2016a; chapter 3 section 3.4). Size-class estimated respiration flux was calculated from individual metabolic rate (chapter 1 equation 1.1) using Hemmingsen's (1960) equation for standard metabolic rate with site-specific temperature-correction (i.e. 2.5 °C; Gillooly et al. 2001), and multiplied by size-class abundance (N_i) (section 3.5). The asterisk indicates the start of the quantitative right-hand side of the spectrum (Bett 2013). Consecutive shaded rows indicate merged data to ensure a minimum of 10 individuals per body-size class. Total seabed area analysed was 85,294 m^2.

Size class	Geometric body size (g wwt)	N_i (ind. m^{-2})	W_i (g wwt m^{-2})	B_i (mg C m^{-2} d^{-1})
13	7.81×10^{-2}	1.04×10^{-4}	6.45×10^{-6}	1.04×10^{-5}
14	1.10×10^{-1}	1.04×10^{-4}	1.06×10^{-5}	1.34×10^{-5}
15	1.56×10^{-1}	2.60×10^{-4}	3.59×10^{-5}	4.36×10^{-5}
16	2.21×10^{-1}	3.12×10^{-4}	5.91×10^{-5}	6.78×10^{-5}
17	3.13×10^{-1}	5.20×10^{-4}	1.43×10^{-4}	1.47×10^{-4}
18	4.42×10^{-1}	8.32×10^{-4}	3.15×10^{-4}	3.04×10^{-4}
19	6.25×10^{-1}	2.18×10^{-3}	1.14×10^{-3}	1.04×10^{-3}
20	8.84×10^{-1}	2.29×10^{-3}	1.73×10^{-3}	1.41×10^{-3}
21*	1.25×10^{0}	6.09×10^{-3}	6.58×10^{-3}	4.86×10^{-3}
22	1.77×10^{0}	1.13×10^{-2}	1.74×10^{-2}	1.17×10^{-2}
23	2.50×10^{0}	1.48×10^{-2}	3.13×10^{-2}	1.99×10^{-2}
24	3.54×10^{0}	2.15×10^{-2}	6.36×10^{-2}	3.75×10^{-2}
25	5.00×10^{0}	1.52×10^{-2}	6.40×10^{-2}	3.44×10^{-2}
26	7.07×10^{0}	1.35×10^{-2}	8.01×10^{-2}	3.97×10^{-2}
27	1.00×10^{1}	1.41×10^{-2}	1.18×10^{-1}	5.37×10^{-2}
28	1.41×10^{1}	1.50×10^{-2}	1.82×10^{-1}	7.42×10^{-2}
29	2.00×10^{1}	2.11×10^{-2}	3.67×10^{-1}	1.35×10^{-1}
30	2.83×10^{1}	1.88×10^{-2}	4.42×10^{-1}	1.56×10^{-1}
31	4.00×10^{1}	1.25×10^{-2}	4.40×10^{-1}	1.35×10^{-1}
32	5.66×10^{1}	6.66×10^{-3}	3.16×10^{-1}	9.31×10^{-2}
33	8.00×10^{1}	4.94×10^{-3}	3.37×10^{-1}	8.97×10^{-2}
34	1.13×10^{2}	4.27×10^{-3}	4.07×10^{-1}	1.00×10^{-1}
35	1.60×10^{2}	3.23×10^{-3}	4.37×10^{-1}	9.85×10^{-2}
36	2.26×10^{2}	3.28×10^{-3}	6.27×10^{-1}	1.30×10^{-1}
37	3.20×10^{2}	1.98×10^{-3}	5.31×10^{-1}	1.02×10^{-1}
38	4.53×10^{2}	9.36×10^{-4}	3.74×10^{-1}	6.24×10^{-2}
39	6.40×10^{2}	6.76×10^{-4}	3.67×10^{-1}	5.85×10^{-2}
40	9.05×10^{2}	3.12×10^{-4}	2.25×10^{-1}	3.20×10^{-2}
41	1.28×10^{3}	2.60×10^{-4}	2.65×10^{-1}	3.46×10^{-2}
42	1.81×10^{3}	-	-	-
43	2.56×10^{3}	5.20×10^{-5}	1.12×10^{-1}	1.16×10^{-2}
44	3.62×10^{3}	1.04×10^{-4}	3.09×10^{-1}	3.02×10^{-2}

G.4 Clarion-Clipperton Zone

Table G.9. Invertebrate megabenthos standing stocks at the Clarion-Clipperton Zone study area in 2015. Geometric size-class data of numerical density (N_i, number of ind. m^{-2}), estimated biomass- (W_i in g wwt m^{-2}), and estimated respiration flux (B_i in mg C m^{-2} d^{-1}). Individual biomass was derived using a generalised volumetric method (GVM) (Benoist et al. 2019b; chapter 3 section 3.4; chapter 4). Size-class estimated respiration flux was calculated from individual metabolic rate (chapter 1 equation 1.1) using Hemmingsen's (1960) equation for standard metabolic rate with site-specific temperature-correction (i.e. 1.5 °C; Gillooly et al. 2001), and multiplied by size-class abundance (N_i) (section 3.5). The asterisk indicates the start of the quantitative right-hand side of the spectrum (Bett 2013). Consecutive shaded rows indicate merged data to ensure a minimum of 10 individuals per body-size class. Total seabed area analysed was 18,582 m^2.

Size class	Geometric body size (g wwt)	N_i (ind. m^{-2})	W_i (g wwt m^{-2})	B_i (mg C m^{-2} d^{-1})
-7	7.63×10^{-5}	2.15×10^{-4}	1.44×10^{-8}	4.85×10^{-8}
-6	1.08×10^{-4}	1.08×10^{-4}	8.43×10^{-9}	3.15×10^{-8}
-5	1.53×10^{-4}	1.61×10^{-4}	2.14×10^{-8}	6.13×10^{-8}
-4	2.16×10^{-4}	7.53×10^{-4}	1.35×10^{-7}	3.71×10^{-7}
-3	3.05×10^{-4}	8.61×10^{-4}	2.25×10^{-7}	5.50×10^{-7}
-2	4.32×10^{-4}	1.08×10^{-3}	3.92×10^{-7}	8.92×10^{-7}
-1	6.10×10^{-4}	1.88×10^{-3}	9.70×10^{-7}	2.02×10^{-6}
0	8.63×10^{-4}	1.40×10^{-3}	1.04×10^{-6}	1.95×10^{-6}
1	1.22×10^{-3}	2.10×10^{-3}	2.17×10^{-6}	3.80×10^{-6}
2	1.73×10^{-3}	7.00×10^{-3}	1.09×10^{-5}	1.64×10^{-5}
3	2.44×10^{-3}	1.40×10^{-2}	2.88×10^{-5}	4.28×10^{-5}
4	3.45×10^{-3}	1.23×10^{-2}	3.59×10^{-5}	4.87×10^{-5}
5	4.88×10^{-3}	8.56×10^{-3}	3.55×10^{-5}	4.38×10^{-5}
6	6.91×10^{-3}	6.78×10^{-3}	3.88×10^{-5}	4.51×10^{-5}
7	9.77×10^{-3}	6.08×10^{-3}	5.07×10^{-5}	5.24×10^{-5}
8	1.38×10^{-2}	6.35×10^{-3}	7.41×10^{-5}	7.10×10^{-5}
9	1.95×10^{-2}	7.59×10^{-3}	1.27×10^{-4}	1.10×10^{-4}
10	2.76×10^{-2}	1.21×10^{-2}	2.87×10^{-4}	2.27×10^{-4}
11	3.91×10^{-2}	1.56×10^{-2}	5.19×10^{-4}	3.81×10^{-4}
12	5.52×10^{-2}	1.96×10^{-2}	9.15×10^{-4}	6.22×10^{-4}
13	7.81×10^{-2}	2.24×10^{-2}	1.49×10^{-3}	9.22×10^{-4}
14*	1.10×10^{-1}	3.01×10^{-2}	2.80×10^{-3}	1.60×10^{-3}
15	1.56×10^{-1}	2.92×10^{-2}	3.85×10^{-3}	2.02×10^{-3}
16	2.21×10^{-1}	2.87×10^{-2}	5.36×10^{-3}	2.57×10^{-3}
17	3.13×10^{-1}	2.72×10^{-2}	7.19×10^{-3}	3.16×10^{-3}

Table G.9. Invertebrate megabenthos standing stocks at the Clarion-Clipperton Zone (CCZ) study area in 2015. *(Continued)*

Size class	Geometric body size (g wwt)	N_i (ind. m^{-2})	W_i (g wwt m^{-2})	B_i (mg C m^{-2} d^{-1})
18	4.42×10^{-1}	2.08×10^{-2}	7.74×10^{-3}	3.14×10^{-3}
19	6.25×10^{-1}	1.81×10^{-2}	9.51×10^{-3}	3.54×10^{-3}
20	8.84×10^{-1}	1.48×10^{-2}	1.10×10^{-2}	3.76×10^{-3}
21	1.25×10^{0}	1.36×10^{-2}	1.43×10^{-2}	4.47×10^{-3}
22	1.77×10^{0}	1.10×10^{-2}	1.62×10^{-2}	4.70×10^{-3}
23	2.50×10^{0}	7.00×10^{-3}	1.46×10^{-2}	3.88×10^{-3}
24	3.54×10^{0}	5.06×10^{-3}	1.50×10^{-2}	3.64×10^{-3}
25	5.00×10^{0}	2.91×10^{-3}	1.23×10^{-2}	2.71×10^{-3}
26	7.07×10^{0}	1.51×10^{-3}	8.97×10^{-3}	1.83×10^{-3}
27	1.00×10^{1}	6.46×10^{-4}	5.15×10^{-3}	1.01×10^{-3}
28	1.41×10^{1}	9.69×10^{-4}	1.18×10^{-2}	1.97×10^{-3}
29	2.00×10^{1}	7.00×10^{-4}	1.17×10^{-2}	1.85×10^{-3}
30	2.83×10^{1}	2.15×10^{-4}	5.22×10^{-3}	7.39×10^{-4}
31	4.00×10^{1}	3.77×10^{-4}	1.25×10^{-2}	1.68×10^{-3}
32	5.66×10^{1}	5.92×10^{-4}	2.85×10^{-2}	3.42×10^{-3}
33	8.00×10^{1}	4.84×10^{-4}	3.22×10^{-2}	3.63×10^{-3}
34	1.13×10^{2}	4.31×10^{-4}	4.04×10^{-2}	4.18×10^{-3}
35	1.60×10^{2}	1.08×10^{-4}	1.42×10^{-2}	1.36×10^{-3}
36	2.26×10^{2}	1.61×10^{-4}	3.16×10^{-2}	2.64×10^{-3}
37	3.20×10^{2}			
38	4.53×10^{2}	4.31×10^{-4}	1.66×10^{-1}	1.19×10^{-2}
39	6.40×10^{2}	1.61×10^{-4}	8.42×10^{-2}	5.76×10^{-3}
40	9.05×10^{2}	5.38×10^{-5}	3.54×10^{-2}	2.49×10^{-3}
41	1.28×10^{3}	1.61×10^{-4}	1.65×10^{-1}	9.70×10^{-3}

Table G.10. Invertebrate megabenthos and demersal fish standing stocks at the Clarion-Clipperton Zone study area in 2015. Geometric size-class data of numerical density (N_i, number of ind. m^{-2}), estimated biomass- (W_i in g wwt m^{-2}), and estimated respiration flux (B_i in mg C m^{-2} d^{-1}). Individual biomass was derived using a generalised volumetric method (GVM) (Benoist et al. 2019b; chapter 3 section 3.4; chapter 4). Size-class estimated respiration flux was calculated from individual metabolic rate (chapter 1 equation 1.1) using Hemmingsen's (1960) equation for standard metabolic rate with site-specific temperature-correction (i.e. 1.5 °C; Gillooly et al. 2001), and multiplied by size-class abundance (N_i) (section 3.5). The asterisk indicates the start of the quantitative right-hand side of the spectrum (Bett 2013). Consecutive shaded rows indicate merged data to ensure a minimum of 10 individuals per body-size class. Total seabed area analysed was 18,582 m^2.

Size class	Geometric body size (g wwt)	N_i (ind. m^{-2})	W_i (g wwt m^{-2})	B_i (mg C m^{-2} d^{-1})
-7	7.63×10^{-5}	2.15×10^{-4}	1.44×10^{-8}	4.85×10^{-8}
-6	1.08×10^{-4}	1.08×10^{-4}	8.43×10^{-9}	3.15×10^{-8}
-5	1.53×10^{-4}	1.61×10^{-4}	2.14×10^{-8}	6.13×10^{-8}
-4	2.16×10^{-4}	7.53×10^{-4}	1.35×10^{-7}	3.71×10^{-7}
-3	3.05×10^{-4}	8.61×10^{-4}	2.25×10^{-7}	5.50×10^{-7}
-2	4.32×10^{-4}	1.08×10^{-3}	3.92×10^{-7}	8.92×10^{-7}
-1	6.10×10^{-4}	1.88×10^{-3}	9.70×10^{-7}	2.02×10^{-6}
0	8.63×10^{-4}	1.40×10^{-3}	1.04×10^{-6}	1.95×10^{-6}
1	1.22×10^{-3}	2.10×10^{-3}	2.17×10^{-6}	3.80×10^{-6}
2	1.73×10^{-3}	7.00×10^{-3}	1.09×10^{-5}	1.64×10^{-5}
3	2.44×10^{-3}	1.40×10^{-2}	2.88×10^{-5}	4.28×10^{-5}
4	3.45×10^{-3}	1.23×10^{-2}	3.59×10^{-5}	4.87×10^{-5}
5	4.88×10^{-3}	8.56×10^{-3}	3.55×10^{-5}	4.38×10^{-5}
6	6.91×10^{-3}	6.78×10^{-3}	3.88×10^{-5}	4.51×10^{-5}
7	9.77×10^{-3}	6.08×10^{-3}	5.07×10^{-5}	5.24×10^{-5}
8	1.38×10^{-2}	6.35×10^{-3}	7.41×10^{-5}	7.10×10^{-5}
9	1.95×10^{-2}	7.59×10^{-3}	1.27×10^{-4}	1.10×10^{-4}
10	2.76×10^{-2}	1.21×10^{-2}	2.87×10^{-4}	2.27×10^{-4}
11	3.91×10^{-2}	1.56×10^{-2}	5.19×10^{-4}	3.81×10^{-4}
12	5.52×10^{-2}	1.96×10^{-2}	9.15×10^{-4}	6.22×10^{-4}
13	7.81×10^{-2}	2.24×10^{-2}	1.49×10^{-3}	9.22×10^{-4}
14*	1.10×10^{-1}	3.01×10^{-2}	2.80×10^{-3}	1.60×10^{-3}
15	1.56×10^{-1}	2.92×10^{-2}	3.85×10^{-3}	2.02×10^{-3}
16	2.21×10^{-1}	2.87×10^{-2}	5.37×10^{-3}	2.58×10^{-3}
17	3.13×10^{-1}	2.72×10^{-2}	7.20×10^{-3}	3.17×10^{-3}
18	4.42×10^{-1}	2.09×10^{-2}	7.76×10^{-3}	3.15×10^{-3}
19	6.25×10^{-1}	1.83×10^{-2}	9.63×10^{-3}	3.58×10^{-3}

Table G.10. Invertebrate megabenthos and demersal fish standing stocks at the Clarion-Clipperton Zone study area in 2015. *(Continued)*

Size class	Geometric body size (g wwt)	N_i (ind. m-2)	W_i (g wwt m-2)	B_i (mg C m-2 d-1)
19	6.25×10^{-1}	1.83×10^{-2}	9.63×10^{-3}	3.58×10^{-3}
20	8.84×10^{-1}	1.52×10^{-2}	1.13×10^{-2}	3.87×10^{-3}
21	1.25×10^{0}	1.40×10^{-2}	1.48×10^{-2}	4.63×10^{-3}
22	1.77×10^{0}	1.12×10^{-2}	1.66×10^{-2}	4.81×10^{-3}
23	2.50×10^{0}	7.53×10^{-3}	1.57×10^{-2}	4.18×10^{-3}
24	3.54×10^{0}	5.70×10^{-3}	1.71×10^{-2}	4.11×10^{-3}
25	5.00×10^{0}	3.66×10^{-3}	1.55×10^{-2}	3.42×10^{-3}
26	7.07×10^{0}	2.21×10^{-3}	1.32×10^{-2}	2.67×10^{-3}
27	1.00×10^{1}	9.69×10^{-4}	7.71×10^{-3}	1.52×10^{-3}
28	1.41×10^{1}	1.02×10^{-3}	1.24×10^{-2}	2.08×10^{-3}
29	2.00×10^{1}	9.69×10^{-4}	1.62×10^{-2}	2.56×10^{-3}
30	2.83×10^{1}	4.31×10^{-4}	1.06×10^{-2}	1.48×10^{-3}
31	4.00×10^{1}	4.31×10^{-4}	1.41×10^{-2}	1.92×10^{-3}
32	5.66×10^{1}	5.92×10^{-4}	2.85×10^{-2}	3.42×10^{-3}
33	8.00×10^{1}	5.38×10^{-4}	3.63×10^{-2}	4.03×10^{-3}
34	1.13×10^{2}	4.31×10^{-4}	4.04×10^{-2}	4.18×10^{-3}
35	1.60×10^{2}	1.08×10^{-4}	1.42×10^{-2}	1.36×10^{-3}
36	2.26×10^{2}	2.15×10^{-4}	4.17×10^{-2}	3.52×10^{-3}
37	3.20×10^{2}			
38	4.53×10^{2}	4.31×10^{-4}	1.66×10^{-1}	1.19×10^{-2}
39	6.40×10^{2}	1.61×10^{-4}	8.42×10^{-2}	5.76×10^{-3}
40	9.05×10^{2}	5.38×10^{-5}	3.54×10^{-2}	2.49×10^{-3}
41	1.28×10^{3}	2.15×10^{-4}	2.20×10^{-1}	1.29×10^{-2}
42	1.81×10^{3}	-	-	-
43	2.56×10^{3}	-	-	-
44	3.62×10^{3}	-	-	-
45	5.12×10^{3}	-	-	-
46	7.24×10^{3}	5.38×10^{-5}	3.00×10^{-1}	1.19×10^{-2}

Table G.11. Xenophyophore standing stocks at the Clarion-Clipperton Zone (CCZ) study area in 2015. Geometric size-class data of numerical density (N_i, number of ind. m^{-2}). Individual body size was derived using a generalised volumetric method (GVM) (Benoist et al. 2019b; chapter 3 section 3.4; chapter 4) and converted to protoplasm biomass using different values found in literature: $corr_a$= 0.01%; $corr_b$= 5%; $corr_c$; = 0.8%; $corr_d$= 3.12%; $corr_e$ is taxon specific (Levin and Gooday 1992; Gooday et al. 2018). The asterisk followed by subscript (a-e) indicates the start of the quantitative right-hand side of the corresponding spectrum (Bett 2013). Consecutive shaded rows indicate merged data to ensure a minimum of 10 individuals per body-size class. Total seabed area analysed was 18,582 m^2.

Size class	Geometric body size (g wwt)	M_{E-corr_a} (g wwt m^{-2})	M_{E-corr_b} (g wwt m^{-2})	M_{E-corr_c} (g wwt m^{-2})	M_{E-corr_d} (g wwt m^{-2})	M_{E-corr_e} (g wwt m^{-2})
-21	5.96×10^{-7}	4.31×10^{-4}	-	-	-	-
-20	8.43×10^{-7}	1.61×10^{-3}	-	-	-	-
-19	1.19×10^{-6}	3.98×10^{-3}	-	-	-	-
-18	1.69×10^{-6}	6.24×10^{-3}	-	-	-	-
-17	2.38×10^{-6}	1.09×10^{-2}	-	-	-	-
-16	3.37×10^{-6}	2.16×10^{-2}	-	-	-	-
-15	4.77×10^{-6}	2.63×10^{-2}	-	-	-	-
-14	6.74×10^{-6}	3.09×10^{-2}	-	-	-	9.15×10^{-4}
-13	9.54×10^{-6}	3.96×10^{-2}	-	-	-	2.37×10^{-3}
-12	1.35×10^{-5}	4.59×10^{-2}	-	-	-	4.63×10^{-3}
-11	1.91×10^{-5}	6.52×10^{-2}	-	-	-	7.96×10^{-3}
-10	2.70×10^{-5}	8.91×10^{-2}	-	-	-	1.17×10^{-2}
-9	3.81×10^{-5}	1.21×10^{-1}	-	-	-	1.65×10^{-2}
-8	5.39×10^{-5}	1.41×10^{-1}	-	9.15×10^{-4}	-	2.10×10^{-2}
-7*(a)	7.63×10^{-5}	1.53×10^{-1}	-	2.37×10^{-3}	-	2.17×10^{-2}
-6	1.08×10^{-4}	1.42×10^{-1}	-	4.63×10^{-3}	-	2.21×10^{-2}
-5	1.53×10^{-4}	1.24×10^{-1}	-	8.07×10^{-3}	-	1.91×10^{-2}
-4	2.16×10^{-4}	8.87×10^{-2}	-	1.38×10^{-2}	9.15×10^{-4}	1.71×10^{-2}
-3	3.05×10^{-4}	5.83×10^{-2}	4.84×10^{-4}	2.30×10^{-2}	2.74×10^{-3}	1.80×10^{-2}
-2	4.32×10^{-4}	3.23×10^{-2}	1.67×10^{-3}	3.00×10^{-2}	5.00×10^{-3}	1.82×10^{-2}
-1	6.10×10^{-4}	1.66×10^{-2}	3.98×10^{-3}	3.40×10^{-2}	8.13×10^{-3}	1.92×10^{-2}
0	8.63×10^{-4}	6.83×10^{-3}	6.35×10^{-3}	3.99×10^{-2}	1.49×10^{-2}	2.34×10^{-2}
1	1.22×10^{-3}	2.26×10^{-3}	1.17×10^{-2}	5.19×10^{-2}	2.30×10^{-2}	3.72×10^{-2}
2	1.73×10^{-3}	7.00×10^{-4}	2.25×10^{-2}	7.14×10^{-2}	3.00×10^{-2}	5.94×10^{-2}
3	2.44×10^{-3}	2.15×10^{-4}	2.71×10^{-2}	9.95×10^{-2}	3.45×10^{-2}	9.16×10^{-2}
4	3.45×10^{-3}	1.08×10^{-4}	3.12×10^{-2}	1.31×10^{-1}	4.00×10^{-2}	1.23×10^{-1}
5	4.88×10^{-3}	-	4.00×10^{-2}	1.47×10^{-1}	5.38×10^{-2}	1.39×10^{-1}
6*(c, e)	6.91×10^{-3}	5.38×10^{-5}	4.51×10^{-2}	1.49×10^{-1}	7.44×10^{-2}	1.44×10^{-1}
7	9.77×10^{-3}	-	6.62×10^{-2}	1.39×10^{-1}	1.00×10^{-1}	1.33×10^{-1}
8	1.38×10^{-2}	-	9.26×10^{-2}	1.10×10^{-1}	1.32×10^{-1}	1.07×10^{-1}
9*(d)	1.95×10^{-2}	-	1.23×10^{-1}	8.02×10^{-2}	1.52×10^{-1}	7.84×10^{-2}
10	2.76×10^{-2}	-	1.44×10^{-1}	4.81×10^{-2}	1.47×10^{-1}	4.75×10^{-2}
11*(b)	3.91×10^{-2}	-	1.52×10^{-1}	2.67×10^{-2}	1.35×10^{-1}	2.64×10^{-2}
12	5.52×10^{-2}	-	1.39×10^{-1}	1.15×10^{-2}	1.10×10^{-1}	1.12×10^{-2}
13	7.81×10^{-2}	-	1.21×10^{-1}	4.84×10^{-3}	7.60×10^{-2}	4.84×10^{-3}
14	1.10×10^{-1}	-	8.73×10^{-2}	1.45×10^{-3}	4.62×10^{-2}	1.45×10^{-3}
15	1.56×10^{-1}	-	5.54×10^{-2}	5.38×10^{-4}	2.61×10^{-2}	5.38×10^{-4}
16	2.21×10^{-1}	-	3.23×10^{-2}	2.69×10^{-4}	1.03×10^{-2}	2.69×10^{-4}
17	3.13×10^{-1}	-	1.52×10^{-2}	-	4.63×10^{-3}	-
18	4.42×10^{-1}	-	6.40×10^{-3}	-	1.40×10^{-3}	-
19	6.25×10^{-1}	-	2.15×10^{-3}	5.38×10^{-5}	4.84×10^{-4}	5.38×10^{-5}
20	8.84×10^{-1}	-	6.46×10^{-4}	-	2.69×10^{-4}	-
21	1.25×10^{0}	-	2.15×10^{-4}	-	-	-
22	1.77×10^{0}	-	1.08×10^{-4}	-	-	-
23	2.50×10^{0}	-	-	-	5.38×10^{-5}	-
24	3.54×10^{0}	-	5.38×10^{-5}	-	-	-